Modal Analysis of General Cyclically Symmetric Systems with Applications to Multi-Stage Structures

Bin Dong

Dissertation submitted to the Faculty of the
Virginia Polytechnic Institute and State University
in partial fulfillment of the requirements for the degree of

Doctor of Philosophy
in
Mechanical Engineering

Robert G. Parker, Chair
Corina Sandu
Lei Zuo
Michael K. Philen
Brian J. Olson

August 4, 2019
Blacksburg, Virginia

Keywords: Cyclic Symmetry, Group Theory, Modal Properties, Multi-Stage System

Modal Analysis of General Cyclically Symmetric Systems with Applications to Multi-Stage Structures

Bin Dong

(ABSTRACT)

This work investigates the modal properties of general cyclically symmetric systems and the multi-stage systems with cyclically symmetric stages. The work generalizes the modal properties of engineering applications, such as planetary gears, centrifugal pendulum vibration absorber (CPVA) systems, multi-stage planetary gears, *etc.*, and provides methods to improve the computational efficiency to numerically solve the system modes when cyclically symmetric structures exist.

Modal properties of cyclically symmetric systems with vibrating central components as three-dimensional rigid bodies are studied without any assumptions on the system matrix symmetries: asymmetric inertia matrix, damping, gyroscopic, and circulatory terms can be present. In the equation of motion of such a cyclically symmetric system, the matrix operators are proved to have properties related to the cyclic symmetry. These symmetry-related properties are used to prove the modal properties of general cyclically symmetric systems. Only three types of modes can exist: substructure modes, translational-tilting modes, and rotational-axial modes. Each mode type is characterized by specific central component modal deflections and substructure phase relations. Instead of solving the full eigenvalue problem, all vibration modes and natural frequencies can be obtained by solving smaller eigenvalue problems associated with each mode type. This computational advantage is dramatic for systems with many substructures or many degrees of freedom per substructure.

Group theory is applied to further generalize the modal properties of cyclically symmetric systems when both rigid-body and compliant central components exist, such as planetary

gears with an elastic continuum ring gear. The group theory for symmetry groups is introduced, and the group-theory-based modal analysis does not rely on any knowledge of the properties of system matrices in system equations of motion. The three types of modes (substructure modes, translational-tilting modes, and rotational-axial modes) are characterized by specific rigid-body central component modal deflections, substructure phase relations, and nodal diameter components of compliant central components. The general formulation of reduced eigenvalue problems for each mode type is obtained through group-theory-based method, and it applies to discrete, continuous, or hybrid discrete-continuous cyclically symmetric systems. The group-theory-based modal analysis also applies to systems with other symmetry types.

The group-theory-based modal analysis is generalized to analyze the multi-stage systems that are composed of symmetric stages coupled through the motions of rigid-body central components. The proposed group-theory-based modal analysis applies to multi-stage systems with cyclically symmetric stages, such as multi-stage planetary gears and CPVA systems with multiple groups of absorbers. The method also applies to multi-stage systems with component stages that have different types of symmetry. For a multi-stage system with symmetric stages, a unitary transformation matrix can be built through an algorithmic and computationally inexpensive procedure. The obtained unitary transformation matrix provides the foundation to analyze the modal properties based on the principles of group-theory-based modal analysis. For general multi-stage systems with symmetric component stages, the vibration modes are classified into two general types, single-stage substructure modes and overall modes, according to the non-zero modal deflections in each component stage. Reduced eigenvalue problems for each mode type are formulated to reduce the computational cost for eigensolutions.

Finite element models of multi-stage bladed disk assemblies consist of multiple cyclically

symmetric bladed disks that are coupled through the boundary nodes at the inter-stage interface. To improve the computational efficiency of calculating the full system modes, a numerical method is proposed by combination of the multi-stage cyclic symmetry reduction method and the subspace iteration method. Compared to the multi-stage cyclic symmetry reduction method, the proposed method improves the accuracy of obtained eigensolutions through an iterative process that is derived from the subspace iteration method. Based on the cyclic symmetry in each component stage of bladed disk, the proposed iterative method can be performed using single stage sector models only, instead of using matrix operators for the full multi-stage bladed disks. Parallel computations can be performed in the proposed iterative method, and the computational speed for eigensolutions can be increased significantly.

Modal Analysis of General Cyclically Symmetric Systems with Applications to Multi-Stage Structures

Bin Dong

(GENERAL AUDIENCE ABSTRACT)

Cyclically symmetric structures exist in many engineering applications such as bladed disks, circular plates, planetary gears, centrifugal pendulum vibration absorbers (CPVA), *etc.* During steady operation, these cyclically symmetric systems are subjected to traveling wave dynamic loading. Component vibrations result in undesirable effects, including high cycle fatigue (HCF) failure, noise, performance reduction, *etc.* Knowledge of the modal properties of cyclically symmetric systems is helpful to analyze the system forced response and understand experimental modal testing.

In this work, single stage cyclically symmetric systems are proved to have highly structured modes. The single stage systems considered in this work can have both rigid bodies and elastic continua as components. Group theory is used to study the modal properties, including the system mode types and the characteristics of different mode types. All the vibration modes of single stage cyclically symmetric systems can be solved from reduced eigenvalue problems. The methodology also applies to systems with other types of symmetry. For multi-stage systems with cyclically symmetric substructures, such as multi-stage planetary gears, a group-theory-based method is developed to analyze the modal properties. For industrial applications, such as multi-stage bladed disk assemblies, this work develops an iterative method to facilitate the calculations of system modes. The modal properties and methods for solving system modes apply to mechanical systems, including CPVA systems, the single/multi-stage planetary gears in power transmission systems, bladed disk assemblies in turbines, circular plates, elastic rings, *etc.*

Acknowledgments

I sincerely thank my advisor, Professor Robert G. Parker, for his guidance and assistance during my graduate studies. Professor Parker enthusiastically supported my academic interest in the vibrations of symmetric systems. His excellent expertise in dynamics is a treasure to me whenever I need academic guidance. His rigorous attitude to high-quality research and his devotion to spreading knowledge through technical writing are invaluable lessons.

I thank Professors Corina Sandu, Lei Zuo, Michael K. Philen, and Dr. Brian J. Olson for serving on my doctoral committee. I am grateful to have had the opportunity to learn from each of them. Their comments and suggestions are more than helpful to my research.

Finally, I thank my family for their support and encouragement throughout my life. I thank my parents for their unconditional trust, timely encouragement, and endless patience during the journey of discovering myself. They are the source of my courage. I thank with love to Wanni, my best friend and companion. As a Ph.D. herself, she understands me best. She loves, encourages, entertains, and helps me to get through the agonizing but fruitful years in the most positive way.

Contents

List of Figures

List of Tables

Chapter 1

Introduction

1.1 Motivation

Many rotating systems consist of an array of identical substructures that are equally spaced circumferentially around the central components, and these systems are referred to as *cyclically symmetric systems*. Many engineering applications are cyclically symmetric, including bladed discs, circular plates, planetary gears, centrifugal pendulum vibration absorbers (CPVA), *etc.* In planetary gears, for example, the substructures are the planet gears, and the central components are the carrier, ring gear, and sun gear. During steady operation, these cyclically symmetric systems are subjected to traveling wave dynamic loading, which excites the system at the frequencies that are proportional to the rotational speed of the system. Under such loading, component vibrations occur and result in undesirable effects, including high cycle fatigue (HCF) failure, noise, performance reduction (such as the higher transmission error in transmission systems with planetary gears), *etc.* Knowledge of the modal properties of cyclically symmetric systems is helpful to analyze the system forced response. Although much is known about the modal properties of specific cyclically sym-

metric systems, such as CPVA and planetary gears, a generalized theory that applies to any cyclically symmetric systems is not developed in previous works.

To analyze the modal properties of a general cyclically symmetric system, the difficulties in directly applying any previous works are two-fold. First, the degrees of freedom of any system component should be arbitrary, *i.e.*, any restrictions to the degrees of freedom of any component should be avoided. The general cyclically symmetric system considered in this research should allow the rigid-body central components to have all three-dimensional motions (six degrees of freedom). In previous works, however, the central components, such as the sun gears in planetary gears, are assumed to have planar motions only. Second, according to the significance of the components' elastic deformations in the frequency range of interest, the components of a cyclically symmetric system can be treated as rigid bodies or elastic continua. For example, in planetary gears with a thin ring gear (commonly used in aerospace applications), the ring gear is treated as an elastic continuum while the other planetary gear components, such as the sun gear, carrier, planet gears, are modeled as rigid bodies. No previous work has studied the general modal properties of cyclically symmetric systems with both rigid bodies and elastic continua. One aim of this work is to obtain the modal properties of general cyclically symmetric systems consisting of components that can be any three-dimensional rigid bodies or elastic continua.

Besides the modal properties of single stage cyclically symmetric systems, this work also aims at developing a general theory to analyze the modal properties of multi-stage systems with symmetric stages. A multi-stage symmetric structure consist of multiple symmetric structures (stages) that are coupled with each other. Bladed disk assemblies and multi-stage compound planetary gears, for example, consist of component stages that are cyclically symmetric. A challenge of studying the modal properties of multi-stage symmetric systems is that the whole systems are not generally symmetric although each stage is symmetric. For

example, a structure composed of multiple cyclically symmetric stages can be asymmetric if the numbers of substructures per stage are coprime. In such cases, mathematical tools that apply to perfectly symmetric systems, such as the circulant matrix theory for cyclically symmetric systems, are not proper to analyze the modal properties of multi-stage symmetric systems. This work aims to develop a systematic method to analyze the modal properties of multi-stage systems with symmetric stages. The method is not restricted to the cases where all the stages are cyclically symmetric.

In practical applications, the finite element models of systems with cyclic symmetry and multi-stage systems with multiple symmetric stages, such as the bladed disk assemblies, can have many degrees of freedom. The computational cost to numerically solve the vibration modes of such large systems can be expensive. Therefore, it is important to establish systematic methodologies to reduce the computational cost for solving the eigensolutions. For single stage cyclically symmetric systems, the existing method to improve the computational efficiency is to formulate sector models based on the circulant matrix theory. This method, however, can not apply to the cases where there are three-dimensional rigid-body central components and/or compliant central components that are elastic continua. For multi-stage systems with symmetric stages, although the existing methods, such as the multi-stage cyclic symmetry reduction method, can reduce the computational cost for multi-stage bladed disks (a type of multi-stage systems with symmetric stages), the eigensolutions obtained are not accurate. Also, for multi-stage systems such as multi-stage planetary gears and CPVA systems with multiple groups of absorbers (another type of multi-stage systems with symmetric stages considered in this dissertation), although similar structured modes are found in previous studies, there is no work attempting to formulate general reduced eigenvalue problems for such systems. Therefore, this work aims to develop methods to efficiently solve the systems modes for each type of systems considered in this work.

1.2 Literature Review

1.2.1 Systems with Cyclic Symmetry

A system is symmetric if there exist operations which bring the system into self-coincidence and leave it indistinguishable from its original configuration. For a system being cyclically symmetric, concretely, the system is invariant to rotations by the spacing angle of substructures. From previous works on cyclically symmetric systems, including bladed disks [2–4], circular plates [5], circular rings [6–8], disc-spindle systems [9, 10], planetary gears [11–16], and centrifugal pendulum vibration absorbers (CPVA) [17–21], unique modal vibration properties are found in such symmetric structures.

The modes of a cyclically symmetric system are highly structured. In early studies on the wave propagation of substructure chains, the linear free response of a cyclically symmetric structure is characterized by identical motions of each substructure and a unique phase relations exist between the adjacent substructures [22–24]. Therefore, unique substructure phase relations are indicated in different modes. In each mode, the substructure phase relation can be characterized by *phase index* [9, 10], the integer quotient of the substructure phase difference divided by the substructure spacing angle. For cyclically symmetric continuum systems, such as circular disks and rings, the mode shapes are characterized by nodal lines across the continua, which are referred to as *nodal diameters*. The numbers of nodal diameters in cyclically symmetric continuum vibrations is analogous to the phase indices in discrete cyclically symmetric systems [6, 10].

In previous studies on cyclically symmetric systems, the theory of circulant matrix played an important role in reducing the computational effort. In a cyclically symmetric system without vibrating central components, the full-system mass and stiffness matrices are

circulant or block circulant, because all the substructures are identical. The circulant matrix theory indicates there exists an appropriate unitary transformation that block diagonalizes all circulant matrices with the same matrix structure. Therefore, the original full-system equations of motion or eigenvalue problems are decomposed into reduced order formulations. The basic theory of circulant matrices [25] was applied to the vibration modes of bladed discs by Óttarson [3] and Olson [17]. The dynamics of a cyclically symmetric system can be captured by analyzing a single substructure, and the eigenvalue problems are significantly reduced in size. A summary of the theory of circulant matrices is provided in a later work by Olson *et al.* [26]. The theory is directly applicable to the modeling and analysis of free and forced vibration of cyclically symmetric systems without vibrating central components.

Although circulant matrix theory is a powerful tool to study cyclically symmetric systems that can be exactly divided into identical substructures or sectors, the existence of vibrating central components limits the direct application of circulant matrix theory. When the central components are modeled as vibrating rigid bodies, the full system matrix formulations in the equations of motion are no longer circulant or block circulant. In many past works, the central components are restricted to planar vibration with two translational degrees of freedom and one rotational degree of freedom along the system's central axis. One example of this case is spur planetary gears [11–16], where the sun gear, ring gear and carrier are the central components and the planet gears are the substructures. Another example is CPVA systems [18–20], where the rotor is the central component and the pendulum absorbers are the substructures. In both examples, three types of modes are found, namely, rotational modes, translational modes, and planet or absorber modes. Ericson and Parker [27, 28] experimentally proved the existence of these three types of modes, and clustering phenomenon of natural frequencies are found. Such highly structured modal properties are mathematically proved by Shi and Parker [29], assuming the central components have only

planar motions. The same authors [21] also studied the modal properties of three-dimensional CPVA system. The structure of vibration modes is similar to that of cyclically symmetric systems with planar vibrating central components, but some modal properties differ. The vibration modes of helical planetary gears, where the motions of the central component also involve all six rigid-body degrees of freedom, are studied by Eritenel and Parker [30].

Besides the studies on the modal properties of linear systems, a variety of nonlinear dynamic behaviors are studied for perfectly cyclically symmetric systems. In a series of papers, Vakakis *et al.* demonstrated nonlinear mode localization may occur in perfectly cyclically symmetric nonlinear systems [31–34]. This mode localization is result of symmetry-breaking process of bifurcation because of frequency dependence on amplitudes. Such nonlinear dynamic behavior is also studied by Georgiades *et al.* [35] using the nonlinear normal mode theory [36–38]. Nonlinear responses are studied for CPVA systems [39–41] with a range of path types. It is shown that the unison response of the absorbers can undergo two basic types of stabilities: one type maintains the symmetry of response, while the other does not. The design of the optimal absorber paths is also studied in the context of the nonlinear behaviors of CPVA systems [42–44]. The nonlinear dynamic behaviors of planetary gears, another example of perfectly cyclically symmetric systems, are also widely studied. Ambarisha and Parker [45] analytically derived design rules to suppress certain harmonics of planet mode response through mesh phasing, ans strong nonlinear behaviors, such as chaotic motions, and period-doubling bifurcations, that are observed from the analytical results are validated by using finite element method [46]. Bahk and Parker gave close-form approximation for the dynamic response of planetary gears over a meaningful mesh frequency range [47], the work gave insight into the impact of system parameter on dynamic response. There are also rich studies of nonlinear planetary gears considering the effects such as bearing clearance [48], tooth wedging [49], gravity effects [50], tooth profile modification [51], *etc.*

1.2.2 Application of Group Theory to Symmetric Engineering Structures

For many years, group theory has been a powerful mathematical tool for studying symmetric systems within areas such as molecular chemistry and condensed matter physics [1, 52]. Relatively recently, applications have emerged in engineering. Bifurcation phenomena in symmetric engineering systems are widely studied [53–55], and the computation of bifurcation points are simplified by using group theory. Group theory has also been used to simplify the vibration problems of engineering structures, including high-tension cable nets [56, 57], shells [58, 59], plates [60, 61], and skeletal structures, such as space trusses and frames [57, 62].

Group theory is an advantageous tool to analyze symmetric systems for two main reasons. First, the group theory provides a systematic method to reduce the order (or size) of the original problems. The essential procedure of a group theoretic method is to decompose the vector space of the original problem into a number of smaller subspaces, where the original problem is reduced into smaller formulations that can be solved with less computational effort. This advantage extends the application of group theory to numerical methods. Healy and Treacy combined the group theory and substructuring techniques in the study of space truss vibrations [62]. Application of group theory to finite element method [60, 63, 64] and finite difference method [61] are also explored.

Second, the group theoretic analysis directly provides qualitative symmetry-related modal properties of the symmetric system. According to the group theory, any eigenvector of a symmetric system is a linear combination of the same species of symmetry vectors that are obtained when decomposing the vector space of the original problem. (This idea is explained in more details in Chapter 3.) Therefore, without solving any eigensolutions, we have known

the number of subspaces that compose the eigenspace, and the number of eigenvectors existing in each subspace. In the context of vibration, this means group theoretic analysis can predict the number of mode types (corresponding to the number of subspaces that compose the eigenspace) and the number of modes for each type. In Refs. [57–59, 61, 65], the modal properties of symmetric systems are directly predicted, and a natural scheme for a physical classification of the mode shapes is suggested [59].

1.2.3 Multi-Stage Systems with Symmetric Stages

In many engineering applications, multiple symmetric structures are coupled with each other to form a multi-stage system. For example, such multi-stage structure exists in bladed disks [66–73], compound planetary gears [74–78], and CPVA with multiple groups of absorbers [19, 20, 79]. Most of the existing studies on multi-stage systems focus on systems consisting of cyclically symmetric stages only. Depending on how the stages are coupled with each other, modeling strategies of multi-stage systems with symmetric stages are generally classified into two types: one type is characterized by the direct couplings between the substructure (or sector) degrees of freedom; in the other type, the stages of symmetric systems are coupled through the rigid-body vibrating central components.

An example system using the first modeling strategy is the multi-stage bladed disks. In previous studies on multi-stage bladed disks, the inter-stage couplings are modeled using constraint equations for the interface degrees of freedoms of different single stages. Bladh *et al.* [66] showed the necessity of modeling multi-stage bladed disks because the behavior of bladed disks is influenced by the interaction between different stages. Reduced order models of multi-stage bladed disks are built by two general strategies, component mode synthesis, and the multi-stage cyclic symmetry reduction. Component mode synthesis method, such

as Craig-Bampton method [80], are widely used [67–69, 81]. When this divide-and-conquer scheme applies, each stage can be analyzed as a single stage, and the mistuning effects can be added to each stage by component mode mistuning techniques [82]. Another strategy to reduce the model order is referred to as the multi-stage cyclic symmetry reduction [70–73, 83]. Laxalde *et al.* first applied this method to tuned multi-stage bladed disks [70, 71], where each stage is modeled cyclically by its elementary substructure and the inter-stage coupling is achieved through a cyclic recombination of the interface degrees of freedom. Mistuning effects are later combined with this idea by Laxalde and Pierre [83]. For multi-stage systems with different number of substructures per stage, the phase indices in different stages are different. In a multi-stage system mode, which is approximated by combining modes of single stage, different combinations of single stage modes influence the accuracy and computational efficiency of this method [73]. Analytical model of multi-stage bladed disks are built by Sinha [84] to study the impact of mistuning.

On the other hand, in the models of compound planetary gears [74, 76] and CPVA systems with multiple groups of absorbers [19, 20], different stages of symmetric systems are coupled through the motions of vibrating rigid-body central components. Similar modal properties are obtained for such multi-stage structures [19, 74–78]. Furthermore, Shi *et al.* [20, 79] applied these modal properties to reduce the translational and rotational rotor vibrations by tuning multiple groups of absorbers.

1.2.4 Mistuned Systems

Although cyclically symmetric systems are meant to be composed of identical substructures, there are always small random variations among substructures. Such nearly symmetric systems are referred to as *mistuned* systems. Mistuning is commonly caused by manufactur-

ing tolerances, material imperfections, in-operation wear, *etc.* The vibrations of mistuned systems arouse great interest when engineers improve the performance and life of bladed disks. Although mistuning is typically small, the blades can experience extremely larger forced response compared to the tuned design. This increase in stresses can lead to premature high cycle fatigue failure of the blades.

The mechanism of the increased forced response in a mistuned system is studied using lumped parameter models [85–87]. Compared to its tuned nominal system, the mode shapes of a mistuned system become confined in a few substructures. Such confinement of vibration mode shapes (or energy) is known as *localization*, and it was discovered by Anderson [88] in the field of solid-state physics.

To estimate the statistics of the forced response for a population of randomly mistuned system with the same nominal design, Monte Carlo simulations are widely performed. Depending on the mistuning strength and the sensitivity of the system, it may require many thousands of realizations to estimate the worst-case forced response. To reduce the computational cost, three strategies are developed: predicting the distribution of mistuned forced response without using Monte Carlo simulations, reducing the number of necessary realizations of Monte Carlo, and generating reduced-order models from a parent model for a frequency range of interest. Sinha and Chen [89] and Mignolet and coworkers [90–92] developed methods of predicting the mistuned forced response distribution without using Monte Carlo simulations. Bladh *et al.* [93] accelerated the Monte Carlo simulations by reducing the number of realizations. The idea is to apply the theory of extreme value statistics to the problem. In extreme value theory, the distribution of the maximum of a set of independently and identically distributed random trials approaches one of three extreme value distribution as the number of trials becomes larger [68]. It was shown that the distribution of the largest forced responding blade amplitudes will asymptotically approach the Weibull distribution.

Therefore, relatively few realizations of Monte Carlo simulations are necessary to fit to the Weibull distribution. The topic of reduced order modeling, the third strategy for reducing the computational cost, is discussed next.

Reduced order modeling is a widely studied topic in bladed disk vibrations. This method lowers the computational cost for each realizations of Monte Carlo simulations. Because the huge amount of literature about this topic, only a brief survey on two categories of the reduced-order modeling strategies is provided here. These two types of methods are summarized as *component-mode-based methods* and *system-mode-based methods*. The component-mode-based methods are based on component mode synthesis (CMS), such as the famous Craig-Bampton method [80]. The strategy is to calculate the modes of each component separately and then synthesize the reduced order model by enforcing the compatibility conditions at the component interface. One important CMS method was developed by Óttarson. He found that the vibration of a blade in a bladed disk can be represented with a basis of cantilevered blade modes plus a set of shapes corresponding to the blade deformation induced by the disk vibration [3]. To calculate the latter set, the modes of the disk are calculated by finite element method with zero-mass blades attached. This approach made it trivial to synthesize the full system model from the component modes. This method was extended by Pierre and coworkers [93–95]. In contrast, the system-mode-based methods are based on the assumption that a selected set of tuned system modes provides a good basis for representing the vibration of mistuned systems [96]. Yang and Griffin called such strategy the subset of nominal modes (SNM) method [97]. The reduced-order model is constructed by selecting a frequency range that includes a family of blade-dominated system modes, typically including at least one mode or mode pair per nodal diameter to span the space of the mistuned modes. The mistuning is then introduced into the model by using an appropriate coordinate transformation to express the mistuning in system modal coordinates.

1.3 Scope of Investigation

This work studies the modal properties of systems with cyclically symmetric structures, and it is partitioned into four chapters according to the system characteristics. Single stage cyclically symmetric systems are studied in Chapters 2 and 3, while multi-stage systems with cyclically symmetric component stages are studied in Chapters 4 and 5.

In Chapter 2, the modal properties of cyclically symmetric systems with three-dimensional vibrating central components are studied. This chapter generalizes the modal properties in Ref. [29]. The mode classifications and the reduced eigenvalue problems of each mode type apply to systems such as planetary gears and CPVA systems, regardless of whether the central components motions are planar or three-dimensional. For cyclically symmetric systems with vibrating central components, the properties of matrices in system equations of motion are obtained based on the system symmetry. These properties are used to prove the modal properties in this chapter, and they can also facilitate derivation of the equations of motion for cyclically symmetric systems. All eigensolutions are solved from the proposed reduced eigenvalue problems, and the computational cost for solving full system modes is enormously reduced.

In Chapter 3, the modal properties of cyclically symmetric systems with both rigid-body and compliant central components are studied based on group theory. The modal properties obtained in this chapter are generalization of those in Chapter 2, because compliant central components, such as the elastic ring gear in planetary gears, are included in the systems in Chapter 3. The group theory for symmetry groups is introduced, and the advantages of group-theory-based modal analysis are discussed. Based on the group-theory-based modal analysis, the modal properties for general cyclically symmetric systems are obtained, and the analysis does not rely on any knowledge of the properties of system matrices in system

equations of motion. The general formulation of reduced eigenvalue problems is provided in the context of group-theory-based method, and it applies to discrete, continuous, or hybrid discrete-continuous cyclically symmetric systems. The group-theory-based modal analysis also applies to systems with other symmetry types.

In Chapter 4, the group-theory-based modal analysis is generalized for multi-stage systems with symmetric component stages. The systems studied in this chapter are composed of symmetric stages that are coupled through the motions of rigid-body central components. The group-theory-based modal analysis applies to multi-stage systems with cyclically symmetric stages, such as multi-stage planetary gears and CPVA systems with multiple groups of absorbers. The method also applies to multi-stage systems with component stages that have different types of symmetry. For general multi-stage systems with symmetric component stages, types of vibration modes are identified and reduced eigenvalue problems for each mode types are formulated based on the principles of group-theory-based modal analysis.

In Chapter 5, a numerical method to solve the system modes of multi-stage bladed disks is developed. In industrial finite element models of multi-stage bladed disks, all the cyclically symmetric component stages are coupled through the boundary nodes at the inter-stage interface instead of through a rigid-body central component. Therefore, the group-theory-based modal analysis developed in Chapter 4 does not apply to multi-stage bladed disks. The multi-stage cyclic symmetry reduction method, as an existing method to obtain eigensolutions of multi-stage bladed disks, is revisited. The advantages and disadvantages of this method is discussed. To improve the accuracy of obtained eigensolutions, a new iterative method is proposed by combination of the multi-stage cyclic symmetry reduction method and the subspace iteration method. The proposed iterative method simplifies the general subspace iteration method based on the cyclic symmetry in each component stages of bladed disk. Accurate full system modes can be obtained through the proposed iterative method

that can be performed using single stage sector models only. Parallel computations can be performed in the proposed iterative method, and the computational speed for eigensolutions can be increased significantly.

Chapter 2

Modal Properties of Cyclically Symmetric Systems with Central Components Vibrating as Three-Dimensional Rigid Bodies

2.1 Introduction

Models for many rotating mechanical systems are cyclically symmetric, including bladed discs [2–4], circular plates [5, 98, 99], circular rings [6–8], disc-spindle systems [9, 10], planetary gears [11–16, 74], centrifugal pendulum vibration absorbers (CPVA) [18–21, 40], *etc.* In such systems, identical *substructures* (*e.g.*, the planets of planetary gears) are equally spaced circumferentially around the *central components*, such as the sun gear, ring gear, and carrier in planetary gears. As shown in Fig. 2.1, a typical cyclically symmetric system is invariant to rotations by the spacing angle. Such structural symmetry results in unique modal vibration

properties, and knowing these properties aids the analysis of the systems.

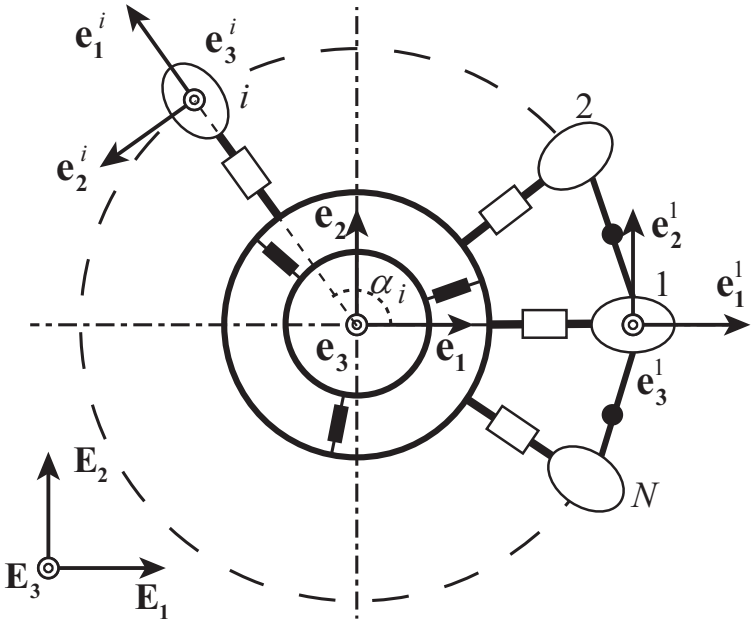

Figure 2.1: Cyclically symmetric systems with multiple central components. The circles represent possible central components, and the ovals are substructures. Some substructures are omitted for conciseness. Couplings may exist between any two substructures (represented by solid lines with solid circles), although only the couplings between the nearest neighboring substructures are depicted. Solid lines with hollow rectangles are the couplings between the central components and the substructures. All the central components and the couplings between them (represented by solid rectangles) are axisymmetric along the nominal rotational axis.

Studies of cyclically symmetric systems date back at least 90 years when physicists studied the lattice vibration of one-dimensional mono-atomic linear chains. With the Born-von Karman periodic boundary condition, the symmetry of a one-dimensional Bravais lattice is cyclic [1], and its dispersion relation shows that the frequency passband widths are determined by the coupling strength between substructures (atoms) [100]. Similar studies of wave propagation in substructure chains indicate unique phase relations exist between the substructures in different modes [22–24]. Such phase relations can be characterized by phase indices [9, 10] that are analogous to the wave vectors in lattice vibrations [101] and the numbers of nodal diameters in cyclically symmetric continuum vibrations [6, 10]. The phase

relations or indices can be mathematically explained by diagonalization of the system mass and stiffness matrices that are circulant or block circulant. The basic theory of circulant matrices [25] was applied to the vibration modes of bladed discs by Óttarson [3] and Olson [17]. The eigenvalue problems are significantly reduced in size after unitary transformation. A summary of the theory of circulant matrices is provided in a later work by Olson *et al.* [26]. The theory is directly applicable to the modeling and analysis of free and forced vibration of cyclically symmetric systems *without* vibrating central components.

The assumption that central components are non-vibrating simplifies the modeling and analysis of cyclically symmetric systems. In many cyclically symmetric systems, however, vibrations of the central components are significant. The central components are circumferentially uniform and axisymmetric along the system's central axis. The full-system matrices are no longer circulant or block circulant when considering the motions of central components. In many past works, the central components are restricted to planar vibration with two translational degrees of freedom and one rotational degree of freedom along the system's central axis. One example of this case is spur planetary gears [11–16, 74], where the sun gear, ring gear and carrier are the central components and the planet gears are the substructures. Another example is CPVA systems [18–20, 40], where the rotor is the central component and the pendulum absorbers are the substructures. Shi and Parker [29] mathematically proved the highly structured modal properties of cyclically symmetric systems assuming the central components have only planar motions, which is a limitation inconsistent with the fact that the substructures can have general three-dimensional geometry and motions.

It remains unknown what modal properties exist when central components are allowed to vibrate as rigid bodies with general six-degree-of-freedom motions, while the substructures can have an arbitrary number of in-plane and out-of-plane degrees of freedom (including general finite element models). For example, the gear mesh interfaces in helical planetary gears

generate three-dimensional forces and moments, and the motions of the central components (the sun gear, ring gear, and carrier) involve all six rigid body degrees of freedom. The modal properties summarized in the prior works are not thoroughly applicable. Eritenel and Parker [30] studied the modal properties of helical planetary gears, and similar work was conducted for the three-dimensional CPVA system [21]. Both works showed that some modal properties of cyclically symmetric systems with planar vibrating central components are preserved, while others differ. General cyclically symmetric systems with central components that can vibrate in all six degrees of freedom have not been studied.

The goal of this paper is to mathematically prove the modal properties of generalized cyclically symmetric systems in which the central components have arbitrary three-dimensional motions. The theory generalizes the properties of cyclically symmetric systems with planar vibrating central components in Ref. [29]. Although the properties are derived for linearized discrete systems, they can be extended to linearized continuum and continuum-discrete hybrid systems if the analogy between phase indices and wavenumbers is established.

This paper is organized as follows. In Section 2.2, the modal properties of cyclically symmetric systems with non-vibrating central components are reviewed, and the basic theory of circulant matrices is distilled from Ref [26]. The study of cyclically symmetric systems with vibrating central components starts by proving essential properties of the system matrices, which is discussed in Section 2.3. In Section 2.4, the modal properties of cyclically symmetric systems with vibrating central components are derived, and we prove that only three categories of modes exist: substructure modes, translational-tilting modes, and rotational-axial modes. Reduced eigenvalue problems for each category are identified, so all eigensolutions can be solved with less computational effort. An example is given to illustrate the properties.

2.2 Cyclically Symmetric Systems with Non-Vibrating Central Components

In many past works [3, 23, 24, 26], vibrations of the central components in the cyclically symmetric systems are neglected. In such cases, we assume the cyclically symmetric system includes N ($N > 2$) identical vibrating substructures and P non-vibrating central components. Although they do not vibrate, the central components may rotate at different constant speeds about the system axis of symmetry that is oriented along $\mathbf{e}_3$. The reference frame $\{\mathbf{e}_1, \mathbf{e}_2, \mathbf{e}_3\}$ rotates at the constant speed Ω of all the substructures. The basis $\{\mathbf{e}_1^i, \mathbf{e}_2^i, \mathbf{e}_3^i\}$ associated with the ith substructure is oriented with a fixed angle, $\alpha_i = 2\pi(i-1)/N$, relative to the $\{\mathbf{e}_1, \mathbf{e}_2, \mathbf{e}_3\}$ basis. The vector $\mathbf{e}_1^i$ is directed radially. Each substructure has arbitrarily many degrees of freedom, so this analysis applies to the cases where a substructure is composed of multiple discrete components or is modeled by the finite element method. With each substructure having L degrees of freedom, the full system has NL degrees of freedom. The linear equation of motion takes the form

$$\mathbf{M}_{ss}\ddot{\mathbf{q}}_s + \mathbf{B}_{ss}\dot{\mathbf{q}}_s + \mathbf{L}_{ss}\mathbf{q}_s = \mathbf{D}_{ss}\mathbf{q}_s = \mathbf{F}_s, \tag{2.1a}$$

$$\mathbf{D}_{ss} = \mathbf{M}_{ss}\frac{\mathrm{d}^2}{\mathrm{d}t^2} + \mathbf{B}_{ss}\frac{\mathrm{d}}{\mathrm{d}t} + \mathbf{L}_{ss}, \tag{2.1b}$$

where $\mathbf{M}_{ss}$ is the inertia matrix (not necessary to be symmetric, *i.e.*, $\mathbf{M}_{ss} \neq \mathbf{M}_{ss}^{\mathrm{T}}$), $\mathbf{B}_{ss}$ includes the damping ($\mathbf{C}_{ss} = \mathbf{C}_{ss}^{\mathrm{T}}$) and gyroscopic ($\mathbf{G}_{ss} = -\mathbf{G}_{ss}^{\mathrm{T}}$) terms, and $\mathbf{L}_{ss}$ includes the stiffness ($\mathbf{K}_{ss} = \mathbf{K}_{ss}^{\mathrm{T}}$) and circulatory ($\mathbf{H}_{ss} = -\mathbf{H}_{ss}^{\mathrm{T}}$) terms; $\mathbf{F}_s$ is the force vector of size $NL \times 1$. The eigenvalue problem of Eq. (2.1) is

$$\lambda^2\mathbf{M}_{ss}\mathbf{u}_s + \lambda\mathbf{B}_{ss}\mathbf{u}_s + \mathbf{L}_{ss}\mathbf{u}_s = \mathbf{A}_{ss}\mathbf{u}_s = \mathbf{0}, \tag{2.2a}$$

$$\mathbf{A}_{ss} = \lambda^2 \mathbf{M}_{ss} + \lambda \mathbf{B}_{ss} + \mathbf{L}_{ss}, \tag{2.2b}$$

where $\mathbf{u}_s$ is the eigenvector. The cases when Eq. (2.2) fails to yield a sufficient number of eigenvectors corresponding to a degenerate eigenvalue are not considered in this work; one such case occurs when critical damping is involved.

An important property of the operator $\mathbf{D}_{ss}$, like the associated matrix $\mathbf{A}_{ss}$, is its block circulant structure. To physically explain this structure, we first consider the equations that govern the first substructure. The matrix operator associated with these equations is the first L rows of $\mathbf{D}_{ss}$, denoted as

$$\mathbf{D}_{s_1 s} = \begin{pmatrix} \mathbf{D}_{s_1 s_1} & \mathbf{D}_{s_1 s_2} & \dots & \mathbf{D}_{s_1 s_N} \end{pmatrix}, \tag{2.3}$$

where the operators $\mathbf{D}_{s_1 s_i}$ for $i = 1, 2, \dots, N$ are $L \times L$ matrices. $\mathbf{D}_{s_1 s_i}$ describes how the dynamics of the first substructure are influenced by motions of the ith substructure. All the matrix operators associated with the other substructures can be similarly divided into N $L \times L$ submatrices, where $\mathbf{D}_{s_i s_l}$ describes the effect of the lth substructure on the ith substructure. In a cyclically symmetric system, the effects of the ith substructure on the first substructure are identical to those of the $(i+1)$th substructure on the second substructure, or that of the $(i+l)$th on the $(l+1)$th. Mathematically, this is expressed as

$$\mathbf{D}_{s_1 s_i} = \cdots = \mathbf{D}_{s_{l+1} s_{i+l}} = \cdots = \mathbf{D}_{s_N s_{i+N-1}}, \ i = 1, 2, \dots, N. \tag{2.4}$$

Any index in Eq. (2.4) outside the range from 1 to N can be adjusted by doing a modulo operation by N (mod N), because the $(i+N)$th substructure is actually the ith substructure. This circulatory adjustment of substructure indices is applied throughout this work. The

operator $\mathbf{D}_{ss}$ can be generated by the N submatrices that build $\mathbf{D}_{s_1 s}$ in Eq. (2.3), *i.e.*,

$$\begin{aligned}\mathbf{D}_{ss} &= \begin{pmatrix} \mathbf{D}_{s_1 s_1} & \mathbf{D}_{s_1 s_2} & \dots & \mathbf{D}_{s_1 s_N} \\ \mathbf{D}_{s_1 s_N} & \mathbf{D}_{s_1 s_1} & \dots & \mathbf{D}_{s_1 s_{N-1}} \\ \vdots & \vdots & \ddots & \vdots \\ \mathbf{D}_{s_1 s_2} & \mathbf{D}_{s_1 s_3} & \dots & \mathbf{D}_{s_1 s_1} \end{pmatrix} \\ &= \text{circulant}(\mathbf{D}_{s_1 s_1},\ \mathbf{D}_{s_1 s_2},\ \dots,\ \mathbf{D}_{s_1 s_N}).\end{aligned} \tag{2.5}$$

The analogous property for $\mathbf{A}_{ss}$ in Eq. (2.2) is

$$\mathbf{A}_{ss} = \text{circulant}(\mathbf{A}_{s_1 s_1},\ \mathbf{A}_{s_1 s_2},\ \dots,\ \mathbf{A}_{s_1 s_N}). \tag{2.6}$$

Compared to solving the $NL \times NL$ eigenvalue problem in Eq. (2.2), a more efficient method is to solve N different $L \times L$ eigenvalue problems that are obtained by block diagonalization of $\mathbf{A}_{ss}$. According to circulant matrix theory [25, 26], any block circulant matrix consisting of N^2 $L \times L$ blocks can be block diagonalized through a unitary transformation by $\mathbf{E}_N \otimes \mathbf{I}_L$, where $\mathbf{I}_L$ is the $L \times L$ identity matrix, and $\mathbf{E}_N$ and $\otimes$ are the $N \times N$ Fourier matrix and the direct product operation, respectively, both of which are defined in Appendix A. Following this path, any eigenvector $\mathbf{u}_s$ of $\mathbf{A}_{ss}$ is expanded as a linear combination of the columns of $\mathbf{E}_N \otimes \mathbf{I}_L$,

$$\mathbf{u}_s = (\mathbf{E}_N \otimes \mathbf{I}_L)\hat{\mathbf{u}}_s. \tag{2.7}$$

Substitution of Eq. (2.7) into Eq. (2.2) and pre-multiplication by the Hermitian of $(\mathbf{E}_N \otimes \mathbf{I}_L)$

give

$$
\begin{aligned}
&(\mathbf{E}_N \otimes \mathbf{I}_L)^{\mathcal{H}} \mathbf{A}_{ss} (\mathbf{E}_N \otimes \mathbf{I}_L) \hat{\mathbf{u}}_s \\
&= \begin{pmatrix} \mathbf{\Lambda}_0 & & & \mathbf{0} \\ & \mathbf{\Lambda}_1 & & \\ & & \ddots & \\ \mathbf{0} & & & \mathbf{\Lambda}_{N-1} \end{pmatrix} \begin{pmatrix} \hat{\mathbf{u}}_{s_{(0)}} \\ \hat{\mathbf{u}}_{s_{(1)}} \\ \vdots \\ \hat{\mathbf{u}}_{s_{(N-1)}} \end{pmatrix} = \mathbf{0},
\end{aligned} \tag{2.8}
$$

where vectors $\hat{\mathbf{u}}_{s_{(i)}}$ are the $L \times 1$ subvectors of $\hat{\mathbf{u}}_s$ [26].

Eq. (2.8) consists of N $L \times L$ reduced eigenvalue problems,

$$\mathbf{\Lambda}_k \hat{\mathbf{u}}_{s_{(k)}} = \mathbf{0}, \ k = 0, 1, ..., N-1, \tag{2.9a}$$

$$\mathbf{\Lambda}_k = \sum_{i=1}^{N} \mathrm{e}^{\frac{2k\pi(i-1)\mathrm{j}}{N}} \mathbf{A}_{s_1 s_i} = \sum_{i=1}^{N} \mathrm{e}^{\mathrm{j}k\alpha_i} \mathbf{A}_{s_1 s_i}, \tag{2.9b}$$

where j is the imaginary unit. Eq. (2.9) is a second-order polynomial eigenvalue problem that has $2L$ eigensolutions for each selection of k. These eigensolutions generate $2L$ eigensolutions of the full eigenvalue problem, Eq. (2.2). For instance, if $(\lambda_{(k)}^{(p)}, \hat{\mathbf{u}}_{s_{(k)}}^{(p)})$ is the pth eigensolution of Eq. (2.9) for a given k and p from 1 to $2L$, then $\lambda_{(k)}^{(p)}$ and $(\mathbf{0}_L, \ldots, \hat{\mathbf{u}}_{s_{(k)}}^{(p)}, \ldots, \mathbf{0}_L)^{\mathrm{T}}$ form an eigensolution of Eq. (2.8). Because the transformation from Eq. (2.2) to Eq. (2.8) is unitary, $\lambda_{(k)}^{(p)}$ is also an eigenvalue of $\mathbf{A}_{ss}$ in Eq. (2.2), and its corresponding $NL \times 1$ eigenvector is (from Eq. (2.7))

$$
\begin{aligned}
\mathbf{u}_{s_{(k)}}^{(p)} &= (\mathbf{E}_N \otimes \mathbf{I}_L)(\mathbf{0}_L, \ldots, \hat{\mathbf{u}}_{s_{(k)}}^{(p)}, \ldots, \mathbf{0}_L)^{\mathrm{T}} \\
&= \frac{1}{\sqrt{N}} \left(\mathrm{e}^{\mathrm{j}k\alpha_1} \hat{\mathbf{u}}_{s_{(k)}}^{(p)}, \mathrm{e}^{\mathrm{j}k\alpha_2} \hat{\mathbf{u}}_{s_{(k)}}^{(p)}, \ldots, \mathrm{e}^{\mathrm{j}k\alpha_N} \hat{\mathbf{u}}_{s_{(k)}}^{(p)} \right)^{\mathrm{T}} \\
&= \mathbf{e}_{(k)} \otimes \hat{\mathbf{u}}_{s_{(k)}}^{(p)},
\end{aligned} \tag{2.10}
$$

where $\mathbf{e}_{(k)}$ is the $(k+1)$th column of $\mathbf{E}_N$. Thus, all eigensolutions of the full eigenvalue problem, Eq. (2.2), are generated from the N reduced eigenvalue problems in Eq. (2.9).

Eq. (2.10) expresses a modal property of cyclically symmetric systems with non-vibrating central components: all the substructures have identical motions (characterized by $\hat{\mathbf{u}}^{(p)}_{s_{(k)}}$), but they vibrate out of phase with the phase difference determined by an integer k, also known as the phase index of the vibration mode [9, 10].

Another modal property is obtained by comparing the full eigenvalue problem (Eq. (2.2)) and the reduced eigenvalue problems (Eq. (2.9)). For Eq. (2.2) being a real-valued, second-order eigenvalue problem, the eigensolutions occur in complex conjugate pairs [102]. If $(\lambda^{(p)}_{(k)}, \mathbf{e}_{(k)} \otimes \hat{\mathbf{u}}^{(p)}_{s_{(k)}})$ is an eigensolution of Eq. (2.2), its complex conjugate $(\overline{\lambda^{(p)}_{(k)}}, \overline{\mathbf{e}_{(k)} \otimes \hat{\mathbf{u}}^{(p)}_{s_{(k)}}})$ is also an eigensolution. From the expansion of the eigenvector $\overline{\mathbf{e}_{(k)} \otimes \hat{\mathbf{u}}^{(p)}_{s_{(k)}}}$,

$$\begin{aligned}\overline{\mathbf{e}_{(k)} \otimes \hat{\mathbf{u}}^{(p)}_{s_{(k)}}} &= \frac{1}{\sqrt{N}} \left(\mathrm{e}^{-\mathrm{j}k\alpha_1} \overline{\hat{\mathbf{u}}^{(p)}_{s_{(k)}}}, \mathrm{e}^{-\mathrm{j}k\alpha_2} \overline{\hat{\mathbf{u}}^{(p)}_{s_{(k)}}}, \ldots, \mathrm{e}^{-\mathrm{j}k\alpha_N} \overline{\hat{\mathbf{u}}^{(p)}_{s_{(k)}}} \right)^{\mathrm{T}} \\ &= \mathbf{e}_{(N-k)} \otimes \overline{\hat{\mathbf{u}}^{(p)}_{s_{(k)}}},\end{aligned} \tag{2.11}$$

we find its phase relation is characterized by phase index $N-k$. $(\overline{\lambda^{(p)}_{(k)}}, \overline{\hat{\mathbf{u}}^{(p)}_{s_{(k)}}})$ falls into the eigensolution set of the reduced eigenvalue problem with phase index $N-k$. Therefore, eigensolutions associated with $k = z$ and $k = N - z$ for $z = 1, 2, \ldots, N-1$ and $z \neq \frac{N}{2}$ are complex conjugate of each other, so only one of the problems with $k = z$ or $k = N - z$ must be solved. For either of the cases when $k = 0$ or $\frac{N}{2}$ (if the number of substructures is even), the reduced eigenvalue problem in Eq. (2.9) is real, thus providing $2L$ eigensolutions in complex conjugate pairs. Therefore, to find the entire eigenspace of the full eigenvalue problem (Eq. (2.2)), one only needs to solve the $L \times L$ reduced eigenvalue problems (Eq. (2.9)) for the cases $k = 0, 1, 2, ..., \frac{N-1}{2}$ or $\frac{N}{2}$, depending on whether N is odd or even.

2.3 Matrix Properties of Cyclically Symmetric Systems with Vibrating Central Components

In many applications with cyclic symmetry, vibrations of the central components occur as rigid body motions [11, 40]. The schematic for such cyclic systems is shown in Fig. 2.1. The N ($N > 2$) identical substructures are connected to P vibrating central components. The central components can rotate at different constant speeds that can be calculated from the rotation speed of the reference frame $\{\mathbf{e}_1, \mathbf{e}_2, \mathbf{e}_3\}$, Ω, multiplied by a known scalar. In planetary gears, for example, the rotation speeds of the sun gear and the ring gear can be expressed by the rotation speed of the carrier multiplied by gear ratios [12].

In the following analysis, each central component has three translational vibrations (x_c, y_c, and z_c) and three rotational vibrations (ζ_c, η_c, and μ_c) along $\mathbf{e}_1$, $\mathbf{e}_2$, and $\mathbf{e}_3$, respectively. The analysis applies to cases where the central components have fewer degrees of freedom. With each substructure having L degrees of freedom, the matrix equation of motion of is

$$\mathbf{M}\ddot{\mathbf{q}} + \mathbf{B}\dot{\mathbf{q}} + \mathbf{L}\mathbf{q} = \mathbf{D}\mathbf{q} = \mathbf{F}, \tag{2.12a}$$

$$\mathbf{D} = \begin{pmatrix} \mathbf{D}_{cc} & \mathbf{D}_{cs} \\ \mathbf{D}_{sc} & \mathbf{D}_{ss} \end{pmatrix} = \mathbf{M}\frac{\mathrm{d}^2}{\mathrm{d}t^2} + \mathbf{B}\frac{\mathrm{d}}{\mathrm{d}t} + \mathbf{L}. \tag{2.12b}$$

$$\mathbf{q} = (\mathbf{q}_c, \mathbf{q}_s)^{\mathrm{T}}, \tag{2.12c}$$

$$\mathbf{q}_c = (\mathbf{q}_{c_1}, \mathbf{q}_{c_2}, \ldots, \mathbf{q}_{c_P})^{\mathrm{T}}, \tag{2.12d}$$

$$\mathbf{q}_{c_i} = (x_{c_i}, y_{c_i}, z_{c_i}, \zeta_{c_i}, \eta_{c_i}, \mu_{c_i})^{\mathrm{T}}, \text{ for } i = 1, 2, \ldots, P, \tag{2.12e}$$

$$\mathbf{q}_s = (\mathbf{q}_{s_1}, \mathbf{q}_{s_2}, \ldots, \mathbf{q}_{s_N})^{\mathrm{T}} \tag{2.12f}$$

$$\mathbf{F} = (\mathbf{F}_c, \mathbf{F}_s)^{\mathrm{T}}, \tag{2.12g}$$

where the subvectors $\mathbf{q}_{c_i}$ and $\mathbf{q}_{s_i}$ describe the dynamics of the ith central component and the ith substructure. Again, no symmetry of $\mathbf{M}$, $\mathbf{B}$, and $\mathbf{L}$ is assumed, so general damping, gyroscopic, stiffness, and circulatory terms are admitted. The eigenvalue problem of Eq. (2.12) is

$$\lambda^2\mathbf{M}\boldsymbol{\Phi} + \lambda\mathbf{B}\boldsymbol{\Phi} + \mathbf{L}\boldsymbol{\Phi} = \mathbf{A}\boldsymbol{\Phi} = \mathbf{0}, \tag{2.13a}$$

$$\mathbf{A} = \begin{pmatrix} \mathbf{A}_{cc} & \mathbf{A}_{cs} \\ \mathbf{A}_{sc} & \mathbf{A}_{ss} \end{pmatrix} = \lambda^2\mathbf{M} + \lambda\mathbf{B} + \mathbf{L}, \tag{2.13b}$$

$$\boldsymbol{\Phi} = (\boldsymbol{\Phi}_c, \boldsymbol{\Phi}_s)^{\mathrm{T}}. \tag{2.13c}$$

Separation of the degrees of freedom into central component and substructure motions as in Eq. (2.12c) leads to a partition of the operator $\mathbf{D}$ in Eq. (2.12b). We derive crucial properties of $\mathbf{D}_{ss}$, $\mathbf{D}_{cc}$, $\mathbf{D}_{cs}$, and $\mathbf{D}_{sc}$ that are necessary for the subsequent modal decomposition. Analogous properties exist among the submatrices of $\mathbf{A}$ in Eq. (2.13b). The properties are derived for the submatrices in $\mathbf{D}$, rather than those in $\mathbf{A}$, because the vector $\mathbf{q}$ in Eq. (2.12) represents an arbitrary configuration. In contrast, $\boldsymbol{\Phi}$ in Eq. (2.13) is restricted to the set of eigenvectors and Eq. (2.13) holds only for selected $\mathbf{A}$ where λ is an eigenvalue. The relevance of these points will arise later.

The relation between the generalized coordinate vector $\mathbf{q}$ and the force vector $\mathbf{F}$ in Eq. (2.12a) is characterized by the operator $\mathbf{D}$. Because the system is brought into self-coincidence by rotations about the symmetry axis by integer multiples of the substructure spacing angle, the operator $\mathbf{D}$ relating $\mathbf{q}$ and $\mathbf{F}$ is invariant if $\mathbf{q}$ and $\mathbf{F}$ are simultaneously rotated by integer multiples of the substructure spacing angle. In the following discussion, this idea is illustrated when proving the properties of submatrices in $\mathbf{D}$, which is achieved by analyzing the same symmetric system using different reference frame definitions. Meanwhile,

it is also proved that the central components must have certain physical properties to be compatible with the full system symmetry.

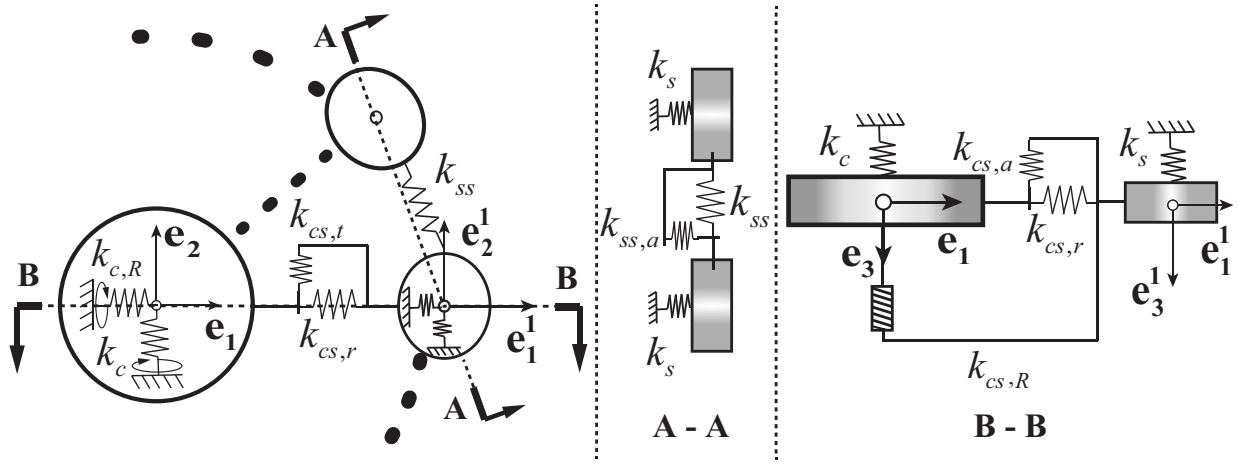

Figure 2.2: An example of a cyclically symmetric system with one vibrating central component and one non-vibrating central component.

To illustrate the properties of $\mathbf{D}_{ss}$, $\mathbf{D}_{cc}$, $\mathbf{D}_{cs}$, and $\mathbf{D}_{sc}$, an example system is given in Fig. 2.2. N equally spaced point mass substructures are connected to a vibrating central component. The substructures and the vibrating central component are installed on a non-vibrating rotor that rotates at constant speed Ω. The ith substructure has three translational vibrations: the radial motion r_i along $\mathbf{e}_1^i$, the tangential motion s_i along $\mathbf{e}_2^i$, and the (out-of-plane) axial motion u_i along $\mathbf{e}_3^i$. Each pair of neighboring substructures are connected by springs k_{ss} and $k_{ss,a}$. Each substructure has mass m_s, and it is isotropically connected to the non-vibrating rotor through springs k_s, and connected to the vibrating central component through springs $k_{cs,r}$, $k_{cs,t}$, and $k_{cs,a}$. The distance between the undeflected position of each substructure and the central axis is L_0. The ith substructure's three translations exert moments on the central component along $\mathbf{e}_1^i$, $\mathbf{e}_2^i$ and $\mathbf{e}_3^i$ through stiffness $k_{cs,R}$ (with units of moment/length). The vibrating central component is connected to the non-vibrating rotor through isotropic stiffness k_c for translations and isotropic torsional stiffness $k_{c,R}$ (with units of moment/rad) for the tilting motions along $\mathbf{e}_1$ or $\mathbf{e}_2$. The vibrating central component has

mass m_c, moment of inertia $J_1 = J_2$ along $\mathbf{e}_1$ and $\mathbf{e}_2$, and moment inertia J_3 along $\mathbf{e}_3$. The linearized equation of motion is

$$\mathbf{M}\ddot{\mathbf{q}} + \Omega\mathbf{G}\dot{\mathbf{q}} + (\mathbf{K}_V - \Omega^2\mathbf{K}_T)\mathbf{q} = \mathbf{F}, \tag{2.14a}$$

$$\mathbf{q} = (x_c, y_c, z_c, \zeta_c, \eta_c, \mu_c, r_1, s_1, u_1, \ldots, r_N, s_N, u_N)^{\mathrm{T}}, \tag{2.14b}$$

where all coordinates are defined in local reference frames. The matrices are

$$\mathbf{M} = \mathrm{diag}(\mathbf{M}_{cc}, \mathbf{M}_{ss}), \tag{2.15a}$$

$$\mathbf{M}_{cc} = \mathrm{diag}(m_c, m_c, m_c, J_1, J_1, J_3), \tag{2.15b}$$

$$\mathbf{M}_{ss} = \mathrm{diag}(\underbrace{m_s, m_s, \ldots, m_s}_{3N}), \tag{2.15c}$$

$$\mathbf{G} = \mathrm{diag}(\mathbf{G}_{cc}, \mathbf{G}_{ss}) = \mathrm{diag}(\mathbf{G}_{cc}, \underbrace{\mathbf{G}_{s_1 s_1}, \ldots, \mathbf{G}_{s_N s_N}}_{N}), \tag{2.15d}$$

$$\mathbf{G}_{cc} = \begin{pmatrix} 0 & -2m_c & 0 & 0 & 0 & 0 \\ 2m_c & 0 & 0 & 0 & 0 & 0 \\ 0 & 0 & 0 & 0 & 0 & 0 \\ 0 & 0 & 0 & 0 & -(2J_1 - J_3) & 0 \\ 0 & 0 & 0 & 2J_1 - J_3 & 0 & 0 \\ 0 & 0 & 0 & 0 & 0 & 0 \end{pmatrix}, \tag{2.15e}$$

$$\mathbf{G}_{s_i s_i} = \begin{pmatrix} 0 & -2m_s & 0 \\ 2m_s & 0 & 0 \\ 0 & 0 & 0 \end{pmatrix}, \tag{2.15f}$$

$$\mathbf{K}_V = \begin{pmatrix} \mathbf{K}_{cc,V} & \mathbf{K}_{cs,V} \\ \mathbf{K}_{cs,V}^{\mathrm{T}} & \mathbf{K}_{ss,V} \end{pmatrix}, \tag{2.15g}$$

$$\mathbf{K}_{cc,V} = \mathrm{diag}(k_x, k_y, k_c + Nk_{cs,a}, k_{x,R}, k_{y,R}, Nk_{cs,t}L_0^2 + Nk_{cs,R}L_0),$$

$$k_x = k_y = k_c + \frac{N}{2}(k_{cs,r} + k_{cs,t}), \tag{2.15h}$$

$$k_{x,R} = k_{y,R} = k_{c,R} + \frac{Nk_{cs,a}L_0^2}{2} + Nk_{cs,R}L_0,$$

$$\mathbf{K}_{cs,V} = \begin{pmatrix} \mathbf{K}_{cs_1,V} & \mathbf{K}_{cs_2,V} & \dots & \mathbf{K}_{cs_N,V} \end{pmatrix},$$

$$\mathbf{K}_{cs_i,V} = \begin{pmatrix} -k_{cs,r}\cos\alpha_i & k_{cs,t}\sin\alpha_i & 0 \\ -k_{cs,r}\sin\alpha_i & -k_{cs,t}\cos\alpha_i & 0 \\ 0 & 0 & -k_{cs,a} \\ -k_{cs,R}\cos\alpha_i & k_{cs,R}\sin\alpha_i & -k_{cs,a}L_0\sin\alpha_i \\ -k_{cs,R}\sin\alpha_i & -k_{cs,R}\cos\alpha_i & k_{cs,a}L_0\cos\alpha_i \\ 0 & -k_{cs,t}L_0 & -k_{cs,R} \end{pmatrix}, \tag{2.15i}$$

$$\mathbf{K}_{ss,V} = \mathrm{circulant}(\mathbf{K}_{s_1s_1,V}, \mathbf{K}_{s_1s_2,V}, \underbrace{\mathbf{0}, \mathbf{0}, \dots, \mathbf{0}}_{N-3}, \mathbf{K}_{s_1s_2,V}^{\mathrm{T}}),$$

$$\mathbf{K}_{s_1s_1,V} = \mathrm{diag}(k_{cs,r} + k_s + 2k_{ss}\sin^2\frac{\pi}{N} + \frac{k_{cs,R}}{L_0},$$

$$k_{cs,t} + k_s + 2k_{ss}\cos^2\frac{\pi}{N} + \frac{k_{cs,R}}{L_0}, k_s + 2k_{ss,a} + \frac{k_{cs,R}}{L_0}), \tag{2.15j}$$

$$\mathbf{K}_{s_1s_2,V} = \begin{pmatrix} k_{ss}\sin^2\frac{\pi}{N} & k_{ss}\sin\frac{\pi}{N}\cos\frac{\pi}{N} & 0 \\ -k_{ss}\sin\frac{\pi}{N}\cos\frac{\pi}{N} & -k_{ss}\cos^2\frac{\pi}{N} & 0 \\ 0 & 0 & -k_{ss,a} \end{pmatrix},$$

$$\mathbf{K}_T = \mathrm{diag}(\mathbf{K}_{cc,T}, \mathbf{K}_{ss,T}) = \mathrm{diag}(\mathbf{K}_{cc,T}, \underbrace{\mathbf{K}_{s_1s_1,T}, \dots, \mathbf{K}_{s_Ns_N,T}}_{N}), \tag{2.15k}$$

$$\mathbf{K}_{cc,T} = \mathrm{diag}(m_c, m_c, 0, J_1, J_1, 0), \tag{2.15l}$$

$$\mathbf{K}_{s_is_i,T} = \mathrm{diag}(m_s, m_s, 0). \tag{2.15m}$$

2.3.1 Properties of $\mathbf{D}_{ss}$

The submatrix operator $\mathbf{D}_{ss}$ captures the connections between the substructures. The effects of central component motions do not appear in $\mathbf{D}_{ss}$. Therefore, although the central components can vibrate, $\mathbf{D}_{ss}$ can be derived from the corresponding system with non-vibrating central components, where all the other aspects are identical to the original system. $\mathbf{D}_{ss}$ is a block circulant matrix, as discussed earlier, and all of its blocks can be obtained by analyzing any one of the substructures. Such block circulant structure of $\mathbf{D}_{ss}$ is illustrated by the operator $\mathbf{K}_{ss,V}$ in Eq. (2.15j) for the example system.

2.3.2 Properties of $\mathbf{D}_{cs}$ and $\mathbf{D}_{sc}$

$\mathbf{D}_{cs}$ and $\mathbf{D}_{sc}$ in Eq. (2.12b) connect the central components with the substructures. $\mathbf{D}_{cs}$ can be partitioned as

$$\mathbf{D}_{cs} = \begin{pmatrix} \mathbf{D}_{c_1 s_1} & \mathbf{D}_{c_1 s_2} & \dots & \mathbf{D}_{c_1 s_N} \\ \mathbf{D}_{c_2 s_1} & \mathbf{D}_{c_2 s_2} & \dots & \mathbf{D}_{c_2 s_N} \\ \vdots & \vdots & \ddots & \vdots \\ \mathbf{D}_{c_P s_1} & \mathbf{D}_{c_P s_2} & \dots & \mathbf{D}_{c_P s_N} \end{pmatrix}, \tag{2.16}$$

where each $6 \times L$ block expresses the impact of the lth substructure on the ith central component. $\mathbf{D}_{sc}$ can be similarly partitioned into NP $L \times 6$ blocks.

To obtain the properties of $\mathbf{D}_{cs}$ and $\mathbf{D}_{sc}$, a general cyclically symmetric system with vibrating central components is analyzed under two different basis definitions depicted in Fig. 2.3. The equations of motion under the reference frames in Fig. 2.3a are formulated in Eq. (2.12). An alternative basis definition is given in Fig. 2.3a. The rotating frame for central component motions, $\{\hat{\mathbf{e}}_1, \hat{\mathbf{e}}_2, \hat{\mathbf{e}}_3\}$, is directed with a fixed angle $2n\pi/N$ relative to the

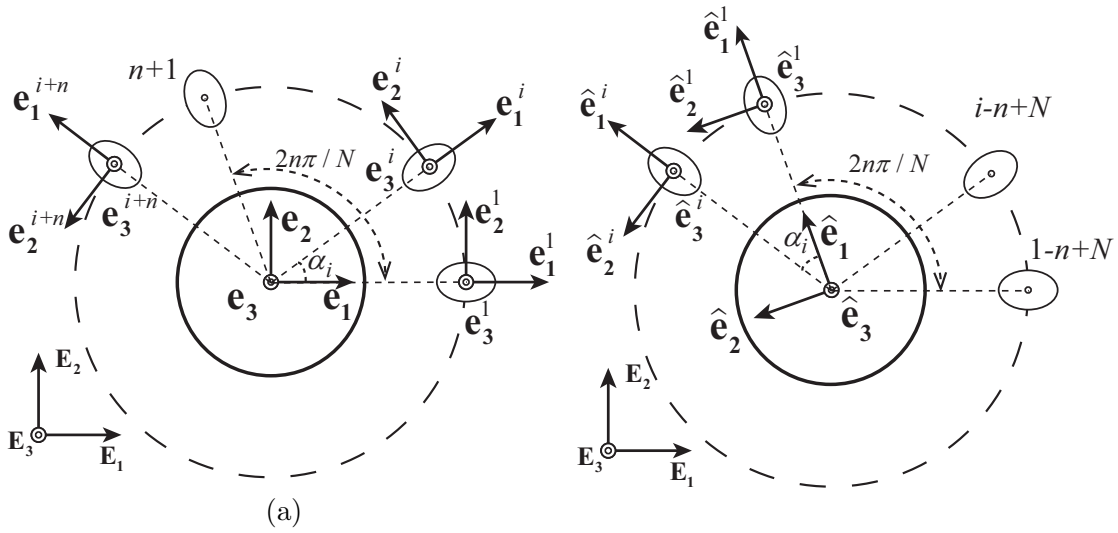

Figure 2.3: Different basis definitions for a generalized cyclically symmetric system. a. The basis $\{\mathbf{e}_1^i, \mathbf{e}_2^i, \mathbf{e}_3^i\}$ is oriented with a fixed angle $\alpha_i = 2\pi(i-1)/N$ to the basis $\{\mathbf{e}_1, \mathbf{e}_2, \mathbf{e}_3\}$. a. $\{\hat{\mathbf{e}}_1^i, \hat{\mathbf{e}}_2^i, \hat{\mathbf{e}}_3^i\}$ is oriented with a fixed angle α_i to $\{\hat{\mathbf{e}}_1, \hat{\mathbf{e}}_2, \hat{\mathbf{e}}_3\}$. The axis $\hat{\mathbf{e}}_1$ in $\{\hat{\mathbf{e}}_1, \hat{\mathbf{e}}_2, \hat{\mathbf{e}}_3\}$ is oriented with the angle $2n\pi/N$ to $\mathbf{e}_1$ in a. $\{\hat{\mathbf{e}}_1^i, \hat{\mathbf{e}}_2^i, \hat{\mathbf{e}}_3^i\}$ in a and $\{\mathbf{e}_1^{i+n}, \mathbf{e}_2^{i+n}, \mathbf{e}_3^{i+n}\}$ in a are identical and applied to the same substructure.

rotating frame $\{\mathbf{e}_1, \mathbf{e}_2, \mathbf{e}_3\}$, where n is an arbitrary integer between 1 and N. $\{\hat{\mathbf{e}}_1^i, \hat{\mathbf{e}}_2^i, \hat{\mathbf{e}}_3^i\}$ is oriented with a fixed angle $\alpha_i = 2\pi(i-1)/N$ relative to $\{\hat{\mathbf{e}}_1, \hat{\mathbf{e}}_2, \hat{\mathbf{e}}_3\}$. A new generalized coordinate vector $\hat{\mathbf{q}}$ is defined similarly to the vector $\mathbf{q}$ in Eq. (2.12c). The equations of motion using the new generalized coordinate vector are

$$\hat{\mathbf{M}}\ddot{\hat{\mathbf{q}}} + \hat{\mathbf{B}}\dot{\hat{\mathbf{q}}} + \hat{\mathbf{L}}\hat{\mathbf{q}} = \hat{\mathbf{D}}\hat{\mathbf{q}} = \hat{\mathbf{F}}, \tag{2.17a}$$

$$\hat{\mathbf{D}} = \begin{pmatrix} \hat{\mathbf{D}}_{cc} & \hat{\mathbf{D}}_{cs} \\ \hat{\mathbf{D}}_{sc} & \hat{\mathbf{D}}_{ss} \end{pmatrix} = \hat{\mathbf{M}}\frac{\mathrm{d}^2}{\mathrm{d}t^2} + \hat{\mathbf{B}}\frac{\mathrm{d}}{\mathrm{d}t} + \hat{\mathbf{L}}. \tag{2.17b}$$

Eqs. (2.12) and (2.17) are different equations of motions for the same system, where the generalized coordinates are defined differently. Proving the properties of $\mathbf{D}_{cs}$ and $\mathbf{D}_{sc}$ requires building a connection between Eqs. (2.12) and (2.17).

The reference frames in Fig. 2.3a can be obtained by rotating their counterpart frames in Fig. 2.3a about the system symmetry axis by an integer (n) multiple of the substructure spacing angle $2\pi/N$. Because the full system is cyclically symmetric, the couplings between all the components are independent of whether the degrees of freedom are defined under the bases in Fig. 2.3a or Fig. 2.3a. For example, the first substructure in Fig. 2.3a couples with any specified substructure or central component identically as the first substructure in Fig. 2.3a couples with the corresponding substructure or central component having the same relative position, although these two substructures are not the same substructure in the global reference frame $\{\mathbf{E}_1, \mathbf{E}_2, \mathbf{E}_3\}$. Therefore, the operator $\hat{\mathbf{D}}$ associated with the basis definition in Fig. 2.3a is identical to the $\mathbf{D}$ in Eq. (2.12),

$$\mathbf{D} = \hat{\mathbf{D}} \tag{2.18}$$

and only $\mathbf{D}$ is used subsequently.

The relations between $\mathbf{q}$ and $\hat{\mathbf{q}}$ (or $\mathbf{F}$ and $\hat{\mathbf{F}}$) can be obtained by observation. In Fig. 2.3, both the subvectors $\mathbf{q}_{s_{i+n}}$ (under $\{\mathbf{e}_1^{i+n}, \mathbf{e}_2^{i+n}, \mathbf{e}_3^{i+n}\}$) and $\hat{\mathbf{q}}_{s_i}$ (under $\{\hat{\mathbf{e}}_1^{i}, \hat{\mathbf{e}}_2^{i}, \hat{\mathbf{e}}_3^{i}\}$) describe the motion of the $(i+n)$th substructure in Fig. 2.3a, *i.e.*,

$$\hat{\mathbf{q}}_{s_i} = \mathbf{q}_{s_{i+n}}. \tag{2.19}$$

Such relation between the subvectors of $\hat{\mathbf{q}}_s$ and $\mathbf{q}_s$ can be expressed as

$$\hat{\mathbf{q}}_s = (\boldsymbol{\sigma}_N^n \otimes \mathbf{I}_L)\mathbf{q}_s, \tag{2.20}$$

where $\boldsymbol{\sigma}_N$ is the $N \times N$ cyclic forward shift matrix

$$\boldsymbol{\sigma}_N = \begin{pmatrix} 0 & 1 & 0 & \dots & 0 & 0 \\ 0 & 0 & 1 & \dots & 0 & 0 \\ \vdots & \vdots & \vdots & \ddots & \vdots & \vdots \\ 0 & 0 & 0 & \dots & 1 & 0 \\ 0 & 0 & 0 & \dots & 0 & 1 \\ 1 & 0 & 0 & \dots & 0 & 0 \end{pmatrix}_{N \times N} . \tag{2.21}$$

When an $N \times 1$ vector $\mathbf{a}$ is multiplied by $\boldsymbol{\sigma}_N^n$ (nth power of $\boldsymbol{\sigma}_N$), it is equivalent to upwardly and cyclically shifting all the elements of $\mathbf{a}$ by n elements. In a similar style, multiplication by $\boldsymbol{\sigma}_N^n \otimes \mathbf{I}_L$ as done in Eq. (2.20) cyclically shifts all the $L \times 1$ subvectors of an $NL \times 1$ vector by nL elements. The vectors expressing the driving forces and moments associated with the substructures are related similarly,

$$\hat{\mathbf{F}}_s = (\boldsymbol{\sigma}_N^n \otimes \mathbf{I}_L)\mathbf{F}_s. \tag{2.22}$$

The subvectors $\hat{\mathbf{q}}_c$ and $\mathbf{q}_c$ (or $\hat{\mathbf{F}}_c$ and $\mathbf{F}_c$) expressing the motions (or driving forces and moments) of the central components are related by a rotational coordinate transformation along the cyclic symmetry axis, *i.e.*,

$$\hat{\mathbf{q}}_c = (\mathbf{I}_{2P} \otimes \mathbf{R}_n^{\mathrm{T}})\mathbf{q}_c, \tag{2.23}$$

$$\hat{\mathbf{F}}_c = (\mathbf{I}_{2P} \otimes \mathbf{R}_n^{\mathrm{T}})\mathbf{F}_c, \tag{2.24}$$

where $\mathbf{I}_{2P}$ is the $2P \times 2P$ identity matrix, $\mathbf{R}_n$ is the rotational transformation matrix,

$$\mathbf{R}_n = \mathbf{R}(\frac{2n\pi}{N}) = \mathbf{R}(\alpha_{n+1}) = \begin{pmatrix} \cos\frac{2n\pi}{N} & -\sin\frac{2n\pi}{N} & 0 \\ \sin\frac{2n\pi}{N} & \cos\frac{2n\pi}{N} & 0 \\ 0 & 0 & 1 \end{pmatrix}, \tag{2.25}$$

and n is the arbitrary integer relating the alternative basis definitions in Fig. 2.3.

Based on Eqs. (2.12b), (2.18), and (2.20)-(2.24), Eqs. (2.12a) and (2.17a) are rewritten as

$$\begin{pmatrix} \mathbf{D}_{cc} & \mathbf{D}_{cs} \\ \mathbf{D}_{sc} & \mathbf{D}_{ss} \end{pmatrix} \begin{pmatrix} \mathbf{q}_c \\ \mathbf{q}_s \end{pmatrix} = \begin{pmatrix} \mathbf{F}_c \\ \mathbf{F}_s \end{pmatrix}, \tag{2.26a}$$

$$\begin{pmatrix} \mathbf{D}_{cc} & \mathbf{D}_{cs} \\ \mathbf{D}_{sc} & \mathbf{D}_{ss} \end{pmatrix} \begin{pmatrix} (\mathbf{I}_{2P} \otimes \mathbf{R}_n^{\mathrm{T}})\mathbf{q}_c \\ (\boldsymbol{\sigma}_N^n \otimes \mathbf{I}_L)\mathbf{q}_s \end{pmatrix} = \begin{pmatrix} (\mathbf{I}_{2P} \otimes \mathbf{R}_n^{\mathrm{T}})\mathbf{F}_c \\ (\boldsymbol{\sigma}_N^n \otimes \mathbf{I}_L)\mathbf{F}_s \end{pmatrix}. \tag{2.26b}$$

Starting separately from Eqs. (2.26a) and (2.26b), each set of L equations governing the motion of a single substructure is written as

$$\sum_{l=1}^{P} \mathbf{D}_{s_i c_l} \mathbf{q}_{c_l} = \mathbf{F}_{s_i} - \sum_{l=1}^{N} \mathbf{D}_{s_i s_l} \mathbf{q}_{s_l}, \ i = 1, 2, \ldots, N, \tag{2.27a}$$

$$\sum_{l=1}^{P} \mathbf{D}_{s_i c_l} (\mathbf{I}_2 \otimes \mathbf{R}_n^{\mathrm{T}}) \mathbf{q}_{c_l} = \mathbf{F}_{s_{i+n}} - \sum_{l=1}^{N} \mathbf{D}_{s_i s_l} \mathbf{q}_{s_{l+n}}, \ i = 1, 2, \ldots, N. \tag{2.27b}$$

Manipulation of Eq. (2.27b) yields

$$\begin{aligned}\sum_{l=1}^{P} \mathbf{D}_{s_i c_l} (\mathbf{I}_2 \otimes \mathbf{R}_n^{\mathrm{T}}) \mathbf{q}_{c_l} &= \mathbf{F}_{s_{i+n}} - \sum_{l=1}^{N} \mathbf{D}_{s_{i+n} s_{l+n}} \mathbf{q}_{s_{l+n}} \\ &= \sum_{l=1}^{P} \mathbf{D}_{s_{i+n} c_l} \mathbf{q}_{c_l},\end{aligned} \tag{2.28}$$

where the first equality uses the block circulant structure of $\mathbf{D}_{ss}$, and the second equality uses Eq. (2.27a). Because Eq. (2.12a) applies for any system configuration $\mathbf{q}$ (as noted in the paragraph following Eq. (2.13)), Eq. (2.28) holds for arbitrary $\mathbf{q}_{c_l}$, where elements of $\mathbf{q}_{c_l}$ are independent. Thus,

$$\mathbf{D}_{s_{i+n} c_l} = \mathbf{D}_{s_i c_l} (\mathbf{I}_2 \otimes \mathbf{R}_n^{\mathrm{T}}), \tag{2.29}$$

or, equivalently,

$$\mathbf{D}_{s_l c_i} = \mathbf{D}_{s_1 c_i} (\mathbf{I}_2 \otimes \mathbf{R}_{l-1}^{\mathrm{T}}). \tag{2.30}$$

Considering the cases when central components are non-vibrating (*i.e.*, $\mathbf{q}_c = \mathbf{0}$), Eqs. (2.26a) and (2.26b) separately yield

$$\mathbf{F}_c = \mathbf{D}_{cs} \mathbf{q}_s, \tag{2.31a}$$

$$(\mathbf{I}_{2P} \otimes \mathbf{R}_n^{\mathrm{T}}) \mathbf{F}_c = \mathbf{D}_{cs} (\boldsymbol{\sigma}_N^n \otimes \mathbf{I}_L) \mathbf{q}_s. \tag{2.31b}$$

Manipulation of Eq. (2.31) yields

$$\mathbf{D}_{cs} (\boldsymbol{\sigma}_N^n \otimes \mathbf{I}_L) = (\mathbf{I}_{2P} \otimes \mathbf{R}_n^{\mathrm{T}}) \mathbf{D}_{cs}, \tag{2.32}$$

which indicates that the submatrices of $\mathbf{D}_{cs}$ are related by

$$\mathbf{D}_{c_i s_{l+n}} = (\mathbf{I}_2 \otimes \mathbf{R}_n)\mathbf{D}_{c_i s_l}, \tag{2.33}$$

or, equivalently,

$$\mathbf{D}_{c_i s_l} = (\mathbf{I}_2 \otimes \mathbf{R}_{l-1})\mathbf{D}_{c_i s_1}. \tag{2.34}$$

Eq. (2.34) indicates that the submatrix connecting the lth substructure and the central components can be obtained by rotationally transforming the submatrix connecting the first substructure and the central components. For substructures being equally spaced, Eqs. (2.30) and (2.34) capture the cyclic symmetry of the coupling between two separate physical subsystems, namely, the periodic substructure chain and the set of axisymmetric coupled central components.

The properties in Eqs. (2.30) and (2.34) can be observed in the example system. $\mathbf{K}_{cs_i,V}$

in Eq. (2.15i), for instance, can be decomposed as

$$
\begin{aligned}
\mathbf{K}_{cs_i,V} &= \begin{pmatrix}
-k_{cs,r}\cos\alpha_i & k_{cs,t}\sin\alpha_i & 0 \\
-k_{cs,r}\sin\alpha_i & -k_{cs,t}\cos\alpha_i & 0 \\
0 & 0 & -k_{cs,a} \\
-k_{cs,R}\cos\alpha_i & k_{cs,R}\sin\alpha_i & -k_{cs,a}L_0\sin\alpha_i \\
-k_{cs,R}\sin\alpha_i & -k_{cs,R}\cos\alpha_i & k_{cs,a}L_0\cos\alpha_i \\
0 & -k_{cs,t}L_0 & -k_{cs,R}
\end{pmatrix} \\
&= \begin{pmatrix}
C & -S & 0 & 0 & 0 & 0 \\
S & C & 0 & 0 & 0 & 0 \\
0 & 0 & 1 & 0 & 0 & 0 \\
0 & 0 & 0 & C & -S & 0 \\
0 & 0 & 0 & S & C & 0 \\
0 & 0 & 0 & 0 & 0 & 1
\end{pmatrix}
\begin{pmatrix}
-k_{cs,r} & 0 & 0 \\
0 & -k_{cs,t} & 0 \\
0 & 0 & -k_{cs,a} \\
-k_{cs,R} & 0 & 0 \\
0 & -k_{cs,R} & k_{cs,a}L_0 \\
0 & -k_{cs,t}L_0 & -k_{cs,R}
\end{pmatrix} \\
&= [\mathbf{I}_2 \otimes \mathbf{R}(\alpha_i)]\mathbf{K}_{cs_1,V} = (\mathbf{I}_2 \otimes \mathbf{R}_{i-1})\mathbf{K}_{cs_1,V},
\end{aligned}
\tag{2.35}
$$

where C and S represent $\cos\alpha_i$ and $\sin\alpha_i$ for brevity.

Eqs. (2.30) and (2.34) greatly simplify the derivation of equations of motion. The components of $\mathbf{D}_{cs_1}$ and $\mathbf{D}_{s_1c}$ can be derived from a free-body diagram containing only the central components and the first substructure. All the other submatrices of $\mathbf{D}_{cs}$ and $\mathbf{D}_{sc}$ can be generated from $\mathbf{D}_{cs_1}$ and $\mathbf{D}_{s_1c}$ according to Eqs. (2.30) and (2.34).

2.3.3 Properties of $\mathbf{D}_{cc}$

The submatrix $\mathbf{D}_{cc}$ associated only with the central components can be partitioned as

$$\mathbf{D}_{cc} = \begin{pmatrix} \mathbf{D}_{c_1c_1} & \mathbf{D}_{c_1c_2} & \dots & \mathbf{D}_{c_1c_P} \\ \mathbf{D}_{c_2c_1} & \mathbf{D}_{c_2c_2} & \dots & \mathbf{D}_{c_2c_P} \\ \vdots & \vdots & \ddots & \vdots \\ \mathbf{D}_{c_Pc_1} & \mathbf{D}_{c_Pc_2} & \dots & \mathbf{D}_{c_Pc_P} \end{pmatrix}, \tag{2.36}$$

where $\mathbf{D}_{c_ic_l}$ $(i, l = 1, 2, \dots, P)$ captures the impact of the lth central component on the ith central component. All the entries of $\mathbf{D}_{cc}$ can be derived from the subsystem of central components with non-vibrating substructures (*i.e.*, $\mathbf{q}_s$ in Eq. (2.12) is zero), where all other aspects are identical to the original system. This subsystem corresponding to $\mathbf{D}_{cc}$ corrects an error in the simplified model for deriving $\mathbf{D}_{cc}$ in Ref. [29], where the stiffnesses between the central components and substructures are mistakenly not included. The error in Ref. [29] leads to incorrect $\mathbf{D}_{cc}$, although the resulting conclusions about the properties of $\mathbf{D}_{cc}$ in Ref. [29] are correct.

The properties of $\mathbf{D}_{cc}$ are obtained in a similar procedure as used above to obtain the properties of of $\mathbf{D}_{cs}$. Starting separately from Eqs. (2.26a) and (2.26b), each set of six equations governing the motion of a single central component is written as

$$\sum_{l=1}^{P} \mathbf{D}_{c_ic_l}\mathbf{q}_{c_l} = \mathbf{F}_{c_i} - \sum_{l=1}^{N} \mathbf{D}_{c_is_l}\mathbf{q}_{s_l},\ i = 1, 2, \dots, P, \tag{2.37a}$$

$$\sum_{l=1}^{P} \mathbf{D}_{c_ic_l}(\mathbf{I}_2 \otimes \mathbf{R}_n^{\mathrm{T}})\mathbf{q}_{c_l} = (\mathbf{I}_2 \otimes \mathbf{R}_n^{\mathrm{T}})\mathbf{F}_{c_i} - \sum_{l=1}^{N} \mathbf{D}_{c_is_l}\mathbf{q}_{s_{l+n}},\ i = 1, 2, \dots, P. \tag{2.37b}$$

Manipulation of Eq. (2.37b) yields

$$\begin{aligned}\sum_{l=1}^{P}\mathbf{D}_{c_ic_l}(\mathbf{I}_2\otimes\mathbf{R}_n^{\mathrm{T}})\mathbf{q}_{c_l} &= (\mathbf{I}_2\otimes\mathbf{R}_n^{\mathrm{T}})\mathbf{F}_{c_i}-\sum_{l=1}^{N}(\mathbf{I}_2\otimes\mathbf{R}_n^{\mathrm{T}})\mathbf{D}_{c_is_{l+n}}\mathbf{q}_{s_{l+n}}\\ &= (\mathbf{I}_2\otimes\mathbf{R}_n^{\mathrm{T}})(\mathbf{F}_{c_i}-\sum_{l=1}^{N}\mathbf{D}_{c_is_l}\mathbf{q}_{s_l})\\ &= (\mathbf{I}_2\otimes\mathbf{R}_n^{\mathrm{T}})\sum_{l=1}^{P}\mathbf{D}_{c_ic_l}\mathbf{q}_{c_l},\end{aligned} \tag{2.38}$$

where the first equality uses Eq. (2.33), the second equality uses the block circulant structure of $\mathbf{D}_{ss}$, and the third uses Eq. (2.27a). Multiplication of Eq. (2.38) by $(\mathbf{I}_2\otimes\mathbf{R}_n)$ from the left yields

$$\sum_{l=1}^{P}(\mathbf{I}_2\otimes\mathbf{R}_n)\mathbf{D}_{c_ic_l}(\mathbf{I}_2\otimes\mathbf{R}_n^{\mathrm{T}})\mathbf{q}_{c_l}=\sum_{l=1}^{P}\mathbf{D}_{c_ic_l}\mathbf{q}_{c_l}, \tag{2.39}$$

where $(\mathbf{I}_2\otimes\mathbf{R}_n)$ and $(\mathbf{I}_2\otimes\mathbf{R}_n^{\mathrm{T}})$ are inverses of each other. For Eq. (2.39) to hold for arbitrary $\mathbf{q}_{c_l}$ having independent elements,

$$(\mathbf{I}_2\otimes\mathbf{R}_n)\mathbf{D}_{c_ic_l}(\mathbf{I}_2\otimes\mathbf{R}_n^{\mathrm{T}})=\mathbf{D}_{c_ic_l}, \tag{2.40}$$

or, equivalently,

$$(\mathbf{I}_{2P}\otimes\mathbf{R}_n)\mathbf{D}_{cc}(\mathbf{I}_{2P}\otimes\mathbf{R}_n^{\mathrm{T}})=\mathbf{D}_{cc}, \tag{2.41}$$

where $n=1,2,\ldots,N$.

Eqs. (2.40) and (2.41) express that the operator $\mathbf{D_{cc}}$ and its submatrix components are invariant under rotation by an integer (n) multiple of the substructure spacing angle $2\pi/N$. This property of $\mathbf{D_{cc}}$ reflects that the symmetry of the central components and the couplings between them are compatible with the full system cyclic symmetry.

Further relations between the elements in $\mathbf{D_{cc}}$ are obtained by summation of Eq. (2.40) over $n = 1, 2, \ldots, N$,

$$\sum_{n=1}^{N} (\mathbf{I}_2 \otimes \mathbf{R}_n) \mathbf{D}_{c_i c_l} (\mathbf{I}_2 \otimes \mathbf{R}_n^{\mathrm{T}}) = N \mathbf{D}_{c_i c_l}. \tag{2.42}$$

Equating the elements in the first row and the first column of both sides of Eq. (2.42) gives

$$\begin{aligned} &\sum_{n=1}^{N} (D_{11}^{(il)} \cos^2 \frac{2n\pi}{N} + D_{22}^{(il)} \sin^2 \frac{2n\pi}{N} + \frac{D_{12}^{(il)}}{2} \sin \frac{4n\pi}{N} + \frac{D_{21}^{(il)}}{2} \sin \frac{4n\pi}{N}) \\ =&\frac{N}{2} (D_{11}^{(il)} + D_{22}^{(il)}) = N D_{11}^{(il)}, \end{aligned} \tag{2.43}$$

where $D_{pq}^{(il)}$ is the element in the pth row and the qth column of $\mathbf{D}_{c_i c_l}$, and the first equality uses the trigonometric identities

$$\sum_{n=1}^{N} \cos^2 \frac{2n\pi}{N} = \sum_{n=1}^{N} \sin^2 \frac{2n\pi}{N} = \frac{N}{2}, \ N = 3, 4, \ldots, \tag{2.44a}$$

$$\sum_{n=1}^{N} \sin \frac{4n\pi}{N} = 0, \ N = 3, 4, \ldots. \tag{2.44b}$$

Eq. (2.43) indicates that $D_{11}^{(il)}$ and $D_{22}^{(il)}$ are identical. Considering other elements of Eq. (2.42) in a similar way gives additional relationships that ensure any submatrix ($\mathbf{D}_{c_i c_l}$) of $\mathbf{D}_{cc}$ in Eq. (2.12b) has the form

$$\mathbf{D}_{c_i c_l} = \begin{pmatrix} D_{11}^{(il)} & D_{12}^{(il)} & 0 & D_{14}^{(il)} & D_{15}^{(il)} & 0 \\ -D_{12}^{(il)} & D_{11}^{(il)} & 0 & -D_{15}^{(il)} & D_{14}^{(il)} & 0 \\ 0 & 0 & D_{33}^{(il)} & 0 & 0 & D_{36}^{(il)} \\ D_{41}^{(il)} & D_{42}^{(il)} & 0 & D_{44}^{(il)} & D_{45}^{(il)} & 0 \\ -D_{42}^{(il)} & D_{41}^{(il)} & 0 & -D_{45}^{(il)} & D_{44}^{(il)} & 0 \\ 0 & 0 & D_{63}^{(il)} & 0 & 0 & D_{66}^{(il)} \end{pmatrix}. \tag{2.45}$$

From Eq. (2.45), one can also prove that $\mathbf{D}_{c_i c_l}$ is invariant under similarity transformation by $\mathbf{I}_2 \otimes \mathbf{R}(\beta)$, *i.e.*,

$$[\mathbf{I}_2 \otimes \mathbf{R}(\beta)]\mathbf{D}_{c_i c_l}[\mathbf{I}_2 \otimes \mathbf{R}(\beta)^{\mathrm{T}}] = \mathbf{D}_{c_i c_l}, \tag{2.46}$$

where β is an arbitrary angle.

Eqs. (2.45) and (2.46) indicate the central components have certain physical properties so that they are compatible with the full system cyclic symmetry. Because the inertia matrix $\mathbf{M}_{c_i c_l}$ of any arbitrary central component has the form in Eq. (2.45), the central component moments of inertia about the system center along $\mathbf{e}_1$ and $\mathbf{e}_2$ are equal, *i.e.*, $J_1 = J_2$, and their centers of mass lie on the system symmetry axis. While these inertia properties are necessary, the central components can be non-uniform such that their geometric shape is not axisymmetric or cyclically symmetric. In addition, Eq. (2.46) indicates the couplings between central components are axisymmetric. Physically, considering when the substructures are non-vibrating, *i.e.*, $\mathbf{q}_s$ in Eq. (2.12) is zero, the operator $\mathbf{D}_{cc}$ that relates the central component generalized coordinate $\mathbf{q}_c$ and the central component force vector $\mathbf{F}_c$ is invariant, whether $\mathbf{q}_c$ and $\mathbf{F}_c$ are defined in the basis $\{\mathbf{e}_1, \mathbf{e}_2, \mathbf{e}_3\}$ or any basis that is rotated from $\{\mathbf{e}_1, \mathbf{e}_2, \mathbf{e}_3\}$ along $\mathbf{e}_3$ by any arbitrary angle.

Crucial properties of the system are evident from Eq. (2.45): (a) there is full coupling between all central component in-plane translations and all out-of-plane tilting degrees of freedom; (b) there is full coupling between all central component axial translations and all in-plane rotations; (c) coupling between the two sets of degrees of freedom defined in (a) and (b) is not possible. These coupling conclusions apply within the six degrees of freedom for each central component and for all $6P$ central component degrees of freedom taken as a whole.

Further understanding of this result can be obtained by considering a fictitious system

where such conditions are not satisfied. The substructures can be ignored for this purpose because $\mathbf{D}_{cc}$ depends only on the central components. For example, we assume that the coupling between the axial ($\mathbf{e}_3$) motion of the ith central component and the translation along $\mathbf{e}_1$ of the lth central component is non-zero, *i.e.*, $D_{31}^{(il)}$ and $D_{13}^{(li)}$ are non-zero. If the system is released such that the axial ($\mathbf{e}_3$) displacement of the ith central components is the only non-zero initial condition, the response should preserve the symmetry of the system and the initial condition, *i.e.*, the other central components are either non-vibrating or translating/rotating purely along the symmetry axis, $\mathbf{e}_3$. The non-zero term $D_{13}^{(li)}$ in the fictitious system, however, would cause the lth central component to vibrate along $\mathbf{e}_1$. The assumed non-zero terms conflict with the system symmetry. Therefore, they should vanish as Eq. (2.45) guarantees.

The components of $\mathbf{D}_{cc}$ in Eq. (2.15), such as $\mathbf{M}_{cc}$ and $\mathbf{G}_{cc}$, have the form in Eq. (2.45).

2.4 Vibration Mode Structure of Cyclically Symmetric Systems with Vibrating Central Components

2.4.1 Properties of A in Eq. (2.13b)

The submatrices of $\mathbf{A}$ in Eq. (2.13b) inherit the previously derived properties from their counterparts in $\mathbf{D}$, namely,

$$\mathbf{A}_{s_i s_l} = \mathbf{A}_{s_{i+n} s_{l+n}},\ n = 1, 2, ..., N, \tag{2.47a}$$

$$\mathbf{A}_{c_i s_l} = (\mathbf{I}_2 \otimes \mathbf{R}_{l-1})\mathbf{A}_{c_i s_1} = [\mathbf{I}_2 \otimes \mathbf{R}(\alpha_l)]\mathbf{A}_{c_i s_1}, \tag{2.47b}$$

$$\mathbf{A}_{s_l c_i} = \mathbf{A}_{s_1 c_i}(\mathbf{I}_2 \otimes \mathbf{R}_{l-1}^{\mathrm{T}}) = \mathbf{A}_{s_1 c_i}[\mathbf{I}_2 \otimes \mathbf{R}^{\mathrm{T}}(\alpha_l)], \tag{2.47c}$$

$$\mathbf{A}_{c_i c_l} = \begin{pmatrix} a_{11}^{(il)} & a_{12}^{(il)} & 0 & a_{14}^{(il)} & a_{15}^{(il)} & 0 \\ -a_{12}^{(il)} & a_{11}^{(il)} & 0 & -a_{15}^{(il)} & a_{14}^{(il)} & 0 \\ 0 & 0 & a_{33}^{(il)} & 0 & 0 & a_{36}^{(il)} \\ a_{41}^{(il)} & a_{42}^{(il)} & 0 & a_{44}^{(il)} & a_{45}^{(il)} & 0 \\ -a_{42}^{(il)} & a_{41}^{(il)} & 0 & -a_{45}^{(il)} & a_{44}^{(il)} & 0 \\ 0 & 0 & a_{63}^{(il)} & 0 & 0 & a_{66}^{(il)} \end{pmatrix}, \tag{2.47d}$$

where the number indices for the central components are bounded from 1 to P.

2.4.2 Modal Decomposition of Generalized Cyclically Symmetric Systems

The eigenvalue problem in Eq. (2.13) can be written as

$$\mathbf{A}_{cc}\mathbf{\Phi}_c + \mathbf{A}_{cs}\mathbf{\Phi}_s = \mathbf{0}, \tag{2.48a}$$

$$\mathbf{A}_{sc}\mathbf{\Phi}_c + \mathbf{A}_{ss}\mathbf{\Phi}_s = \mathbf{0}. \tag{2.48b}$$

Instead of directly solving Eq. (2.48), all the eigensolutions will be found through the following procedure. First, we propose and later confirm that $\mathbf{\Phi}_s$ in Eq. (2.48) has the same phase behavior as proved earlier for systems with non-vibrating central components, that is, all substructures execute the same motion $\hat{\mathbf{\Phi}}_{s_{(k)}}$ but with a phase difference determined by a phase index k. Mathematically, this means

$$\mathbf{\Phi}_{s_{(k)}} = \mathbf{e}_{(k)} \otimes \hat{\mathbf{\Phi}}_{s_{(k)}}, \tag{2.49}$$

where $\mathbf{\Phi}_{s_{(k)}}$ specifies a particular $\mathbf{\Phi}_s$ that is characterized by a phase index k. Because of Eq. (2.49), one only needs to determine the L-dimensional vector $\hat{\mathbf{\Phi}}_{s_{(k)}}$ to generate the full NL-dimensional vector of substructure degrees of freedom $\mathbf{\Phi}_{s_{(k)}}$. Second, a trial subvector for the corresponding central component motions $\mathbf{\Phi}_{c_{(k)}}$ is proposed for a selected phase index k. Based on this proposed form of the full eigenvectors, Eq. (2.48) is reduced to a lower-dimensional eigenvalue problem whose solution yields all the full system eigensolutions $\mathbf{\Phi}_{(k)} = (\mathbf{\Phi}_{c_{(k)}}, \mathbf{\Phi}_{s_{(k)}})^{\mathrm{T}}$ satisfying Eq. (2.13) for the selected phase index k. After completing such procedure for all phase indices $k \in \{0, 1, \ldots, N-1\}$, the vibration modes are explicitly categorized into *substructure* and *coupled* modes depending on whether $\mathbf{\Phi}_{c_{(k)}}$ is a zero vector.

To propose proper central component sub-eigenvectors, Eq. (2.48a) is investigated. Substitution of Eqs. (2.47b) and (2.49) into $\mathbf{A}_{cs}\mathbf{\Phi}_s$ in Eq. (2.48a) yields

$$\mathbf{A}_{cs}\mathbf{\Phi}_s = \left(\mathbf{A}_{c_1 s}\mathbf{\Phi}_s, \mathbf{A}_{c_2 s}\mathbf{\Phi}_s, \ldots, \mathbf{A}_{c_P s}\mathbf{\Phi}_s\right)^{\mathrm{T}}, \tag{2.50a}$$

$$\begin{aligned}\mathbf{A}_{c_m s}\mathbf{\Phi}_s =& \sum_{i=1}^{N} \mathrm{e}^{\mathrm{j}k\alpha_i}[\mathbf{I}_2 \otimes \mathbf{R}(\alpha_i)]\mathbf{A}_{c_m s_1}\hat{\mathbf{\Phi}}_{s_{(k)}} \\ =& \mathbf{T}_k \mathbf{A}_{c_m s_1}\hat{\mathbf{\Phi}}_{s_{(k)}}, \text{ for } m = 1, 2, \ldots, P,\end{aligned} \tag{2.50b}$$

where the operator $\mathbf{T}_k$ is a function of phase index only,

$$\begin{aligned}\mathbf{T}_k &= \sum_{i=1}^{N} \mathrm{e}^{\mathrm{j}k\alpha_i}[\mathbf{I}_2 \otimes \mathbf{R}(\alpha_i)] \\ &= \mathbf{I}_2 \otimes \begin{pmatrix} \sum_{i=1}^{N} \mathrm{e}^{\mathrm{j}k\alpha_i}\cos\alpha_i & -\sum_{i=1}^{N} \mathrm{e}^{\mathrm{j}k\alpha_i}\sin\alpha_i & 0 \\ \sum_{i=1}^{N} \mathrm{e}^{\mathrm{j}k\alpha_i}\sin\alpha_i & \sum_{i=1}^{N} \mathrm{e}^{\mathrm{j}k\alpha_i}\cos\alpha_i & 0 \\ 0 & 0 & \sum_{i=1}^{N} \mathrm{e}^{\mathrm{j}k\alpha_i} \end{pmatrix}.\end{aligned} \tag{2.51}$$

The form of $\mathbf{T}_k$ varies for different selections of phase index k, and it motivates the subsequent

proposed forms of $\mathbf{\Phi}_{c_{(k)}}$.

Substructure modes

For all phase indices $k = 2, 3, ..., N-2$, the trigonometric identities [18]

$$\sum_{i=1}^{N} \mathrm{e}^{\mathrm{j}k\alpha_i} \cos\alpha_i = \sum_{i=1}^{N} \mathrm{e}^{\mathrm{j}k\alpha_i} \sin\alpha_i = \sum_{i=1}^{N} \mathrm{e}^{\mathrm{j}k\alpha_i} = 0, \;\; k = 2, 3, ..., N-2 \tag{2.52}$$

make the operator $\mathbf{T}_k$ in Eq. (2.51) vanish,

$$\mathbf{T}_k = \mathbf{0}, \quad k = 2, 3, ..., N-2. \tag{2.53}$$

Consequently, the second term $\mathbf{A}_{cs}\mathbf{\Phi}_s$ in Eq. (2.48a) vanishes. Thus, the selection $\mathbf{\Phi}_c = \mathbf{0}$, as assumed below, ensures that Eq. (2.48a) is satisfied.

To satisfy Eq. (2.48b) with $\mathbf{\Phi}_c = \mathbf{0}$ already proposed from above, it remains only to find $\mathbf{\Phi}_s$ with the form of Eq. (2.49) such that $\mathbf{A}_{ss}\mathbf{\Phi}_s = \mathbf{0}$. This problem is identical to Eq. (2.2) where $\mathbf{\Phi}_s$ was proved to have the phase relations in Eq. (2.49); $\hat{\mathbf{\Phi}}_{s_{(k)}}$ are the same as the $\hat{\mathbf{u}}_{s_{(k)}}$ in Eq. (2.9) for the $N-3$ phase indices $k = 2, 3, ..., N-2$.

Thus, the full eigenvectors corresponding to the modes with phase index $k = 2, 3, ..., N-2$ are

$$\mathbf{\Phi}_{(k)} = \begin{pmatrix} \mathbf{\Phi}_{c_{(k)}} \\ \mathbf{\Phi}_{s_{(k)}} \end{pmatrix} = \begin{pmatrix} \mathbf{0}_{6P\times 1} \\ \mathbf{e}_{(k)} \otimes \hat{\mathbf{\Phi}}_{s_{(k)}} \end{pmatrix}, \tag{2.54}$$

where $\hat{\mathbf{\Phi}}_{s_{(k)}}$ is solved from the $L \times L$ eigenvalue problem in Eq. (2.9) for each value of k. For each phase index k, $2L$ complex-valued eigensolutions are obtained. These $2L$ eigensolutions are complex conjugates of the eigensolutions for the case with phase index $N-k$ ($k \neq \frac{N}{2}$).

When the number of substructures is even, the reduced eigenvalue problem Eq. (2.9) with phase index $k = \frac{N}{2}$ is real-valued and provides $2L$ eigensolutions in complex conjugate pairs. Therefore, there are $2L \times (N-3)$ eigensolutions with the form in Eq. (2.54), consisting of $L \times (N-3)$ complex conjugate pairs.

In all of these $L \times (N-3)$ pairs of modes, the modal deflections occur only in the substructures, so such modes are named *substructure modes* [29]. The substructure modes are referred to as *planet modes* in planetary gears [12–16, 30, 74] and *absorber modes* in CPVA systems [18–21]. To obtain these modes, one only needs to solve $L \times L$ eigenvalue problems in Eq. (2.9) for the cases when $k = 2, ..., \frac{N-1}{2}$ or $\frac{N}{2}$, depending on whether N is odd or even. This is more computationally efficient than solving the $(NL+6P) \times (NL+6P)$ full system eigenvalue problem, especially when the number of substructures and/or, more commonly, the number of degrees of freedom per substructure is large.

Besides computational efficiency, Eq. (2.9) explains the $N-3$ degeneracy of the eigenvalues in planetary gears and CPVA systems [12–16, 18–21, 30, 74]. Planetary gears and CPVA systems are cyclic systems without interactions between the substructures, *i.e.*, the operator $\mathbf{A}_{ss}$ is block diagonal. All the reduced eigenvalue problems in Eq. (2.9) are equivalent to

$$\mathbf{A}_{s_1 s_1} \hat{\mathbf{\Phi}}_{s_{(k)}} = \mathbf{0}, \quad k = 2, 3, ..., N-2, \tag{2.55}$$

where the ith eigensolution, $(\lambda_{(k)}^{(i)}, \hat{\mathbf{\Phi}}_{s_{(k)}}^{(i)})$, is identical for all the $N-3$ selections of k. Therefore, all the eigenvalues consist of L pairs of eigenvalues with degeneracy $N-3$. Such analysis and conclusions about eigenvalue degeneracy also exist in Ref. [29], although that work considers the central components having in-plane degrees of freedom only. For systems with coupling between the substructures, the above eigenvalue degeneracy is not expected.

The eigenvalue problem of the example system in Fig. 2.2 is solved with the parameters

in Table 2.1. The imaginary parts of the eigenvalues are shown in Fig. 2.4 and Table 2.2. The number of substructure modes ($k = 2, 3$) for the example system with $L = 3$ and $N = 5$ matches the above derivation: there are $L \times (N - 3) = 6$ pairs of substructure modes. The eigenvalues solved from the reduced eigenvalue problems match those from the full eigenvalue problem (Fig. 2.4).

System Parameters	**Value**
radius of substructure undeflected position, L_0 (m)	0.50
rotational speed of the system, Ω (rad s^{-1})	104.72
number of substructures	5
Central component	
mass, m_c (kg)	20
inertia along $\mathbf{e}_1$, J_1 (kg m^2)	5.0
inertia along $\mathbf{e}_3$, J_3 (kg m^2)	10.0
translational stiffness to non-vibrating rotor, k_c (N m^{-1})	5.2×10^6
rotaional stiffness to non-vibrating rotor, $k_{c,R}$ (N m rad^{-1})	1.0×10^6
Coupling between vibrating central component and substructure	
radial stiffness $k_{cs,r}$ (N m^{-1})	2.5×10^6
tangential stiffness $k_{cs,t}$ (N m^{-1})	3.0×10^6
axial stiffness $k_{cs,a}$ (N m^{-1})	2.0×10^6
substructure effect on central component rotations $k_{cs,R}$ (N rad^{-1})	1.5×10^6
Substructures	
mass, m_s (kg)	1
stiffness to non-vibrating rotor k_s (N m^{-1})	1.0×10^6
in-plane stiffness k_{ss} (N m^{-1})	2.0×10^6
axial stiffness substructures $k_{ss,a}$ (N m^{-1})	1.0×10^6

Table 2.1: Parameters of the cyclically symmetric example system in Fig. 2.2. There is one vibrating central component, and each substructure has three degrees of freedom.

Figure 2.5 illustrates two substructure modes (mode 10 and 11) of the example system. The central component has zero modal deflections, while the motions of all substructures are identical in magnitude. Because of the gyroscopic effects, the three degrees of freedom within each substructure are out of phase, although the relative phase differences within each substructure are identical for all substructures. In contrast, the phase differences between

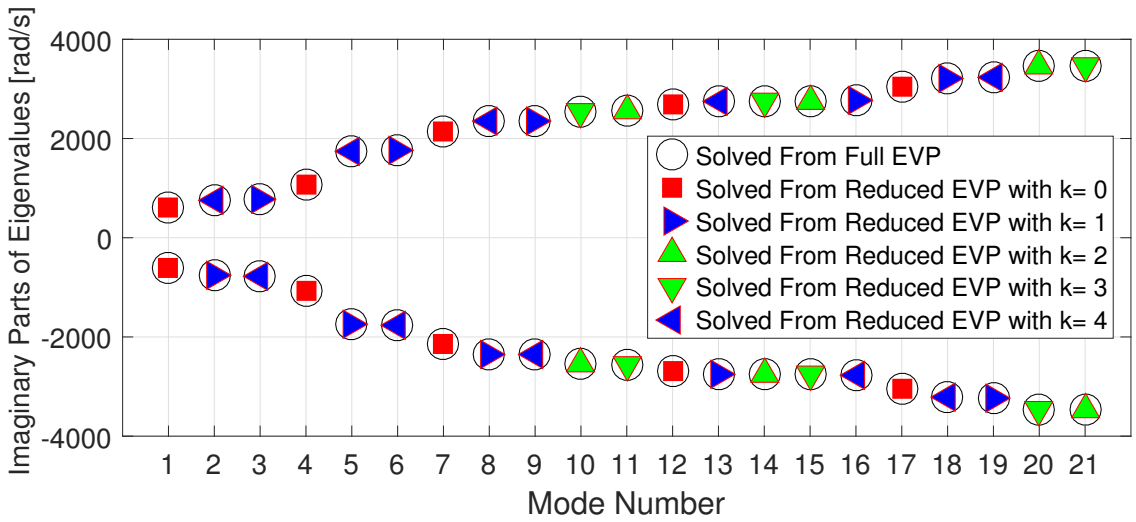

Figure 2.4: Imaginary parts of eigenvalues of the example system in Fig. 2.2. The eigenvalues solved from reduced eigenvalue problems in Eqs. (2.9), (2.67), and (2.72) are compared to those from the full eigenvalue problem in Eq. (2.13).

Mode Type	**Natural Frequency** (rad s^{-1}) **(Mode Number)**
Substructure Modes	2550 (10), 2558 (11), 2760 (14,15), 3456 (20), 3465 (21)
Translation-tilting Modes	763 (2), 784 (3), 1753 (5), 1756 (6), 2353 (8), 2534 (9), 2753 (13), 2771 (16), 3213 (18), 3234 (19)
Axial-rotational Modes	600 (1), 1061 (4), 2140 (7), 2685 (12), 3044 (17)

Table 2.2: Natural frequencies of the cyclically symmetric example system in Fig. 2.2. The number in parentheses denotes the mode number that labels the eigenvalue in Fig. 2.4.

different substructures are characterized by the phase index of the mode. For example, in Fig. 2.5a, the $(i+1)$th substructure vibrates 144 degrees out-of-phase with the ith substructure. This phase relation is characterized by phase index $k = 2$, because the phase difference is k times the substructure spacing angle of 72 degrees. Similarly, the eigenvector in Fig. 2.5b is characterized by phase index $k = 3$.

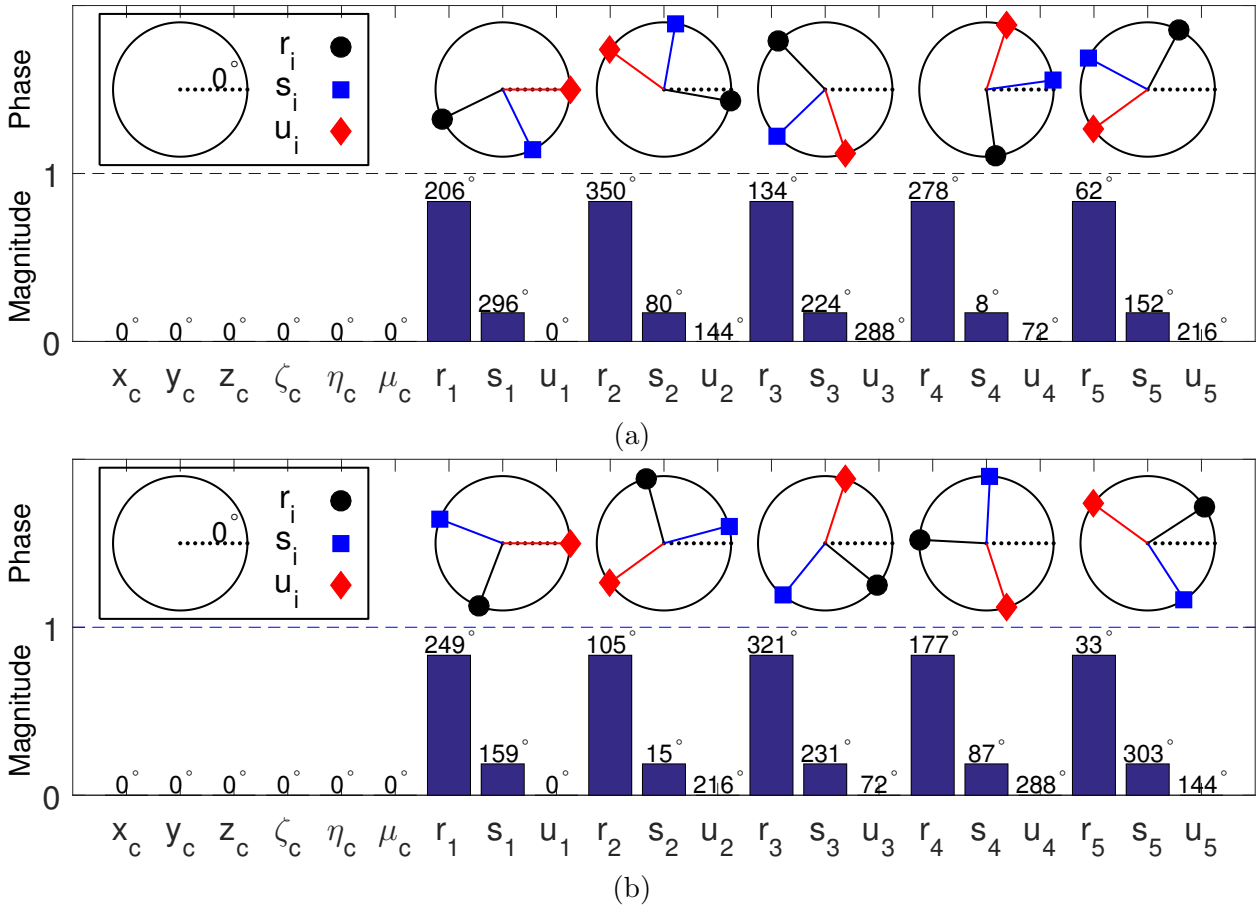

Figure 2.5: Substructure modes of the example system. The phases of all degrees of freedom are labeled in number. Phases of each substructure's motions are illustrated in the upper diagrams, where the symbols correspond to the numerical phase labels. a Eigenvector of the 11th mode, phase index $k = 2$, imaginary part of eigenvalue = 2558 rad s^{-1}. b Eigenvector of the 10th mode, phase index $k = 3$, imaginary part of eigenvalue = 2550 rad s^{-1}.

Coupled Modes

For $k = 0, 1$ and $N - 1$, the matrix $\mathbf{T}_k$ in Eq. (2.51) does not vanish, so neither does the term $\mathbf{A}_{cs}\mathbf{\Phi}_s$ in Eq. (2.48a). Thus, the central component modal deflections ($\mathbf{\Phi}_{c_{(k)}}$) for $k \in \{0, 1, N - 1\}$ that satisfy Eq. (2.48a) are non-zero. In such modes, the substructure motions are coupled with non-zero central component motions.

According to the direction of motion, all six degrees of freedom within a central compo-

nent are categorized into two types. Type-I motions include the out-of-plane axial translation and in-plane rotation. All type-I motions are expressed as vectors parallel to the symmetry axis of the system. In contrast, the two in-plane translations and two out-of-plane tilting motions are defined as type-II motions, and they are expressed as vectors perpendicular to the symmetry axis. In Section 2.3, Eq. (2.45) rules out coupling between type-I and type-II motions, although coupling between motions of the same type may exist. These properties lead to separation of coupled modes into translational-tilting modes and rotational-axial modes.

(i) Translational-Tilting Modes

For the cases when $k = 1$ and $N - 1$, the operator $\mathbf{T}_k$ in Eq. (2.51) is

$$\mathbf{T}_1 = \begin{pmatrix} \frac{N}{2} & -\mathrm{j}\frac{N}{2} & 0 & 0 & 0 & 0 \\ \mathrm{j}\frac{N}{2} & \frac{N}{2} & 0 & 0 & 0 & 0 \\ 0 & 0 & 0 & 0 & 0 & 0 \\ 0 & 0 & 0 & \frac{N}{2} & -\mathrm{j}\frac{N}{2} & 0 \\ 0 & 0 & 0 & \mathrm{j}\frac{N}{2} & \frac{N}{2} & 0 \\ 0 & 0 & 0 & 0 & 0 & 0 \end{pmatrix}, \tag{2.56a}$$

$$\mathbf{T}_{N-1} = \mathbf{T}_1^{\mathrm{T}}. \tag{2.56b}$$

For brevity, only the case when $k = 1$ is considered. Similar analysis applies to the case when $k = N - 1$.

We first consider the term $\mathbf{A}_{cs}\mathbf{\Phi}_s$ in Eq. (2.48a). Combination of Eq. (2.50) and Eq. (2.56a) provides two properties of $\mathbf{A}_{c_m s}\mathbf{\Phi}_s$: (i) the second row of $\mathbf{A}_{c_m s}\mathbf{\Phi}_s$ is j times the first row, and the fifth is j times the fourth; (ii) the third and the sixth rows of $\mathbf{A}_{c_m s}\mathbf{\Phi}_s$ vanish. The term $\mathbf{A}_{cc}\mathbf{\Phi}_c$ in Eq. (2.48a) must have these same two properties. A reasonable trial

$\mathbf{\Phi}_{c_{(1)}}$ for $k = 1$ consists of P 6×1 subvectors that have zero entries in the third and sixth rows. Another clue for finding a reasonable trial $\mathbf{\Phi}_{c_{(1)}}$ is obtained from the axisymmetry of the coupled central components. Such symmetry indicates that there should be no *preferred* directions for any central component type-II motions, *i.e.*, the modal deflection of the two in-plane translations (or tilting motions) should have the same magnitude. The phase difference between two in-plane translations (or tilting motions) is assumed to be the difference between their directions, 90 degrees, multiplied by the phase index $k = 1$. This corresponds to multiplication by j. The proposed mode shape of the mth central component is

$$\mathbf{\Phi}_{c_m} = (x_{c_m}, \mathrm{j}x_{c_m}, 0, \zeta_{c_m}, \mathrm{j}\zeta_{c_m}, 0)^{\mathrm{T}},\ m = 1, 2, ..., P. \tag{2.57}$$

The term $\mathbf{A}_{cc}\mathbf{\Phi}_c$ in Eq. (2.48a) is expanded as

$$\mathbf{A}_{cc}\mathbf{\Phi}_c = \left(\mathbf{A}_{c_1c}\mathbf{\Phi}_c, \mathbf{A}_{c_2c}\mathbf{\Phi}_c, \ldots, \mathbf{A}_{c_Pc}\mathbf{\Phi}_c\right)^{\mathrm{T}}. \tag{2.58}$$

Partitioning Eq. (2.48a) into equations for the P central components gives

$$\mathbf{A}_{c_mc}\mathbf{\Phi}_c + \mathbf{A}_{c_ms}\mathbf{\Phi}_s = \mathbf{0}_{6\times 1},\ m = 1, 2, ..., P. \tag{2.59}$$

Based on Eqs. (2.47d) and (2.57), $\mathbf{A}_{c_m c}\mathbf{\Phi}_c$ in Eq. (2.59) is

$$\mathbf{A}_{c_m c}\mathbf{\Phi}_c = \sum_{i=1}^{P} \begin{pmatrix} a_{11}^{(mi)} x_{c_i} + a_{14}^{(mi)} \zeta_{c_i} + \mathrm{j}(a_{12}^{(mi)} x_{c_i} + a_{15}^{(mi)} \zeta_{c_i}) \\ \mathrm{j}(a_{11}^{(mi)} x_{c_i} + a_{14}^{(mi)} \zeta_{c_i}) - (a_{12}^{(mi)} x_{c_i} + a_{15}^{(mi)} \zeta_{c_i}) \\ 0 \\ a_{41}^{(mi)} x_{c_i} + a_{44}^{(mi)} \zeta_{c_i} + \mathrm{j}(a_{42}^{(mi)} x_{c_i} + a_{45}^{(mi)} \zeta_{c_i}) \\ \mathrm{j}(a_{41}^{(mi)} x_{c_i} + a_{44}^{(mi)} \zeta_{c_i}) - (a_{42}^{(mi)} x_{c_i} + a_{45}^{(mi)} \zeta_{c_i}) \\ 0 \end{pmatrix}. \tag{2.60}$$

Invoking Eqs. (2.50b), (2.56a) and (2.60) into Eq. (2.59) makes the third and the sixth equations in Eq. (2.59) vanish, while the second equation is j times the first equation, and the fifth is j times the fourth. Therefore, the six equations for the mth central component are reduced to only two independent equations. All the $6P$ equations for all central components generate only $2P$ independent equations.

Partitioned from Eq. (2.48b), the governing equation for the nth substructure is

$$\mathbf{A}_{s_n c}\mathbf{\Phi}_c + \mathbf{A}_{s_n s}\mathbf{\Phi}_s = \mathbf{0},\ n = 1, 2, ..., N, \tag{2.61}$$

where $\mathbf{\Phi}_s$ is assumed to satisfy Eq. (2.49) with $k = 1$,

$$\mathbf{\Phi}_s = \mathbf{e}_{(1)} \otimes \hat{\mathbf{\Phi}}_{s_{(1)}} = (\mathrm{e}^{\mathrm{j}\alpha_1}\hat{\mathbf{\Phi}}_{s_{(1)}}, \mathrm{e}^{\mathrm{j}\alpha_2}\hat{\mathbf{\Phi}}_{s_{(1)}}, ..., \mathrm{e}^{\mathrm{j}\alpha_N}\hat{\mathbf{\Phi}}_{s_{(1)}})^{\mathrm{T}}. \tag{2.62}$$

Invoking Eq. (2.62) and the properties of $\mathbf{A}_{sc}$ in Eq. (2.47c), Eq. (2.61) becomes

$$\sum_{i=1}^{P} \mathbf{A}_{s_1 c_i}[\mathbf{I}_2 \otimes \mathbf{R}^{\mathrm{T}}(\alpha_n)]\mathbf{\Phi}_{c_i} + \sum_{l=1}^{N} \mathrm{e}^{\mathrm{j}\alpha_l}\mathbf{A}_{s_n s_l}\hat{\mathbf{\Phi}}_{s_{(1)}} = \mathbf{0},\ n = 1, 2, \ldots, N. \tag{2.63}$$

For the form of $\mathbf{\Phi}_{c_i}$ in Eq. (2.57), one can verify that

$$[\mathbf{I}_2 \otimes \mathbf{R}^{\mathrm{T}}(\alpha_n)]\mathbf{\Phi}_{c_i} = \mathrm{e}^{\mathrm{j}\alpha_n}\mathbf{\Phi}_{c_i}. \tag{2.64}$$

Moreover, the second term in Eq (2.63) can be reformulated as

$$\begin{aligned}\sum_{l=1}^{N} \mathrm{e}^{\mathrm{j}\alpha_l}\mathbf{A}_{s_n s_l}\hat{\mathbf{\Phi}}_{s_{(1)}} &= \sum_{l=1}^{N} \mathrm{e}^{\mathrm{j}\alpha_l}\mathbf{A}_{s_1 s_{l-n+1}}\hat{\mathbf{\Phi}}_{s_{(1)}} = \sum_{l=1}^{N} \mathbf{A}_{s_1 s_{l-n+1}}\mathbf{\Phi}_{s_l} \\ &= \sum_{l=1}^{N} \mathrm{e}^{\mathrm{j}\alpha_n}\mathbf{A}_{s_1 s_{l-n+1}}\mathbf{\Phi}_{s_{l-n+1}} = \sum_{l=1}^{N} \mathrm{e}^{\mathrm{j}\alpha_n}\mathbf{A}_{s_1 s_l}\mathbf{\Phi}_{s_l}, \\ &= \sum_{l=1}^{N} \mathrm{e}^{\mathrm{j}\alpha_l}\mathrm{e}^{\mathrm{j}\alpha_n}\mathbf{A}_{s_1 s_l}\hat{\mathbf{\Phi}}_{s_{(1)}}\end{aligned} \tag{2.65}$$

where the block circulant structure of $\mathbf{A}_{ss}$ in Eq. (2.47a) is applied in the process. Substitution of Eqs. (2.64) and (2.65) into Eq. (2.63) yields

$$\sum_{i=1}^{P} \mathbf{A}_{s_1 c i}\mathbf{\Phi}_{c_i} + \sum_{l=1}^{N} \mathrm{e}^{\mathrm{j}\alpha_l}\mathbf{A}_{s_1 s_l}\hat{\mathbf{\Phi}}_{s_{(1)}} = \mathbf{0}. \tag{2.66}$$

Eq. (2.66) is independent of the substructure index n, *i.e.*, the governing equations in Eq. (2.61) are identical for all N substructures. Therefore, only L independent equations are obtained from Eq. (2.48b).

In summary, Eq. (2.48a) generates $2P$ independent equations and Eq. (2.48b) provides L independent equations. The unknowns include two type-II modal deflections (x_{c_m} and ζ_{c_m}) for each central component and the L unknowns in the substructure mode shape $\hat{\mathbf{\Phi}}_{s_{(1)}}$. Thus, there are altogether $2P+L$ unknowns to be solved, equaling the number of independent equations. These equations formulate a $(2P + L) \times (2P + L)$ complex-valued second-order

reduced eigenvalue problem,

$$\begin{pmatrix} \tilde{\mathbf{A}}_{cc} & \mathbf{I}_2 \otimes \begin{pmatrix} \frac{N}{2} & -\mathrm{j}\frac{N}{2} & 0 \end{pmatrix} \mathbf{A}_{c_m s_1} \\ \tilde{\mathbf{A}}_{s_1 c} & \sum_{l=1}^{N} \mathrm{e}^{\mathrm{j}\alpha_l} \mathbf{A}_{s_1 s_l} \end{pmatrix} \begin{pmatrix} \tilde{\tilde{\mathbf{\Phi}}}_c \\ \hat{\mathbf{\Phi}}_{s_{(1)}} \end{pmatrix} = \mathbf{0}, \tag{2.67a}$$

$$\tilde{\tilde{\mathbf{\Phi}}}_c = (x_{c_1},\ \zeta_{c_1},\ \ldots,\ x_{c_P},\ \zeta_{c_P})^{\mathrm{T}}, \tag{2.67b}$$

$$\tilde{\mathbf{A}}_{c_m c_i} = \begin{pmatrix} a_{11}^{(mi)} + \mathrm{j}a_{12}^{(mi)} & a_{14}^{(mi)} + \mathrm{j}a_{15}^{(mi)} \\ a_{41}^{(mi)} + \mathrm{j}a_{42}^{(mi)} & a_{44}^{(mi)} + \mathrm{j}a_{45}^{(mi)} \end{pmatrix},\ m,\ i = 1, \ldots,\ P, \tag{2.67c}$$

$$\tilde{\mathbf{A}}_{s_1 c_m} = \mathbf{A}_{s_1 c_m} \left[\mathbf{I}_2 \otimes \begin{pmatrix} 1 & 0 & 0 \end{pmatrix}^{\mathrm{T}} \right],\ m = 1, \ldots,\ P, \tag{2.67d}$$

where $\tilde{\mathbf{A}}_{cc}$ is reduced from $\mathbf{A}_{cc}$ in Eq. (2.13b), and $\tilde{\mathbf{A}}_{s_1 c}$ is reduced from $\mathbf{A}_{s_1 c}$ that connects the central components and the first substructure. The blocks of $\tilde{\mathbf{A}}_{cc}$ and $\tilde{\mathbf{A}}_{s_1 c}$ are defined as $\tilde{\mathbf{A}}_{c_m c_i}$ and $\tilde{\mathbf{A}}_{s_1 c_m}$ in Eq. (2.67), respectively. The reduced eigenvalue problem in Eq. (2.67) yields $4P + 2L$ complex-valued eigensolutions. The eigensolutions for the case when $k = N - 1$ are the complex conjugates of those for $k = 1$. Therefore, all $4P + 2L$ pairs of eigenslolutions are determined by solving one reduced eigenvalue problem. The full system eigenvectors are then constructed from Eqs. (2.57) and (2.62).

For the cases when $k = 1$ and $N - 1$, the full eigenvectors are characterized by non-zero type-II vibrations and zero type-I vibrations of the central components. These modes are named *translational-tilting modes*. In prior works, such modes are found in planetary gears [12–16, 74], CPVA systems [18–20], and general cyclically symmetric systems [29], where the central components have in-plane motions only. These planar modes are special cases of translational-tilting modes when the tilting motions of the central components are not modeled.

Figure 2.4 compares the eigenvalues calculated from Eq. (2.67) to those from Eq. (2.13)

for the example system where $P = 1$ and $L = 3$. Consistent with the analysis, there are ten pairs of translational-tilting modes, and the eigenvalues from Eqs. (2.67) and (2.13) are identical. The eigensolutions from Eqs. (2.67) with $k = 4$ are complex conjugates of those with $k = 1$. Figure 2.6 presents two translational-tilting modes for the example system. In Fig. 2.6a, the central component in-plane translations have the same magnitude and the phase difference between them is 90 degrees, *i.e.*, $y_c = \mathrm{j}x_c$. Such relations also exist between the out-of-plane tilting motions. All the substructures vibrate identically (*i.e.*, the magnitudes and relative phases of each substructure's degrees of freedom are identical), but the $(i+1)$th substructure vibrates with a phase difference of 72 degrees relative to the ith substructure. Thus, the mode is characterized by phase index $k = 1$. In contrast, the eigenvector in Fig. 2.6b is characterized by phase index $k = 4$.

(ii)Rotational-Axial modes

For the case when $k = 0$, the operator $\mathbf{T}_k$ in Eq. (2.51) becomes

$$\mathbf{T}_0 = \begin{pmatrix} 0 & 0 & 0 & 0 & 0 & 0 \\ 0 & 0 & 0 & 0 & 0 & 0 \\ 0 & 0 & N & 0 & 0 & 0 \\ 0 & 0 & 0 & 0 & 0 & 0 \\ 0 & 0 & 0 & 0 & 0 & 0 \\ 0 & 0 & 0 & 0 & 0 & N \end{pmatrix}. \tag{2.68}$$

Considering $\mathbf{A}_{cs}\mathbf{\Phi}_s$ in Eq. (2.48a), Eqs. (2.50) and (2.68) reveal that, for each $m = 1, 2, ..., P$, only the third and sixth rows of $\mathbf{A}_{c_m s}\mathbf{\Phi}_s$ in Eq. (2.59) are non-zero. Considering Eq. (2.48a),

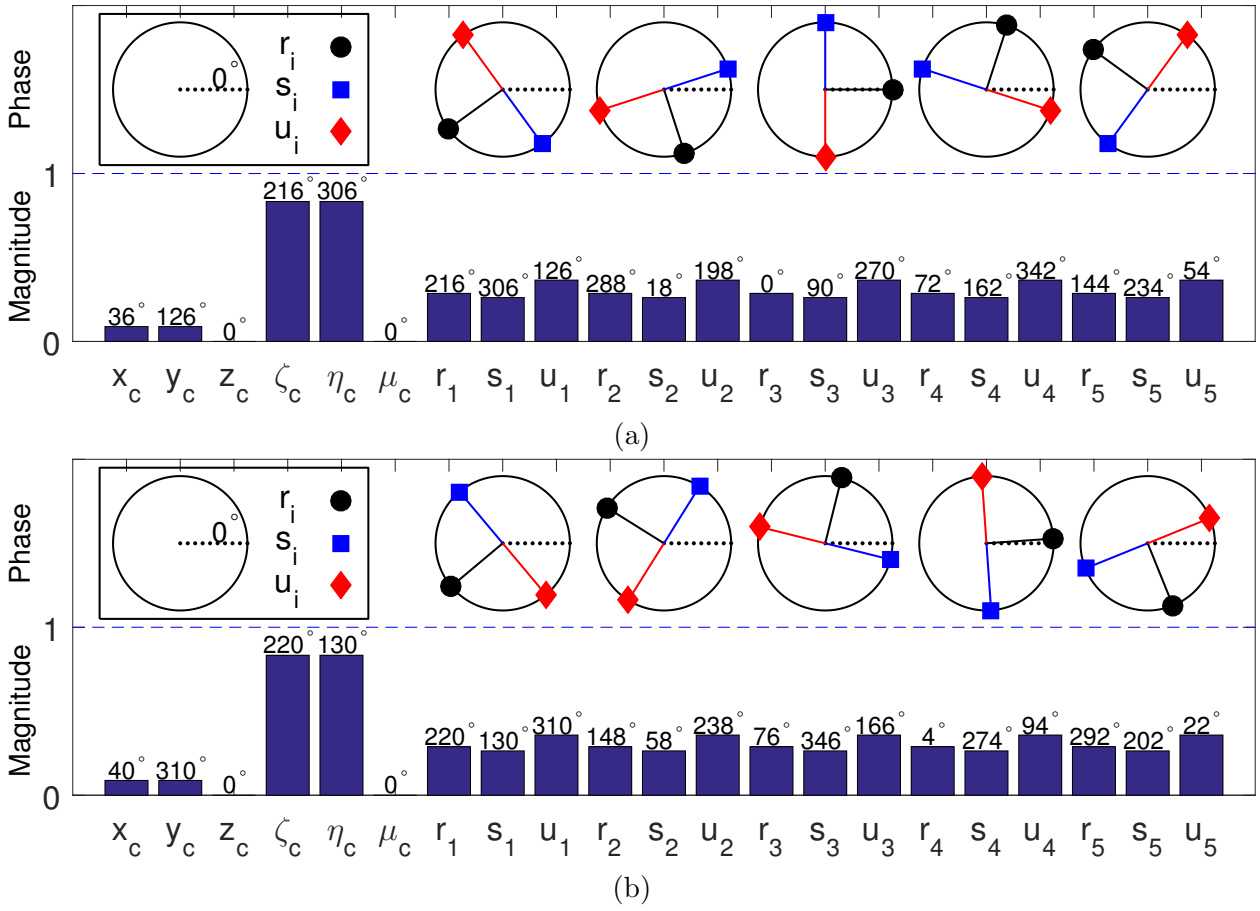

Figure 2.6: Translational-tilting modes of the example system. a Eigenvector of the 6th mode, phase index $k = 1$, imaginary part of eigenvalue = 1756 rad s^{-1}. b Eigenvector of the 5th mode, phase index $k = 4$, imaginary part of eigenvalue = 1753 rad s^{-1}.

the sub-eigenvector of all the central components are proposed to have zero type-II motions,

$$\mathbf{\Phi}_{c_m} = (0, 0, z_{c_m}, 0, 0, \mu_{c_m})^{\mathrm{T}}, \ m = 1, 2, ..., P. \tag{2.69}$$

The term $\mathbf{A}_{c_m c}\mathbf{\Phi}_c$ in Eq. (2.59) then expands to

$$\mathbf{A}_{c_m c}\mathbf{\Phi}_c = \sum_{i=1}^{P} \mathbf{A}_{c_m c_i}\mathbf{\Phi}_{c_i} = \sum_{i=1}^{P} \begin{pmatrix} 0 \\ 0 \\ a_{33}^{(mi)} z_{c_i} + a_{36}^{(mi)} \mu_{c_i} \\ 0 \\ 0 \\ a_{63}^{(mi)} z_{c_i} + a_{66}^{(mi)} \mu_{c_i} \end{pmatrix} . \tag{2.70}$$

Thus, both $\mathbf{A}_{c_m c}\mathbf{\Phi}_c$ and $\mathbf{A}_{c_m s}\mathbf{\Phi}_s$ in Eq. (2.59) have non-zero terms in the third and sixth rows while the other rows vanish, so Eq. (2.59) provides only two independent equations for each value of m. Therefore, Eq. (2.48a) only generates $2P$ independent equations.

Through a procedure analogous to that from Eq. (2.61) to Eq. (2.66), a counterpart of Eq. (2.66) is obtained for the case when $k = 0$,

$$\sum_{i=1}^{P} \mathbf{A}_{s_1 c i}\mathbf{\Phi}_{c_i} + \sum_{l=1}^{N} \mathbf{A}_{s_1 s_l}\hat{\mathbf{\Phi}}_{s_{(0)}} = \mathbf{0}, \tag{2.71}$$

which is again independent of the substructure index n. The N substructure governing equations in Eq. (2.61) are equivalent. Therefore, Eq. (2.48b) provides only L independent equations.

Combining the $2P$ independent equations from Eq. (2.48a) with the L equations from Eq. (2.71), a $(2P + L) \times (2P + L)$ real-valued, second-order reduced eigenvalue problem is

formulated,

$$\begin{pmatrix} \tilde{\mathbf{A}}_{cc} & \mathbf{I}_2 \otimes \begin{pmatrix} 0 & 0 & N \end{pmatrix} \mathbf{A}_{c_m s_1} \\ \tilde{\mathbf{A}}_{s_1 c} & \sum_{l=1}^{N} \mathbf{A}_{s_1 s_l} \end{pmatrix} \begin{pmatrix} \tilde{\boldsymbol{\Phi}}_c \\ \hat{\boldsymbol{\Phi}}_{s_{(0)}} \end{pmatrix} = \mathbf{0}, \tag{2.72a}$$

$$\tilde{\boldsymbol{\Phi}}_c = (z_{c_1},\ \mu_{c_1},\ \ldots,\ z_{c_P},\ \mu_{c_P})^{\mathrm{T}}, \tag{2.72b}$$

$$\tilde{\mathbf{A}}_{c_m c_i} = \begin{pmatrix} a_{33}^{(mi)} & a_{36}^{(mi)} \\ a_{63}^{(mi)} & a_{66}^{(mi)} \end{pmatrix},\ m,\ i = 1, \ldots,\ P, \tag{2.72c}$$

$$\tilde{\mathbf{A}}_{s_1 c_m} = \mathbf{A}_{s_1 c_m} \left[\mathbf{I}_2 \otimes \begin{pmatrix} 0 & 0 & 1 \end{pmatrix}^{\mathrm{T}} \right],\ m = 1, \ldots,\ P. \tag{2.72d}$$

Solution of Eq. (2.72) gives $2(2P+L)$ reduced eigenvectors consisting of the two type-I modal deflections (z_{c_m} and μ_{c_m}) of each central component and the L unknowns in $\hat{\boldsymbol{\Phi}}_{s_{(0)}}$. The full eigenvectors are constructed from Eqs. (2.49) and (2.69). Because Eq. (2.72) is a real-valued, second-order eigenvalue problem whose eigensolutions occur in complex conjugate pairs, the full system eigensolutions for the case when $k = 0$ occur in $2P + L$ complex conjugate pairs.

In such modes, the type-II vibrations of the central components vanish. Central components have only out-of-plane axial translation and in-plane rotation. The modes are named *rotational-axial modes*. All the substructures in such modes vibrate in phase (recall $k = 0$) with the same magnitude. The rotational modes defined in prior works [12–16, 18–20, 29, 74] are special cases of rotational-axial modes when the out-of-plane axial translations of the central components are not modeled.

Figure 2.4 compares the eigenvalues calculated from Eq. (2.72) to those from Eq. (2.13) for the example system ($P = 1$, $L = 3$). Consistent with the analysis, there are five ($2P + L = 5$) complex conjugate pairs of rotational-axial modes, and the eigenvalues from Eqs. (2.72) and (2.13) are identical. An example rotational-axial mode is given in Fig.

2.7. The modal deflections of the central component are only axial and rotational. All the substructures vibrate identically and move in phase.

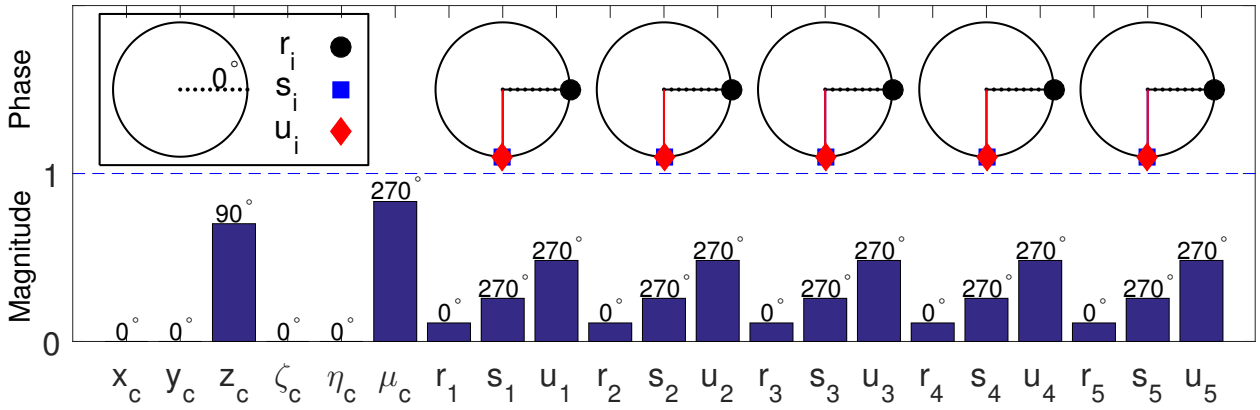

Figure 2.7: Rotational-axial mode (phase index $k = 0$) of the example system. The imaginary part of the eigenvalue is 1061 rad s^{-1} (mode number = 4).

Completeness of the modal decomposition

The above modal decomposition provides $(N-3) \times L$ complex conjugate pairs of substructure modes, $2 \times (2P + L)$ pairs of translational-tilting modes, and $2P + L$ pairs of rotational-axial modes. The total of $6P + NL$ complex conjugate pairs of modes equals the total degrees of freedom. Therefore, the derived eigenvectors form the complete set of eigenvectors. No other mode type exists. The results apply for systems with arbitrary matrix symmetries, *i.e.*, $\mathbf{M} \neq \mathbf{M}^{\mathrm{T}}$, $\mathbf{B} \neq \mathbf{B}^{\mathrm{T}}$, and $\mathbf{L} \neq \mathbf{L}^{\mathrm{T}}$ in Eq. (2.12). For the example system in Fig. 2.2, Fig. 2.4 confirms that the number of eigensolutions from all the reduced eigenvalue problems for $k = 0, 1, 2, 3, 4$ exactly matches that from the full eigenvalue problem in Eq. (2.13).

2.4.3 Consistency with Conservative, Non-Gyroscopic Systems

In many previous works [12, 16, 26], the eigenvalues associated with the substructure modes and translational-tilting modes exhibit two-fold degeneracy when the cyclically symmetric systems are conservative and non-gyroscopic. The following analysis explains that this eigenvalue degeneracy results from two properties of $\mathbf{A}$ in Eq. (2.13b): $\mathbf{A}$ and its components (*e.g.*, $\mathbf{M}$) satisfy the properties in Eq. (2.47) for cyclically symmetric systems; and, $\mathbf{A}$ has the properties associated with conservative, non-gyroscopic systems.

The eigenvalue problem for conservative, non-gyroscopic systems is

$$\lambda^2\mathbf{M}\boldsymbol{\Phi} + \mathbf{K}\boldsymbol{\Phi} = \mathbf{0}, \tag{2.73}$$

where $\mathbf{M}$ and $\mathbf{K}$ are symmetric mass and stiffness matrices. This real-valued, first-order eigenvalue problem (λ^2 is the eigenvalue) admits real-valued eigenvalues and eigenvectors [102]. Meanwhile, Eq. (2.73) is a specific case of Eq. (2.13) when $\mathbf{M} = \mathbf{M}^{\mathrm{T}}$, $\mathbf{B} = \mathbf{0}$, and $\mathbf{L} = \mathbf{K} = \mathbf{K}^{\mathrm{T}}$, so the modal properties derived for general cyclically symmetric systems apply. The foregoing derivation concludes that: (a) substructure modes with phase index $k = 2, 3, ..., N-2$ ($k \neq \frac{N}{2}$) and translational-tilting modes with $k = 1$ and $N-1$ are complex-valued; (b) the eigensolutions with phase index k ($k = 1, 2, ..., N-1$ and $k \neq \frac{N}{2}$) are complex conjugates of the modes with phase index $N-k$.

Combination of the properties of conservative, non-gyroscopic systems with the modal properties of general cyclically symmetric systems ((a) and (b) above) indicates:

1. For cases when $k = 1, 2, ..., N-1$ and $k \neq \frac{N}{2}$, complex-valued $\boldsymbol{\Phi}$ and real-valued λ^2 satisfy Eq. (2.73). Consequently, both the real and imaginary parts of $\boldsymbol{\Phi}$ are eigenvectors. Two real independent eigenvectors are associated with the same eigenvalue

λ^2, so all substructure modes and translational-tilting modes have two-fold degenerate eigenvalues.

2. Eigenvectors with phase index k ($k = 1, 2, ..., N-1$ and $k \neq \frac{N}{2}$) and those with phase index $N-k$ provide the same real and imaginary parts of $\mathbf{\Phi}$ because of (b). Therefore, modes with phase index k ($k = 1, 2, ..., N-1$ and $k \neq \frac{N}{2}$) and $N-k$ have the same set of two-fold degenerate eigenvalues (λ^2) with the two corresponding eigenvectors for each eigenvalue given by the real and imaginary components of the complex-valued $\mathbf{\Phi}$.

3. For the cases when $k = 0$ or $\frac{N}{2}$, both Eq. (2.73) and its reduced eigenvalue problems provide real-valued eigensolutions, and the eigenvalues are distinct in general.

2.5 Conclusions

This work derives essential matrix properties and the resulting highly structured vibration modes of general cyclically symmetric systems with central components vibrating as three-dimensional rigid bodies. While cyclic symmetry of the structure is necessary, no matrix symmetry is assumed; all of asymmetric mass matrix, damping, gyroscopic, and circulatory terms can be present. All the modes are characterized by substructures that vibrate identically but with particular phase relations between the substructures for different mode types. The phase between adjacent substructures' vibrations equals the spacing angle multiplied by an integer phase index. The modes are further classified by how the central components vibrate. Only three types of modes can exist:

1. Substructure modes: all central components are non-vibrating, while the substructures vibrate identically with phase differences characterized by phase indices from 2 to $N-2$;

2. Translational-tilting modes: the central components tilt out-of-plane and translate in-plane, but do not rotate or move axially. The phase relations between the substructures are labeled with phase indices 1 and $N-1$;

3. Rotational-axial modes: the only non-zero central component motions are axial translation and rotation about the symmetry axis, while the substructures all vibrate in phase.

In the equation of motion of a general cyclically symmetric system, the matrix operators are shown to have specific properties related to the cyclic symmetry. These important symmetry-related properties allow proof of the modal properties. Furthermore, they facilitate derivation of the equations of motion by considering simpler subsystems (*e.g.*, only the central components and one substructure) to obtain the smaller matrix partitions that are assembled to construct the full system model.

All the vibration modes and natural frequencies can be obtained by solving smaller eigenvalue problems associated with each mode type. This computational advantage is dramatic for systems with many substructures or many degrees of freedom per substructure.

Appendix A. Fourier Matrix and Direct Product

Fourier Matrix

The $N \times N$ Fourier matrix is defined as [26]

$$\begin{aligned}\mathbf{E}_N &= \frac{1}{\sqrt{N}} \begin{bmatrix} 1 & 1 & 1 & \dots & 1 \\ 1 & w_N & w_N^2 & \dots & w_N^{N-1} \\ 1 & w_N^2 & w_N^4 & \dots & w_N^{2(N-1)} \\ \vdots & \vdots & \vdots & \ddots & \vdots \\ 1 & w_N^{N-1} & w_N^{2(N-1)} & \dots & w_N^{(N-1)(N-1)} \end{bmatrix} \\ &= \begin{bmatrix} \mathbf{e}_{(0)} & \mathbf{e}_{(1)} & \mathbf{e}_{(2)} & \dots & \mathbf{e}_{(N-1)} \end{bmatrix},\end{aligned} \tag{2.74}$$

where $w_N^k = \mathrm{e}^{\mathrm{j}\frac{2k\pi}{N}}$ with j as the imaginary unit, and vector $\mathbf{e}_{(k)} = (1, w_N^k, w_N^{2k}, \dots, w_N^{(N-1)k})^{\mathrm{T}}$ is the $(k+1)$th column of the Fourier matrix.

Direct Product

For $\mathbf{a}, \mathbf{b} \in \mathbb{C}^n$, the direct product of $\mathbf{a}$ and $\mathbf{b}^{\mathrm{T}}$ is the $n \times n$ matrix

$$\mathbf{a} \otimes \mathbf{b}^{\mathrm{T}} = \begin{pmatrix} a_1 b_1 & a_1 b_2 & \dots & a_1 b_n \\ a_2 b_1 & a_2 b_2 & \dots & a_2 b_n \\ \vdots & \vdots & \ddots & \vdots \\ a_n b_1 & a_n b_2 & \dots & a_n b_n \end{pmatrix}. \tag{2.75}$$

If $\mathbf{A} \in \mathbb{C}^{m \times n}$ and $\mathbf{B} \in \mathbb{C}^{p \times q}$, the direct product of $\mathbf{A}$ and $\mathbf{B}$ is

$$\mathbf{A} \otimes \mathbf{B} = \begin{pmatrix} a_{11}\mathbf{B} & a_{12}\mathbf{B} & \dots & a_{1n}\mathbf{B} \\ a_{21}\mathbf{B} & a_{22}\mathbf{B} & \dots & a_{2n}\mathbf{B} \\ \vdots & \vdots & \ddots & \vdots \\ a_{m1}\mathbf{B} & a_{m2}\mathbf{B} & \dots & a_{mn}\mathbf{B} \end{pmatrix} \tag{2.76}$$

with dimension $mp \times nq$. Consider Eq (2.10) as an example:

$$\mathbf{u}_{s_{(k)}}^{(p)} = \mathbf{e}_{(k)} \otimes \hat{\mathbf{u}}_{s_{(k)}}^{(p)} = \frac{1}{\sqrt{N}} \begin{bmatrix} \hat{\mathbf{u}}_{s_{(k)}}^{(p)} \\ w_N^k \hat{\mathbf{u}}_{s_{(k)}}^{(p)} \\ w_N^{2k} \hat{\mathbf{u}}_{s_{(k)}}^{(p)} \\ \vdots \\ w_N^{(N-1)k} \hat{\mathbf{u}}_{s_{(k)}}^{(p)} \end{bmatrix}. \tag{2.77}$$

In Eq (2.77), each subvector has a phase difference of $\frac{2k\pi}{N}$ relative to its neighboring subvector.

Chapter 3

Group-Theory-Based Modal Analysis of Cyclically Symmetric Systems with Rigid-Body and Compliant Central Components

3.1 Introduction

Cyclically symmetric or rotationally periodic structures exist in many mechanical systems, such as planetary gears [11, 12, 15, 16, 28, 30, 103], circular rings[6–8], circular plates [5, 99, 104], centrifugal pendulum vibration absorber (CPVA) systems [18, 21, 38, 79], and *etc.* The cyclic symmetry of these systems results in highly structured vibration modes. In a vibration mode, the rotationally repeated structures, or *substructures*, are vibrating with a phase difference. The phase relations between substructures can be characterized by phase indices [9, 10]. The phase relations between substructures can be fully explained by the

circulant matrix theory [26]. For cyclically symmetric systems consisting of repeated substructures only, application of the circulant matrix theory can improve the computational efficiency, because the full system problem of a cyclically symmetric system can be reduced into several problems with smaller size [26].

In cyclically symmetric systems with *rigid-body central components* (*e.g.*, the rotor in a CPVA system), although the phase relations between substructures still exist in a system mode, the mode structure of these systems can not be directly obtained from the circulant matrix theory. In many previous works, the modal properties of such structures are obtained for specific mechanical systems, such as planetary gears [11, 12, 16, 30] and CPVA systems [18, 21]. Shi and Parker [29] derived the modal properties for general cyclically symmetric systems with rigid-body central components that can have planar motions. Dong and Parker [105] further generalized the modal properties in Ref. [29] to systems with three-dimensional central components, and the theory can fully explain the structured modes in helical planetary gears [30]. Although the modal properties of cyclically symmetric systems with rigid-body central components are obtained in these previous studies, the modal properties for general cyclically symmetric systems with *compliant central components* are still unknown. For example, the ring gear in the planetary gears in Ref. [15] is modeled as an elastic continuum, the mode structure of such a system can not be identified based on the previous works, such as Refs. [26, 29, 105], which attempted to summarize the modal properties of general cyclically symmetric systems.

In previous works, the modal properties of cyclically symmetric systems are obtained based on the circulant matrix theory and the properties of the matrix operators in system equations of motion. In a cyclically symmetric system with compliant central components, the system is a hybrid discrete-continuous system, and the circulant matrix theory does not directly apply. To analyze a hybrid discrete-continuous system with cyclic symmetry, group

theory, as a powerful tool to study symmetric systems, is used in this work.

Group theory is widely used in areas such as molecular chemistry and condensed matter physics [1, 52], and applications of group theory have emerged in engineering. In many previous works, group theory is used to reduce the computational costs for symmetric systems. For example, bifurcation phenomena in symmetric engineering systems are studied by using group theory to simplify the computation of bifurcation points [53–55]. Group theory is also used to simplify the vibration problems of engineering structures, including high-tension cable nets [56, 57], shells [58, 59], and skeletal structures, such as space trusses and frames [57, 62]. Group theory applies to any discrete, continuous or hybrid discrete-continuous systems with symmetry.

The aim of this work is to obtain the modal properties of cyclically symmetric systems with both rigid-body and compliant central components through group theory. The rigid-body central components are allowed to have six degrees of freedom, and the number of degrees of freedom for substructures and compliant central components can be arbitrary. Gyroscopic effect is also considered. The modal properties obtained generalize the modal properties obtained in Ref. [26, 29, 105] and other works that studies specific systems [11, 12, 15, 16, 18, 21, 30, 30]. The mode types in general cyclically symmetric systems are identified, and each mode type can be solved from a reduced eigenvalue problem that is formulated based on group theory. Although this work focuses on systems with cyclic symmetry, the analysis procedure can also apply to systems with other symmetry types.

This paper is organized as follows. In Section 3.2, the basics of group theory for symmetry groups are first reviewed. The theory in this section is distilled from Refs. [1, 52], and application of group theory to a symmetric system is illustrated by an example system. In Section 3.3, group theory is applied to general cyclically symmetric systems with both rigid-body and compliant central components. Modal properties of such systems are

obtained, and the reduced eigenvalue problems are formulated to reduce the computational cost. An example cyclically symmetric system with both rigid-body and compliant central components is given to illustrate the properties.

3.2 Group Theory and Its Application to Symmetric System Vibrations

3.2.1 Basics of Group Theory

A collection of elements $\{A, B, \ldots, R, \ldots\}$ is a group $\mathcal{G}$ under an operation denoted by $\bullet$ if it satisfies the following requirements:

1. **closure** For all A and B in $\mathcal{G}$, the result of the operation $A \bullet B$ is also in $\mathcal{G}$;
2. **associativity** For all A, B and C in $\mathcal{G}$, $(A \bullet B) \bullet C = A \bullet (B \bullet C)$;
3. **existence of identity** There exists a unit element E in $\mathcal{G}$ such that $R \bullet E = E \bullet R = R$ for all R in $\mathcal{G}$;
4. **existence of inverse** Every element R in $\mathcal{G}$ has an inverse in $\mathcal{G}$, denoted as R^{-1}, such that $R \bullet R^{-1} = E$.

The symmetry group of an object is the group of all symmetry operations that bring the object into coincidence with itself and leave it indistinguishable from its original configuration. For example, for an object with $\mathcal{C}_N$ cyclic symmetry, the object is brought into self-coincidence by the N symmetry operations consisting of identity and the rotations by $2\pi/N$, $4\pi/N$,..., and $2(N-1)\pi/N$. The object in Fig. 3.1 exhibits $\mathcal{C}_3$ group symmetry, and

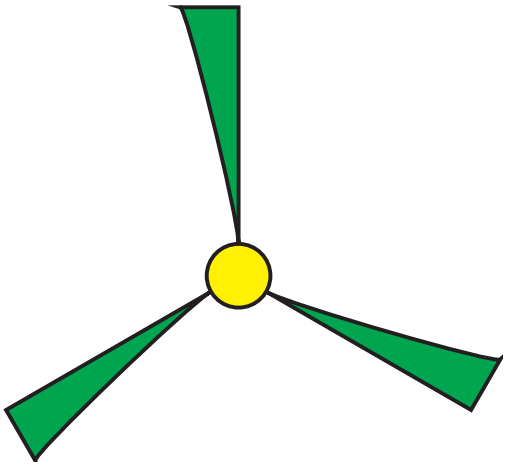

Figure 3.1: An object that exhibits $\mathcal{C}_3$ group symmetry.

the symmetry operations include identity, rotation by $2\pi/3$, and rotation by $-2\pi/3$ (equivalent to $4\pi/3$) around the center. These three operations are denoted as E, C_3, and C_3^{-1}, respectively, and they satisfy the above four requirements to form a group.

By the definition of a symmetry group, the process to identify the symmetry of an object only involves graphically intuitive consideration in most cases. To apply group theory to mechanics, however, the identification of the symmetry group of a system requires more rigorous work. To build the connection between group theory and mechanics problems, it is necessary to identify the symmetry operations which leave the operator in the equations to be solved invariant. In Ref. [52], Section 1.8 discusses that the symmetry of a molecular system is defined by the group of the symmetry operations which leave the Hamiltonian in the Schrödinger equation invariant. In this work, a more convenient but also rigorous method to identify the system symmetry is introduced. To consider the vibration of a system, the symmetry operation that forms the symmetry group of the system can transform an arbitrary system configuration (deflection) to an equivalent configuration. Starting with any configuration in a set of equivalent configurations as the initial condition, the free vibration of the system is physically identical to the cases starting with any other configurations

in the set. The only difference between the free vibrations starting from two equivalent configurations can be regarded as the result of changing the observation perspectives. This method is equivalent to identifying the group of symmetry operations which can leave the operators in the system equations of motion invariant.

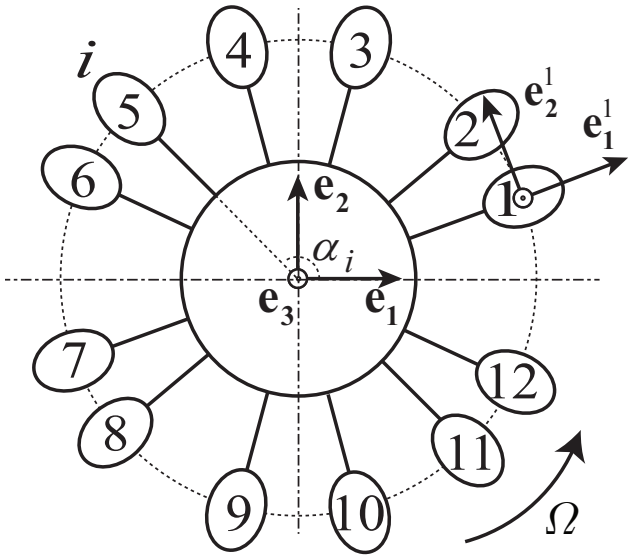

Figure 3.2: An example system with $\mathcal{D}_2$ symmetry. The ovals represent identical substructures and the circle is the vibrating central components. All the substructures and the vibrating central components are connected to a rotating ground (with rotational speed Ω) through stiffness. The reference frame $\{\mathbf{e}_1, \mathbf{e}_2, \mathbf{e}_3\}$ associated with the central component motions rotates at the same speed Ω. The axes $\mathbf{e}_1^i$ and $\mathbf{e}_2^i$ associated with the ith substructure defines the direction of substructure radial and tangential motions, and are oriented with a fixed angle, α^i, relative to the $\{\mathbf{e}_1, \mathbf{e}_2, \mathbf{e}_3\}$ basis.

To illustrate the identification of system symmetry, the symmetry of the system in Fig. 3.2 is analyzed. In this system, all substructures (the ovals) have two degrees of freedom, the planar radial and tangential motions, and the vibrating central component (the circle) has three planar degrees of freedom. The substructures are distributed in the four phases divided by the axes $\mathbf{e}_1$ and $\mathbf{e}_2$, and the geometry of the system is symmetric along the axes $\mathbf{e}_1$ and $\mathbf{e}_2$. The geometry of the system is brought into self-coincidence by four symmetry operations: identity (E), rotation by π along $\mathbf{e}_3$ (C_2), rotation by π along

$\mathbf{e}_1$ ($C_2^{(1)}$), and rotation by π along $\mathbf{e}_2$ ($C_2^{(2)}$). To consider the symmetry of the system, an arbitrary deflection of the system is given in Fig. 3.3(a), and the symmetry operations $C_2^{(1)}$, $C_2^{(2)}$, C_2 transform the deflection to the deflections in Fig. 3.3(b) , (c), and (d), respectively. For the case when the system rotational speed Ω is zero, the four deflections in Fig. 3.3 are equivalent because when they serve as initial conditions the free vibrations of the system are physically identical if the perspective of observers is changed according to the associated symmetry operation (the numbers in Fig. 3.3 are used to identify the change of observation perspective). Therefore, the symmetry group for the system with zero rotational speed contains four symmetry operations, E, $C_2^{(1)}$, $C_2^{(2)}$, C_2, and the group is $\mathcal{D}_2$ (a dihedral group). For the case when the system rotational speed is not zero, the Coriolis force influences the dynamics of the system. Because the rotational speed, as a system parameter, is not transformed by symmetry operations, only the deflection in Fig. 3.3(d) is equivalent to the deflection in Fig. 3.3(a). Therefore, the symmetry group for the system with non-zero rotational speed contains only two symmetry operations, E, C_2, and the system is cyclically symmetric ($\mathcal{C}_2$ symmetry).

Quantitative studies of a symmetry group rely on the concept of group representations. For a symmetry group $\mathcal{G} = \{A, B, \ldots, R, \ldots\}$ with g elements, a representation of $\mathcal{G}$ consists of g matrices $\{\mathbf{D}(A), \mathbf{D}(B), \ldots, \mathbf{D}(R), \ldots\}$ associated with the elements of the group in such a way that when $R \bullet S = T$ then $\mathbf{D}(R)\mathbf{D}(S) = \mathbf{D}(T)$. For example, three representations of $\mathcal{C}_3$ are shown as the rows in Table 3.1. All these three representations are one-dimensional, because each symmetry operation is represented by a scalar (one-dimensional matrix). (Therefore, they are also irreducible representations as defined later.) These rows can be verified as representations using the foregoing definition. For example, the relation

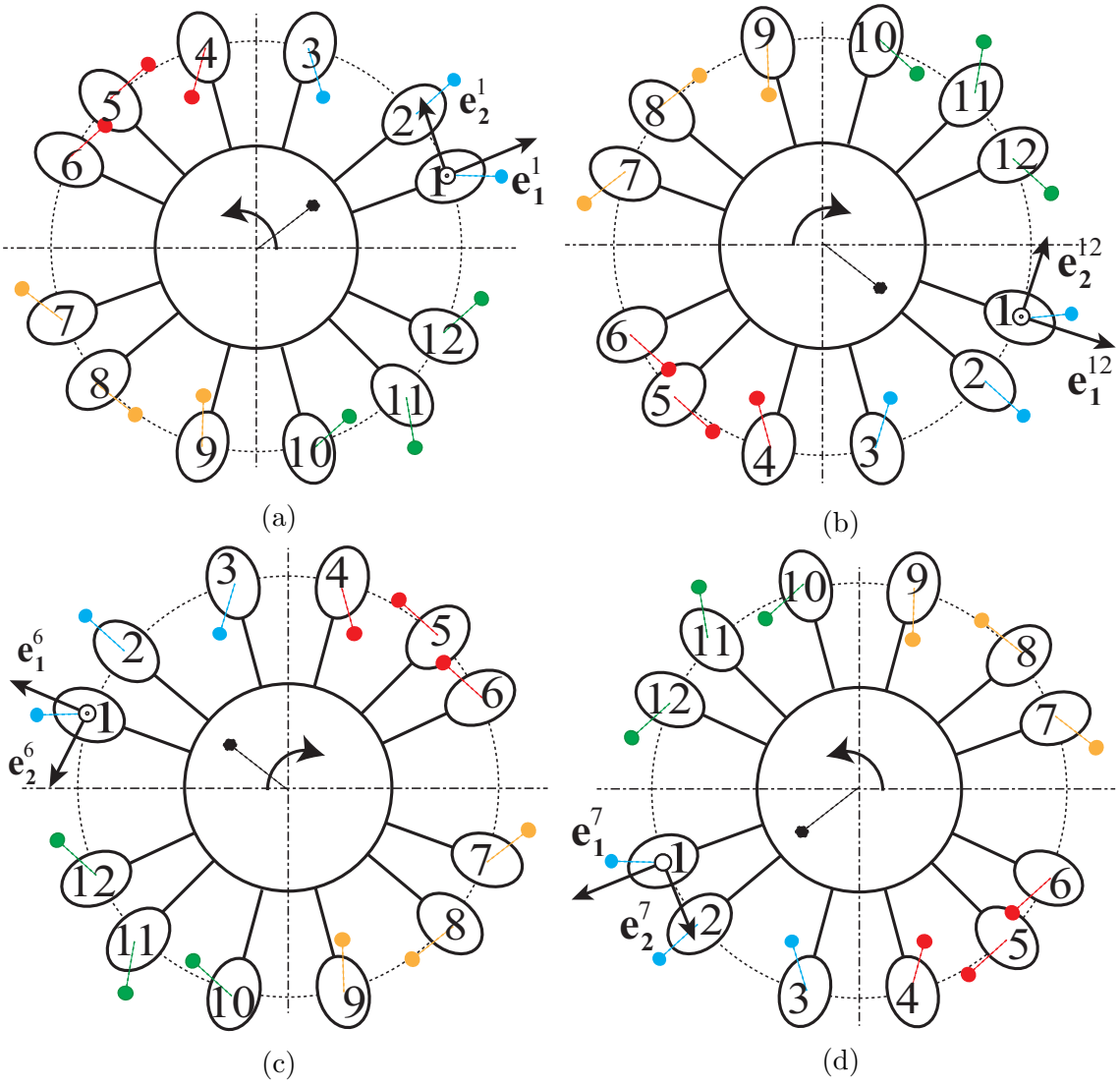

Figure 3.3: (a) An arbitrary deflection of the example system in Fig. 3.2. The dots represent the deflected position of the components and the curve with arrow represent the rotational deflection of the central component. (b), (c), and (d) are the three deflections obtained by transforming the deflection in (a) by symmetry operation $C_2^{(1)}$, $C_2^{(2)}$, and C_2, respectively.

$C_3 \bullet C_3^{-1} = E$ in the group $\mathcal{C}_3$ is quantitatively represented by the following equation,

$$\mathbf{D}^{(E_{11})}(C_3)\mathbf{D}^{(E_{11})}(C_3^{-1}) = e^{\frac{2\pi \mathrm{j}}{3}} e^{-\frac{2\pi \mathrm{j}}{3}} = 1 = \mathbf{D}^{(E_{11})}(E), \tag{3.1}$$

when the group elements in $\mathcal{C}_3$ are represented by the representations labeled as E_{11}.

Representation label	E	C_3	C_3^{-1}
A	1	1	1
E_{11}	1	$e^{\frac{2\pi \mathrm{j}}{3}}$	$e^{\frac{-2\pi \mathrm{j}}{3}}$
E_{22}	1	$e^{\frac{-2\pi \mathrm{j}}{3}}$	$e^{\frac{2\pi \mathrm{j}}{3}}$

Table 3.1: Irreducible representations of $\mathcal{C}_3$. Representations are named according to Ref. [1], and j is the imaginary unit.

Two properties about group representations are important.

1. If $\{\mathbf{D}(A), \mathbf{D}(B), \ldots, \mathbf{D}(R), \ldots\}$ is a representation of $\mathcal{G}$, $\{\tilde{\mathbf{D}}(A), \tilde{\mathbf{D}}(B), \ldots, \tilde{\mathbf{D}}(R), \ldots\}$ is also a representation of $\mathcal{G}$, where $\tilde{\mathbf{D}}(R) = \mathbf{U}^\dagger \mathbf{D}(R)\mathbf{U}$ and $\mathbf{U}$ is a unitary matrix ($\mathbf{U}^\dagger\mathbf{U} = \mathbf{I}$, where $\mathbf{U}^\dagger$ is the Hermitian transpose of $\mathbf{U}$). For the elements R, S, and T in $\mathcal{G}$ satisfying $R \bullet S = T$, the matrices $\tilde{\mathbf{D}}(R)$, $\tilde{\mathbf{D}}(S)$, and $\tilde{\mathbf{D}}(T)$ are related as

$$\tilde{\mathbf{D}}(R)\tilde{\mathbf{D}}(S) = \mathbf{U}^\dagger \mathbf{D}(R)\mathbf{U}\mathbf{U}^\dagger \mathbf{D}(S)\mathbf{U} = \mathbf{U}^\dagger \mathbf{D}(R)\mathbf{D}(S)\mathbf{U} = \mathbf{U}^\dagger \mathbf{D}(T)\mathbf{U} = \tilde{\mathbf{D}}(T). \tag{3.2}$$

   The two representations ($\{\mathbf{D}(A), \mathbf{D}(B), \ldots, \mathbf{D}(R), \ldots\}$ and $\{\tilde{\mathbf{D}}(A), \tilde{\mathbf{D}}(B), \ldots, \tilde{\mathbf{D}}(R), \ldots\}$) are said to be *equivalent*.

2. From any two representations of $\mathcal{G}$, $\{\mathbf{D}^{(\alpha)}(A), \ldots, \mathbf{D}^{(\alpha)}(R), \ldots\}$ and $\{\mathbf{D}^{(\beta)}(A), \ldots, \mathbf{D}^{(\beta)}(R), \ldots\}$, a new representation is formed from the *direct sums* of the matrices in these two rep-

resentations, *i.e.*,

$$\left\{ \begin{pmatrix} \mathbf{D}^{(\alpha)}(A) & \mathbf{0} \\ \mathbf{0} & \mathbf{D}^{(\beta)}(A) \end{pmatrix}, \ \ldots, \begin{pmatrix} \mathbf{D}^{(\alpha)}(R) & \mathbf{0} \\ \mathbf{0} & \mathbf{D}^{(\beta)}(R) \end{pmatrix}, \ \ldots \right\}. \tag{3.3}$$

Based on the two properties above, any representation of a group is either equivalent to the direct sum of some lower-dimensional representations (meaning all the matrices in the representation can be block diagonalized by a unitary transformation), or *irreducible* as the simplest form that can not be further block diagonalized through a unitary transformation. For example, the representations of $\mathcal{C}_3$ in Table 3.1 are all one-dimensional and so irreducible, because they can not be further block diagonalized. Deriving irreducible representations for any symmetry group is usually unnecessary, because the irreducible representations of the typical symmetry groups are available in mathematics literature [1, 52].

Knowing the irreducible representations of a symmetry group, the configuration space of the system with the group symmetry can be decomposed into subspaces, onto which the original problem can be projected as problems with smaller size and be solved separately. To explain this methodology, the decomposition of the configuration space is discussed for discrete and continuous systems separately as follows.

For a discrete symmetric system, the configuration of the system is described by a vector whose elements are the values of the system deflections. For any deflection $\mathbf{v}$ of the symmetric system, the following quantities

$$\sum_R \mathbf{D}^{(\gamma)}(R^{-1})^T_{l1} R\mathbf{v}, \ \ \sum_R \mathbf{D}^{(\gamma)}(R^{-1})^T_{l2} R\mathbf{v}, \ \ \ldots, \ \ \sum_R \mathbf{D}^{(\gamma)}(R^{-1})^T_{lg_\gamma} R\mathbf{v}, \ \ l = 1, 2, ..., g_\gamma, \tag{3.4}$$

can be calculated with respect to an irreducible representation of the symmetry group, where $R\mathbf{v}$ is the deflection transformed by performing the operation R on $\mathbf{v}$, γ is the dummy index

for irreducible representation labels, $\mathbf{D}^{(\gamma)}(R^{-1})_{li}$ is the element in the lth row and the ith column of $\mathbf{D}^{(\gamma)}(R^{-1})$, and g_γ is the dimension of the matrix $\mathbf{D}^{(\gamma)}(R^{-1})$. According to the group theory, no matter what deflection $\mathbf{v}$ and index l are selected, the resulting quantities in Eq. (3.4) are always in g_γ separate subspaces. Meanwhile, the subspaces generated by the irreducible representation γ are also separated from those generated by any other irreducible representations. Therefore, the full configuration space is decomposed into $W = \sum_\gamma g_\gamma$ subspaces. The basis for the ith subspace generated by the irreducible representation γ are denoted as $\{\mathbf{u}_1^{(\gamma,i)},\ \mathbf{u}_2^{(\gamma,i)},\ \ldots,\ \mathbf{u}_{g_{(\gamma,i)}}^{(\gamma,i)}\}$, where $g_{(\gamma,i)}$ is the number of basis vectors. With each vector in the basis being normalized such that

$$\mathbf{u}_\mu^{(\gamma,i)\dagger}\mathbf{u}_\mu^{(\gamma,i)} = 1,\ \mu = 1, 2, \ldots, g_{(\gamma,i)}, \tag{3.5}$$

these basis vectors are called *symmetry vectors*, $\mathbf{u}_\mu^{(\gamma,i)}$ is said to be of *symmetry species* (γ, i), and the basis is a *symmetry-adapted basis* for the subspace of symmetry species (γ, i). By calculating the set of quantities in Eq. (3.4) for each irreducible representation, all symmetry vectors are obtained for the symmetric system. They form a matrix with the following structure,

$$\begin{aligned}\mathbf{U} &= \Big(\underbrace{\mathbf{u}_1^{(\alpha,1)}\ \mathbf{u}_2^{(\alpha,1)}\ \ldots}_{\text{Species } (\alpha,1)}\ \underbrace{\mathbf{u}_1^{(\alpha,2)}\ \mathbf{u}_2^{(\alpha,2)}\ \ldots}_{\text{Species } (\alpha,2)}\ \ldots\ \underbrace{\mathbf{u}_1^{(\beta,1)}\ \mathbf{u}_2^{(\beta,1)}\ \ldots}_{\text{Species } (\beta,1)}\ \underbrace{\ldots}_{etc.}\Big) \\ &= \Big(\underbrace{\mathbf{U}^{(\alpha,1)}\quad \mathbf{U}^{(\alpha,2)}\quad \ldots\quad \mathbf{U}^{(\beta,1)}\quad \ldots}_{W\,submatrices}\Big).\end{aligned} \tag{3.6}$$

Based on group theory [1], the matrix $\mathbf{U}$ in Eq. (3.6) has the following properties,

$$\mathbf{U}^\dagger\mathbf{U} = \mathbf{I}, \tag{3.7a}$$

$$\mathbf{U}^{(\gamma,i)\dagger}\mathbf{A}\mathbf{U}^{(\rho,h)} = \begin{cases} \mathbf{0} & \gamma \neq \rho \text{ or } i \neq h \\ \tilde{\mathbf{A}}^{(\gamma,i)} & \gamma = \rho \text{ and } i = h \end{cases}, \tag{3.7b}$$

where $\mathbf{A}$ is the operator in the full system eigenvalue problem,

$$\mathbf{A}(\lambda)\boldsymbol{\phi} = [\lambda^2\mathbf{M} + \lambda\mathbf{C} + \mathbf{K}]\boldsymbol{\phi} = \mathbf{0}. \tag{3.8}$$

The matrix operator $\mathbf{A}$ is a polynomial of the eigenvalue λ, including the inertia matrix $\mathbf{M}$, the damping matrix $\mathbf{C}$, and the stiffness matrix $\mathbf{K}$, (and these matrices are not necessary to be symmetric). The property in Eq. (3.7b) is defined as the orthogonality of symmetry species, and it provides a benefit of reducing the size of the eigenvalue problem. Firstly, because the columns of $\mathbf{U}$ in Eq. (3.6) form a basis for the configuration space, the eigenvector $\boldsymbol{\phi}$ can be expanded as a linear combination of the columns of $\mathbf{U}$,

$$\boldsymbol{\phi} = \mathbf{U}\hat{\boldsymbol{\phi}} = \begin{pmatrix} \mathbf{U}^{(\alpha,1)} & \mathbf{U}^{(\alpha,2)} & \dots & \mathbf{U}^{(\beta,1)} & \dots \end{pmatrix} \hat{\boldsymbol{\phi}}. \tag{3.9}$$

The coefficients (elements in the vector $\hat{\boldsymbol{\phi}}$) of this combination are the unknowns to be solved. Substitution of Eq. (3.9) into Eq. (3.8) and pre-multiplication by the Hermitian of $\mathbf{U}$ give

$$\mathbf{U}^\dagger\mathbf{A}\mathbf{U}\hat{\boldsymbol{\phi}} = \tilde{\mathbf{A}}\hat{\boldsymbol{\phi}} = \begin{pmatrix} \tilde{\mathbf{A}}^{(\alpha,1)} & & & & \\ & \tilde{\mathbf{A}}^{(\alpha,2)} & & & \\ & & \ddots & & \\ & & & \tilde{\mathbf{A}}^{(\beta,1)} & \\ & & & & \ddots \end{pmatrix} \begin{pmatrix} \hat{\boldsymbol{\phi}}^{(\alpha,1)} \\ \hat{\boldsymbol{\phi}}^{(\alpha,2)} \\ \vdots \\ \hat{\boldsymbol{\phi}}^{(\beta,1)} \\ \vdots \end{pmatrix} = 0, \tag{3.10}$$

where $(\hat{\boldsymbol{\phi}}^{(\alpha,1)}, \hat{\boldsymbol{\phi}}^{(\alpha,2)}, \dots, \hat{\boldsymbol{\phi}}^{(\beta,1)}, \dots)^T = \hat{\boldsymbol{\phi}}$. The eigenvalues in Eq. (3.10) are identical to those in Eq. (3.8) because $\mathbf{U}$ is unitary. Solving Eq. (3.10) is equivalent to solving W

(number of symmetry species) reduced eigenvalue problems,

$$\tilde{\mathbf{A}}^{(\gamma,i)}\hat{\boldsymbol{\phi}}^{(\gamma,i)} = \mathbf{0}, \tag{3.11a}$$

$$\tilde{\mathbf{A}}^{(\gamma,i)} = \mathbf{U}^{(\gamma,i)\dagger}\mathbf{A}\mathbf{U}^{(\gamma,i)}, \tag{3.11b}$$

because every eigensolution $(\lambda, \hat{\boldsymbol{\phi}}^{(\gamma,i)})$ of Eq. (3.11) can generate an eigensolution of Eq. (3.10), where the eigenvalue is λ, and the eigenvector is

$$\hat{\boldsymbol{\phi}} = (\mathbf{0}, \ldots, \mathbf{0}, \hat{\boldsymbol{\phi}}^{(\gamma,i)}, \mathbf{0}, \ldots, \mathbf{0})^T. \tag{3.12}$$

Therefore, the eigenvalues of the W reduced eigenvalue problems in Eq. (3.11) are also the eigenvalues of the full eigenvalue problem in Eq. (3.8). Meanwhile, substitution of Eq. (3.12) into Eq. (3.9) gives

$$\boldsymbol{\phi} = \mathbf{U}^{(\gamma,i)}\hat{\boldsymbol{\phi}}^{(\gamma,i)}, \tag{3.13}$$

which indicates the eigenvectors solved from Eq. (3.11) generate full system eigenvectors.

For a continuous system, the configuration of the system is described by a vector consisting of functions, *i.e.*, the configuration $\mathbf{v}$ of the symmetric system is

$$\mathbf{v} = \begin{pmatrix} f_1(\mathbf{r}) \\ f_2(\mathbf{r}) \\ \vdots \\ f_n(\mathbf{r}) \end{pmatrix}, \tag{3.14}$$

where $f_m(\mathbf{r})$ is a function of the position vector $\mathbf{r}$ (such a function is referred to as a field) and n is the number of such functions (fields) in $\mathbf{v}$. For the mth field $f_m(\mathbf{r})$ in Eq. (3.14), $f_m(\mathbf{r})$ can be written as a linear combination of the basis functions that spans the function

space, *i.e.,*

$$f_m(\mathbf{r}) = \sum_{l=1}^{\infty} c_{m,l}\psi_{m,l}(\mathbf{r}), \tag{3.15}$$

where $\psi_{m,1}$, $\psi_{m,2}$, ... form a complete set of basis functions on the domain of the field $f_m(\mathbf{r})$. The full configuration space is the sum of the extended vector spaces that are obtained by extending all the function spaces for all the field functions. Specifically, the basis of the full configuration space is

$$\begin{aligned}
&\left\{\mathbf{\Psi}_{1,1}, \mathbf{\Psi}_{1,2}, \ldots, \mathbf{\Psi}_{2,1}, \mathbf{\Psi}_{2,2}, \ldots, \mathbf{\Psi}_{n,1}, \mathbf{\Psi}_{n,2}, \ldots,\right\} \\
&= \left\{ \begin{pmatrix} \psi_{1,1} \\ 0 \\ \vdots \\ 0 \end{pmatrix}, \begin{pmatrix} \psi_{1,2} \\ 0 \\ \vdots \\ 0 \end{pmatrix}, \ \ldots, \begin{pmatrix} 0 \\ \psi_{2,1} \\ \vdots \\ 0 \end{pmatrix}, \begin{pmatrix} 0 \\ \psi_{2,2} \\ \vdots \\ 0 \end{pmatrix}, \ \ldots, \begin{pmatrix} 0 \\ 0 \\ \vdots \\ \psi_{n,1} \end{pmatrix}, \begin{pmatrix} 0 \\ 0 \\ \vdots \\ \psi_{n,2} \end{pmatrix}, \ \ldots \right\}.
\end{aligned} \tag{3.16}$$

Analogous to the decomposition of configuration space for a discrete system, by calculating the quantities in Eq. (3.4) with respect to the irreducible representation γ, g_γ separate subspaces of the full configuration space is generated, and the full configuration space is decomposed into $W = \sum_\gamma g_\gamma$ subspaces. The basis for the ith subspace generated by the irreducible representation γ is denoted as $\{\mathbf{u}_1^{(\gamma,i)}, \ \mathbf{u}_2^{(\gamma,i)}, \ \ldots,\}$, but the elements in these basis vectors are fields in general, instead of scalars as in the case for discrete systems. These basis vectors, although each element in them are functions in general, are said to be of the symmetry species (γ, i), and the basis is the symmetry-adapted basis in context of continuous systems. All the symmetry-adapted basis vectors of all the symmetry species span the full configuration space.

The eigenvalue problem of a continuous system can be written in a general form,

$$\mathbf{L}(\lambda)\boldsymbol{\phi} = \mathbf{0}, \tag{3.17}$$

where $\mathbf{L}$ is an operator for multiple degrees of freedom, and it is a polynomial of the eigenvalue λ. To solve the eigenvalue problem numerically, the complete set of basis functions for the function space of $f_m(\mathbf{r})$ in Eq. (3.15) is truncated by selecting L_m basis functions only. $f_m(\mathbf{r})$ in Eq. (3.15) is approximated as

$$f_m(\mathbf{r}) = \sum_{l=1}^{L_m} c_{m,l}\psi_{m,l}(\mathbf{r}), \tag{3.18}$$

and the complete set of basis vectors that span the full configuration space is consequently truncated as

$$\left\{ \boldsymbol{\Psi}_{1,1}, \boldsymbol{\Psi}_{1,2}, \ldots, \boldsymbol{\Psi}_{1,L_1}, \boldsymbol{\Psi}_{2,1}, \boldsymbol{\Psi}_{2,2}, \ldots, \boldsymbol{\Psi}_{2,L_2}, \ldots, \boldsymbol{\Psi}_{n,1}, \boldsymbol{\Psi}_{n,2}, \ldots, \boldsymbol{\Psi}_{n,L_n} \right\}. \tag{3.19}$$

The eigenvector $\boldsymbol{\phi}$ in Eq. (3.17) is expanded as a linear combination of the basis vectors in Eq. (3.19),

$$\boldsymbol{\phi} = \sum_{m=1}^{n} \sum_{l=1}^{L_m} a_{m,l}\boldsymbol{\Psi}_{m,l}. \tag{3.20}$$

Through weighted residual methods, such as the Galerkin method, Eq. (3.17) can be discretized into a matrix form, where the dimension of the matrices is the total number of basis vectors in the truncated set, $\sum_{m=1}^{n} L_m$. The discretization in weighted residual methods is omitted in this work, but it can be found in Ref. [102].

To reduce the size of the discretized eigenvalue problem, the configuration subspace spanned by the truncated set of basis vectors in Eq. (3.19) are decomposed into $W = \sum_\gamma g_\gamma$ subspaces by substitution of Eq. (3.20) into Eq. (3.14) and calculation of the quantities in

Eq. (3.4). The symmetry-adapted basis for the ith subspace generated by the irreducible representation γ is $\{\mathbf{u}_1^{(\gamma,i)},\ \mathbf{u}_2^{(\gamma,i)},\ \ldots,\mathbf{u}_{g_{(\gamma,i)}}^{(\gamma,i)}\}$. $g_{(\gamma,i)}$ is the number of basis vectors of symmetry species (γ,i), and the sum of $g_{(\gamma,i)}$ for all symmetry species is equal to the number of basis vectors in Eq. (3.19), *i.e.*,

$$\sum_{(\gamma,i)} g_{(\gamma,i)} = \sum_{m=1}^{n} L_m, \tag{3.21}$$

According to group theory, all the eigenvectors $\boldsymbol{\phi}$ in Eq. (3.17) is a linear combination of the basis vectors of one symmetry species only,

$$\boldsymbol{\phi} = \sum_{l=1}^{g_{(\gamma,i)}} b_l^{(\gamma,i)} \mathbf{u}_l^{(\gamma,i)}. \tag{3.22}$$

Based on this expansion of eigenvectors, Eq. (3.17) can be discretized into a matrix form for each symmetry species (γ,i), where the dimension of the matrices for the symmetry species (γ,i) is $g_{(\gamma,i)}$. Therefore, the discretized eigenvalue problem with dimension $\sum_{m=1}^{n} L_m$ by using the basis in Eq. (3.19) is decomposed into W reduced eigenvalue problems.

By comparing the applications of group theory to discrete and continuous systems, the methodology for discrete systems can be regarded as a more special case of the one for continuous systems, where $\mathbf{L}(\lambda)$ in Eq. (3.17) is a matrix of numbers, $f_m(\mathbf{r})$ in Eq. (3.14) is a number, the domain of $f_m(\mathbf{r})$ is a single point, and the expansion in Eq. (3.15) can be written as $f_m(\mathbf{r}) = c_m$ because the basis of a function space on a single point includes only one basis function which values 1 on the domain point. Therefore, the decomposition of configuration space into subspaces spanned by symmetry-adapted basis vectors can be performed for discrete, continuous, and hybrid continuous-discrete systems, as long as the system symmetry is identified.

Once the symmetry-adapted basis vectors are obtained, two general benefits are provided immediately. Firstly, the computation efficiency for solving the eigenvalue problem

is improved. The original eigenvalue problem in the full configuration space is now decomposed into $W = \sum_\gamma g_\gamma$ independent reduced problems, and each reduced eigenvalue problem is obtained by projecting the original eigenvalue problem onto the subspace spanned by the symmetry-adapted basis of a symmetry species. The dimension of each reduced eigenvalue problem is the number of basis vectors in the symmetry-adapted basis of each symmetry species ($g_{(\gamma,i)}$ in the foregoing discussion).

Secondly, the modal properties of a symmetric system are obtained once its symmetry-adapted basis vectors are known. Eqs. (3.13) and (3.22) indicate any full system eigenvector is a linear combination of symmetry-adapted basis vectors of one symmetry species only. Once all symmetry species are obtained, the vibration modes of the symmetric system can be classified into different types corresponding to the different symmetry species. The vibration modes of a given type have the properties of the symmetry-adapted basis vectors of the symmetry species that defines the mode type. The number of mode types (W), number of modes in each type ($g_{(\gamma,i)}$), and the characteristic modal deflection in each mode type are all available. Such analysis can be done by algorithmic and computationally inexpensive calculations (*i.e.*, by calculating the quantities in Eq. (3.4)) instead of numerically solving the original eigenvalue problem in Eq. (3.8) or Eq. (3.17), which is computationally expensive. Even if one solved the eigenvalue problem in Eq. (3.8) or Eq. (3.17), the vibration modes are not separated into types, nor the modal properties are naturally revealed. Because the calculations only involve the system symmetry and the definitions of the degrees of freedom, the system equation of motion are not even necessary to determine the modal properties.

3.2.2 Example: Systems with $\mathcal{D}_2$ Symmetry in Fig. 3.2

To illustrate the application of group theory, the system in Fig. (3.2) is solved as an example. As discussed earlier, the system has the $\mathcal{D}_2$ symmetry when the rotational speed Ω is zero, and the following discussion in this section is for this non-gyroscopic case. The system parameters are given in Tables 3.5 and 3.6, and the equation of motion is formulated in Eqs. (3.55) and (3.56).

To obtain symmetry-adapted basis vectors (symmetry vectors for discrete systems), the generalized coordinate vector $\mathbf{q}$ in Eq. (3.55) is used as the vector $\mathbf{v}$ in Eq. (3.4). For this example, $\mathbf{q}$ in Eq. (3.55) is

$$\mathbf{q} = (\underbrace{x_c, y_c, \mu_c}_{\mathbf{q}_c}, \underbrace{r_1, s_1}_{\mathbf{q}_{s_1}}, \underbrace{r_2, s_2}_{\mathbf{q}_{s_2}}, \ldots, \underbrace{r_{12}, s_{12}}_{\mathbf{q}_{s_{12}}})^T. \tag{3.23}$$

where the subvector $\mathbf{q}_c$ contains three planar degrees of freedom of the vibrating central component, and the $\mathbf{q}_{s_i}$ contains two planar translations the ith substructure (r denotes the radial translation and s denotes the tangential translation). From Fig. (3.3), the deflections transformed by different symmetry operations can be obtained. The transformed deflections for the central component can be directly obtained from observation, as tabulated in Table 3.2. To consider the transformed configurations of the substructures, all substructures are can be divided into several sets because of the system symmetry, and the substructures in each set can coincide with each other by symmetry operations. For example, the 1st, 6th, 7th, and 12th substructures are in one set. As shown in Fig. (3.3), by different symmetry operations, the deflections of a substructure are 'passed' to the substructures in the same set, and the transformed deflections can have different values from the untransformed ones, because they are measured in the coordinate system of the substructure that 'receives' the deflection. For example, by the symmetry operation $C_2^{(1)}$, the deflections of the first substructure are

'passed' to the 12th substructure, and the deflection subvector for that are measured under the frame $\{\mathbf{e}_1^{12}, \mathbf{e}_2^{12}\}$ is $(r_1, -s_1)^T$. The transformed subvector for all the substructures by the symmetry operation $C_2^{(1)}$ is,

$$\begin{aligned} C_2^{(1)}\mathbf{q}_s =& C_2^{(1)}(\mathbf{q}_{s_1}, \ldots, \mathbf{q}_{s_{12}})^T \\ =& (r_{12}, -s_{12}, r_{11}, -s_{11}, r_{10}, -s_{10}, r_9, -s_9, r_8, -s_8, r_7, -s_7, \\ & r_6, -s_6, r_5, -s_5, r_4, -s_4, r_3, -s_3, r_2, -s_2, r_1, -s_1)^T. \end{aligned} \tag{3.24}$$

To avoid this long vector form of $C_2^{(1)}\mathbf{q}_s$ in Eq. (3.24), the relation between $C_2^{(1)}\mathbf{q}_s$ and $\mathbf{q}_s$ can be written as,

$$C_2^{(1)}\mathbf{q}_s = \mathbf{D}(C_2^{(1)})\mathbf{q}_s, \tag{3.25a}$$

$$\mathbf{D}(C_2^{(1)}) = \begin{pmatrix} 0 & 0 & 0 & 1 \\ 0 & 0 & 1 & 0 \\ 0 & 1 & 0 & 0 \\ 1 & 0 & 0 & 0 \end{pmatrix} \otimes \mathbf{I}_{f,3} \otimes \mathbf{J}, \tag{3.25b}$$

$$\mathbf{J}_2 = \begin{pmatrix} 1 & 0 \\ 0 & -1 \end{pmatrix}, \ \mathbf{I}_{f,N} = \begin{pmatrix} 0 & 0 & \ldots & 0 & 1 \\ 0 & 0 & \ldots & 1 & 0 \\ \vdots & \vdots & \iddots & \vdots & \vdots \\ 0 & 1 & \ldots & 0 & 0 \\ 1 & 0 & \ldots & 0 & 0 \end{pmatrix}, \tag{3.25c}$$

where $\mathbf{I}_N$ is the N-dimensional identity matrix, $\mathbf{I}_{f,N}$ is the N-dimensional flipped identity matrix, $\otimes$ is the direct product [26]. Similarly, the transformed subvector for all the

substructures by the other symmetry operations in $\mathcal{D}_2$ can be obtained as

$$E\mathbf{q}_s = \mathbf{D}(E)\mathbf{q}_s,\ \mathbf{D}(E) = \begin{pmatrix} 1 & 0 & 0 & 0 \\ 0 & 1 & 0 & 0 \\ 0 & 0 & 1 & 0 \\ 0 & 0 & 0 & 1 \end{pmatrix} \otimes \mathbf{I}_3 \otimes \mathbf{I}_2, \tag{3.26a}$$

$$C_2^{(2)}\mathbf{q}_s = \mathbf{D}(C_2^{(2)})\mathbf{q}_s,\ \mathbf{D}(C_2^{(2)}) = \begin{pmatrix} 0 & 1 & 0 & 0 \\ 1 & 0 & 0 & 0 \\ 0 & 0 & 0 & 1 \\ 0 & 0 & 1 & 0 \end{pmatrix} \otimes \mathbf{I}_{f,3} \otimes \mathbf{J}, \tag{3.26b}$$

$$C_2\mathbf{q}_s = \mathbf{D}(C_2)\mathbf{q}_s,\ \mathbf{D}(C_2^{(2)}) = \begin{pmatrix} 0 & 0 & 1 & 0 \\ 0 & 0 & 0 & 1 \\ 1 & 0 & 0 & 0 \\ 0 & 1 & 0 & 0 \end{pmatrix} \otimes \mathbf{I}_3 \otimes \mathbf{I}_2. \tag{3.26c}$$

The transformed deflection for the whole system by the operation R in the group $\mathcal{D}_2$ can be obtained by assembling the transformed deflections of the central component and the substructures in Table 3.2 through the relation

$$R\mathbf{q} = \begin{pmatrix} R\mathbf{q}_c \\ R\mathbf{q}_s \end{pmatrix},\ \text{for } R \in \mathcal{D}_2. \tag{3.27}$$

The calculation of the quantities in Eq. (3.4) is then performed with respect to each irreducible representation of the group $\mathcal{D}_2$. As tabulated in Table 3.3, there are four irreducible representations of the $\mathcal{D}_2$ group, and all of them are one-dimensional because each symmetry operation is represented by a scalar (one-dimensional matrix). Because all the irreducible

Transformed Vector $R\mathbf{q}$	Central Component $R\mathbf{q}_c$	Substructures $R\mathbf{q}_s$
$E\mathbf{q}$	$(x_c, y_c, \mu_c)^T$	$\mathbf{D}(E)\mathbf{q}_s$
$C_2^{(1)}\mathbf{q}$	$(x_c, -y_c, -\mu_c)^T$	$\mathbf{D}(C_2^{(1)})\mathbf{q}_s$
$C_2^{(2)}\mathbf{q}$	$(-x_c, y_c, -\mu_c)^T$	$\mathbf{D}(C_2^{(2)})\mathbf{q}_s$
$C_2\mathbf{q}$	$(-x_c, -y_c, \mu_c)^T$	$\mathbf{D}(C_2)\mathbf{q}_s$

Table 3.2: Transformed vector of $\mathbf{q}$ by symmetry operations in group $\mathcal{D}_2$.

Representation label	E	$C_2^{(1)}$	$C_2^{(2)}$	C_2
A	1	1	1	1
B1	1	-1	-1	1
B2	1	-1	1	-1
B3	1	1	-1	-1

Table 3.3: Irreducible representations of $\mathcal{D}_2$ [1].

representations are one-dimensional ($g_\gamma = 1$), the quantity series in Eq. (3.4) contains only one item. Consequently, the calculation of the one quantity in Eq. (3.4) with respect to each irreducible representation (labeled as γ) yields only one subspace of the symmetry species (γ,1). For example, based on Eqs. (3.25)-(3.27) and Table 3.2, the quantity in Eq. (3.4) with respect to the irreducible representation A in Table 3.3 is

$$
\begin{aligned}
&\sum_R \mathbf{D}^{(A)}(R^{-1})^T\mathbf{q} \\
=&1\times\begin{pmatrix} x_c \\ y_c \\ \mu_c \\ \mathbf{D}(E)\mathbf{q}_s \end{pmatrix} + 1\times\begin{pmatrix} x_c \\ -y_c \\ -\mu_c \\ \mathbf{D}(C_2^{(1)})\mathbf{q}_s \end{pmatrix} + 1\times\begin{pmatrix} -x_c \\ y_c \\ -\mu_c \\ \mathbf{D}(C_2^{(2)})\mathbf{q}_s \end{pmatrix} + 1\times\begin{pmatrix} -x_c \\ -y_c \\ \mu_c \\ \mathbf{D}(C_2)\mathbf{q}_s \end{pmatrix} \\
=&\begin{pmatrix} \mathbf{0}_{3\times 1} \\ \\ \hat{\mathbf{D}}^{(A)}\mathbf{q}_s \end{pmatrix},
\end{aligned}
\tag{3.28}
$$

where

$$\hat{\mathbf{D}}^{(A)} = \begin{pmatrix} \mathbf{I}_3 \otimes \mathbf{I}_2 & \mathbf{I}_{f,3} \otimes \mathbf{J} & \mathbf{I}_3 \otimes \mathbf{I}_2 & \mathbf{I}_{f,3} \otimes \mathbf{J} \\ \mathbf{I}_{f,3} \otimes \mathbf{J} & \mathbf{I}_3 \otimes \mathbf{I}_2 & \mathbf{I}_{f,3} \otimes \mathbf{J} & \mathbf{I}_3 \otimes \mathbf{I}_2 \\ \mathbf{I}_3 \otimes \mathbf{I}_2 & \mathbf{I}_{f,3} \otimes \mathbf{J} & \mathbf{I}_3 \otimes \mathbf{I}_2 & \mathbf{I}_{f,3} \otimes \mathbf{J} \\ \mathbf{I}_{f,3} \otimes \mathbf{J} & \mathbf{I}_3 \otimes \mathbf{I}_2 & \mathbf{I}_{f,3} \otimes \mathbf{J} & \mathbf{I}_3 \otimes \mathbf{I}_2 \end{pmatrix}. \tag{3.29}$$

For any arbitrary deflection $\mathbf{q}$, all possible quantity in Eq. (3.28) are contained in a subspace spanned by the symmetry-adapted basis (symmetry vectors) of the symmetry species $(A, 1)$. Based on the structure of the right-hand-side of Eq. (3.28), the symmetry-adapted basis (symmetry vectors) is obtained if the set of all linearly independent columns in $\hat{\mathbf{D}}^{(A)}$ is known. By simple algebraic calculations, columns of $\hat{\mathbf{D}}^{(A)}$ in Eq. (3.29) can only provided 6 linearly independent columns and they are contained in the first column of blocks $(\mathbf{I}_3 \otimes \mathbf{I}_2,\ \mathbf{I}_{f,3} \otimes \mathbf{J},\ \mathbf{I}_3 \otimes \mathbf{I}_2,\ \mathbf{I}_{f,3} \otimes \mathbf{J})^T$. On normalization (Eq. (3.5)), the symmetry-adapted basis for species (A,1) is obtained. Similarly, another three symmetry-adapted bases can be obtained in the same procedure, and the unitary transformation matrix with the structure in Eq. (3.6) is written as

$$\mathbf{U}_{\mathcal{D}_2} = \begin{pmatrix} \mathbf{U}_{\mathcal{D}_2}^{(A,1)} & \mathbf{U}_{\mathcal{D}_2}^{(B1,1)} & \mathbf{U}_{\mathcal{D}_2}^{(B2,1)} & \mathbf{U}_{\mathcal{D}_2}^{(B3,1)} \end{pmatrix}, \tag{3.30a}$$

$$\mathbf{U}_{\mathcal{D}_2}^{(A,1)} = \frac{1}{2}\begin{pmatrix} \mathbf{0} \\ \hdashline \mathbf{I}_3 \otimes \mathbf{I}_2 \\ \mathbf{I}_{f,3} \otimes \mathbf{J}_2 \\ \mathbf{I}_3 \otimes \mathbf{I}_2 \\ \mathbf{I}_{f,3} \otimes \mathbf{J}_2 \end{pmatrix}, \quad \mathbf{U}_{\mathcal{D}_2}^{(B1,1)} = \frac{1}{2}\left(\begin{array}{c:c} 0 & \\ 0 & \mathbf{0} \\ 2 & \\ \hdashline & \mathbf{I}_3 \otimes \mathbf{I}_2 \\ & -\mathbf{I}_{f,3} \otimes \mathbf{J}_2 \\ \mathbf{0} & \mathbf{I}_3 \otimes \mathbf{I}_2 \\ & -\mathbf{I}_{f,3} \otimes \mathbf{J}_2 \end{array}\right),$$

$$\mathbf{U}_{\mathcal{D}_2}^{(B2,1)} = \frac{1}{2}\left(\begin{array}{c:c} 0 & \\ 2 & \mathbf{0} \\ 0 & \\ \hdashline & \mathbf{I}_3 \otimes \mathbf{I}_2 \\ & \mathbf{I}_{f,3} \otimes \mathbf{J}_2 \\ \mathbf{0} & -\mathbf{I}_3 \otimes \mathbf{I}_2 \\ & -\mathbf{I}_{f,3} \otimes \mathbf{J}_2 \end{array}\right), \mathbf{U}_{\mathcal{D}_2}^{(B3,1)} = \frac{1}{2}\left(\begin{array}{c:c} 2 & \\ 0 & \mathbf{0} \\ 0 & \\ \hdashline & \mathbf{I}_3 \otimes \mathbf{I}_2 \\ & -\mathbf{I}_{f,3} \otimes \mathbf{J}_2 \\ \mathbf{0} & -\mathbf{I}_3 \otimes \mathbf{I}_2 \\ & \mathbf{I}_{f,3} \otimes \mathbf{J}_2 \end{array}\right). \tag{3.30b}$$

Although the unitary matrix in Eq. (3.30) is generated for a specific system, the formulation can be generalized to a system with $\mathcal{D}_2$ symmetry, which consists of one planar rigid-body central component and $N = 4N_q$ substructures (N_q is the number of substructure in one quadrant). In such a case, the only modification in Eq. (3.30) is to replace the number of substructures in one quadrant (3) by N_q.

With the unitary matrix in Eq. (3.30), the modal properties of the example system in Fig. 3.2 are known without numerically solving the eigenvalue problem. Because there are four symmetry species in the unitary matrix, four types of modes can exist. One type of modes are linear combinations of symmetry vectors in $\mathbf{U}_{\mathcal{D}_2}^{(A,1)}$, and six modes fall into this category because the subspace is spanned by six columns of $\mathbf{U}_{\mathcal{D}_2}^{(A,1)}$. All of these modes

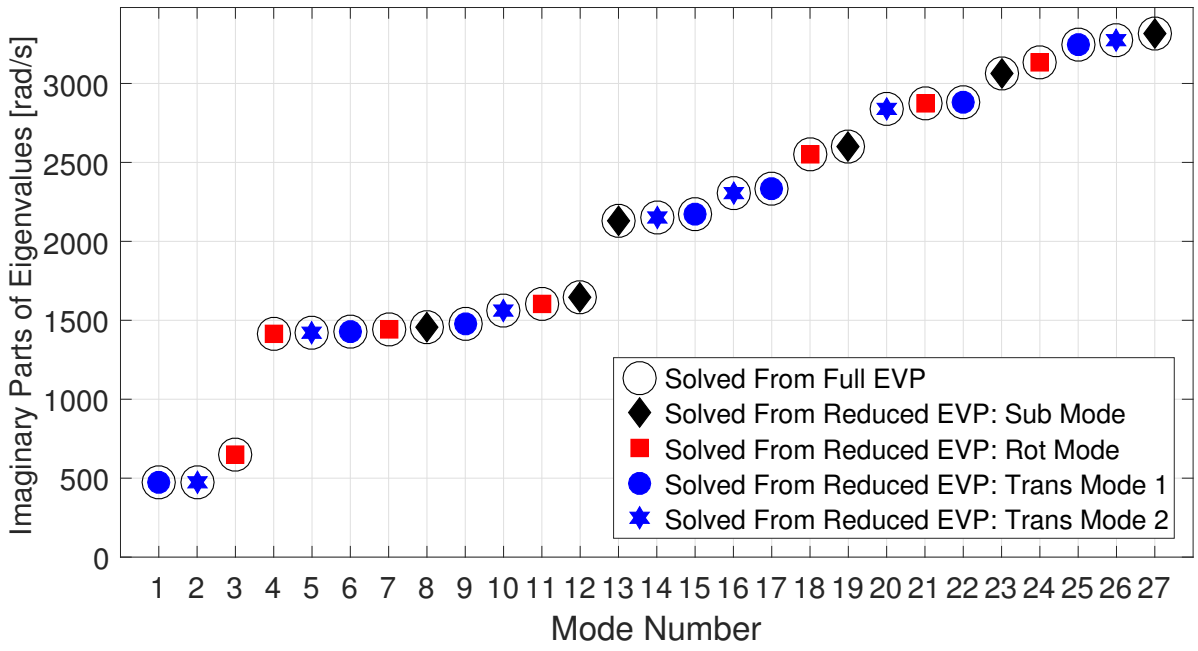

Figure 3.4: Natural frequencies of the example system in Fig. 3.2. The complex conjugates of the presented eigenvalues are also eigenvalues but omitted for conciseness.

are characterized by the zero deflection of the vibrating central component, and they are called the *substructure* modes. Similarly, seven modes are linear combinations of symmetry vectors in $\mathbf{U}_{\mathcal{D}_2}^{(B1,1)}$, and they are characterized by the non-zero rotational deflection of the vibrating central component, thus are called the *rotational* modes. The modes that are linear combinations of symmetry vectors in $\mathbf{U}_{\mathcal{D}_2}^{(B2,1)}$ or $\mathbf{U}_{\mathcal{D}_2}^{(B3,1)}$ are *translational modes* because of the non-zero central component translations. Seven of them (of the species $(B2,1)$) have central component deflections purely along the $\mathbf{e}_2$, and the other seven (of the species $(B3,1)$) have central component deflections purely along the $\mathbf{e}_1$.

According to Eq. (3.11), four reduced eigenvalue problems are formulated. To validate the group-theory-based method, Fig. 3.4 compares the eigenvalues solved from the reduced eigenvalue problems to those from the full eigenvalue problem for the example system in Figure 3.2. The two sets of eigenvalues match with each other. Meanwhile, the number of modes in each mode type also satisfies the above analysis. Figure 3.5 illustrates a substruc-

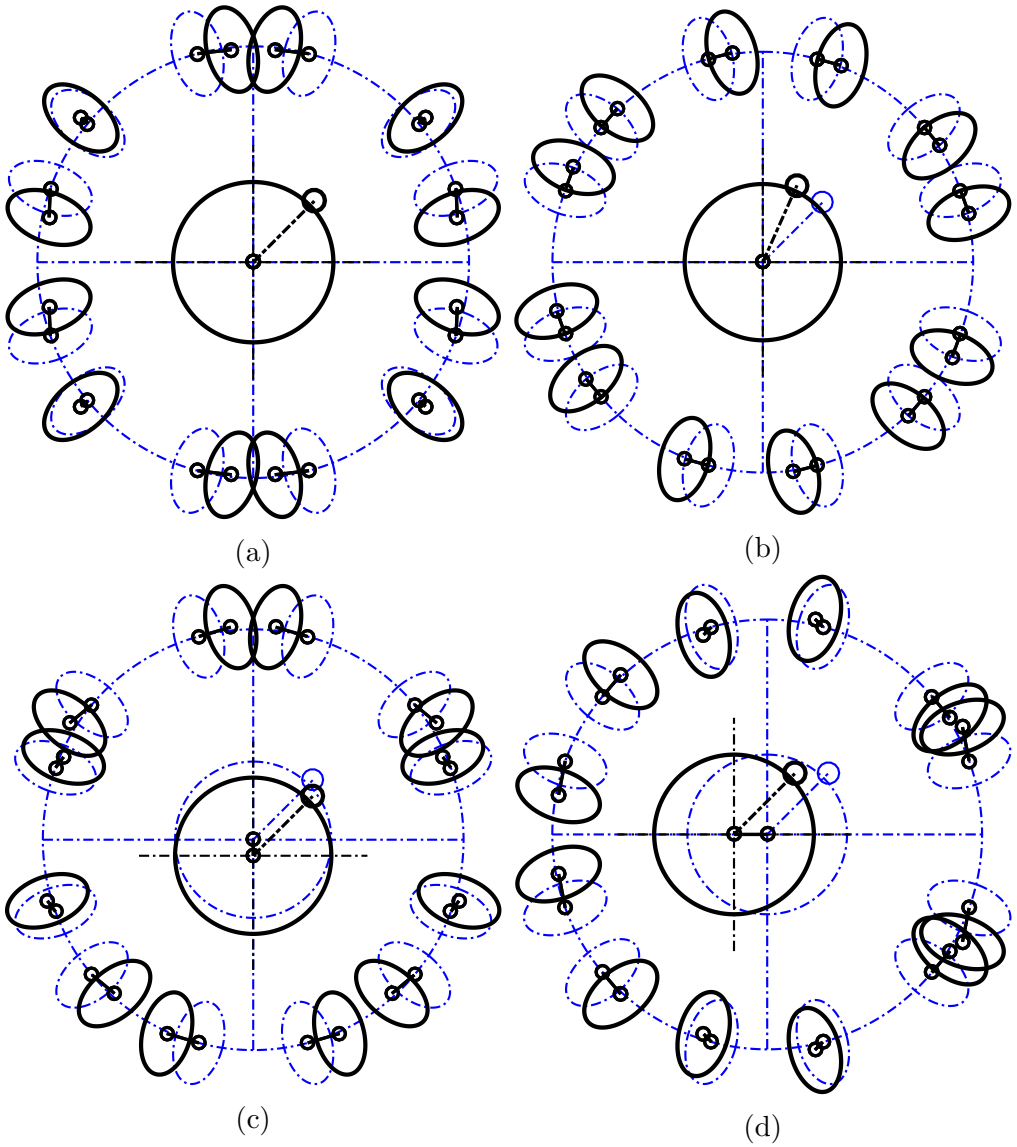

Figure 3.5: Modes of the example in Fig. 3.2. (a) A substructure mode (the 23rd mode). (b) A rotational mode (the 21th mode). (c) A translational mode (the 25th mode). (d) A translational mode (the 26th mode).

ture mode, a rotational mode, and two translational modes. The four example modes are associated with the four symmetry species in Eq. (3.30b), as determined by group-theory-based analysis.

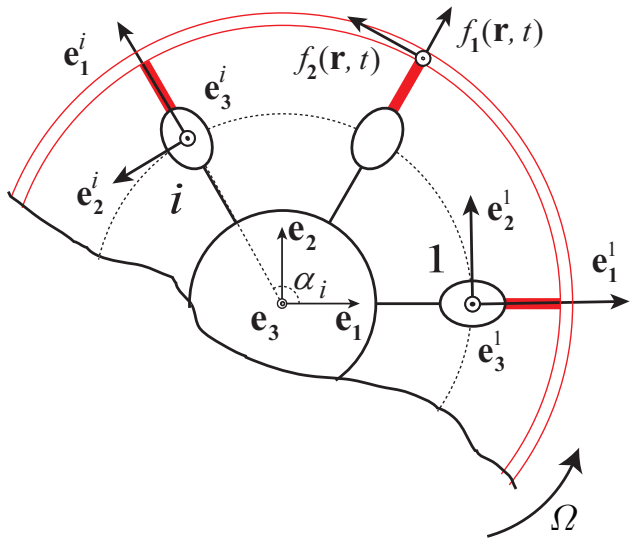

Figure 3.6: Schematic of a general cyclically symmetric system.

3.3 Group-Theory-Based Modal Analysis of General Cyclically Symmetric Systems

In this section, modal properties of general cyclically symmetric systems are derived based on group theory. The general cyclically symmetric system considered are allowed to have both rigid-body and compliant vibrating central components, the substructures can have any number of degrees of freedom. The derived modal properties generalize the relevant past works on cyclically symmetric systems [6, 12, 15, 18, 21, 29, 105].

3.3.1 Derivation of Symmetry-Adapted Basis

For a system with $\mathcal{C}_N$ symmetry, the symmetry operations that bring the system into self-coincidence are N rotations about an axis by the angle of $i \times 2\pi/N$ for $i = 0, 1, ..., N-1$. For convenience, the N symmetry operations are denoted as C_N^i $(i = 0, 1, ..., N-1)$, where $C_N^0 = E$ is the identity operation, and C_N^i and C_N^{N-i} are inverses of each other. In the following

derivation, the general cyclically symmetric system is supposed to have M_R rigid-body central components (each has six-degrees of freedom), M_C degrees of freedom for compliant central components, and N identical substructures (each has L degrees of freedom). The system is allowed to rotate about the system symmetry axis at a constant speed Ω that describes the angular speed of substructure about the symmetry axis. The schematic of the general system is given in Fig. 3.6. The deflections of rigid-body central components are defined under the coordinate system $\{\mathbf{e}_1,\mathbf{e}_2,\mathbf{e}_3\}$, which can rotate at a constant speed (this speed can be different from Ω). The coordinate systems under which the substructure deflections are defined are coordinated according to the angular positions of the substructures, so that the axes $\mathbf{e}_1^i$, $\mathbf{e}_2^i$, and $\mathbf{e}_3^i$ are in the radial, tangential, and axial directions of the ith substructure. The deformations of the compliant central components are defined as functions (fields as defined in Section 3.2) of the position vector $\mathbf{r}$. For convenience, the vector $\mathbf{r}$ that describes a material point of a compliant central component is not changed as the system rotates, and $\mathbf{r}$ can be written in cylindrical coordinate system, *i.e.*,

$$\mathbf{r} = (r, \theta, z)^T \tag{3.31}$$

where r, θ, and z are the radial, azimuth, and axial coordinates, respectively.

To obtain the symmetry-adapted basis vectors by calculating the quantities in Eq. (3.4), it is necessary to obtain $R\mathbf{v}$ that is transformed from any configuration vector $\mathbf{v}$ by any symmetry operation R in the cyclic group. Any configuration vector contains three parts. The first part of a general configuration vector consists of functions (fields as defined in Section 3.2) that describe the deformations of the compliant central components, the other two parts are vectors of scalars that describe the deflections of the rigid-body central components and

substructures. An arbitrary configuration vector is in the form of

$$\mathbf{v} = \begin{pmatrix} \mathbf{f} \\ \mathbf{q}_c \\ \mathbf{q}_s \end{pmatrix}, \tag{3.32a}$$

$$\mathbf{f} = \begin{pmatrix} f_1(r,\theta,z) \\ f_2(r,\theta,z) \\ \vdots \\ f_{M_C}(r,\theta,z) \end{pmatrix} \tag{3.32b}$$

$$\mathbf{q}_c = (\mathbf{q}_{c_1}, \mathbf{q}_{c_2}, \ldots, \mathbf{q}_{c_{M_R}})^T,\ \mathbf{q}_{c_m} = (x_{c_m}, y_{c_m}, z_{c_m}, \zeta_{c_m}, \eta_{c_m}, \mu_{c_m})^T, \tag{3.32c}$$

$$\mathbf{q}_s = (\mathbf{q}_{s_1}, \mathbf{q}_{s_2}, \ldots, \mathbf{q}_{s_N})^T, \tag{3.32d}$$

where x_{c_m}, y_{c_m}, z_{c_m}, ζ_{c_m}, η_{c_m}, and μ_{c_m} are the three translations and three rotations of the mth rigid-body central component along the axes $\mathbf{e}_1$, $\mathbf{e}_2$, and $\mathbf{e}_3$, respectively. By performing any symmetry operation C_N^i $(i = 0, 1, ..., N-1)$ in $\mathcal{C}_N$, the transformed configuration $C_N^i\mathbf{v}$ is

$$C_N^i\mathbf{v} = \begin{pmatrix} C_N^i\mathbf{f} \\ C_N^i\mathbf{q}_c \\ C_N^i\mathbf{q}_s \end{pmatrix} \tag{3.33a}$$

$$C_N^i\mathbf{f} = \begin{pmatrix} f_1(r,\theta-\frac{2i\pi}{N},z) \\ f_2(r,\theta-\frac{2i\pi}{N},z) \\ \vdots \\ f_{M_C}(r,\theta-\frac{2i\pi}{N},z) \end{pmatrix} \tag{3.33b}$$

$$C_N^i\mathbf{q}_c = (\mathbf{I}_{M_R} \otimes \mathbf{I}_2 \otimes \mathbf{R}_i)\mathbf{q}_c \tag{3.33c}$$

$$C_N^i \mathbf{q}_s = (\sigma_N^i \otimes \mathbf{I}_L)\mathbf{q}_s \tag{3.33d}$$

where $\mathbf{R}_i$ is the rotation transformation matrix

$$\mathbf{R}_i = \mathbf{R}(\frac{2i\pi}{N}) = \begin{pmatrix} \cos\frac{2i\pi}{N} & -\sin\frac{2i\pi}{N} & 0 \\ \sin\frac{2i\pi}{N} & \cos\frac{2i\pi}{N} & 0 \\ 0 & 0 & 1 \end{pmatrix}, \tag{3.34}$$

and σ_N^i is the ith power of the $N \times N$ cyclic backward shift matrix

$$\sigma_N = \begin{pmatrix} 0 & 0 & 0\ldots & 0 & 1 \\ 1 & 0 & 0\ldots & 0 & 0 \\ 0 & 1 & 0\ldots & 0 & 0 \\ \vdots & \vdots & \ddots & \vdots & \vdots \\ 0 & 0 & \ldots & 1 & 0 \end{pmatrix}_{N\times N} . \tag{3.35}$$

For systems with central components that only have planar degrees of freedom, Eq. (3.33c) should be revised by excluding $\mathbf{I}_2$ accordingly.

To understand the structure of the transformed configuration $C_N^i\mathbf{v}$ in Eq. (3.33), Fig. 3.7 illustrates how an arbitrary configuration of a system with the $\mathbf{C}_6$ symmetry is transformed to its equivalent configuration by the symmetry operation C_6^1, *i.e.,* the rotation about the axis $\mathbf{e}_3$ by $\pi/3$. This example is a special case of the general cyclically symmetric system in the foregoing discussion, where the degrees of freedom of each substructure are two planar translations, the rigid body central component has three planar degrees of freedom, and the deformation of compliant central component (a ring) is fully described by the tangential deformation (the radial deformation is related to the tangential deformation as discussed in 3.4). By comparing the two configurations in Fig. 3.7, the compliant central component

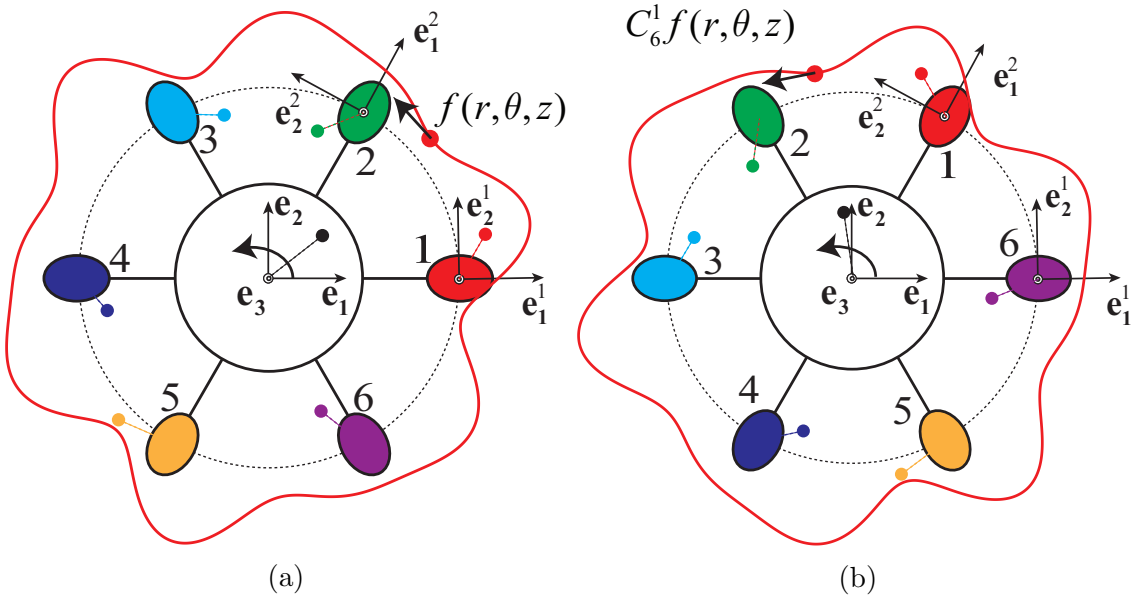

Figure 3.7: (a) An arbitrary deflection $\mathbf{v}$ of the example system with $\mathcal{C}_6$ symmetry. (b) The deflection $C_6^1\mathbf{v}$ transformed from $\mathbf{v}$ by C_6^1.

deformation in the transformed configuration is physically identical to that in the original configuration, and the relation between these two configurations satisfy the relation in Eq. (3.33): $C_6^1 f(r,\theta,z)$ that describes the transformed deformation is obtained by translating the azimuth coordinate by $\pi/3$, *i.e.*, $C_6^1 f(r,\theta,z) = f(r,\theta-\pi/3,z)$. The deflections of the rigid-body central component in two configurations are related as $C_6^1\mathbf{q}_c = \mathbf{R}(\pi/3)\mathbf{q}_c$. As shown in Fig. 3.7, the substructure deflections that are measured in the frame $\{\mathbf{e}_1^2, \mathbf{e}_2^2\}$ in Fig. 3.7(b) are the deflections of the first substructure in Fig. 3.7(a). This relation between the substructure deflections in Figs. 3.7(a) and (b) is described by Eq. (3.33d) (when $i = 1$ and $N = 6$), which indicates the deflections of the first substructure are passed to the second substructure, those of the second substructure to the third, *etc.*

To calculate the quantities in Eq. (3.4), the irreducible representations of $\mathcal{C}_N$ are given in Table 3.4. For the purpose of convenience, the convention of labeling the irreducible representations in Ref. [1] is avoided. For the group $\mathcal{C}_N$, there are N irreducible representations,

and all these representations are one-dimensional, *i.e.*, each symmetry operation in $\mathcal{C}_N$ is associated with a scalar. In this work, the N irreducible representations are labeled by the numbers from 0 to $N-1$, and the representation labeled by k is given in Table 3.4.

Symmetry Operation	E	C_N^1	C_N^2	...	C_N^{N-1}
Irreducible Representation Labeled by k ($k = 0, \ldots, N-1$)	1	$e^{-\frac{2k\pi \mathrm{j}}{N}}$	$e^{-\frac{4k\pi \mathrm{j}}{N}}$	...	$e^{-\frac{2k(N-1)\pi \mathrm{j}}{N}}$

Table 3.4: Irreducible representation labeled by k of the group $\mathcal{C}_N$. j is the imaginary unit.

Because all the irreducible representations for the group $\mathcal{C}_N$ are one-dimensional, only one quantity in Eq. (3.4) needs to be calculated with respect to any one of the irreducible representations. For the irreducible representation labeled by k in Table 3.4, substitution of Eq. (3.33) into Eq. (3.4) yields

$$\sum_{R\in\mathcal{C}_N} \mathbf{D}^{(k)}(R^{-1})^T R\mathbf{v} = \sum_{i=0}^{N-1} e^{\frac{2ik\pi \mathrm{j}}{N}} C_N^i \mathbf{v} = \begin{pmatrix} \tilde{\mathbf{f}}^{(k)} \\ \tilde{\mathbf{q}}_c^{(k)} \\ \tilde{\mathbf{q}}_s^{(k)} \end{pmatrix}, \tag{3.36a}$$

$$\tilde{\mathbf{f}}^{(k)} = \begin{pmatrix} \tilde{f}_1^{(k)}(r,\theta,z) \\ \tilde{f}_2^{(k)}(r,\theta,z) \\ \cdots \\ \tilde{f}_{M_C}^{(k)}(r,\theta,z) \end{pmatrix}, \tag{3.36b}$$

$$\tilde{f}_m^{(k)}(r,\theta,z) = \sum_{i=0}^{N-1} e^{\frac{2ik\pi \mathrm{j}}{N}} f_m(r,\theta - \frac{2i\pi}{N}, z), \text{ for } m = 1,,2,\ldots,M_C,$$

$$\tilde{\mathbf{q}}_c^{(k)} = \sum_{i=0}^{N-1} e^{\frac{2ik\pi \mathrm{j}}{N}} (\mathbf{I}_{M_R} \otimes \mathbf{I}_2 \otimes \mathbf{R}_i)\mathbf{q}_c, \tag{3.36c}$$

$$\tilde{\mathbf{q}}_s^{(k)} = \sum_{i=0}^{N-1} e^{\frac{2ik\pi \mathrm{j}}{N}} (\sigma_N^i \otimes \mathbf{I}_L)\mathbf{q}_s, \tag{3.36d}$$

where the quantity in Eq. (3.36a) is a vector of the same size with the vector $\mathbf{v}$ in Eq. (3.32).

To obtain the symmetry-adapted basis, the subvectors of the quantity in Eq. (3.36a) are analyzed to identify the subspace that includes all possible resulted vectors in Eq. (3.36a) for any arbitrary configuration vector $\mathbf{v}$.

Firstly, the quantity $\tilde{f}_m^{(k)}(r,\theta,z)$ in Eq. (3.36b) for the mth field of compliant central components is proved to satisfy the following relation,

$$\begin{aligned}
&\tilde{f}_m^{(k)}(r,\theta+\frac{2n\pi}{N},z)\\
=&\sum_{i=0}^{N-1} e^{\frac{2ik\pi \mathrm{j}}{N}} f_m(r,\theta-\frac{2(i-n)\pi}{N},z)\\
=&e^{\frac{2nk\pi \mathrm{j}}{N}} \sum_{i=0}^{N-1} e^{\frac{2(i-n)k\pi \mathrm{j}}{N}} f_m(r,\theta-\frac{2(i-n)\pi}{N},z)\\
=&e^{\frac{2nk\pi \mathrm{j}}{N}} \sum_{i-n} e^{\frac{2(i-n)k\pi \mathrm{j}}{N}} f_m(r,\theta-\frac{2(i-n)\pi}{N},z)\\
=&e^{\frac{2nk\pi \mathrm{j}}{N}} \tilde{f}_m^{(k)}(r,\theta,z), \qquad n=0,1,\ldots,N-1,
\end{aligned} \tag{3.37}$$

where the first and the fourth equalities are based on Eq. (3.36b), and the third equality is a result of changing the dummy index from i to $i-n$. This relation indicates an important property of the configuration subspace generated by the irreducible representation labeled by k. In this subspace, any field (such as the mth) of compliant central components satisfies a phase relation,

$$\tilde{f}_m^{(k)}(r,\theta+\frac{2n\pi}{N},z) = e^{\frac{2nk\pi \mathrm{j}}{N}} \tilde{f}_m^{(k)}(r,\theta,z), \qquad n=0,1,\ldots,N-1. \tag{3.38}$$

In previous works, this phase relation is said to be characterized by the phase index k [9, 10]. To obtain the symmetry-adapted basis characterized by the phase index k for the mth compliant central component field, $f_m(r,\theta,z)$ in Eq. (3.32b) is expanded over the azimuth

coordinate θ after the separation of variables, *i.e.*,

$$f_m(r,\theta,z) = h_m(r,z)\sum_{l=-\infty}^{\infty} c_{m,l}e^{\mathrm{j}l\theta}, \tag{3.39}$$

where $h_m(r,z)$ is not discretized, and $c_{m,l}$ is the coefficient of the Fourier component $e^{\mathrm{j}l\theta}$ with the harmonic order l. The function space of the field $f_m(r,\theta,z)$ can be spanned by the basis $\{e^{\mathrm{j}l\theta}h_m(r,z) : l = 0, \pm 1, \dots\}$. Substitution of Eq. (3.39) into Eq. (3.36b) yields

$$\begin{aligned}
\tilde{f}_m^{(k)}(r,\theta,z) &= h_m(r,z)\sum_{i=0}^{N-1} e^{\frac{2ik\pi\mathrm{j}}{N}} \sum_{l=-\infty}^{\infty} c_{m,l}e^{\mathrm{j}l(\theta-\frac{2i\pi}{N})} \\
&= h_m(r,z)\sum_{l=-\infty}^{\infty} c_{m,l}e^{\mathrm{j}l\theta} \sum_{i=0}^{N-1} e^{\mathrm{j}\frac{2i\pi}{N}(k-l)} \\
&= Nh_m(r,z)\sum_{l=-\infty}^{\infty} c_{m,l}e^{\mathrm{j}l\theta}\delta_{l,k+SN} \\
&= Nh_m(r,z)\sum_{\substack{l=k+SN,\\ S=0,\pm1,\dots}} c_{m,l}e^{\mathrm{j}l\theta},
\end{aligned} \tag{3.40}$$

where S is any integer, and the third equality uses the identity

$$\sum_{i=0}^{N-1} e^{\mathrm{j}\frac{2i\pi}{N}(k-l)} = N\delta_{l,k+SN} = \begin{cases} N & l = k+SN \\ 0 & l \neq k+SN \end{cases}. \tag{3.41}$$

Eq. (3.40) indicates that in the configuration subspace generated by the irreducible representation labeled by k, any compliant central component deformation only have Fourier (nodal diameter) components whose harmonic orders are $k + SN$. The function space of any field $f_m(r,\theta,z)$ can be decomposed into N subspaces characterized by k ($k = 0, 1, \dots, N-1$), and the symmetry-adapted basis for the kth subspace is $\{e^{\mathrm{j}(k+SN)\theta}h_m(r,z) : S = 0, \pm 1, \dots\}$.

For the cases when $f_m(r,\theta,z)$ in Eq. (3.39) is expanded with a limited number of Fourier

components, the range of l for the summation in Eq. (3.39) is considered between $-L_mN$ to L_mN in this derivation. The symmetry-adapted basis that spans the function space for $f_m(r,\theta,z)$ is $\{e^{\mathrm{j}l\theta}h_m(r,z) : l = 0, \pm1, \ldots, \pm L_mN\}$. The truncated basis for the space of $\mathbf{f}$ in Eq. (3.32b) contains $\sum_{m=1}^{M_C}(2L_mN+1)$ basis vectors, and each vector is in the form of

$$\mathbf{\Psi}_{m,l} = (0,\ \ldots,\ \underbrace{h_m(r,z)e^{\mathrm{j}l\theta}}_{m\text{th field}},\ 0,\ \ldots,\ 0)^T, \tag{3.42}$$

where $m = 1, 2, \ldots, M_R$ and $l = 0, \pm1, \pm2, \ldots, \pm L_mN$. All these vectors forms a basis that is analogous to the basis in Eq. (3.19). According to the harmonic order of the Fourier components in each field function, the vectors in Eq. (3.42) can be categorized into N sets, and the set characterized by k ($k = 0, 1, \ldots, N-1$) is

$$\tilde{\mathbf{\Psi}}^{(k)} = \{\mathbf{\Psi}_{m,l} : m = 1, 2, \ldots, M_C,\ -L_mN \leqslant l = SN + k \leqslant L_mN\}, \tag{3.43}$$

where S is any integer that satisfies the inequality $-L_mN \leqslant SN + k \leqslant L_mN$. Because of the structure of $\tilde{\mathbf{f}}^{(k)}$ in Eq. (3.36b) and the relation in Eq. (3.40), the set $\tilde{\mathbf{\Psi}}^{(k)}$ in Eq. (3.43) contains all the basis vectors that spans the space of $\tilde{\mathbf{f}}^{(k)}$ in Eq. (3.36b) (for the cases when bases of all field functions are truncated). $\tilde{\mathbf{\Psi}}^{(k)}$ in Eq. (3.43) is the symmetry-adapted basis that spans the subspace (of $\mathbf{f}$ in Eq. (3.32b)) generated by the irreducible representation labeled by k. For convenience, $\tilde{\mathbf{\Psi}}^{(k)}$ in Eq. (3.43) can be regarded as a matrix whose columns are vectors of functions in the form of Eq. (3.42).

The vectors that span the subspace which contains all the possible vectors $\tilde{\mathbf{q}}_c^{(k)}$ and $\tilde{\mathbf{q}}_s^{(k)}$ in Eq. (3.36a) also contribute to the symmetry-adapted basis generated by the irreducible representation labeled by k. Substitution of Eq. (3.34) into Eq. (3.36c) yields

$$\tilde{\mathbf{q}}_c^{(k)} = \hat{\mathbf{D}}_c^{(k)}\mathbf{q}_c, \tag{3.44a}$$

$$\hat{\mathbf{D}}_c^{(k)} = (\mathbf{I}_{M_R} \otimes \mathbf{I}_2) \otimes (\sum_{i=0}^{N-1} e^{\mathrm{j}\frac{2i\pi}{N}k} \begin{pmatrix} \cos\frac{2i\pi}{N} & -\sin\frac{2i\pi}{N} & 0 \\ \sin\frac{2i\pi}{N} & \cos\frac{2i\pi}{N} & 0 \\ 0 & 0 & 1 \end{pmatrix})$$

$$= \begin{cases} \mathbf{I}_{M_R} \otimes \mathbf{I}_2 \otimes \begin{pmatrix} 0 & 0 & 0 \\ 0 & 0 & 0 \\ 0 & 0 & N \end{pmatrix} & k = 0 \\ \mathbf{I}_{M_R} \otimes \mathbf{I}_2 \otimes \begin{pmatrix} \frac{N}{2} & \mp\mathrm{j}\frac{N}{2} & 0 \\ \pm\mathrm{j}\frac{N}{2} & \frac{N}{2} & 0 \\ 0 & 0 & 0 \end{pmatrix} & k = 1, N-1 \\ \mathbf{I}_{M_R} \otimes \mathbf{I}_2 \otimes \mathbf{0}_{3\times 3} & k = 2, 3, \ldots, N-2 \end{cases} \tag{3.44b}$$

where the elements in $\hat{\mathbf{D}}_c^{(k)}$ is determined by k because of the following identities,

$$\sum_{i=0}^{N-1} e^{\mathrm{j}\frac{2i\pi}{N}k} = \begin{cases} N & k = 0 \\ 0 & k \neq 0 \end{cases}, \tag{3.45a}$$

$$\sum_{i=0}^{N-1} e^{\mathrm{j}\frac{2i\pi}{N}k} \cos\frac{2i\pi}{N} = \begin{cases} \frac{N}{2} & k = 1, N-1 \\ 0 & k = 2, 3, \ldots, N-2 \end{cases}, \tag{3.45b}$$

$$\sum_{i=0}^{N-1} e^{\mathrm{j}\frac{2i\pi}{N}k} \sin\frac{2i\pi}{N} = \begin{cases} \mathrm{j}\frac{N}{2} & k = 1 \\ -\mathrm{j}\frac{N}{2} & k = N-1 \\ 0 & k = 2, 3, \ldots, N-2 \end{cases}. \tag{3.45c}$$

Based on Eq. (3.44), for each irreducible representation (labeled by k), the symmetry-adapted subspace containing all $\tilde{\mathbf{q}}_c^{(k)}$ in Eq. (3.36c) is identified. For $k = 2, 3, \ldots, N-2$,

$\tilde{\mathbf{q}}_c^{(k)}$ in Eq. (3.44) is always a zero vector, and there is no symmetry-adapted basis vectors (symmetry vectors) for the subspace (a vanished subspace) that contains all such $\tilde{\mathbf{q}}_c^{(k)}$. For $k = 0$, the subspace containing all $\tilde{\mathbf{q}}_c^{(0)}$ is spanned by the columns of $\hat{\mathbf{D}}_c^{(0)}$ in Eq. (3.44b). By eliminating the zero vectors in $\hat{\mathbf{D}}_c^{(0)}$, the symmetry vectors (after being normalized based on Eq. (3.5)) for this subspace are the columns of the matrix

$$\tilde{\mathbf{U}}_c^{(0)} = \mathbf{I}_{M_R} \otimes \mathbf{I}_2 \otimes \begin{pmatrix} 0 & 0 & 1 \end{pmatrix}^T. \tag{3.46}$$

For the cases when $k = 1$ and $k = N - 1$, the symmetry vectors of the subspaces containing all $\tilde{\mathbf{q}}_c^{(k)}$ are also obtained similarly as the columns of

$$\tilde{\mathbf{U}}_c^{(1)} = \mathbf{I}_{M_R} \otimes \mathbf{I}_2 \otimes \begin{pmatrix} 1/\sqrt{2} & \mathrm{j}/\sqrt{2} & 0 \end{pmatrix}^T, \tag{3.47a}$$

$$\tilde{\mathbf{U}}_c^{(N-1)} = \mathbf{I}_{M_R} \otimes \mathbf{I}_2 \otimes \begin{pmatrix} 1/\sqrt{2} & -\mathrm{j}/\sqrt{2} & 0 \end{pmatrix}^T. \tag{3.47b}$$

For the cases when the central components only have planar degrees of freedom, Eqs. (3.46) and (3.47b) should be revised by excluding $\mathbf{I}_2$.

Similarly, substitution of Eq. (3.35) into Eq. (3.36d) yields

$$\tilde{\mathbf{q}}_s^{(k)} = \hat{\mathbf{D}}_s^{(k)} \mathbf{q}_s, \tag{3.48a}$$

$$\hat{\mathbf{D}}_s^{(k)} = \begin{pmatrix} \mathbf{I}_L & e^{\mathrm{j}\frac{2k\pi}{N}(N-1)}\mathbf{I}_L & e^{\mathrm{j}\frac{2k\pi}{N}(N-2)}\mathbf{I}_L & \dots & e^{\mathrm{j}\frac{2k\pi}{N}}\mathbf{I}_L \\ e^{\mathrm{j}\frac{2k\pi}{N}}\mathbf{I}_L & \mathbf{I}_L & e^{\mathrm{j}\frac{2k\pi}{N}(N-1)}\mathbf{I}_L & \dots & e^{\mathrm{j}\frac{4k\pi}{N}}\mathbf{I}_L \\ e^{\mathrm{j}\frac{4k\pi}{N}}\mathbf{I}_L & e^{\mathrm{j}\frac{2k\pi}{N}}\mathbf{I}_L & \mathbf{I}_L & \dots & e^{\mathrm{j}\frac{6k\pi}{N}}\mathbf{I}_L \\ \vdots & \vdots & \vdots & \ddots & \vdots \\ e^{\mathrm{j}\frac{2k\pi}{N}(N-1)}\mathbf{I}_L & e^{\mathrm{j}\frac{2k\pi}{N}(N-2)}\mathbf{I}_L & e^{\mathrm{j}\frac{2k\pi}{N}(N-3)}\mathbf{I}_L & \dots & \mathbf{I}_L \end{pmatrix}. \tag{3.48b}$$

For $\tilde{\mathbf{q}}_s^{(k)}$ in Eq. (3.48a) being partitioned into N $L\times 1$ subvectors, *i.e.*, $\tilde{\mathbf{q}}_s^{(k)} = (\tilde{\mathbf{q}}_{s_1}^{(k)}, \tilde{\mathbf{q}}_{s_2}^{(k)}, \dots, \tilde{\mathbf{q}}_{s_N}^{(k)})^T$,

the relation between these subvectors is obtained by substitution of Eq. (3.32d) into Eq. (3.48). The relation between the ith and $(i+1)$th subvectors of $\tilde{\mathbf{q}}_s^{(k)}$ is

$$\begin{aligned}\tilde{\mathbf{q}}_{s_{i+1}}^{(k)} &= \sum_{p=1}^{N} e^{\mathrm{j}\frac{2k\pi}{N}(i+1-p)}\mathbf{I}_L\mathbf{q}_{s_p} \\ &= e^{\mathrm{j}\frac{2k\pi}{N}}\sum_{p=1}^{N} e^{\mathrm{j}\frac{2k\pi}{N}(i-p)}\mathbf{I}_L\mathbf{q}_{s_p} \\ &= e^{\mathrm{j}\frac{2k\pi}{N}}\tilde{\mathbf{q}}_{s_i}^{(k)}.\end{aligned} \tag{3.49}$$

Eq. (3.49) indicates that, in the configuration subspace generated by the irreducible representation labeled by k, the deflections of adjacent substructures are identical in magnitude but with a phase difference characterized by the integer k. Such phase relation between substructures and the concept of phase index (the integer k) are widely used in previous work [12, 26, 29, 105]. The symmetry-adapted basis for the subspace containing all $\tilde{\mathbf{q}}_s^{(k)}$ in Eq. (3.36d) is the set of all the linearly independent vectors in $\hat{\mathbf{D}}_s^{(k)}$. By observation, the columns of blocks in $\hat{\mathbf{D}}_s^{(k)}$ are all related to the first column of blocks by a scalar factor, for example, the second column of blocks is equal to the first column multiplied by $e^{-\mathrm{j}\frac{2k\pi}{N}}$. Meanwhile, all the vectors in the first column of blocks in $\hat{\mathbf{D}}_s^{(k)}$ are linearly independent. Therefore, the first column of blocks provides the symmetry-adapted basis vectors for the subspace containing all $\tilde{\mathbf{q}}_s^{(k)}$, and this symmetry-adapted basis vectors form the matrix

$$\tilde{\mathbf{U}}_s^{(k)} = \frac{1}{\sqrt{N}}\begin{pmatrix}1 & e^{\mathrm{j}\frac{2k\pi}{N}} & e^{\mathrm{j}\frac{4k\pi}{N}} & \dots & e^{\mathrm{j}\frac{2k\pi}{N}(N-1)}\end{pmatrix}^T \otimes \mathbf{I}_L, \tag{3.50}$$

where the factor $\frac{1}{\sqrt{N}}$ is resulted from the normalization process in Eq. (3.5).

In summary, for each given irreducible representation labeled by k, the subvectors $\tilde{\mathbf{f}}^{(k)}$, $\tilde{\mathbf{q}}_c^{(k)}$, and $\tilde{\mathbf{q}}_s^{(k)}$ in Eq. (3.36a) are in the spaces spanned by the columns of $\tilde{\mathbf{\Psi}}^{(k)}$ (Eq. (3.43)), $\tilde{\mathbf{U}}_c^{(k)}$ (Eqs. (3.46) and (3.47)), and $\tilde{\mathbf{U}}_s^{(k)}$ (Eq. (3.50)), respectively. These spaces include all

possible $\tilde{\mathbf{f}}^{(k)}$, $\tilde{\mathbf{q}}_c^{(k)}$, and $\tilde{\mathbf{q}}_s^{(k)}$ for any arbitrary configuration $\mathbf{v}$ in Eq. (3.36a). According to Eq. (3.36a), the space includes any $\sum_{R\in\mathcal{C}_N}\mathbf{D}^{(k)}(R^{-1})^T R\mathbf{v}$ in Eq. (3.36a) for any arbitrary configuration $\mathbf{v}$ is spanned by the column vectors of the matrix

$$\boldsymbol{\chi}^{(k,1)} = \begin{cases} \begin{pmatrix} \tilde{\boldsymbol{\Psi}}^{(k)} & \mathbf{0} & \mathbf{0} \\ \mathbf{0} & \tilde{\mathbf{U}}_c^{(k)} & \mathbf{0} \\ \mathbf{0} & \mathbf{0} & \tilde{\mathbf{U}}_s^{(k)} \end{pmatrix} & k = 0, 1, N-1 \\ \begin{pmatrix} \tilde{\boldsymbol{\Psi}}^{(k)} & \mathbf{0} \\ \mathbf{0} & \mathbf{0} \\ \mathbf{0} & \tilde{\mathbf{U}}_s^{(k)} \end{pmatrix} & k = 2, 3, \ldots, N-2 \end{cases} \tag{3.51}$$

Therefore, these vectors form the full system symmetry-adapted basis generated by the irreducible representation labeled by k. Based on Section 3.2.1, all of these vectors are of the same symmetry species $(k, 1)$ because they are generated with respect to the one-dimensional irreducible representation labeled by k.

Based on Eqs. (3.43), (3.46), (3.50), and (3.51), the number of symmetry-adapted basis vectors of the symmetry species $(0, 1)$ is $2M_R + L + \sum_{m=1}^{M_C}(2L_m + 1)$ because $\tilde{\boldsymbol{\Psi}}^{(k)}$, $\tilde{\mathbf{U}}_c^{(k)}$, $\tilde{\mathbf{U}}_s^{(k)}$ have $\sum_{m=1}^{M_C}(2L_m+1)$, $2M_R$, and L columns, respectively. Similarly, the number of symmetry-adapted basis vectors of the symmetry species $(1, 1)$ or $(N-1, 1)$ is $2M_R + L + 2\sum_{m=1}^{M_C} L_m$, and the number of symmetry-adapted basis vectors of the symmetry species $(k, 1)$ when $k = 2, 3, \ldots, N-2$ is $L + 2\sum_{m=1}^{M_C} L_m$. The sum of all symmetry-adapted basis vectors of all symmetry species is $6M_R+NL+\sum_{m=1}^{M_C}(2L_mN+1)$, which equals the sum of the number of all basis vectors for all compliant central component fields, $\sum_{m=1}^{M_C}(2L_mN+1)$, and the number of degrees of freedom for all discrete components, $6M_R + NL$. Therefore, the full configuration space is completely decomposed into N subspaces spanned by the symmetry-adapted bases.

3.3.2 Modal Properties of Cyclically Symmetric Systems

After the symmetry-adapted bases of the all symmetry species are obtained, the modal properties of general cyclically symmetric systems with both rigid-body and compliant central components are known. According to the group theory in Section 3.2.1, any eigenvector is a linear combination of the symmetry-adapted basis vectors of one symmetry species only. Therefore, the N symmetry species in Eq. (3.51) indicate there are N types of modes. Meanwhile, the characteristic modal deflections for each mode type are also known. Because both the quantity $\sum_{R\in\mathcal{C}_N} \mathbf{D}^{(k)}(R^{-1})^T R\mathbf{v}$ in Eq. (3.36a) and the full system eigenvectors are linear combinations of the symmetry-adapted basis vectors of one symmetry species, the properties of $\tilde{\mathbf{f}}^{(k)}$ (or $\tilde{f}_m^{(k)}(r,\theta,z)$), $\tilde{\mathbf{q}}_c^{(k)}$, and $\tilde{\mathbf{q}}_s^{(k)}$ in Eq. (3.36a) can be directly regarded as the properties of the eigenvectors of the symmetry species $(k,1)$. These properties include:

1. For any integer $k = 0, 1, \ldots, N-1$, the modal deformation of any compliant central component degree of freedom satisfies the phase relation analogous to Eq. (3.38). This property does not rely on the discretization process when the system is numerically solved. If the deformations of compliant central components are expanded over the azimuth coordinate, nodal diameter components in the compliant central component modal deformations must be of the harmonic order $k + NS$, where S is an arbitrary integer.

2. For any integer $k = 0, 1, \ldots, N-1$, the modal deflections of substructures satisfy the phase relation analogous to Eq. (3.49). The modal deflections of all substructures are identical in magnitude, but different substructures are vibrating with phase differences characterized by the phase index k.

3. For the cases when $k = 2, 3, \ldots, N-2$, the rigid-body central components are not vibrating because all the symmetry-adapted basis vectors in $\boldsymbol{\chi}^{(k,1)}$ (Eq. (3.51)) have

only zero entries for the rigid-body central component degrees of freedom. For the cases when $k = 0$, based on the structures of $\boldsymbol{\chi}^{(k,1)}$ in Eq. (3.51) and $\tilde{\mathbf{U}}_c^{(0)}$ in Eq. (3.46), the rigid-body central components only have non-zero out-of-plane translations and in-plane rotations along the axis $\mathbf{e}_3$ (referred to as the *type-I* motions in Ref. [105]). Similarly, for the cases when $k = 1$ (or $N-1$), the rigid-body central components only have non-zero in-plane translations and out-of-plane tilting motions along the axes $\mathbf{e}_1$ and $\mathbf{e}_2$ (referred to as the *type-II* motions).

4. Any full system eigenvector of the symmetry species $(k, 1)$ generally has all the above properties simultaneously, *i.e.*, the motions of the compliant central components and the substructures satisfies the phase relation characterized by the phase index k, and the rigid-body central component has the modal deflections characterized by k. It is accidental if a full system eigenvector of the symmetry species $(k, 1)$ only has a part of the above properties, for example, a mode when the substructures vibrate in phase $(k = 0)$ while the rigid-body central components do not vibrate is a special case.

Based on the above modal properties, all N (for $k = 0, 1, \ldots, N-1$) types of modes are commonly classified into three categories, each of which is characterized by the modal deflections of the rigid-body central components. For the cases when the phase index $k = 0$, the modes are called the *rotational-axial modes* because the rigid-body central components can only have non-zero type-I motions. This category of modes generalizes the rotational modes in cyclically symmetric systems with planar central components, such as the planet gears in Refs. [12, 15] and the centrifugal pendulum vibration absorber (CPVA) systems in Refs. [18, 20]. Similarly, the modes characterized by the phase indices $k = 1$ and $N-1$ are called the *translational-tilting modes* because of the non-zero type-II motions of the rigid-body central components. This category of modes and its special cases (translational modes) for systems with planar central components, are found in previous works [12, 15, 16, 18, 20,

21, 29, 30, 105]. For the cases when the phase index $k = 2, 3, \ldots, N-2$, the modes are called the *substructure modes* [29, 105], which generalize the planet modes in planet gears [12, 15, 16, 30] and the absorber modes in CPVA systems [18, 79]. For general cyclically symmetric systems with compliant central components, the compliant central components in a *substructure mode* can also vibrate.

3.3.3 Numerical Solution by Solving Reduced Eigenvalue Problems

For general cyclically symmetric systems with both rigid-body and compliant central components, the eigenvalue problem can be written in the form of Eq. (3.17), where the elements of in the matrix operator $\mathbf{L}(\lambda)$ can be operators or scalars (for example, the operators in Eq. (3.60)). To numerically solve the problem, the eigenvector $\boldsymbol{\phi}$ in Eq. (3.17) can be written as a linear combination of a number of basis vectors. Without any knowledge of the symmetry-adapted bases obtained from group theory, a commonly used selection of the basis vectors are the columns of the matrix

$$\boldsymbol{\chi} = \begin{pmatrix} \boldsymbol{\Psi} & \mathbf{0} & \mathbf{0} \\ \mathbf{0} & \mathbf{I}_{6M_R} & \mathbf{0} \\ \mathbf{0} & \mathbf{0} & \mathbf{I}_{NL} \end{pmatrix}, \tag{3.52}$$

where $\boldsymbol{\Psi} = \{\boldsymbol{\Psi}_{m,l} : m = 1, 2, \ldots, M_C,\ -L_m N \leqslant l \leqslant L_m N\}$ ($\boldsymbol{\Psi}_{m,l}$ is defined in Eq. (3.42)) for the case when the mth compliant central component field is approximated by considered a limited number of Fourier components (l from $-L_m N$ to $L_m N$). Then, the eigenvalue problem in Eq. (3.17) can be discretized through weighted residual methods, such as the Galerkin method. The discretization for such a hybrid continuous-discrete system is based

on the inner product

$$\langle \mathbf{W}_1, \mathbf{W}_2 \rangle = \int_D \mathbf{f}_1^\dagger \mathbf{f}_2 \, \mathrm{d}D + \mathbf{p}_1^\dagger \mathbf{p}_2, \tag{3.53}$$

where $\mathbf{W}_i = (\mathbf{f}_i, \mathbf{p}_i)^T$ consists of a subvector of field functions on D (denoted as $\mathbf{f}_i$) and a subvector of numbers (denoted as $\mathbf{p}_i$). Because the number of basis vectors (columns in $\boldsymbol{\chi}$) is $6M_R + NL + \sum_{m=1}^{M_C}(2L_m N + 1)$, the size of the discretized eigenvalue problem is also $6M_R + NL + \sum_{m=1}^{M_C}(2L_m N + 1)$.

Based on group theory, the space spanned by the columns of $\boldsymbol{\chi}$ in Eq. (3.52) is decomposed into N subspaces that are spanned by the symmetry-adapted bases in Eq. (3.51), and any full system eigenvector must fall into one of these subspaces. Therefore, the eigenvalue problem in Eq. (3.17) is decomposed into N reduced discretized eigenvalue problems, and the problem characterized by the phase index k ($k = 0, 1, \ldots, N-1$) is obtained by discretizing Eq. (3.17) using the columns of $\boldsymbol{\chi}^{(k,1)}$ in Eq. (3.51) as the basis vectors. The size of the reduced discretized eigenvalue problem is determined by the number of basis vectors in $\boldsymbol{\chi}^{(k,1)}$ in Eq. (3.51) for the symmetry species $(k, 1)$. The number of full system modes obtained by solving each reduced eigenvalue problem equals the number of basis vectors multiplied by the order of the eigenvalue problems (the power number of the eigenvalue), and these modes are of the same mode type as discussed before.

According to Eqs. (3.43), (3.46), (3.50), and (3.51), the symmetry-adapted basis vectors of the symmetry species $(N - k, 1)$ are the complex conjugates of those of the symmetry species $(k, 1)$, where $k \neq 0$ or $N/2$. Because the inner product in Eq. (3.53) has the following property,

$$\langle \overline{\mathbf{W}}_1, \overline{\mathbf{W}}_2 \rangle = \int_D \overline{\mathbf{f}}_1^\dagger \overline{\mathbf{f}}_2 \, \mathrm{d}D + \overline{\mathbf{p}}_1^\dagger \overline{\mathbf{p}}_2 = \overline{\int_D \mathbf{f}_1^\dagger \mathbf{f}_2 \, \mathrm{d}D + \mathbf{p}_1^\dagger \mathbf{p}_2} = \overline{\langle \mathbf{W}_1, \mathbf{W}_2 \rangle}, \tag{3.54}$$

where $\overline{\mathbf{W}}_1$ is the complex conjugate of $\mathbf{W}_1$, the discretized matrix operators in the reduced

eigenvalue problems characterized by k and $N-k$ are complex conjugates to each other. The eigensolutions obtained from these two reduced eigenvalue problems are also in complex conjugate pairs. The symmetry-adapted basis vectors of the symmetry species $(0,1)$ or $(N/2,1)$ (when N is even) are real valued, and the eigensolutions obtained from the reduced eigenvalue problems characterized by $k=0$ or $N/2$ are in complex conjugate pairs. Therefore, all the eigensolutions can be obtained from solving the reduced eigenvalue problems characterized by $k=0,1,\ldots,N/2$, when N is even, or $k=0,1,\ldots,(N-1)/2$, when N is odd.

3.3.4 Numerical Validation: Example System in Fig. 3.7

In this section, the example system in Fig. 3.7 is solved to illustrate the modal properties and validate the effectiveness of reduced eigenvalue problems obtained from the above group-theory-based analysis. The system includes six substructures ($N=6$), each of which has two degrees of freedom ($L=2$). As mentioned in Section 3.3.1, a minor revision on Eqs. (3.46) and (3.47) (by excluding $\mathbf{I}_2$ in the these equations) is necessary because the vibrating rigid-body central component ($M_R=1$) has three planar degrees of freedom. As discussed in Appendix B, the compliant central component is a ring whose deformation can be described by the tangential motion of the points on the ring ($M_C=1$). The radial and axial coordinates that of a point on the ring can be ignored, *i.e.*, $f(\mathbf{r},t)=f(\theta,t)$ and $h_m(r,z)$ in Eq. (3.42) is the constant 1. The equation of motion and eigenvalue problem are given in Eqs. (3.58) and (3.60).

To numerically solve the system eigensolutions, $f(\theta,t)$ is approximated by a linear combination of the Fourier components whose harmonic orders vary from -6 to 6, *i.e.*, L_m in Eq. (3.42) is 1. The eigenvalue problem in Eq. (3.60) is first discretized using the columns

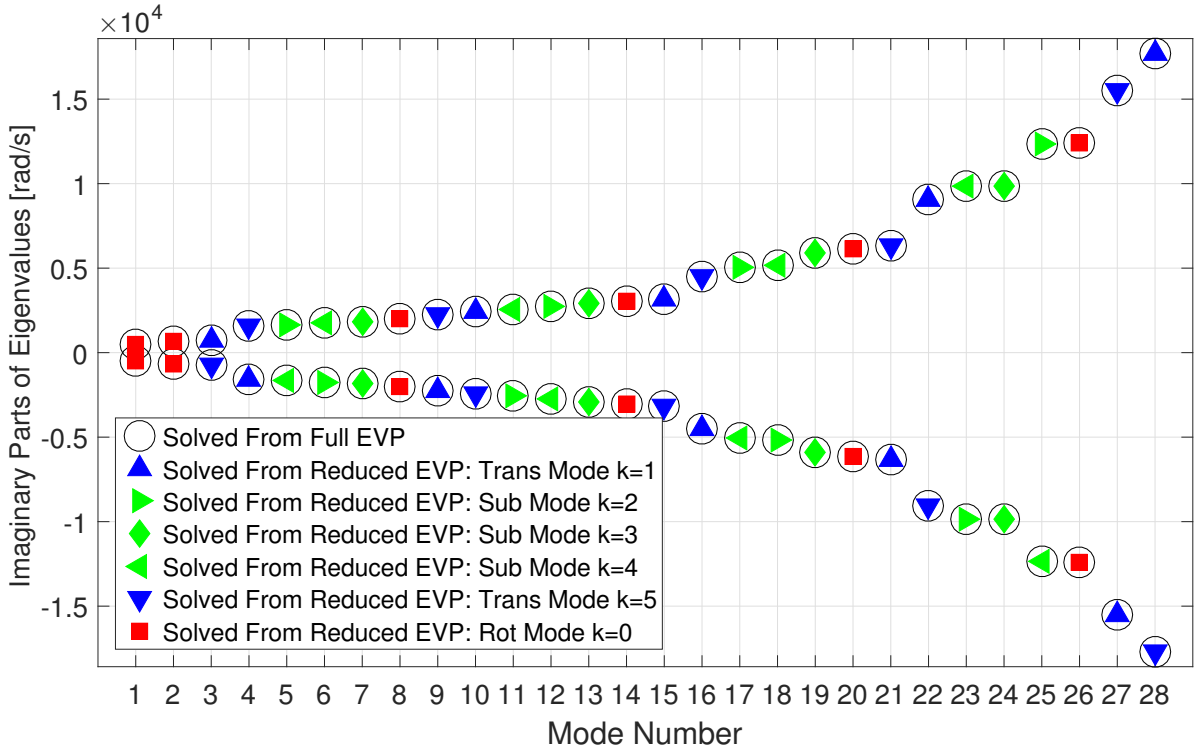

Figure 3.8: Natural frequencies of the example system in Fig. 3.7.

of $\boldsymbol{\chi}$ in Eq. (3.52) as the basis vectors, and the size of the discretized eigenvalue problem is $3M_C + NL + \sum_{m=1}^{M_C}(2L_mN + 1) = 28$. This discretized eigenvalue problem is referred to as the full discretized eigenvalue problem of this example system. 56 eigensolutions are obtained by solving this full discretized eigenvalue problem, and the eigenvalues are shown in Fig. 3.8.

According to the analysis in Sections 3.3.2 and 3.3.3, all the eigensolutions can be solved from 6 reduced discretized eigenvalue problems, each of which is characterized by a phase index k. For the case when $k = 0$, the number of columns in $\boldsymbol{\chi}^{(0,1)}$ in Eq. (3.51) is $M_C + L + \sum_{m=1}^{M_C}(2L_m + 1) = 6$, so the reduced eigenvalue problem characterized by $k = 0$ is of the size 6×6. 12 rotational modes (in 6 complex conjugate pairs) can be obtained by solving the reduced eigenvalue problem characterized by $k = 0$. Similarly, for the cases when $k = 1$ and $N - 1$, the two reduced eigenvalue problems are of the size

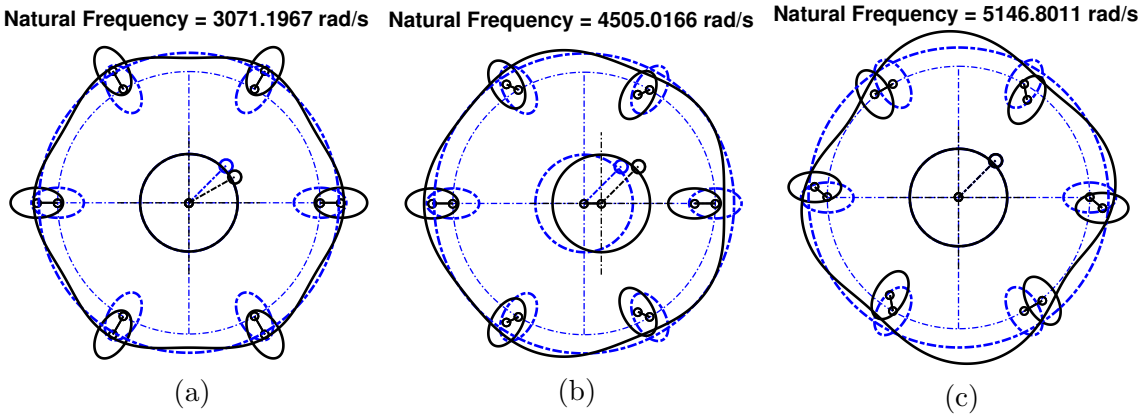

Figure 3.9: Example modes of the example system in Fig. 3.7. Only the real parts of the eigenvectors are illustrated. (a) A rotational mode (mode number 14). (b) A translational mode mode number 16). (c) A substructure mode (mode number 18).

5×5 ($M_C + L + 2\sum_{m=1}^{M_C} L_m = 5$). 10 translational modes are obtained by solving either of the problems, and the eigensolutions of these two reduced eigenvalue problems are complex conjugates to each other. For the cases when $k = 2, 3, \ldots, N-2$, the reduced eigenvalue problems are all of the size 4×4 ($L + 2\sum_{m=1}^{M_C} L_m = 4$). By solving each of these problems, 8 substructure modes can be obtained. Therefore, before numerically solving these reduced eigenvalue problems, the number of modes in each mode types are known.

As shown in Fig. 3.8, the eigenvalues obtained by solving all the 6 reduced eigenvalue problems match those from the full eigenvalue problem. Figure 3.9 illustrates three example modes (the mode numbers are 14, 16, and 18) solved from the full eigenvalue problem. Based on Fig. 3.8, these three modes can also be solved from the reduced eigenvalue problems characterized by $k = 0$, 5, and 4, respectively. Therefore, these three modes are a substructure modes, a rotational modes, and a translational modes according to their phase indices. As shown in Fig. 3.9, the modal deflection characteristics in these three modes match the modal properties obtained in Section 3.3.2.

3.4 Conclusions

In this work, modal properties of general cyclically symmetric systems with rigid-body and compliant central components are obtained through group-theory-based modal analysis. This work generalizes the previous studies on the modal properties of cyclically symmetric systems in Refs. [26, 29, 105], where compliant central components, such as the elastic ring gear in planetary gears [15], are not considered. In this work, the general cyclically symmetric systems studied are allowed to have arbitrary numbers of substructures, rigid-body central components, and compliant central components. The rigid-body central components are allowed to have six degrees of freedom, and the number of degrees of freedom in each substructure or compliant central component is arbitrary. The modal properties of a cyclically symmetric system with $\mathcal{C}_N$ symmetry include:

1. In any mode, substructures vibrate identically but with particular phase relations between them. The phase relations between substructures can be characterized by phase indices k from 0 to $N-1$. Similar phase relations also exists between the N equally partitioned sectors of any compliant central component. For any mode, the phase relations between the substructures and between the sectors of compliant central components are characterized by the same phase index.

2. According to the modal deflections of the rigid-body central components, all the modes are classified into three categories, rotational-axial modes, translational-tilting modes, and substructure modes.

3. In rotational-axial modes, the only non-zero modal deflections of any rigid-body central component are the axial translation and the rotation about the system symmetry axis. The substructures vibrate in phase (phase index $k = 0$), and the modal deformations of compliant central components only have the nodal diameter components of the

harmonic order equal to NS, where S is an arbitrary integer.

4. In translational-tilting modes, the rigid-body central components can only tilt out-of-plane and translate in-plane, while the phase relation between substructures is characterized by the phase index $k = 1$ or $N - 1$. The modal deformations of compliant central components only have the nodal diameter components of the harmonic order $NS \pm 1$.

5. In substructure modes, the rigid-body central components are non-vibrating, but both the substructures and compliant central components can vibrate. Substructure modes are characterized by phase indices from 2 to $N - 2$. The modal deformations of compliant central components only have the nodal diameter components of the harmonic order $NS + k$, when a substructure mode is characterized by the phase index k.

Through group theory, the derivation of all the above modal properties does not rely on any preliminary knowledge of the properties of matrix operators in system equation of motion, which is required in previous studies [29, 105]. The symmetry-adapted bases of different symmetry species can be obtained through algorithmic, computationally inexpensive calculations. Once the symmetry-adapted bases are obtained, the above modal properties are known. All the eigensolutions can be obtained by solving smaller eigenvalue problems that are built based on the symmetry-adapted bases characterized by different phase indices. Therefore, group-theory-based modal analysis is advantageous in improving the computational efficiency and identifying modal properties of symmetric systems.

Appendix B. Equation of Motion and Eigenvalue Problem of the Example Systems

The example systems in Figs. 3.2 and 3.7 can be assembled by the components and coupling elements in Fig. 3.10. The example system in Fig. 3.2 consists of the rigid-body

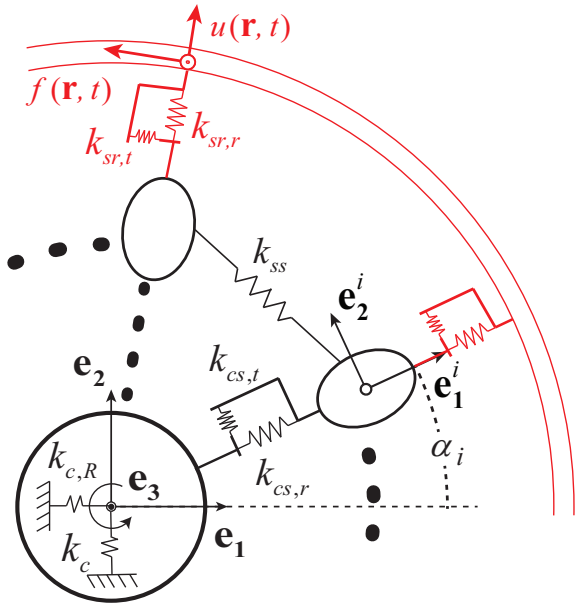

Figure 3.10: Components and coupling elements that assemble the example systems.

central components and the substructures, but the compliant central component, the ring, is not included. The equation of motion for the example system in Fig. 3.2 (free vibration cases) is formulated as

$$\mathbf{M}\ddot{\mathbf{q}} + \Omega\mathbf{G}\dot{\mathbf{q}} + (\mathbf{K}_V - \Omega^2\mathbf{K}_T)\mathbf{q} = \mathbf{0}, \tag{3.55a}$$

$$\mathbf{q} = (x_c, y_c, \mu_c, \underbrace{r_1, s_1, r_2, s_2, \ldots}_{2N})^T, \tag{3.55b}$$

where all coordinates are defined in local reference frames and there are N substructures. The matrices are

$$\mathbf{M} = \mathrm{diag}(\mathbf{M}_{cc}, \mathbf{M}_{ss}), \tag{3.56a}$$

$$\mathbf{M}_{cc} = \mathrm{diag}(m_c, m_c, J_z),\ \mathbf{M}_{ss} = \mathrm{diag}(\underbrace{m_s, m_s, \ldots, m_s}_{2N}), \tag{3.56b}$$

$$\mathbf{G} = \mathrm{diag}(\mathbf{G}_{cc}, \mathbf{G}_{s_1 s_1}, \mathbf{G}_{s_2 s_2}, \ldots, \mathbf{G}_{s_N s_N}), \tag{3.56c}$$

$$\mathbf{G}_{cc} = \begin{pmatrix} 0 & -2m_c & 0 \\ 2m_c & 0 & 0 \\ 0 & 0 & 0 \end{pmatrix},\ \mathbf{G}_{s_i s_i} = \begin{pmatrix} 0 & -2m_s \\ 2m_s & 0 \end{pmatrix}, \tag{3.56d}$$

$$\mathbf{K}_V = \begin{pmatrix} \mathbf{K}_{cc,V} & \mathbf{K}_{cs,V} \\ \mathbf{K}_{cs,V}^T & \mathbf{K}_{ss,V} \end{pmatrix}, \tag{3.56e}$$

$$\mathbf{K}_{cc,V} = \mathrm{diag}(k_c, k_c, k_{c,R}) + \sum_{i=1}^{N} \hat{\mathbf{K}}_{cc,V}^i,$$

$$\hat{\mathbf{K}}_{cc,V}^i = \begin{pmatrix} k_{cs,r}\cos^2\alpha_i + k_{cs,t}\sin^2\alpha_i & \frac{1}{2}(k_{cs,r} - k_{cs,t})\sin 2\alpha_i & 0 \\ \frac{1}{2}(k_{cs,r} - k_{cs,t})\sin 2\alpha_i & k_{cs,t}\cos^2\alpha_i + k_{cs,r}\sin^2\alpha_i & 0 \\ 0 & 0 & k_{cs,t}L_0^2 \end{pmatrix} \tag{3.56f}$$

$$\mathbf{K}_{cs,V} = \begin{pmatrix} \mathbf{K}_{cs_1,V} & \mathbf{K}_{cs_2,V} & \ldots & \mathbf{K}_{cs_N,V} \end{pmatrix},$$

$$\mathbf{K}_{cs_i,V} = \begin{pmatrix} -k_{cs,r}\cos\alpha_i & k_{cs,t}\sin\alpha_i \\ -k_{cs,r}\sin\alpha_i & -k_{cs,t}\cos\alpha_i \\ 0 & -k_{cs,t}L_0 \end{pmatrix}, \tag{3.56g}$$

$$\mathbf{K}_{ss,V} = \{\mathbf{K}_{s_i s_l,V}\}_{N\times N \text{ blocks}}$$

$$\mathbf{K}_{s_i s_i,V} = \text{the } i\text{th diagonal block of } \mathbf{K}_{ss,V}$$

$$= \begin{pmatrix} k_{cs,r} + k_{ss}(\sin^2 a_i + \sin^2 b_i) & \frac{1}{2}k_{ss}(\sin 2b_i - \sin 2a_i) \\ \frac{1}{2}k_{ss}(\sin 2b_i - \sin 2a_i) & k_{cs,t} + k_{ss}(\cos^2 a_i + \cos^2 b_i) \end{pmatrix},$$

$$\mathbf{K}_{s_i s_{i+1},V} = \begin{pmatrix} k_{ss}\sin^2 a_i & \frac{1}{2}k_{ss}\sin 2a_i \\ -\frac{1}{2}k_{ss}\sin 2a_i & -k_{ss}\cos^2 a_i \end{pmatrix}, \tag{3.56h}$$

$$\mathbf{K}_{s_i s_{i-1},V} = \begin{pmatrix} k_{ss}\sin^2 b_i & -\frac{1}{2}k_{ss}\sin 2b_i \\ \frac{1}{2}k_{ss}\sin 2b_i & -k_{ss}\cos^2 b_i \end{pmatrix},$$

$$a_i = \alpha_{i+1} - \alpha_i,\ b_i = \alpha_i - \alpha_{i-1},$$

$$\mathbf{K}_T = \text{diag}(\mathbf{K}_{cc,T}, \mathbf{K}_{s_1 s_1,T}, \mathbf{K}_{s_2 s_2,T}, \ldots, \mathbf{K}_{s_N s_N,T}), \tag{3.56i}$$

$$\mathbf{K}_{cc,T} = \text{diag}(m_c, m_c, 0), \tag{3.56j}$$

$$\mathbf{K}_{s_i s_i,T} = \text{diag}(m_s, m_s). \tag{3.56k}$$

For the example system in Fig. 3.7, an elastic ring is coupled with the substructures, and the ring is rotating with the same constant speed as the substructures. The bending of the ring is considered to be the only source of the ring deformation, and the ring radial deflection is determined from the inextensibility condition [6]

$$u(\mathbf{r}, t) = -\partial f(\mathbf{r}, t)/\partial\theta, \tag{3.57}$$

where u and f are the radial and tangential deformations of the ring. Therefore, the deformation of the ring can be purely described by the tangential deflections of the points on the ring. Because the azimuth coordinate θ is sufficient to identify a point on a ring, $f(\mathbf{r}, t)$ can be written as $f(\theta, t)$. The full system vibration can be described by an extended variable

$\mathbf{q}_e = (f(\theta,t), \mathbf{q})^T$, and the full system equation of motion is

$$\mathbf{M}_e\ddot{\mathbf{q}}_e + \Omega\mathbf{G}_e\dot{\mathbf{q}}_e + (\mathbf{K}_{eV} - \Omega^2\mathbf{K}_{eT})\mathbf{q}_e = \mathbf{0}, \tag{3.58a}$$

$$\mathbf{M}_e = \begin{pmatrix} \rho(\frac{\partial^2}{\partial t^2} - \frac{\partial^4}{\partial t^2\partial\theta^2}) & \mathbf{0} \\ \mathbf{0} & \mathbf{M} \end{pmatrix}, \tag{3.58b}$$

$$\mathbf{G}_e = \begin{pmatrix} -4\rho\frac{\partial^2}{\partial t\partial\theta} & \mathbf{0} \\ \mathbf{0} & \mathbf{G} \end{pmatrix}, \tag{3.58c}$$

$$\mathbf{K}_{eT} = \begin{pmatrix} \rho(1 - \frac{\partial^2}{\partial\theta^2}) & \mathbf{0} \\ \mathbf{0} & \mathbf{K}_T \end{pmatrix}, \tag{3.58d}$$

$$\mathbf{K}_{eV} = \begin{pmatrix} L_1 & \mathbf{L}_2 \\ \mathbf{L}_3 & \mathbf{K}_V + \mathbf{L}_4 \end{pmatrix},$$

$$L_1 = k_{sr,t} - \sum_{i=1}^{N} k_{sr,r}\Big[\delta(\theta-\alpha_i)\frac{\partial^2}{\partial\theta^2} + \frac{\partial\delta(\theta-\alpha_i)}{\partial\theta}\frac{\partial}{\partial\theta}\Big] - k_{bend}\Big(\frac{\partial^6}{\partial\theta^6} + 2\frac{\partial^4}{\partial\theta^4} + \frac{\partial^2}{\partial\theta^2}\Big),$$

$$\mathbf{L}_2 = \begin{pmatrix} \mathbf{0}_{1\times3} & -k_{sr,r}\frac{\partial\delta(\theta-\alpha_1)}{\partial\theta} & -k_{sr,t}\delta(\theta-\alpha_1) & \dots & -k_{sr,r}\frac{\partial\delta(\theta-\alpha_N)}{\partial\theta} & -k_{sr,t}\delta(\theta-\alpha_N) \end{pmatrix},$$

$$\mathbf{L}_3 = \begin{pmatrix} \mathbf{0}_{1\times3} & -k_{sr,r}\frac{\partial}{\partial\theta}|_{\theta=\alpha_1} & -k_{sr,t}(\bullet)|_{\theta=\alpha_1} & \dots & -k_{sr,r}\frac{\partial}{\partial\theta}|_{\theta=\alpha_N} & -k_{sr,t}(\bullet)|_{\theta=\alpha_N} \end{pmatrix}^T,$$

$$\mathbf{L}_4 = \mathrm{diag}(0,0,0,\underbrace{k_{sr,r}, k_{sr,t}, \dots, k_{sr,r}, k_{sr,t}}_{2N}),$$

(3.58e)

where $\delta()$ is the Dirac delta function, and $(\bullet)|_{\theta=x}$ is the operator to evaluate the function when $\theta = x$, *i.e.*, $(\bullet)|_{\theta=x} f(\theta,t) = f(\theta,t)|_{\theta=x} = f(x,t)$.

The eigenvalue problem of Eq. (3.55) is

$$(\lambda^2\mathbf{M} + \lambda\Omega\mathbf{G} + \mathbf{K}_V - \Omega^2\mathbf{K}_T)\boldsymbol{\phi} = \mathbf{0}, \tag{3.59}$$

where λ and $\boldsymbol{\phi}$ are the system eigenvalue and eigenvector, respectively. The eigenvalue problem of Eq. (3.58) is

$$(\lambda_e^2\tilde{\mathbf{M}}_e + \lambda_e\Omega\tilde{\mathbf{G}}_e + \mathbf{K}_{eV} - \Omega^2\mathbf{K}_{eT})\boldsymbol{\phi}_e = \mathbf{0}, \tag{3.60a}$$

$$\tilde{\mathbf{M}}_e = \begin{pmatrix} \rho(1 - \frac{\partial^2}{\partial\theta^2}) & \mathbf{0} \\ \mathbf{0} & \mathbf{M} \end{pmatrix}, \tag{3.60b}$$

$$\tilde{\mathbf{G}}_e = \begin{pmatrix} -4\rho\frac{\partial}{\partial\theta} & \mathbf{0} \\ \mathbf{0} & \mathbf{G} \end{pmatrix}. \tag{3.60c}$$

Different sets of parameters apply to the example systems. The parameters in Table 3.5 apply to all the examples, while Table 3.6 provides the parameters that vary with different systems.

System Parameters	**Value**
C.C. mass, m_c (kg)	20
C.C. moment of inertia along $\mathbf{e}_3$, J_z (kg-m^2)	10.0
C.C. translational stiffness to non-vibrating rotor, k_c (N/m)	5.2×10^6
C.C. rotational stiffness to non-vibrating rotor, $k_{c,R}$ (N-m/rad)	1.0×10^7
Radius of Sub. undeflected position, L_0 (m)	1
Radial stiffness between C.C. and a Sub., $k_{cs,r}$ (N/m)	2.5×10^6
Tangential stiffness between C.C. and a Sub., $k_{cs,t}$ (N/m)	3.0×10^6

Table 3.5: System parameters for all example systems consisting of the components and coupling elements in Fig. 3.10. These parameters apply to both example systems in Figs. 3.2 and 3.7. Abbreviations C.C. and Sub. represent rigid-body central component and substructure, respectively, and they are also used in Table 3.6.

System Parameters	**Value**
System with $\mathcal{D}_2$ symmetry (Fig. 3.2)	
Angular positions of Subs., α_i (deg)	20, 40, 75, 105, 140, 160, 200, 220, 255, 285, 320, 340
Mass of a Sub., m_s (kg)	1.5
Stiffness between Subs., k_{ss} (N/m)	2.5×10^6
Rotational speed of non-vibrating C.C., Ω (rad/s)	0
Cyclically symmetric system (Fig. 3.7)	
Angular positions of Subs., α_i (deg)	0, 60, 120, 180, 240, 300
Radial stiffness between the ring and a Sub., $k_{sr,r}$ (N/m)	2.0×10^6
Tangential stiffness between the ring and a Sub., $k_{sr,t}$ (N/m)	2.0×10^6
Mass of a Sub., m_s (kg)	1
Stiffness between Subs., k_{ss} (N/m)	2.0×10^6
Angular density of the ring, ρ (kg/rad)	0.05
Bending stiffness of the ring, k_{bend} (N/m)	1.0×10^4
Rotational speed of non-vibrating C.C., Ω (rad/s)	100

Table 3.6: Parameters of the components and coupling elements in Fig. 3.10 that are different in the example systems in Figs. 3.2 and 3.7.

Chapter 4

Group-Theory-Based Modal Analysis of Multi-Stage Systems with Arbitrary Symmetry of Component Stages

4.1 Introduction

A system is symmetric if there exist operations that bring the system into self-coincidence and leave it indistinguishable from its original configuration. Many mechanical systems have symmetric structures. For example, rotating systems such as bladed disks [2, 3], circular rings [6, 8], planetary gears [11, 12, 16], and centrifugal pendulum vibration absorbers (CPVA) [18, 40] are cyclically symmetric, while systems such as thin plates [57] and space-truss domes [106] may have other types of symmetry.

Group theory has been a powerful mathematical tool for studying symmetric systems

within areas such as molecular chemistry and condensed matter physics [1, 52]. The essential procedure of a group-theory-based method is to decompose the vector space of the original problem into a number of smaller subspaces, where the original problem is reduced into smaller formulations that can be solved with less computational effort. Meanwhile, some qualitative symmetry-related modal properties of the system are obtained by the group-theory-based analysis [57]. Group theory is advantageous for analyzing symmetric systems, but it has not been widely used in engineering vibration problems.

In many engineering applications, multiple symmetric structures are coupled with each other to form a multi-stage system. For example, such multi-stage structures exist in bladed disks [66–73], compound planetary gears [74, 76], and CPVA systems with multiple groups of absorbers [19, 20]. In studies on multi-stage bladed disks [66–73], the inter-stage couplings are modeled using constraint equations for the interface degrees of freedom for different single-stages. Bladh *et al.* [66] showed the necessity of modeling multi-stage bladed disks because the behavior of bladed disks is influenced by the interaction between different stages. Reduced order models of multi-stage bladed disks are built using component mode synthesis [67–69] and multi-stage cyclic symmetry reduction [70–73]. On the other hand, in the models of compound planetary gears [74, 76] and CPVA systems with multiple groups of absorbers [19, 20], different stages of symmetric systems are coupled through a vibrating central component (*e.g.*, the rotor in CPVA). Similar modal properties are obtained for such multi-stage structures [19, 74, 76]. Furthermore, Shi *et al.* [20] applied these modal properties to reduce the translational and rotational rotor vibrations by tuning multiple groups of absorbers.

A challenge of studying the modal properties of a system with multiple symmetric stages is that the whole multi-stage system is not symmetric even though individual stages are. For example, a structure composed of two cyclically symmetric stages is not symmetric if the numbers of substructures (*e.g.*, the absorbers in CPVA) per stage are coprime, *i.e.*, the only

positive integer that divides both the numbers is one. In this case, mathematical tools that apply to perfectly symmetric systems, such as circulant matrix theory for cyclically symmetric systems [26], are not proper to analyze the modal properties of multi-stage symmetric systems.

The goal of this work is to build a group-theory-based method to analyze the modal properties of multi-stage systems with symmetric component stages. Specifically, the multi-stage systems considered are composed of stages that may exhibit any type of symmetry with no constraint that the type of symmetry be the same in each stage, and these stages are coupled through the motions of rigid-body central components. For example, stages in multi-stage planetary gears are coupled with other stages through the motions of central (*i.e.,* sun and ring) gears, shafts, and carriers [74]. Cases where the stages are coupled through the motions of components that are off the symmetry axes of individual stages are out of the scope of this work.

This paper is organized as follows. In Section 4.2, the general principles of group-theory-based modal analysis are summarized, and they apply to both single-stage and multi-stage systems with symmetric structures. In Section 4.3, group theory for single-stage symmetric systems is introduced. In Section 4.4, the mode classification for single-stage symmetric systems with rigid-body central components is studied in preparation to generalize group theory to multi-stage systems. In Section 4.5, a group-theory-based method is developed to analyze the modal properties of multi-stage systems with symmetric stages. Through the proposed method, reduced eigenvalue problems for multi-stage systems with symmetric stages are formulated and qualitative modal properties are obtained. Two examples of multi-stage systems with symmetric stages are given, one of which is a multi-stage system with cyclically symmetric stages that generalizes multi-stage planetary gears and CPVA systems with multiple groups of absorbers.

4.2 Principles of Group-Theory-Based Modal Analysis

Eigenvalue problems for multi-degrees-of-freedom systems take the general form

$$\mathbf{A}(\lambda)\boldsymbol{\phi} = [\lambda^2\mathbf{M} + \lambda\mathbf{C} + \mathbf{K}]\boldsymbol{\phi} = \mathbf{0}, \tag{4.1}$$

where the matrix operator $\mathbf{A}$ is a polynomial of the eigenvalue λ, including the inertia matrix $\mathbf{M}$, the stiffness matrix $\mathbf{K}$, and $\mathbf{C}$ can include the damping and gyroscopic matrices. All these matrices are not necessary to be symmetric. Instead of directly solving a full eigenvalue problem, a more computationally efficient method is to transform the full problem into problems of smaller size. To achieve this goal, the eigenvector $\boldsymbol{\phi}$ is expanded as a linear combination of the columns of a square, unitary transformation matrix $\mathbf{U}$ ($\mathbf{U}^\dagger\mathbf{U} = \mathbf{I}$, where $\mathbf{I}$ is the identity matrix and $\mathbf{U}^\dagger$ is the hermitian transpose of $\mathbf{U}$),

$$\boldsymbol{\phi} = \mathbf{U}\hat{\boldsymbol{\phi}} = \begin{pmatrix} \mathbf{U}_1 & \mathbf{U}_2 & \dots & \mathbf{U}_W \end{pmatrix} \hat{\boldsymbol{\phi}}. \tag{4.2}$$

If the matrix $\mathbf{U}$ has the following property,

$$\mathbf{U}_i^\dagger \mathbf{A} \mathbf{U}_h = \begin{cases} \mathbf{0} & i \neq h \\ \tilde{\mathbf{A}}_i & i = h \end{cases}, \tag{4.3}$$

the matrix $\mathbf{U}^\dagger\mathbf{A}\mathbf{U}$ is block diagonal. Substitution of Eq. (4.2) into Eq (4.1) and pre-multiplication by $\mathbf{U}^\dagger$ give

$$\mathbf{U}^\dagger\mathbf{A}\mathbf{U}\hat{\boldsymbol{\phi}} = \tilde{\mathbf{A}}\hat{\boldsymbol{\phi}} = \begin{pmatrix} \tilde{\mathbf{A}}_1 & & & \\ & \tilde{\mathbf{A}}_2 & & \\ & & \ddots & \\ & & & \tilde{\mathbf{A}}_W \end{pmatrix} \begin{pmatrix} \hat{\boldsymbol{\phi}}_1 \\ \hat{\boldsymbol{\phi}}_2 \\ \vdots \\ \hat{\boldsymbol{\phi}}_W \end{pmatrix} = \mathbf{0}, \tag{4.4}$$

where $\tilde{\mathbf{A}}_i = \mathbf{U}_i^\dagger\mathbf{A}\mathbf{U}_i$ and $(\hat{\boldsymbol{\phi}}_1, \hat{\boldsymbol{\phi}}_2, \ldots, \hat{\boldsymbol{\phi}}_W)^T = \hat{\boldsymbol{\phi}}$.

Solving Eq. (4.4) is equivalent to solving the W reduced eigenvalue problems,

$$\tilde{\mathbf{A}}_i\hat{\boldsymbol{\phi}}_i = \mathbf{0}, \ \ i = 1, 2, ..., W, \tag{4.5}$$

Every eigensolution $(\lambda, \hat{\boldsymbol{\phi}}_i)$ of Eq. (4.5) generates an eigensolution of Eq. (4.4) where the eigenvalue is λ and the eigenvector is

$$\hat{\boldsymbol{\phi}} = (\mathbf{0}, \ldots, \mathbf{0}, \hat{\boldsymbol{\phi}}_i, \mathbf{0}, \ldots, \mathbf{0})^T. \tag{4.6}$$

Because $\mathbf{U}$ is unitary, the eigenvalues in Eqs. (4.4) and (4.1) are identical. Therefore, the eigenvalues of the W reduced eigenvalue problems in Eq. (4.5) are also the eigenvalues of the full eigenvalue problem in Eq. (4.1). Meanwhile, substitution of Eq. (4.6) into Eq. (4.2) gives

$$\boldsymbol{\phi} = \mathbf{U}_i\hat{\boldsymbol{\phi}}_i, \tag{4.7}$$

which indicates the eigenvectors solved from Eq. (4.5) generate full system eigenvectors of the original problem. Thus, the full eigenvalue problem in Eq. (4.1) can be decomposed into W reduced problems if a unitary matrix with the property in Eq. (4.3) is found.

Applying a unitary transformation to block diagonalize the full system matrix operator $\mathbf{A}$ in Eq. (4.1) provides two significant benefits. First, the computational efficiency is improved by solving the W reduced eigenvalue problems in Eq. (4.5), instead of solving the full eigenvalue problem (Eq. (4.1)). The size of the ith reduced eigenvalue problem in Eq. (4.5) is determined by the number of columns in the matrix $\mathbf{U}_i$, which is a portion (averaging $1/W$ in size) of the number of total degrees of freedom. Such improvement of computational efficiency is more significant when the system has many degrees of freedom or W is large.

Second, the properties of the full system modes can be obtained. Eq. (4.7) indicates the reduced eigenvectors solved from Eq. (4.5) generate modes that are linear combinations of the columns in $\mathbf{U}_i$ only. The modal deflection properties of a mode type are determined by the properties of the column vectors that comprise $\mathbf{U}_i$. Thus, the full system modes can be categorized into W types, and each type can be obtained from a reduced eigenvalue problem in Eq. (4.5). The number of modes in the ith type equals the number of reduced eigenvectors from Eq. (4.5), which equals the number of columns in $\mathbf{U}_i$ multiplied by the order of λ in Eq. (4.5). All these qualitative modal properties can be obtained based on the matrix $\mathbf{U}$ in Eq. (4.6) without need to numerically solve any eigenvalue problems.

Although application of unitary transformations is beneficial as shown above, obtaining such a unitary matrix (satisfying Eq. (4.3)) for an arbitrary system can be hard. Although the modal matrix of a system can serve as a proper unitary transformation matrix, this option is not helpful because it requires the computationally expensive numerical solution of Eq. (4.1) and does not provide the two benefits described above. Therefore, the focus of the following sections is to obtain the unitary matrix for a symmetric system or a multi-stage system with symmetric stages.

4.3 Group-Theory-Based Modal Analysis for Single-Stage Symmetric Systems

For a single-stage symmetric system, group theory provides a systematic method to identify the desired unitary matrix with trivial computational cost. This process relies only on the symmetry of the system and does not rely on the equations of motion. According to group theory [1, 52], for any single-stage symmetric system, the configuration space of the system can be decomposed into a number of separated subspaces that are spanned by the symmetry-adapted bases. The number of these subspaces (denoted as W) are determined by the number of irreducible representations of the symmetry group and the dimensions of the representations. These numbers for a symmetry group are independent of the equation of motion for specific symmetric system, and they are available in mathematics literature [1, 52]. The process of obtaining the symmetry-adapted bases is provided in details in Chapter 3, and the methodology can also be found in Refs. [1, 52]. For brevity, this process in Chapter 3 is not introduced.

The basis vectors (referred to as the *symmetry vectors* in Ref. [1]) that form a symmetry-adapted basis for one subspace are said to be of the same symmetry species. The matrix containing all the symmetry vectors is a unitary matrix. According to the symmetry species of the symmetry vectors, it can be partitioned as

$$\begin{aligned}\mathbf{U} &= \Big(\underbrace{\mathbf{u}_1^{(\alpha,1)}\ \mathbf{u}_2^{(\alpha,1)}\ \dots}_{\text{Species } (\alpha,1)}\ \underbrace{\mathbf{u}_1^{(\alpha,2)}\ \mathbf{u}_2^{(\alpha,2)}\ \dots}_{\text{Species } (\alpha,2)}\ \dots\ \underbrace{\mathbf{u}_1^{(\beta,1)}\ \mathbf{u}_2^{(\beta,1)}\ \dots}_{\text{Species } (\beta,1)}\ \underbrace{\dots}_{etc.} \Big) \\ &= \Big(\underbrace{\mathbf{U}^{(\alpha,1)}\quad \mathbf{U}^{(\alpha,2)}\quad \dots\quad \mathbf{U}^{(\beta,1)}\quad \dots}_{W\,submatrices} \Big),\end{aligned} \tag{4.8}$$

where the vector $\mathbf{u}_\mu^{(\gamma,i)}$ is the μth symmetry vector of the symmetry species (γ, i). Based on

group theory [1], this matrix has the property analogous to those of $\mathbf{U}$ in Eq. (4.3), *i.e.*,

$$\mathbf{U}^{(\gamma,i)\dagger}\mathbf{A}\mathbf{U}^{(\rho,h)} = \begin{cases} \mathbf{0} & \gamma \neq \rho \text{ or } i \neq h \\ \tilde{\mathbf{A}}^{(\gamma,i)} & \gamma = \rho \text{ and } i = h \end{cases} . \tag{4.9}$$

The property in Eq. (4.9) is the orthogonality of symmetry species. With $\mathbf{U}$ in Eq. (4.2) determined as shown above, the full eigenvalue problem in Eq. (4.1) is decomposed into reduced eigenvalue problems in the form of Eq. (4.5), with the subscript i in Eq. (4.5) being replaced by the superscript (γ, i) labeling the symmetry species, as shown in Eq. (4.9). The number of reduced eigenvalue problems equals the number of symmetry species W.

Because any eigenvector in Eq. (4.1) is a linear combination of symmetry vectors in one symmetry species only (as shown in Eq. (4.7) with $\mathbf{U}_i$ being replaced by $\mathbf{U}^{(\gamma,i)}$). The vibration modes of a symmetric system can be classified into different types corresponding to the different symmetry species. Meanwhile, the vibration modes of a given type have the properties of the symmetry vectors in the symmetry species that defines the mode type. Thus, the number of mode types, the number of modes in each type, and the characteristic modal deflection of each mode type are all available. Such analysis can be done by algorithmic and computationally inexpensive calculations as shown in Chapter 3. Because the calculations only involve the system symmetry and the definitions of all degrees of freedom, the system equation of motion are not even necessary to determine the modal properties. This benefit of group theory is preferred, because even if one solved the full eigenvalue problem in Eq. (4.1), the modes are not naturally separated into types nor the modal properties are revealed.

4.4 Mode Classification of Single-Stage Symmetric Systems with Rigid-Body Central Components

In a general single-stage symmetric system, a central component is a component that is left unmoved when a symmetry operation applies to the whole system, while substructures are the other components in the system. For example, in planetary gears with cyclic symmetry, the ring and sun gears are central components, while the planet gears are substructures. For symmetric systems with rigid-body central components, both the assembly of all central components and the assembly of all substructures can be regarded as two sub-systems, and the symmetry of both sub-systems are identical to the symmetry of the full system. Therefore, the symmetry vectors for these two sub-systems can be obtained separately. Both sub-systems have the same number of symmetry species, because the number of symmetry species is determined by the system symmetry. The symmetry vectors of the symmetry species (γ, i) for the sub-system including all central components are columns of the matrix $\mathbf{U}_c^{(\gamma,i)}$, while the symmetry vectors of the symmetry species (γ, i) for the sub-system including all substructures comprise the matrix $\mathbf{U}_s^{(\gamma,i)}$. In the following analysis, we consider $\mathbf{U}_c^{(\gamma,i)}$ and $\mathbf{U}_s^{(\gamma,i)}$ can be zero matrices. $\mathbf{U}_c^{(\gamma,i)} = \mathbf{0}$, for example, indicates the subspace of the symmetry species (γ, i) for the sub-system including all the central components vanishes.

As mentioned in Section 4.3, the symmetry vectors for a symmetric system are determined by the system symmetry and the definition of all degrees of freedom. The degrees of freedom of the full single-stage symmetric system include and only include the degrees of freedom of the two sub-systems, and the two sub-systems and the full system have the same symmetry type. Therefore, the submatrix $\mathbf{U}^{(\gamma,i)}$ in Eq. (4.8) for a full single-stage symmetric system can be obtained by assembling $\mathbf{U}_c^{(\gamma,i)}$ and $\mathbf{U}_s^{(\gamma,i)}$. The eigenvector $\boldsymbol{\phi}$ in Eq. (4.1) can

be partitioned as

$$\boldsymbol{\phi} = \begin{pmatrix} \boldsymbol{\phi}_c & \boldsymbol{\phi}_s \end{pmatrix}^T . \tag{4.10}$$

If the eigenvector $\boldsymbol{\phi}$ is of the symmetry species (γ, i), $\boldsymbol{\phi}_c$ in Eq. (4.10) is a linear combination of the columns in $\mathbf{U}_c^{(\gamma,i)}$ and $\boldsymbol{\phi}_s$ in Eq. (4.10) is a linear combination of the columns in $\mathbf{U}_s^{(\gamma,i)}$. Therefore, the submatrix $\mathbf{U}^{(\gamma,i)}$ in Eq. (4.8) have the general structure

$$\mathbf{U}^{(\gamma,i)} = \left[\begin{array}{c|c} \mathbf{U}_c^{(\gamma,i)} & \mathbf{0} \\ \hline \mathbf{0} & \mathbf{U}_s^{(\gamma,i)} \end{array} \right]^* , \tag{4.11}$$

where $[\ ]^*$ is the operation to retain only the linearly independent columns of a matrix.

Considering that $\mathbf{U}_c^{(\gamma,i)}$ and $\mathbf{U}_s^{(\gamma,i)}$ in Eq. (4.11) can be zero matrices, the general structure of $\mathbf{U}^{(\gamma,i)}$ in Eq. (4.11) leads to three possible non-empty structures of $\mathbf{U}^{(\gamma,i)}$,

$$\mathbf{U}^{(\gamma,i)} = \left(\begin{array}{c} \mathbf{0} \\ \hline \mathbf{U}_s^{(\gamma,i)} \end{array} \right) , \left(\begin{array}{c|c} \mathbf{U}_c^{(\gamma,i)} & \mathbf{0} \\ \hline \mathbf{0} & \mathbf{U}_s^{(\gamma,i)} \end{array} \right) , \text{ or } \left(\begin{array}{c} \mathbf{U}_c^{(\gamma,i)} \\ \hline \mathbf{0} \end{array} \right) , \tag{4.12}$$

where $\mathbf{U}_c^{(\gamma,i)}$ and $\mathbf{U}_s^{(\gamma,i)}$ are matrices with non-zero elements. Based on Eq. (4.7) (with the subscript i being replace by the superscript (γ, i)), these three structures in Eq. (4.12) are associated with substructure modes and coupled modes, pure central component modes, respectively, and these mode types are named according the non-zero deflections in a vibration mode. For a general symmetric system that include both central components and substructures, only the first two structures $\mathbf{U}^{(\gamma,i)}$ in Eq. (4.12) can exist, although not any symmetric systems are guaranteed to have submatrices in both forms. The third structure of $\mathbf{U}^{(\gamma,i)}$ in Eq. (4.12) can not exist in a general symmetric system that include both central components and substructures. The reasons are as follows.

The three possible structures of $\mathbf{U}^{(\gamma,i)}$ in Eq. (4.12) are obtained by assembling the

symmetry species of the two sub-systems (defined early) of the full systems. Because the derivation of symmetry species only relies on the system symmetry and the definition of the system degrees of freedom, if all the three possible structures of $\mathbf{U}^{(\gamma,i)}$ in Eq. (4.12) exist for a symmetric system, they should exist for any other system that has the same symmetry and definition of degrees of freedom. The third structure of $\mathbf{U}^{(\gamma,i)}$ in Eq. (4.12), however, can not meet this criterion when the system includes both the central components and the substructures. If the third structure of $\mathbf{U}^{(\gamma,i)}$ in Eq. (4.12) can exist for a given symmetric system, it indicates there are always some modes where the central components can move without influencing any substructure for any other system that has the same system symmetry and definition of degrees of freedom, no matter how the central components and the substructures are coupled. Based on the reaction forces between the central components and substructures, however, as long as substructures exist, such types of modes can always be ruled out by properly defining the couplings between the central components and substructures. Therefore, the third structure of $\mathbf{U}^{(\gamma,i)}$ in Eq. (4.12) can exist only when substructures do not exist in the symmetric system (a trivial case). In contrast, if the first two structures of $\mathbf{U}^{(\gamma,i)}$ in Eq. (4.12) can exist for a symmetric system, no contradiction is resulted for them to exist for any other system that has the same symmetry and definition of degrees of freedom. Therefore, the modes of a general single-stage symmetric systems with both central components and substructures are classified into two general categories, substructure modes and coupled modes.

Eq. (4.12) also leads to additional information of the orthogonality between symmetry species (Eq. (4.9)). Partitioning the eigenvector $\boldsymbol{\phi}$ in Eq. (4.1) as done in Eq. (4.10) leads

to a partition of the operator $\mathbf{A}$ in Eq. (4.1) as

$$\mathbf{A} = \begin{pmatrix} \mathbf{A}_{cc} & \mathbf{A}_{cs} \\ \mathbf{A}_{sc} & \mathbf{A}_{ss} \end{pmatrix}, \tag{4.13}$$

where $\mathbf{A}_{cc}$ connects the central components only, $\mathbf{A}_{ss}$ connects the substructures only, and $\mathbf{A}_{cs}$ and $\mathbf{A}_{sc}$ connects the central components and the substructures. Substitution of Eqs. (4.12) and (4.13) into Eq. (4.9) yields

$$\mathbf{U}_c^{(\gamma,i)} \mathbf{A}_{cc} \mathbf{U}_c^{(\rho,h)} = \mathbf{0}, \tag{4.14a}$$

$$\mathbf{U}_c^{(\gamma,i)} \mathbf{A}_{cs} \mathbf{U}_s^{(\rho,h)} = \mathbf{0}, \tag{4.14b}$$

$$\mathbf{U}_s^{(\gamma,i)} \mathbf{A}_{sc} \mathbf{U}_c^{(\rho,h)} = \mathbf{0}, \tag{4.14c}$$

$$\mathbf{U}_s^{(\gamma,i)} \mathbf{A}_{ss} \mathbf{U}_s^{(\rho,h)} = \mathbf{0}, \tag{4.14d}$$

where $\gamma \neq \rho$ or $i \neq h$. Eq. (4.14) will be used to build the unitary transformation matrices for multi-stage systems from the symmetry species of all component stages.

4.5 Group-Theory-Based Modal Analysis of Multi-Stage Structures with Symmetric Component Stages

Prior studies on multi-stage compound planetary gears [74] and centrifugal pendulum vibration absorbers with multiple groups of absorbers [19] indicate multi-stage structures with symmetric component stages possess unique mode structures. The systems in these works consist of cyclically symmetric stages that are coupled through the vibrating central components (*e.g.*, the ring gear, sun gear, and carrier in planetary gears). In this section, the

modal properties of multi-stage structures with symmetric component stages are analyzed based on group theory. The analysis applies to any multi-stage system with component stages having arbitrary symmetry. The component stages can have different symmetry types (*e.g.*, the example system in Fig. 4.1(b)). The component stages are coupled through the central component vibrations.

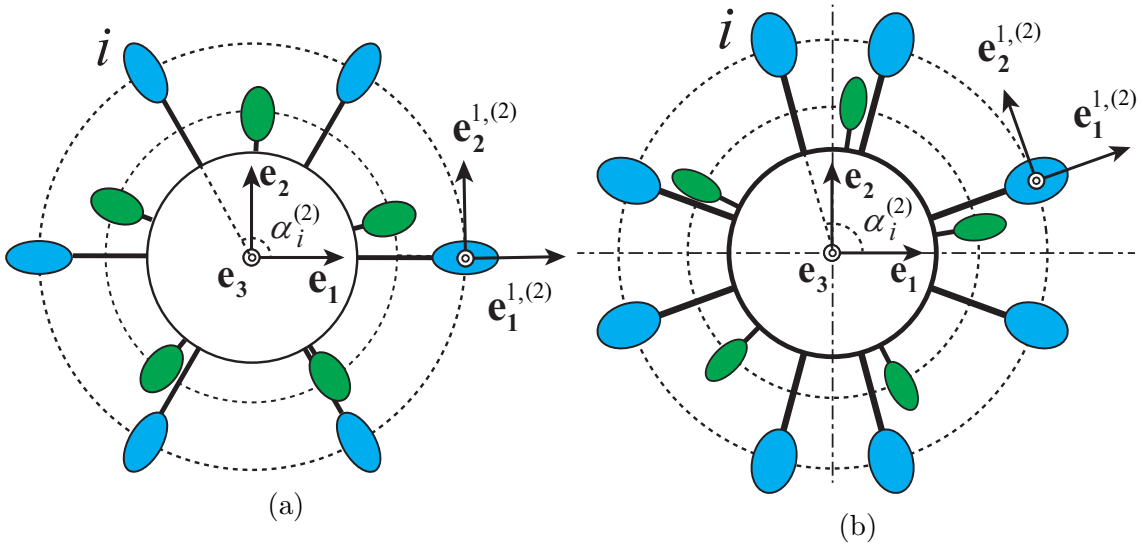

Figure 4.1: (a) An example multi-stage cyclically symmetric system. The two component stages exhibit $\mathcal{C}_5$ and $\mathcal{C}_6$ symmetry, respectively. (b) An example multi-stage symmetric system with two component stages that exhibit $\mathcal{C}_5$ and $\mathcal{D}_2$ symmetry, respectively.

An obstacle in studying the general modal properties of multi-stage systems with symmetric stages using conventional mathematical tools, such as the circulant matrix theory for cyclically symmetric systems [26], is that multi-stage systems are not generally symmetric (*e.g.*, the examples in Fig. 4.1). Although this precludes direct application of group theory to a multi-stage system, group-theory-based modal analysis of the component stages allows formulation of the unitary transformation matrix for multi-stage systems with symmetric component stages. Thus, as shown in what follows, the modal properties and the reduced eigenvalue problems are obtained through the general principles in Section 4.2.

To illustrate the proposed group-theory-based modal analysis, the example systems in

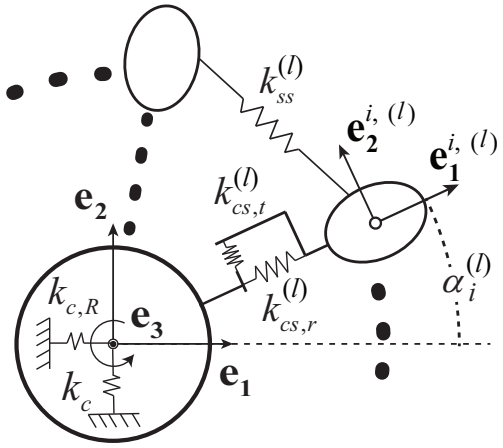

Figure 4.2: Components and coupling elements that assemble the example systems.

Fig. 4.1 are analyzed after the unitary transformation matrix for general multi-stage systems is formulated. Either of the examples consist of a vibrating central component (solid circle in Fig. 4.1) that has three planar degrees of freedom and substructures (ovals in Fig. 4.1) that have two planar translational degrees of freedom. The axes $\mathbf{e}_1^{i,(l)}$ and $\mathbf{e}_2^{i,(l)}$ associated with the ith substructure in the lth stage defines the direction of substructure radial and tangential motions, and are oriented with a fixed angle, $\alpha_i^{(l)}$, relative to the $\{\mathbf{e}_1, \mathbf{e}_2, \mathbf{e}_3\}$ basis that is associated with the central component motions. The couplings in these example systems are illustrated in Fig. 4.2. The full system is installed on a non-vibrating rotor that rotates at a constant speed Ω about $\mathbf{e}_3$ through the stiffness between the vibrating and non-vibrating rotor. The reference frames $\{\mathbf{e}_1, \mathbf{e}_2, \mathbf{e}_3\}$ and $\{\mathbf{e}_1^{i,(l)}, \mathbf{e}_2^{i,(l)}\}$ rotate at the same speed Ω about $\mathbf{e}_3$. The equations of motion of these example systems are given in Appendix C, and the parameters of these example systems are tabulated in Tables 4.1 and 4.2.

4.5.1 Formulation of Unitary Transformation Matrix

The unitary transformation matrix for a multi-stage system with arbitrarily symmetric component stages coupled through the central component vibrations is formulated in the following steps: 1) the multi-stage system is decomposed into symmetric component stages; 2) each component stage is analyzed through group theory; 3) the symmetry species of all component stages are used as building blocks to obtain the unitary transformation matrix for the multi-stage system.

To decompose a multi-stage system into component stages, all central components are classified into two types. The first type of central components (type-A) are the central components that only exist in one component stage and are not directly coupled with the substructures in other stages. For example, in a two-stage planetary gear system where the sun gear of one stage and the carrier of the other stage are connected and modeled as a rigid-body component, the ring gears are the type-A central components in the two stages because they are not directly coupled with the planet gears (substructures) of the other stage. In some cases, some central component may not couple with any substructures. If the symmetry of such a central component is identical to the symmetry of an adjacent component stages that it is connected to, this central component is regarded as a type-A central component of this adjacent stage. If a central component without connecting substructures has a symmetry type that is different from all the symmetry types of its adjacent stages, the central component alone is regarded as a component stage without substructures, and it is also the type-A central component of this stage. The other type of central components (type-B) are directly coupled with the substructures of different stages, *i.e.*, they are the common parts of multiple stages. This type of central components is considered when analyzing the component stages that include them. For example, the example system in Fig. 4.1(a) can be decomposed into two component systems that exhibit $\mathcal{C}_5$ and $\mathcal{C}_6$ symmetry ($\mathcal{C}_N$

denotes the cyclic symmetry with N rotationally periodic substructures), respectively, and the type-B central component is included in both stages.

A general system consisting of two symmetric stages is considered. The developed method generalizes to systems with more stages. For a two-stage system with symmetric stages, the eigenvector $\boldsymbol{\phi}$ and the operator $\mathbf{A}$ in the general eigenvalue problem (Eq. (4.1)) can be partitioned as

$$\boldsymbol{\phi}_M = \begin{pmatrix} \boldsymbol{\phi}_c^{(1A)} & \boldsymbol{\phi}_c^{(B)} & \boldsymbol{\phi}_c^{(2A)} & \boldsymbol{\phi}_s^{(1)} & \boldsymbol{\phi}_s^{(2)} \end{pmatrix}^T, \tag{4.15a}$$

$$\mathbf{A}_M = \begin{pmatrix} \mathbf{A}_{M,cc} & \mathbf{A}_{M,cs} \\ \mathbf{A}_{M,sc} & \mathbf{A}_{M,ss} \end{pmatrix} = \left(\begin{array}{ccc|cc} \mathbf{A}_{cc}^{(1)} & & \mathbf{A}_{cc}^{(1A),(2A)} & & \mathbf{0} \\ & \mathbf{A}_{cc}^{(B)} & & \mathbf{A}_{cs}^{(1)} & \\ & & & & \mathbf{A}_{cs}^{(2)} \\ \mathbf{A}_{cc}^{(2A),(1A)} & & \mathbf{A}_{cc}^{(2)} & \mathbf{0} & \\ \hline \mathbf{A}_{sc}^{(1)} & & \mathbf{0} & \mathbf{A}_{ss}^{(1)} & \mathbf{0} \\ \mathbf{0} & & \mathbf{A}_{sc}^{(2)} & \mathbf{0} & \mathbf{A}_{ss}^{(2)} \end{array}\right), \tag{4.15b}$$

where the subscript M emphasizes this operator is derived for the multi-stage system. $\mathbf{A}_{cc}^{(B)}$ represents the coupling between the type-B central components shared by the two stages. $\mathbf{A}_{cc}^{(1A),(2A)}$ connects the type-A central components in the two stages, and $\mathbf{A}_{cc}^{(1)}$ (a rectangular matrix that includes $\mathbf{A}_{cc}^{(B)}$) connects the central components (including type-A and type-B) in the first stage (and similarly for $\mathbf{A}_{cc}^{(2)}$ and the second stage). The zero submatrices in $\mathbf{A}_M$ result from the fact that the substructures of one stage do not couple with either of the type-A central components or the substructures of the other stage.

As introduced in Section 4.3, the unitary transformation matrix of each component stage is obtained from group theory, and the modal properties are determined without numerically

solving the eigenvalue problems. Eq. (4.14) holds for all component stages. With the stage index labeled by the additional superscript (l), Eq. (4.14) gives

$$\mathbf{U}_c^{(l,\gamma,i)}\mathbf{A}_{cc}^{(l)}\mathbf{U}_c^{(l,\rho,h)} = \mathbf{0}, \tag{4.16a}$$

$$\mathbf{U}_c^{(l,\gamma,i)}\mathbf{A}_{cs}^{(l)}\mathbf{U}_s^{(l,\rho,h)} = \mathbf{0}, \tag{4.16b}$$

$$\mathbf{U}_s^{(l,\gamma,i)}\mathbf{A}_{sc}^{(l)}\mathbf{U}_c^{(l,\rho,h)} = \mathbf{0}, \tag{4.16c}$$

$$\mathbf{U}_s^{(l,\gamma,i)}\mathbf{A}_{ss}^{(l)}\mathbf{U}_s^{(l,\rho,h)} = \mathbf{0}. \tag{4.16d}$$

The submatrices $\mathbf{U}_c^{(l,\gamma,i)}$ and $\mathbf{U}_s^{(l,\gamma,i)}$ are obtained from the symmetry vectors of symmetry species (γ, i) for the lth stage. The set of all the symmetry species that are associated with the substructure modes of the lth stage is $S^{(l)}$, while the set of all the symmetry species that are associated with the coupled modes of the lth stage is $C^{(l)}$. The number of symmetry species in $S^{(l)}$ is denoted as $N_S^{(l)}$.

Based on the structure of the operator $\mathbf{A}_M$ in Eq. (4.15b), the unitary transformation matrix $\mathbf{U}_M$ for the two-stage system is built from the matrices $\mathbf{U}_c^{(l,\gamma,i)}$ and $\mathbf{U}_s^{(l,\gamma,i)}$ in Eq. (4.16). To decompose the full system eigenvalue problem into reduced eigenvalue problems analogously to the process from Eq. (4.1) to Eq. (4.5), $\mathbf{U}_M$ are proposed to have a similar structure to the operator $\mathbf{U}$ in Eq. (4.8),

$$\mathbf{U}_M = \Bigg(\underbrace{\mathbf{U}_M^{G_1}\ \mathbf{U}_M^{G_2}\ \ldots \mathbf{U}_M^{G_X}}_{X\,submatrices}\ \underbrace{\mathbf{U}_M^{(1,\alpha,1)}\ \mathbf{U}_M^{(1,\alpha,2)}\ \ldots}_{N_S^{(1)}\,submatrices}\ \underbrace{\mathbf{U}_M^{(2,\alpha,1)}\ \mathbf{U}_M^{(2,\alpha,2)}\ \ldots}_{N_S^{(2)}\,submatrices} \Bigg), \tag{4.17}$$

where each submatrix can generate a group of full system modes from a reduced eigenvalue problem in the form of Eq. (4.5). The submatrices of $\mathbf{U}_M$ are built as follows.

$\mathbf{U}_M^{(1,\gamma,i)}$ and $\mathbf{U}_M^{(2,\rho,h)}$ in Eq. (4.17) are structured as

$$\mathbf{U}_M^{(1,\gamma,i)} = \left(\begin{array}{c:c:c|c:c} \mathbf{0} & \mathbf{0} & \mathbf{0} & \mathbf{U}_s^{(1,\gamma,i)} & \mathbf{0} \end{array} \right)^T, \ (1,\gamma,i) \in S^{(1)}, \tag{4.18a}$$

$$\mathbf{U}_M^{(2,\rho,h)} = \left(\begin{array}{c:c:c|c:c} \mathbf{0} & \mathbf{0} & \mathbf{0} & \mathbf{0} & \mathbf{U}_s^{(2,\rho,h)} \end{array} \right)^T, \ (2,\rho,h) \in S^{(2)}, \tag{4.18b}$$

respectively. Because the set $S^{(1)}$ contains $N_S^{(1)}$ symmetry species denoted by the triples $(1,\gamma,i)$, Eq. (4.18a) formulates $N_S^{(1)}$ submatrices of $\mathbf{U}_M$. Similarly, Eq. (4.18b) formulates $N_S^{(2)}$ submatrices.

The submatrices $\mathbf{U}_M^{G_\zeta}$ in Eq. (4.17) ($\zeta = 1, 2, ..., X$) are generated from symmetry vectors of the symmetry species (l,γ,i) that are in the set $C^{(l)}$ ($l = 1, 2$ in a two-stage system). To obtain these submatrices $\mathbf{U}_M^{G_\zeta}$, all the symmetry species in $C^{(1)}$ and $C^{(2)}$ are re-grouped into the sets G_1, G_2, ..., G_X, and the number of such sets X is unknown until the re-grouping process ends. To determine how the symmetry species (l,γ,i) that are in the set $C^{(l)}$ are re-grouped, the quantity

$$\left(\begin{array}{c} \mathbf{U}_c^{(1,\eta,f)} \\ \hdashline \mathbf{0} \end{array} \right)^\dagger \mathbf{A}_{M,cc} \left(\begin{array}{c} \mathbf{0} \\ \hdashline \mathbf{U}_c^{(2,\xi,g)} \end{array} \right) \tag{4.19}$$

is calculated for any symmetry species $(1,\eta,f) \in C^{(1)}$ and any symmetry species $(2,\xi,g) \in C^{(2)}$. If the quantity in Eq. (4.19) is non-zero, these two species $(1,\eta,f)$ and $(2,\xi,g)$ are defined as being coupled. The coupled symmetry species are re-grouped in the same set of symmetry species (*e.g.*, the set G_ζ). If a symmetry species for the one stage is coupled with multiple symmetry species for the other stages, all these symmetry species are categorized in the same set. After all the symmetry species in $C^{(1)}$ and $C^{(2)}$ are re-grouped into X sets, there are no common symmetry species between any two sets. The submatrix $\mathbf{U}_M^{G_\zeta}$ in Eq.

(4.17) for the set G_ζ (where $\zeta = 1, 2, ..., X$) is then formulated as

$$\mathbf{U}_M^{G_\zeta} = \begin{pmatrix} \mathbf{U}_c^{G_\zeta} & \mathbf{0} \\ \mathbf{0} & \mathbf{U}_s^{G_\zeta} \end{pmatrix} = \left(\begin{array}{c|c} \left[\begin{array}{c|c} \mathbf{U}_c^{G_\zeta^{(1)}} & \mathbf{0} \\ \hline \mathbf{0} & \mathbf{U}_c^{G_\zeta^{(2)}} \end{array} \right]^* & \mathbf{0} \\ \hline \mathbf{0} & \begin{array}{c|c} \mathbf{U}_s^{G_\zeta^{(1)}} & \mathbf{0} \\ \hline \mathbf{0} & \mathbf{U}_s^{G_\zeta^{(2)}} \end{array} \end{array} \right), \tag{4.20a}$$

$$\mathbf{U}_c^{G_\zeta^{(l)}} = \begin{pmatrix} \dots & \mathbf{U}_c^{(l,\eta,f)} & \dots \end{pmatrix}, \; \mathbf{U}_s^{G_\zeta^{(l)}} = \begin{pmatrix} \dots & \mathbf{U}_s^{(l,\eta,f)} & \dots \end{pmatrix}, \quad (l,\eta,f) \in G_\zeta^{(l)} = C^{(l)} \bigcap G_\zeta, \tag{4.20b}$$

where $[\,]^*$ is the operation to retain only the linearly independent columns of a matrix. This re-grouping scheme for the symmetry species in $C^{(1)}$ and $C^{(2)}$ guarantees that $\mathbf{U}_c^{G_\zeta}$ in Eq. (4.20a) is orthogonal to its counterpart for the symmetry species set G_κ, *i.e.*,

$$(\mathbf{U}_c^{G_\zeta})^\dagger \mathbf{A}_{M,cc} \mathbf{U}_c^{G_\kappa} = \begin{cases} \mathbf{0} & \zeta \neq \kappa \\ \tilde{\mathbf{A}}_{M,cc}^{G_\zeta} & \zeta = \kappa \end{cases}. \tag{4.21}$$

The process of building the unitary matrix $\mathbf{U}_M$ is summarized by the flowchart in Fig. 4.3.

The proposed matrix $\mathbf{U}_M$ in Eq. (4.17) has an analogous function to the unitary transformation matrix for single-stage systems, because $\mathbf{U}_M$ have the property in Eq. (4.3), *i.e.*,

$$(\mathbf{U}_M^m)^\dagger \mathbf{A}_M \mathbf{U}_M^n = \begin{cases} \mathbf{0} & m \neq n \\ \tilde{\mathbf{A}}_M^m & m = n \end{cases}, \tag{4.22}$$

where m and n can be G_ζ (for $\zeta = 1, 2, ..., X$) or any symmetry species (labeled by triples) in $S^{(1)}$ and $S^{(2)}$. For example, for any symmetry species $(1, \gamma, i) \in S^{(1)}$ and the $(2, \rho, h) \in S^{(2)}$,

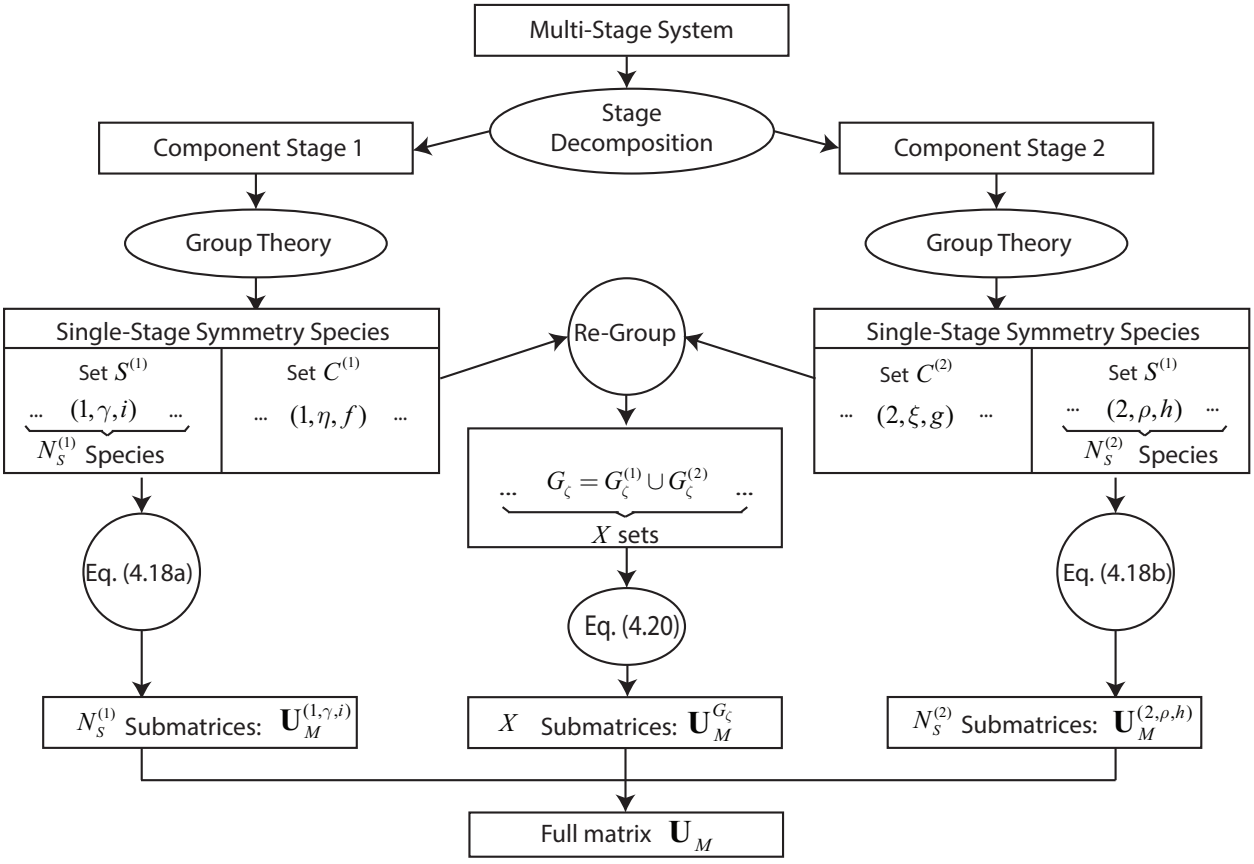

Figure 4.3: Flowchart of building $\mathbf{U}_M$ in Eq. (4.17).

substitution of Eqs. (4.15b) and (4.18) into Eq. (4.22) gives

$$(\mathbf{U}_M^{(1,\gamma,i)})^\dagger \mathbf{A}_M \mathbf{U}_M^{(2,\rho,h)} = \left(\begin{array}{c:c:c|c:c} \mathbf{0} & \mathbf{0} & \mathbf{0} & \mathbf{U}_s^{(1,\gamma,i)} & \mathbf{0} \end{array} \right)^\dagger \left(\begin{array}{c} \mathbf{0} \\ \hdashline \mathbf{A}_{cs}^{(2)} \mathbf{U}_s^{(2,\rho,h)} \\ \hline \mathbf{0} \\ \hdashline \mathbf{A}_{ss}^{(2)} \mathbf{U}_s^{(2,\rho,h)} \end{array} \right) = \mathbf{0}. \tag{4.23}$$

For two symmetry species $(1,\gamma,i)$ and $(1,\rho,h) \in S^{(1)}$, substitution of Eqs. (4.15b) and (4.18a) into Eq. (4.22) gives

$$\begin{aligned} (\mathbf{U}_M^{(1,\gamma,i)})^\dagger \mathbf{A}_M \mathbf{U}_M^{(1,\rho,h)} &= \left(\begin{array}{c:c:c|c:c} \mathbf{0} & \mathbf{0} & \mathbf{0} & \mathbf{U}_s^{(1,\gamma,i)} & \mathbf{0} \end{array} \right)^\dagger \left(\begin{array}{c} \mathbf{A}_{cs}^{(1)} \mathbf{U}_s^{(1,\rho,h)} \\ \hdashline \mathbf{0} \\ \hline \mathbf{A}_{ss}^{(1)} \mathbf{U}_s^{(1,\rho,h)} \\ \hdashline \mathbf{0} \end{array} \right) \\ &= (\mathbf{U}_s^{(1,\gamma,i)})^\dagger \mathbf{A}_{ss}^{(1)} \mathbf{U}_s^{(1,\rho,h)} \\ &= \begin{cases} \mathbf{0} & \gamma \neq \rho \text{ or } i \neq h \\ \tilde{\mathbf{A}}_M^{(1,\gamma,i)} & \gamma = \rho \text{ and } i = h \end{cases}, \end{aligned} \tag{4.24}$$

where the last equality is a result of Eq. (4.16). Both Eqs. (4.23) and (4.24) satisfy the properties of $\mathbf{U}_M$ in Eq. (4.22). Similarly, Eq. (4.22) can be validated for different selections of superscripts m and n (G_ζ for $\zeta = 1, 2, ..., X$ or any symmetry species in $S^{(1)}$ and $S^{(2)}$) through simple algebraic manipulation based on Eqs. (4.15b), (4.16), (4.18), (4.20), and (4.21). The algebraic details are omitted in this paper.

After the unitary transformation matrix $\mathbf{U}_M$ is built, reduced eigenvalue problems can

be formulated similarly to the procedure from Eq. (4.2) to Eq. (4.5). The columns of $\mathbf{U}_M$ are analogous to the symmetry vectors in single-stage systems, and the superscripts in Eq. (4.17) (*e.g.,* G_1, G_2, $(2, \alpha, 2)$, ...) are analogous to the symmetry species in group theory for single-stage symmetric systems.

The structure of $\mathbf{U}_M$ in Eq. (4.17) indicates two types of modes exist in general multi-stage structures with symmetric component stages. *Overall modes* that involve the deflections of central components are linear combinations of the columns in $\mathbf{U}_M^{G_\zeta}$ (Eq. (4.20)). Substructure deflections occur in different stages. The other type of modes is associated with $\mathbf{U}_M^{(1,\gamma,i)}$ and $\mathbf{U}_M^{(2,\rho,h)}$ in Eq. (4.18). In these modes, the central components do not vibrate, and only the substructures in one of the stages vibrate. Such modes are defined as *single-stage substructure modes*.

To carry out the above group-theory-based analysis, only the matrix operator associated with the central components ($\mathbf{A}_{M,cc}$ in Eq. (4.19)) is needed. The full system equations of motion are not required until one intends to numerically solve for the eigensolutions. Because all central components are rigid bodies and there are only a finite number of them, the process of building the unitary transformation matrix is computationally trivial. In return, the computational efficiency by applying the above group-theory-based analysis is improved because the full system eigenvalue problem in Eq. (4.1) is decomposed into $X + N_S^{(1)} + N_S^{(2)}$ smaller eigenvalue problems that are formulated in Eq. (4.5). This improvement of computational efficiency is apparent when the full system eigenvalue problems has many degrees of freedom.

4.5.2 Example 1: Multi-Stage System with Cyclically Symmetric Stages

In Fig. 4.1(a), the example system consists of two cyclically symmetric stages that exhibit $\mathcal{C}_5$ and $\mathcal{C}_6$ symmetry, respectively. An axisymmetric rigid-body central component is coupled to the substructures in both stages, so it is a type-B central component as defined in Section 4.5.1. According to the substructure angular positions of both component stages in Table 4.2, the full system is not symmetric, *i.e.*, there are no symmetry operations (except for the identity) that can be applied to the whole system to bring it to self-coincidence with the original system.

The full system is first decomposed into two cyclically symmetric systems, each of which includes the planar rigid-body central component. For a cyclically symmetric system with N substructures (each has two degrees of freedom) and one rigid-body central component, the unitary transformation matrix $\mathbf{U}_{\mathcal{C}_N}$ can be built according to the analysis for general cyclically symmetric systems in Chapter 3 as

$$\mathbf{U}_{\mathcal{C}_N} = \begin{pmatrix} \mathbf{U}_{\mathcal{C}_N}^{(0,1)} & \mathbf{U}_{\mathcal{C}_N}^{(1,1)} & \mathbf{U}_{\mathcal{C}_N}^{(2,1)} & \dots & \mathbf{U}_{\mathcal{C}_N}^{(N-1,1)} \end{pmatrix}, \tag{4.25a}$$

$$\mathbf{U}_{\mathcal{C}_N}^{(k,1)} = \begin{cases} \begin{pmatrix} \mathbf{U}_{\mathcal{C}_N,c}^{(k,1)} & \mathbf{0} \\ \mathbf{0} & \mathbf{f}_N^{(k)} \otimes \mathbf{I}_2 \end{pmatrix} & k = 0, 1, N-1 \\ \begin{pmatrix} \mathbf{0} \\ \mathbf{f}_N^{(k)} \otimes \mathbf{I}_2 \end{pmatrix} & k = 2, 3, \dots, N-2 \end{cases}, \tag{4.25b}$$

$$\begin{gathered} \mathbf{U}_{\mathcal{C}_N,c}^{(0,1)} = \begin{pmatrix} 0 & 0 & 1 \end{pmatrix}^T, \\ \mathbf{U}_{\mathcal{C}_N,c}^{(1,1)} = \begin{pmatrix} 1/\sqrt{2} & \mathrm{j}/\sqrt{2} & 0 \end{pmatrix}^T, \ \mathbf{U}_{\mathcal{C}_N,c}^{(N-1,1)} = \begin{pmatrix} 1/\sqrt{2} & -\mathrm{j}/\sqrt{2} & 0 \end{pmatrix}^T \end{gathered} \tag{4.25c}$$

where j is the imaginary unit, $\mathbf{I}_2$ is the 2×2 identity matrix, and

$$\mathbf{f}_N^{(k)} = \frac{1}{\sqrt{N}} \begin{pmatrix} 1 & e^{\mathrm{j}\frac{2k\pi}{N}} & e^{\mathrm{j}\frac{4k\pi}{N}} & \dots & e^{\mathrm{j}\frac{2k\pi}{N}(N-1)} \end{pmatrix}^T. \tag{4.26}$$

In this example, the set of all the symmetry species that are associated with the coupled modes of the first stage includes the symmetry species $(0,1)$, $(1,1)$, and $(4,1)$, *i.e.*, the set $C^{(1)}$ (as defined in Section 4.5.1) is

$$C^{(1)} = \{(1,0,1),(1,1,1),(1,4,1)\}, \tag{4.27}$$

where the stage label 1 is added into the labels of symmetry species. Similarly, the other sets of symmetry species are obtained as

$$C^{(2)} = \{(2,0,1),(2,1,1),(2,5,1)\}, \tag{4.28a}$$

$$S^{(1)} = \{(1,2,1),(1,3,1)\}, \tag{4.28b}$$

$$S^{(2)} = \{(2,2,1),(2,3,1),(2,4,1)\}. \tag{4.28c}$$

To build the unitary transformation matrix for the full multi-stage system, denoted as $\mathbf{U}_{\mathcal{C}_5-\mathcal{C}_6}$, the quantity in Eq. (4.19) is first calculated to determine the possible coupling between the single-stage symmetry species in the set $C^{(1)}$ and $C^{(2)}$. Calculating the following quantities for the matrices $\mathbf{M}_{cc}$, $\mathbf{G}_{cc}$, $\mathbf{K}_{cc,V}$, and $\mathbf{K}_{cc,T}$ in Eq. (4.43) (only the case for $\mathbf{M}_{cc}$

is shown here),

$$
\begin{aligned}
&\begin{pmatrix} \mathbf{U}_c^{(1,0,1)} & \mathbf{U}_c^{(1,1,1)} & \mathbf{U}_c^{(1,4,1)} \end{pmatrix}^{\dagger} \mathbf{M}_{cc} \begin{pmatrix} \mathbf{U}_c^{(2,0,1)} & \mathbf{U}_c^{(2,1,1)} & \mathbf{U}_c^{(2,5,1)} \end{pmatrix} \\
&= \begin{pmatrix} \mathbf{U}_{\mathcal{C}_5,c}^{(0,1)} & \mathbf{U}_{\mathcal{C}_5,c}^{(1,1)} & \mathbf{U}_{\mathcal{C}_5,c}^{(4,1)} \end{pmatrix}^{\dagger} \mathbf{M}_{cc} \begin{pmatrix} \mathbf{U}_{\mathcal{C}_6,c}^{(0,1)} & \mathbf{U}_{\mathcal{C}_6,c}^{(1,1)} & \mathbf{U}_{\mathcal{C}_6,c}^{(5,1)} \end{pmatrix} \\
&= \begin{pmatrix} 0 & 1/\sqrt{2} & 1/\sqrt{2} \\ 0 & \mathrm{j}/\sqrt{2} & -\mathrm{j}/\sqrt{2} \\ 1 & 0 & 0 \end{pmatrix}^{\dagger} \mathbf{M}_{cc} \begin{pmatrix} 0 & 1/\sqrt{2} & 1/\sqrt{2} \\ 0 & \mathrm{j}/\sqrt{2} & -\mathrm{j}/\sqrt{2} \\ 1 & 0 & 0 \end{pmatrix} = \begin{pmatrix} J_z & 0 & 0 \\ 0 & m_c & 0 \\ 0 & 0 & m_c \end{pmatrix},
\end{aligned}
\tag{4.29}
$$

is equivalent to calculating altogether nine quantities in Eq. (4.19), so that it is examined whether any of the three symmetry species $(1,0,1)$, $(1,1,1)$, and $(1,4,1)$ is coupled with any of the three symmetry species $(2,0,1)$, $(2,1,1)$, and $(2,5,1)$. The non-zero values on the diagonal entries of the results in Eq. (4.29) indicates the symmetry species $(1,0,1)$ and the symmetry species $(2,0,1)$ are coupled, and so are the symmetry species $(1,1,1)$ and the symmetry species $(2,1,1)$, and the symmetry species $(1,4,1)$ and the symmetry species $(2,5,1)$. Therefore, according to whether the symmetry species are coupled, all the symmetry species in the sets $C^{(1)}$ and $C^{(2)}$ (in Eqs. (4.27) and (4.28a)) are re-grouped into three sets, $Rot = \{(1,0,1),(2,0,1)\}$, $T_1 = \{(1,1,1),(2,1,1)\}$, and $T_2 = \{(1,4,1),(2,5,1)\}$ (corresponding to the sets G_1, G_2, and G_3 that appear in Eq. (4.20)).

According to Eq. (4.20), a matrix $\mathbf{U}_{\mathcal{C}_5-\mathcal{C}_6}^{Rot}$ (corresponding to $\mathbf{U}_M^{G_\zeta}$) is built from $\mathbf{U}_{\mathcal{C}_5}^{(0,1)}$

and $\mathbf{U}_{\mathcal{C}_6}^{(0,1)}$ in Eq. (4.25),

$$\mathbf{U}_{\mathcal{C}_5-\mathcal{C}_6}^{Rot} = \left(\begin{array}{c:cc} 0 & & \\ 0 & \mathbf{0} & \mathbf{0} \\ 1 & & \\ \hline \mathbf{0} & \mathbf{f}_5^{(0)} \otimes \mathbf{I}_2 & \mathbf{0} \\ \mathbf{0} & \mathbf{0} & \mathbf{f}_6^{(0)} \otimes \mathbf{I}_2 \end{array}\right), \tag{4.30}$$

where the superscript *Rot* indicates that the central component motions are purely rotational. Similarly, another two matrices, $\mathbf{U}_{\mathcal{C}_5-\mathcal{C}_6}^{T_1}$ and $\mathbf{U}_{\mathcal{C}_5-\mathcal{C}_6}^{T_2}$, are obtained from $\mathbf{U}_{\mathcal{C}_5}^{(1,1)}$ and $\mathbf{U}_{\mathcal{C}_6}^{(1,1)}$, and $\mathbf{U}_{\mathcal{C}_5}^{(4,1)}$ and $\mathbf{U}_{\mathcal{C}_6}^{(5,1)}$, respectively,

$$\mathbf{U}_{\mathcal{C}_5-\mathcal{C}_6}^{T_1} = \left(\begin{array}{c:cc} 1/\sqrt{2} & & \\ \mathrm{j}/\sqrt{2} & \mathbf{0} & \mathbf{0} \\ 0 & & \\ \hline \mathbf{0} & \mathbf{f}_5^{(1)} \otimes \mathbf{I}_2 & \mathbf{0} \\ \mathbf{0} & \mathbf{0} & \mathbf{f}_6^{(1)} \otimes \mathbf{I}_2 \end{array}\right), \tag{4.31a}$$

$$\mathbf{U}_{\mathcal{C}_5-\mathcal{C}_6}^{T_2} = \left(\begin{array}{c:cc} 1/\sqrt{2} & & \\ -\mathrm{j}/\sqrt{2} & \mathbf{0} & \mathbf{0} \\ 0 & & \\ \hline \mathbf{0} & \mathbf{f}_5^{(4)} \otimes \mathbf{I}_2 & \mathbf{0} \\ \mathbf{0} & \mathbf{0} & \mathbf{f}_6^{(5)} \otimes \mathbf{I}_2 \end{array}\right), \tag{4.31b}$$

where the superscripts T_1 and T_2 distinguish the two kinds of purely translational central component motions in these two submatrices. Meanwhile, according to Eq. (4.18), the other

parts of the desired matrix $\mathbf{U}_{\mathcal{C}_5-\mathcal{C}_6}$ that involves no central component motions are obtained,

$$\mathbf{U}^{(1,k1,1)}_{\mathcal{C}_5-\mathcal{C}_6} = \begin{pmatrix} \mathbf{0} \\ \hline \mathbf{f}_5^{(k1)} \otimes \mathbf{I}_2 \\ \mathbf{0} \end{pmatrix}, \; k1 = 2, 3, \tag{4.32a}$$

$$\mathbf{U}^{(2,k2,1)}_{\mathcal{C}_5-\mathcal{C}_6} = \begin{pmatrix} \mathbf{0} \\ \hline \mathbf{0} \\ \mathbf{f}_6^{(k2)} \otimes \mathbf{I}_2 \end{pmatrix}, \; k2 = 2, 3, 4. \tag{4.32b}$$

The full unitary transformation matrix for the example multi-stage system, $\mathbf{U}_{\mathcal{C}_5-\mathcal{C}_6}$, is built by its submatrices in Eqs. (4.30), (4.31), and (4.32).

Based on the structure of the constructed transformation matrix, $\mathbf{U}_{\mathcal{C}_5-\mathcal{C}_6}$,the modal properties of the example multi-stage cyclically symmetric system are obtained. Because eight submatrices of $\mathbf{U}_{\mathcal{C}_5-\mathcal{C}_6}$ are obtained in Eqs (4.30), (4.31), and (4.32), there are eight types of modes that fall into three categories. One category of modes are linear combinations of the columns in $\mathbf{U}^{Rot}_{\mathcal{C}_5-\mathcal{C}_6}$ only, and these modes are characterized by the non-zero central component rotational deflection and the identical, in-phase substructure motions in each stage. Therefore, these modes are defined as *overall rotational modes*. Similarly, $\mathbf{U}^{T_1}_{\mathcal{C}_5-\mathcal{C}_6}$ and $\mathbf{U}^{T_2}_{\mathcal{C}_5-\mathcal{C}_6}$ in Eq. (4.31) are associated with two types of *overall translational modes*, where the central component deflection is purely translational. In such modes, the substructures in each stage vibrate with the phase difference characterized by the phase indices associated with the single-stage translational modes ($k1$ =1 or 4, and $k2$ =1 or 5). The other category of modes are the single-stage substructure modes spanned by the columns in $\mathbf{U}^{(1,k1,1)}_{\mathcal{C}_5-\mathcal{C}_6}$ for $k1 = 2, 3$ or $\mathbf{U}^{(2,k2,1)}_{\mathcal{C}_5-\mathcal{C}_6}$ for $k2 = 2, 3, 4$ in Eq. (4.32). In these modes, the central component does not vibrate, and the substructures in only one stage vibrate while the others do not. Meanwhile, the number of modes in each mode type is also obtained because it equals to the

number of columns in the submatrix multiplied by the order of eigenvalue. Therefore, five complex conjugate pairs of overall rotational modes, ten complex conjugate pairs of overall translational modes (in two sets, with ten modes in each set), and ten pairs of single-stage substructure modes (in five sets, with four modes in each set) are expected. The total number of mode pairs $5 + 10 + 10 = 25$ equals the total degrees of freedom in this example.

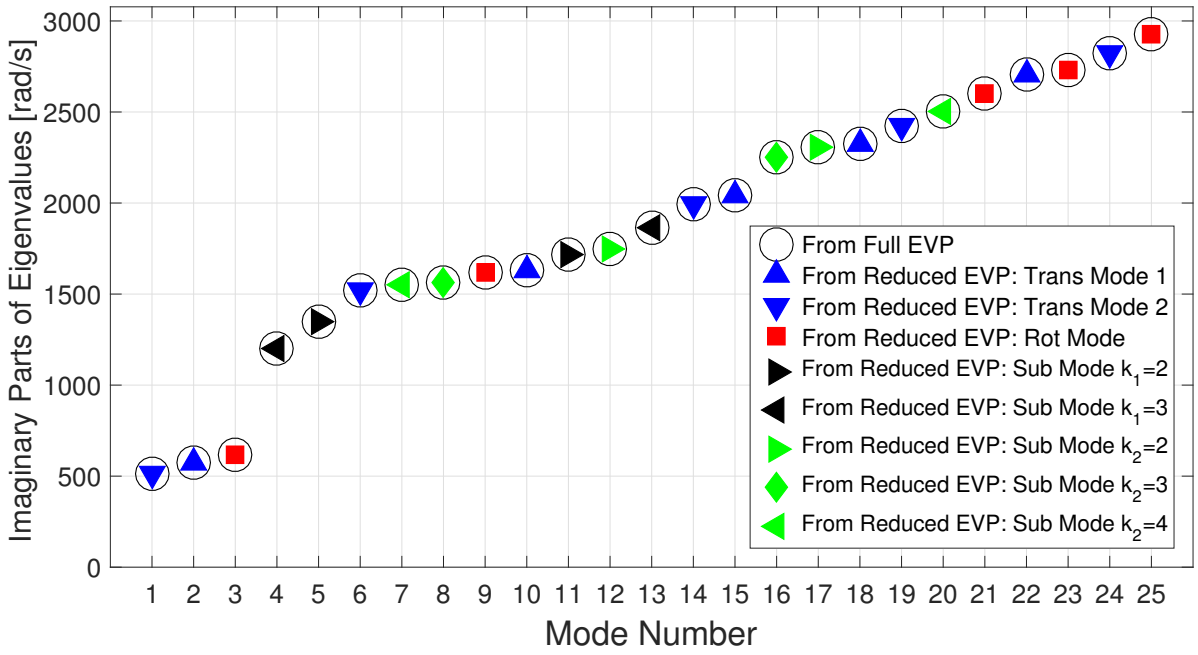

Figure 4.4: Natural frequencies of the example system in Fig. 4.1(a). The complex conjugates of the presented eigenvalues are also eigenvalues but omitted for conciseness.

To numerically solve the eigensolutions of the example system, eight reduced eigenvalue problems can be formulated based on Eq. (4.5), where the matrix $\mathbf{U}^{(\gamma,i)}$ in Eq. (4.5) is replaced by the eight submatrices of $\mathbf{U}_{\mathcal{C}_5-\mathcal{C}_6}$ in Eqs. (4.30)-(4.32). The eigenvalues of the example multi-stage cyclically symmetric system in Fig. 4.1(a) are shown in Fig. 4.4. The eigenvalues solved from the reduced eigenvalue problems match those from the full eigenvalue problem in Eq. (4.44). Fig. 4.5 shows the 9th, 6th, 4th, and 7th modes of this example system. These modes are illustrated to have the modal properties that are directly obtained from the above group-theory-based analysis. Specifically, they are an overall rotational mode,

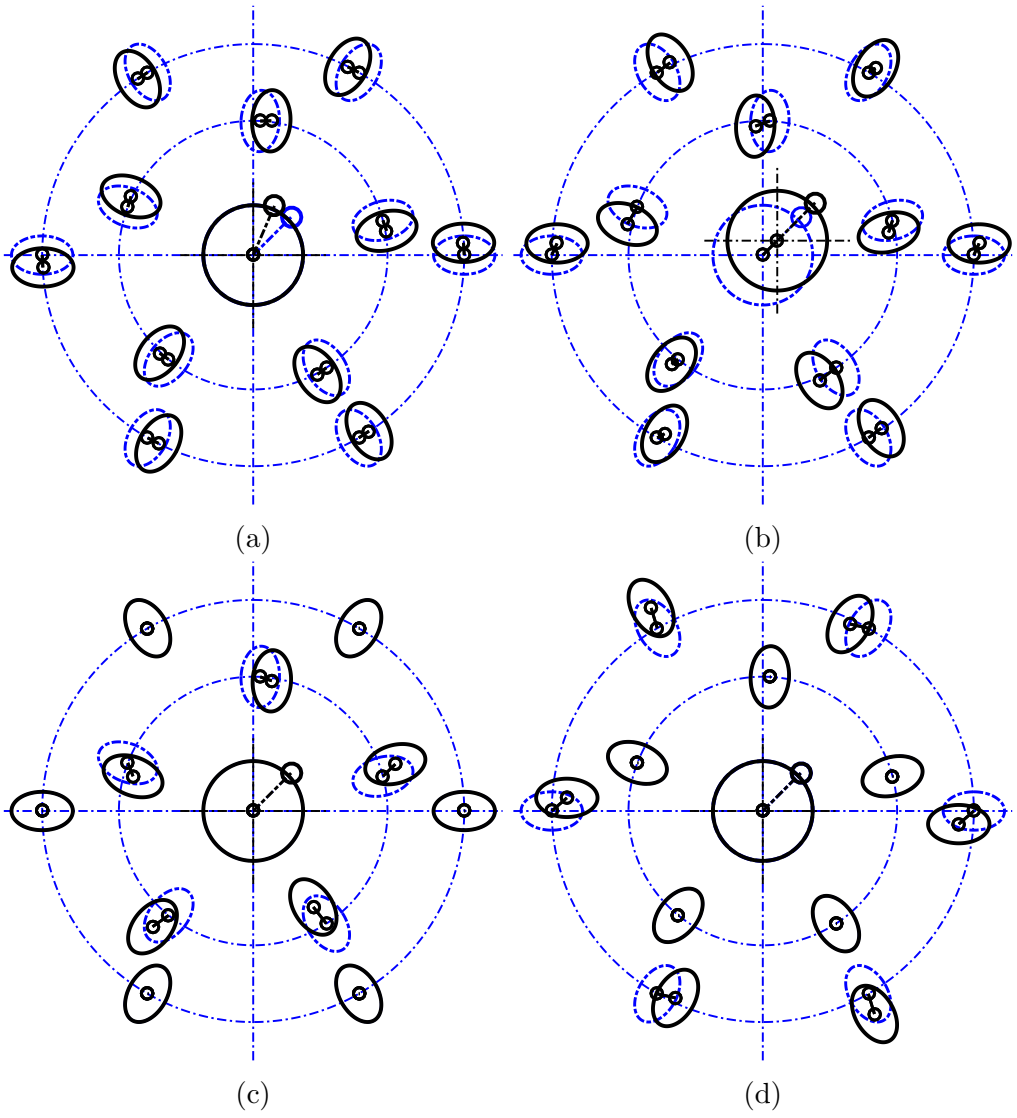

Figure 4.5: Modes of the example in Fig. 4.1(a). (a) An overall rotational mode (the 9th mode). (b) An overall translational mode (the 6th mode). (c) A single-stage substructure mode in the $\mathcal{C}_5$ stage (the 4th mode). (d) A single-stage substructure mode in the $\mathcal{C}_6$ stage (the 7th mode)

. .

an overall translational mode, a single-stage substructure mode for the first stage, and a single-stage substructure mode for the second stage, respectively. Fig. 4.4 also illustrates that the number of modes in each mode type also match the above group-theory-based analysis.

4.5.3 Example 2: Multi-Stage System with $\mathcal{C}_5$ and $\mathcal{D}_2$-Symmetric Stages

The example system in Fig. 4.1(b) consists of two stages that exhibit $\mathcal{C}_5$ and $\mathcal{D}_2$ symmetries, respectively. The first stage is the cyclically symmetric stage, while the second stage has the $\mathcal{D}_2$ symmetry. In the stage with the $\mathcal{D}_2$ symmetry, the substructures are distributed in the four phases divided by the axes $\mathbf{e}_1$ and $\mathbf{e}_2$, and the geometry of the system is symmetric along the axes $\mathbf{e}_1$ and $\mathbf{e}_2$. The geometry of the system is brought into self-coincidence by four symmetry operations: identity (E), rotation by π along $\mathbf{e}_3$ (C_2), rotation by π along $\mathbf{e}_1$ ($C_2^{(1)}$), and rotation by π along $\mathbf{e}_2$ ($C_2^{(2)}$). This example is to illustrate that the group-theory based modal analysis developed in this work applies to multi-stage systems consisting of stages with different symmetry types.

According to the analysis for $\mathcal{D}_2$-symmetric systems in Chapter 3, the unitary transformation matrix for the $\mathcal{D}_2$-symmetric stage is obtained

$$\mathbf{U}_{\mathcal{D}_2} = \begin{pmatrix} \mathbf{U}_{\mathcal{D}_2}^{(A,1)} & \mathbf{U}_{\mathcal{D}_2}^{(B1,1)} & \mathbf{U}_{\mathcal{D}_2}^{(B2,1)} & \mathbf{U}_{\mathcal{D}_2}^{(B3,1)} \end{pmatrix}, \tag{4.33a}$$

$$\mathbf{U}_{\mathcal{D}_2}^{(A,1)} = \begin{pmatrix} \mathbf{0} \\ \mathbf{U}_{\mathcal{D}_2,s}^{(A,1)} \end{pmatrix} = \frac{1}{2} \left(\begin{array}{c} \mathbf{0} \\ \hdashline \mathbf{I}_2 \otimes \mathbf{I}_2 \\ \mathbf{I}_{f,2} \otimes \mathbf{J}_2 \\ \mathbf{I}_2 \otimes \mathbf{I}_2 \\ \mathbf{I}_{f,2} \otimes \mathbf{J}_2 \end{array}\right),$$

$$\mathbf{U}_{\mathcal{D}_2}^{(B1,1)} = \begin{pmatrix} \mathbf{U}_{\mathcal{D}_2,c}^{(B1,1)} & \mathbf{0} \\ \mathbf{0} & \mathbf{U}_{\mathcal{D}_2,s}^{(B1,1)} \end{pmatrix} = \frac{1}{2} \left(\begin{array}{c:c} 0 & \\ 0 & \mathbf{0} \\ 2 & \\ \hdashline & \mathbf{I}_2 \otimes \mathbf{I}_2 \\ & -\mathbf{I}_{f,2} \otimes \mathbf{J}_2 \\ \mathbf{0} & \mathbf{I}_2 \otimes \mathbf{I}_2 \\ & -\mathbf{I}_{f,2} \otimes \mathbf{J}_2 \end{array}\right),$$

$$\mathbf{U}_{\mathcal{D}_2}^{(B2,1)} = \begin{pmatrix} \mathbf{U}_{\mathcal{D}_2,c}^{(B2,1)} & \mathbf{0} \\ \mathbf{0} & \mathbf{U}_{\mathcal{D}_2,s}^{(B2,1)} \end{pmatrix} = \frac{1}{2} \left(\begin{array}{c:c} 0 & \\ 2 & \mathbf{0} \\ 0 & \\ \hdashline & \mathbf{I}_2 \otimes \mathbf{I}_2 \\ & \mathbf{I}_{f,2} \otimes \mathbf{J}_2 \\ \mathbf{0} & -\mathbf{I}_2 \otimes \mathbf{I}_2 \\ & -\mathbf{I}_{f,2} \otimes \mathbf{J}_2 \end{array}\right), \tag{4.33b}$$

$$\mathbf{U}_{\mathcal{D}_2}^{(B3,1)} = \begin{pmatrix} \mathbf{U}_{\mathcal{D}_2,c}^{(B3,1)} & \mathbf{0} \\ \mathbf{0} & \mathbf{U}_{\mathcal{D}_2,s}^{(B3,1)} \end{pmatrix} = \frac{1}{2} \left(\begin{array}{c:c} 2 & \\ 0 & \mathbf{0} \\ 0 & \\ \hdashline & \mathbf{I}_2 \otimes \mathbf{I}_2 \\ & -\mathbf{I}_{f,2} \otimes \mathbf{J}_2 \\ \mathbf{0} & -\mathbf{I}_2 \otimes \mathbf{I}_2 \\ & \mathbf{I}_{f,2} \otimes \mathbf{J}_2 \end{array}\right),$$

where

$$\mathbf{I}_{f,2} = \begin{pmatrix} 0 & 1 \\ 1 & 0 \end{pmatrix}, \ \mathbf{J}_2 = \begin{pmatrix} 1 & 0 \\ 0 & -1 \end{pmatrix}. \tag{4.34}$$

The set of all the symmetry species that are associated with the coupled modes of the second stage includes the symmetry species $(B1,1)$, $(B2,1)$, and $(B3,1)$, while the set of all the symmetry species that are associated with the substructure modes of the second stage only includes $(A,1)$, *i.e.*,

$$C^{(2)} = \{(2,B1,1),(2,B2,1),(2,B3,1)\}, \tag{4.35a}$$

$$S^{(2)} = \{(2,A,1)\}. \tag{4.35b}$$

To build the unitary transformation matrix for the full multi-stage system, denoted as $\mathbf{U}_{\mathcal{C}_5-\mathcal{D}_2}$, the couplings between the symmetry species in $C^{(1)}$ (Eq. (4.27)) and $C^{(2)}$ (Eq.(4.35a)) are identified by the following equation (similar to the process in Eq. (4.29)):

$$\begin{aligned} &\begin{pmatrix} \mathbf{U}_c^{(1,0,1)} & \mathbf{U}_c^{(1,1,1)} & \mathbf{U}_c^{(1,4,1)} \end{pmatrix}^{\dagger} \mathbf{M}_{cc} \begin{pmatrix} \mathbf{U}_c^{(2,B1,1)} & \mathbf{U}_c^{(2,B2,1)} & \mathbf{U}_c^{(2,B3,1)} \end{pmatrix} \\ &= \begin{pmatrix} \mathbf{U}_{\mathcal{C}_5,c}^{(0,1)} & \mathbf{U}_{\mathcal{C}_5,c}^{(1,1)} & \mathbf{U}_{\mathcal{C}_5,c}^{(4,1)} \end{pmatrix}^{\dagger} \mathbf{M}_{cc} \begin{pmatrix} \mathbf{U}_{\mathcal{D}_2,c}^{(B1,1)} & \mathbf{U}_{\mathcal{D}_2,c}^{(B2,1)} & \mathbf{U}_{\mathcal{D}_2,c}^{(B3,1)} \end{pmatrix} \\ &= \begin{pmatrix} 0 & 1/\sqrt{2} & 1/\sqrt{2} \\ 0 & \mathrm{j}/\sqrt{2} & -\mathrm{j}/\sqrt{2} \\ 1 & 0 & 0 \end{pmatrix}^{\dagger} \mathbf{M}_{cc} \begin{pmatrix} 0 & 0 & 1 \\ 0 & 1 & 0 \\ 1 & 0 & 0 \end{pmatrix} = \begin{pmatrix} J_z & 0 & 0 \\ 0 & -\mathrm{j}m_c/\sqrt{2} & m_c/\sqrt{2} \\ 0 & \mathrm{j}m_c/\sqrt{2} & m_c/\sqrt{2} \end{pmatrix}, \end{aligned} \tag{4.36}$$

The non-zero entries on the right-hand-side of Eq. (4.36) indicate that the symmetry species $(1,0,1)$ and $(2,B1,1)$ are coupled with each other but uncoupled with the other symmetry species in the sets $C^{(1)}$ and $C^{(2)}$. Meanwhile, the other four symmetry species in the sets $C^{(1)}$ and $C^{(2)}$ are coupled. Therefore, all the symmetry species in the sets $C^{(1)}$ and $C^{(2)}$

(in Eqs. (4.27) and (4.35a)) are re-grouped into two sets, $Rot = \{(1,0,1),(2,B1,1)\}$ and $Trans = \{(1,1,1),(1,4,1),(2,B2,1),(2,B3,1)\}$.

Based on the above two sets of symmetry species, two submatrices in the form of $\mathbf{U}_M^{G_\zeta}$ in Eq. (4.20) are built. One submatrix is built from the matrix $\mathbf{U}_{\mathcal{C}_5}^{(0,1)}$ in Eq. (4.25) and the matrix $\mathbf{U}_{\mathcal{D}_2}^{(B1,1)}$ in Eq. (4.33b), while the other is built from the matrices $\mathbf{U}_{\mathcal{C}_5}^{(1,1)}$ and $\mathbf{U}_{\mathcal{C}_5}^{(4,1)}$ in Eq. (4.25) and the matrices $\mathbf{U}_{\mathcal{D}_2}^{(B2,1)}$ and $\mathbf{U}_{\mathcal{D}_2}^{(B3,1)}$ in Eq. (4.33b). According to Eq. (4.20), these two submatrices are formulated as

$$\mathbf{U}_{\mathcal{C}_5-\mathcal{D}_2}^{Rot} = \left(\begin{array}{c:cc} 0 & & \\ 0 & \mathbf{0} & \mathbf{0} \\ 1 & & \\ \hdashline \mathbf{0} & \mathbf{f}_5^{(0)} \otimes \mathbf{I}_2 & \mathbf{0} \\ \mathbf{0} & \mathbf{0} & \mathbf{U}_{\mathcal{D}_2,s}^{(B1,1)} \end{array}\right), \tag{4.37a}$$

$$\mathbf{U}_{\mathcal{C}_5-\mathcal{D}_2}^{Trans} = \left(\begin{array}{cc:cccc} 0 & 1 & & & & \\ 1 & 0 & \mathbf{0} & \mathbf{0} & \mathbf{0} & \mathbf{0} \\ 0 & 0 & & & & \\ \hdashline \mathbf{0} & & \mathbf{f}_5^{(1)} \otimes \mathbf{I}_2 & \mathbf{f}_5^{(4)} \otimes \mathbf{I}_2 & \mathbf{0} & \mathbf{0} \\ \mathbf{0} & & \mathbf{0} & \mathbf{0} & \mathbf{U}_{\mathcal{D}_2,s}^{(B2,1)} & \mathbf{U}_{\mathcal{D}_2,s}^{(B3,1)} \end{array}\right), \tag{4.37b}$$

where $\mathbf{U}_{\mathcal{D}_2,s}^{(B1,1)}$, $\mathbf{U}_{\mathcal{D}_2,s}^{(B2,1)}$, and $\mathbf{U}_{\mathcal{D}_2,s}^{(B3,1)}$ are submatrices of $\mathbf{U}_{\mathcal{D}_2}^{(B1,1)}$, $\mathbf{U}_{\mathcal{D}_2}^{(B2,1)}$, and $\mathbf{U}_{\mathcal{D}_2}^{(B3,1)}$ in Eq. (4.33b). Meanwhile, the other submatrices of $\mathbf{U}_{\mathcal{C}_5-\mathcal{D}_2}$ that are associated with the single-stage substructure modes are obtained from Eq. (4.18),

$$\mathbf{U}_{\mathcal{C}_5-\mathcal{D}_2}^{(1,k1,1)} = \left(\begin{array}{c} \mathbf{0} \\ \hline \mathbf{f}_5^{(k1)} \otimes \mathbf{I}_2 \\ \mathbf{0} \end{array}\right), \; k1 = 2,3, \tag{4.38a}$$

$$\mathbf{U}^{(2,A,1)}_{\mathcal{C}_5-\mathcal{D}_2} = \begin{pmatrix} \mathbf{0} \\ \hline \mathbf{0} \\ \mathbf{U}^{(A,1)}_{\mathcal{D}_2,s} \end{pmatrix}. \tag{4.38b}$$

Therefore, the unitary transformation matrix for the example system is

$$\mathbf{U}_{\mathcal{C}_5-\mathcal{D}_2} = \begin{pmatrix} \mathbf{U}^{Rot}_{\mathcal{C}_5-\mathcal{D}_2} & \mathbf{U}^{Trans}_{\mathcal{C}_5-\mathcal{D}_2} & \mathbf{U}^{(1,2,1)}_{\mathcal{C}_5-\mathcal{D}_2} & \mathbf{U}^{(1,3,1)}_{\mathcal{C}_5-\mathcal{D}_2} & \mathbf{U}^{(2,A,1)}_{\mathcal{C}_5-\mathcal{D}_2} \end{pmatrix}. \tag{4.39}$$

Similar to the analysis for the example system in Fig. 4.1(a), the modal properties of the example system in Fig. 4.1(b) are obtained based on Eqs. (4.37) to (4.39). There are five types of modes that fall into three categories according to the non-zero central component modal deflections: overall rotational modes, overall translational modes, and single-stage substructure modes. $\mathbf{U}^{Rot}_{\mathcal{C}_5-\mathcal{D}_2}$ in Eq. (4.37) is associated with the overall rotational modes, and there are seven pairs of such modes (in complex conjugate pairs) because $\mathbf{U}^{Rot}_{\mathcal{C}_5-\mathcal{D}_2}$ has seven columns. $\mathbf{U}^{Trans}_{\mathcal{C}_5-\mathcal{D}_2}$ in Eq. (4.37) is associated with the overall translational modes, and there are 14 pairs of translational modes. The single-stage substructure modes are associated with $\mathbf{U}^{(1,k1,1)}_{\mathcal{C}_5-\mathcal{D}_2}$ ($k1 = 2, 3$) and $\mathbf{U}^{(2,A,1)}_{\mathcal{C}_5-\mathcal{D}_2}$ in Eq. (4.38). The structure of $\mathbf{U}^{(1,k1,1)}_{\mathcal{C}_5-\mathcal{D}_2}$ ($k1 = 2, 3$) indicates two types of single-stage substructure modes are characterized by the phase relations of single-stage cyclically symmetric systems, and there are 4 complex conjugate pairs of such single-stage substructure modes. The other type of single-stage substructure modes (four pairs of modes associated with $\mathbf{U}^{(2,A,1)}_{\mathcal{C}_5-\mathcal{D}_2}$) have the modal properties of the substructure modes in single-stage $\mathcal{D}_2$-symmetric systems.

The eigensolutions of the example system are solved from the full eigenvalue problem in Eq. (4.44) and the reduced eigenvalue problems that are formulated based on Eqs. (4.5), (4.37) and (4.38). As shown in Fig. (4.6), the eigenvalue solved from the reduced eigenvalue problems match those from the full eigenvalue problems. Meanwhile, the selected modes in

Fig. (4.7) have the modal properties of each mode type, which have been obtained from the above group-theory-based analysis.

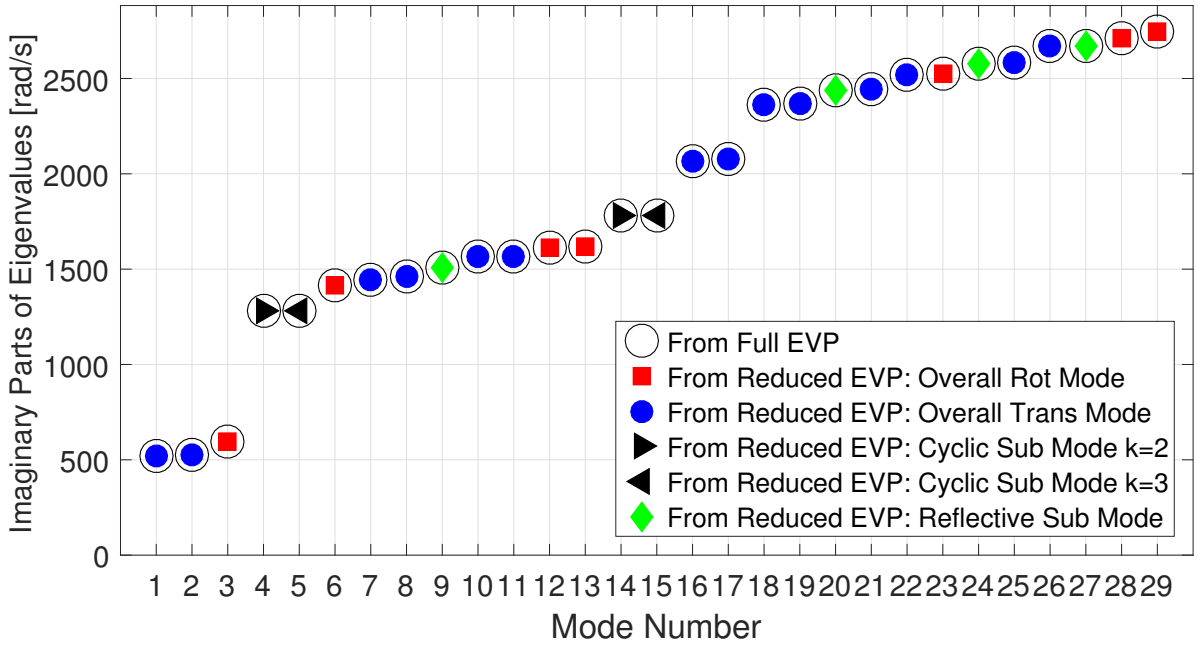

Figure 4.6: Natural frequencies of the example system in Fig. 4.1(b). The complex conjugates of the presented eigenvalues are also eigenvalues but omitted for conciseness.

4.5.4 Remarks

For both examples, the overall modes are further categorized into overall rotational modes and overall translational modes. Such decomposition of the overall modes are the results of re-grouping scheme for the symmetry species associated with the single-stage coupled modes (symmetry species in $C^{(1)}$ and $C^{(2)}$). More specifically, the right-hand-side of Eq. (4.29) for the first example is completely diagonalized, while its counterpart in Eq. (4.36) for the second example is not. Therefore, the overall translational modes are further classified into two types in the first example, but are not decomposed in the second example.

In previous works, the modal properties of multi-stage planetary gears [74, 76] and

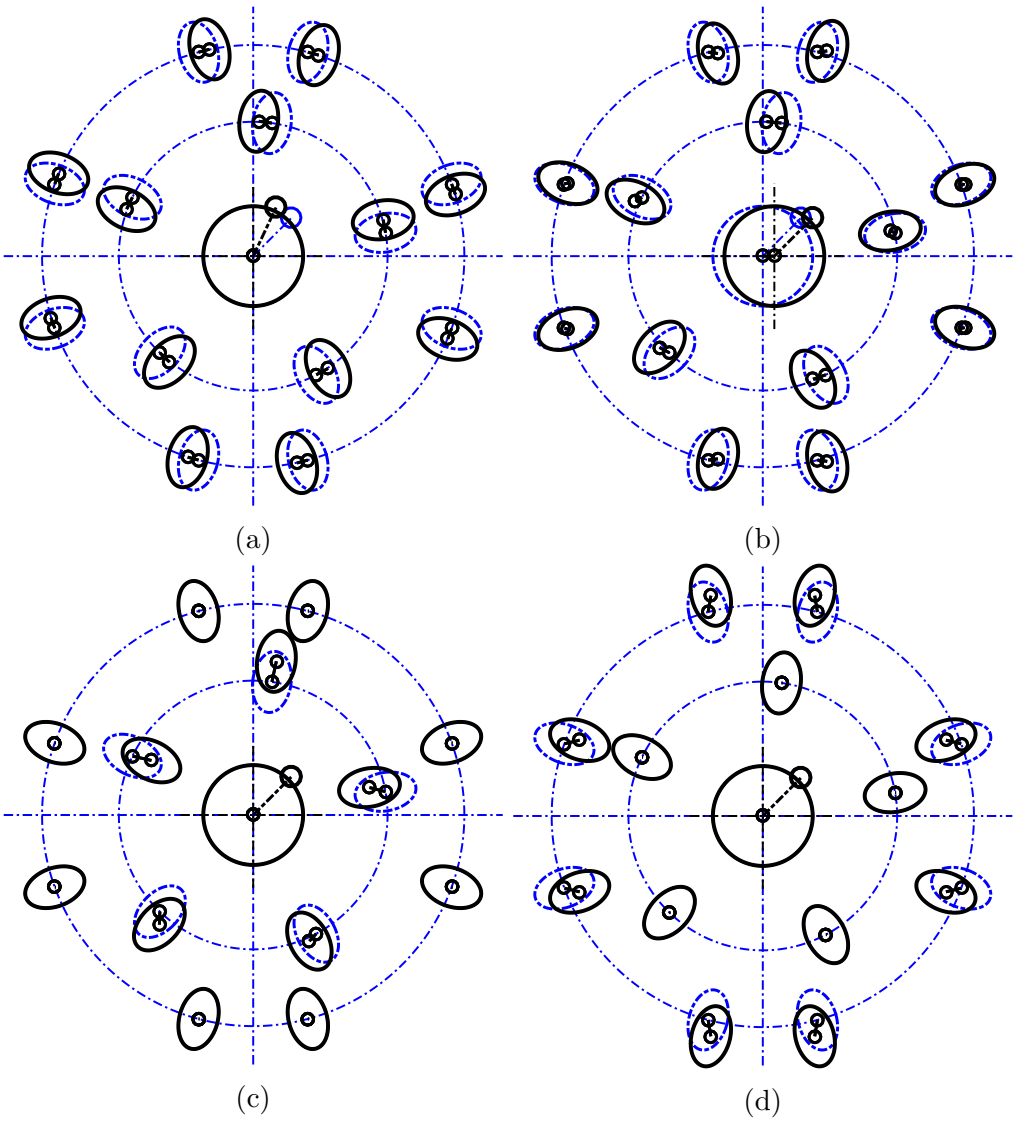

Figure 4.7: Modes of the example in Fig. 4.1(b). (a) An overall rotational mode (the 12th mode). (b) An overall translational mode (the 11th mode). (c) A single-stage substructure mode in the $\mathcal{C}_5$-symmetric stage (the 4th mode). (d) A single-stage substructure mode in the $\mathcal{D}_2$-symmetric stage (the 9th mode)

. .

CPVA with multiple groups of absorbers [19, 20] are studied using analytical models. Only three categories of modes are found in these studies: planet (or absorber) modes, overall rotational modes, and overall translational modes. In Ref. [21, 79], the overall translational modes are replaced by the overall translational-tilting modes when the rotor has out-of-plane tilting degrees of freedom. All of these modal properties can be obtained by the group-theory-based method developed in this work. For example, in Ref. [19], the CPVA system consists of one rotor (a type-B central component) with three planar degrees of freedom and n groups of absorbers. Each group of absorbers and the rotor are regarded a cyclically symmetric component stage, and the symmetries of all stages are generally different because the number of absorbers ($N^{(l)} \geq 3$ for the lth group) varies in each group of absorbers. To re-group the symmetry species associated with the single-stage coupled modes (symmetry species in $C^{(1)}$, $C^{(2)}$, ..., $C^{(n)}$), the couplings between these symmetry species in any two stages are identified through a process similar to Eq. (4.29). Because all the stages are cyclically symmetric and the all stages are connected through the same type-B central component, this calculation is repetitive for any two stages. Through simple calculations similar to Eq. (4.29), the symmetry species in $C^{(1)}$, $C^{(2)}$, ..., $C^{(n)}$ are proved to be coupled similarly as their counterparts are coupled in the example system in Fig. 4.1(a). All the symmetry species in $C^{(1)}$, $C^{(2)}$, ..., $C^{(n)}$ are categorized into three sets,

$$Rot = \{(l, 0, 1) : l = 1, 2, \ldots, n\}, \tag{4.40a}$$

$$Trans1 = \{(l, 1, 1) : l = 1, 2, \ldots, n\}, \tag{4.40b}$$

$$Trans2 = \{(l, N^{(l)} - 1, 1) : l = 1, 2, \ldots, n\}, \tag{4.40c}$$

where the set Rot is associated with the overall rotational modes and the other two sets are associated with the overall translational modes. For the lth group of absorbers, the

symmetry species in the set

$$S^{(l)} = \{(l, i, 1) : i = 2, 3, \ldots, N^{(l)} - 2\} \tag{4.41}$$

are associated with the absorber modes (single-stage substructure modes). Such reasoning also explains the similar mode structures in multi-stage planetary gears [74, 76].

For multi-stage cyclically symmetric systems where the stages are coupled through the type-A central components or substructures, the further classification of overall modes is not expected as a property for general multi-stage systems with symmetric component stages.

4.6 Conclusions

This work develops a group-theory-based method to analyze the multi-stage systems with arbitrary symmetry of component stages. In this work, the component stages in multi-stage systems are coupled through the rigid-body central components. This method applies to multi-stage compound planetary gears and CPVA systems with multiple groups of absorbers, and the modal properties of these systems derived in previous works [19, 20, 74, 76] can be achieved in a more simple, general, and systematic way. Meanwhile, this method applies to the multi-stage systems composed of stages with different symmetry types, and the full systems are allowed to be asymmetric.

Group theory is shown powerful to study multi-stage systems with symmetric component stages, although the full multi-stage systems can be asymmetric. The group-theory-based method provides the following advantages:

1. For a multi-stage symmetric system, this method provides a unitary matrix transformation that can block diagonalize the full system matrix operators, and therefore, reduced

eigenvalue problems are formulated. All vibration modes and natural frequencies can be solved from the reduced eigenvalue problems, which improves the computational efficiency.

2. The computational cost to build the unitary matrix for a multi-stage system is small, although the full systems may have many degrees of freedom.

3. Modal properties of multi-stage systems are obtained without numerically solving the eigenvalue problems. The unitary transformation matrix for a multi-stage system is sufficient to obtain the qualitative modal properties, including the number of mode types, the number of modes in each mode type, and the characteristic modal deflections in each mode type.

For general multi-stage systems with component stages coupled through central components, all modes fall into two categories:

1. Single-stage substructure modes: the central components are not vibrating, and only the substructures in one of the component stages vibrate, while the others do not.

2. Overall modes: there are non-zero central component modal deflections, and the substructure deflections occur in different stages.

Appendix C. Equations of Motion for the Example Multi-Stage Systems in Fig. 4.1

The equations of motion for all these example systems are expressed as

$$\mathbf{M}\ddot{\mathbf{q}} + \Omega\mathbf{G}\dot{\mathbf{q}} + (\mathbf{K}_V - \Omega^2\mathbf{K}_T)\mathbf{q} = \mathbf{F}, \tag{4.42a}$$

$$\mathbf{q} = (x_c, y_c, \mu_c, \underbrace{r_1^{(1)}, s_1^{(1)}, r_2^{(1)}, s_2^{(1)}, \ldots}_{2N^{(1)}}, \ldots, \underbrace{r_1^{(n)}, s_1^{(n)}, \ldots}_{2N^{(n)}})^T, \tag{4.42b}$$

where all coordinates are defined in local reference frames. The superscript (l) labels the lth stage that has $N^{(l)}$ substructures. There are n stages in total. The matrices are

$$\mathbf{M} = \mathrm{diag}(\mathbf{M}_{cc}, \mathbf{M}_{ss}^{(1)}, \ldots, \mathbf{M}_{ss}^{(n)}), \tag{4.43a}$$

$$\mathbf{M}_{cc} = \mathrm{diag}(m_c, m_c, J_z),\ \mathbf{M}_{ss}^{(l)} = \mathrm{diag}(\underbrace{m_s^{(l)}, m_s^{(l)}, \ldots, m_s^{(l)}}_{2N^{(l)}}), \tag{4.43b}$$

$$\mathbf{G} = \mathrm{diag}(\mathbf{G}_{cc}, \underbrace{\mathbf{G}_{s_1s_1}^{(1)}, \mathbf{G}_{s_2s_2}^{(1)}, \ldots}_{N^{(1)}}, \ldots, \underbrace{\mathbf{G}_{s_1s_1}^{(n)}, \mathbf{G}_{s_2s_2}^{(n)}, \ldots}_{N^{(n)}}), \tag{4.43c}$$

$$\mathbf{G}_{cc} = \begin{pmatrix} 0 & -2m_c & 0 \\ 2m_c & 0 & 0 \\ 0 & 0 & 0 \end{pmatrix},\ \mathbf{G}_{s_is_i}^{(l)} = \begin{pmatrix} 0 & -2m_s^{(l)} \\ 2m_s^{(l)} & 0 \end{pmatrix}, \tag{4.43d}$$

$$\mathbf{K}_V = \begin{pmatrix} \mathbf{K}_{cc,V} & \mathbf{K}_{cs,V} \\ \mathbf{K}_{cs,V}^T & \mathbf{K}_{ss,V} \end{pmatrix}, \tag{4.43e}$$

$$\mathbf{K}_{cc,V} = \mathrm{diag}(k_c, k_c, k_{c,R}) + \sum_{l=1}^{n} \sum_{i=1}^{N^{(l)}} \hat{\mathbf{K}}_{cc,V}^{i,(l)},$$

$$\hat{\mathbf{K}}_{cc,V}^{i,(l)} = \begin{pmatrix} k_{cs,r}^{(l)} \cos^2\alpha_i^{(l)} + k_{cs,t}^{(l)} \sin^2\alpha_i^{(l)} & \frac{1}{2}(k_{cs,r}^{(l)} - k_{cs,t}^{(l)}) \sin 2\alpha_i^{(l)} & 0 \\ \frac{1}{2}(k_{cs,r}^{(l)} - k_{cs,t}^{(l)}) \sin 2\alpha_i^{(l)} & k_{cs,t}^{(l)} \cos^2\alpha_i^{(l)} + k_{cs,r}^{(l)} \sin^2\alpha_i^{(l)} & 0 \\ 0 & 0 & k_{cs,t}^{(l)} L_0^2 \end{pmatrix} \tag{4.43f}$$

$$\mathbf{K}_{cs,V} = \left(\underbrace{\mathbf{K}_{cs_1,V}^{(1)} \quad \mathbf{K}_{cs_2,V}^{(1)} \quad \ldots}_{N^{(1)}} \quad \cdots \quad \underbrace{\mathbf{K}_{cs_1,V}^{(n)} \quad \mathbf{K}_{cs_2,V}^{(n)} \quad \ldots}_{N^{(n)}} \right),$$

$$\mathbf{K}_{cs_i,V}^{(l)} = \begin{pmatrix} -k_{cs,r}^{(l)} \cos\alpha_i^{(l)} & k_{cs,t}^{(l)} \sin\alpha_i^{(l)} \\ -k_{cs,r}^{(l)} \sin\alpha_i^{(l)} & -k_{cs,t}^{(l)} \cos\alpha_i^{(l)} \\ 0 & -k_{cs,t}^{(l)} L_0 \end{pmatrix}, \tag{4.43g}$$

$$\mathbf{K}_{ss,V} = \text{diag}(\mathbf{K}^{(1)}_{ss,V}, \mathbf{K}^{(2)}_{ss,V}, \ldots, \mathbf{K}^{(n)}_{ss,V}),$$

$$\mathbf{K}^{(l)}_{s_i s_i,V} = \text{the } i\text{th diagonal block of } \mathbf{K}^{(l)}_{ss,V}$$

$$= \begin{pmatrix} k^{(l)}_{cs,r} + k^{(l)}_{ss}(\sin^2 a^{(l)}_i + \sin^2 b^{(l)}_i) & \frac{1}{2}k^{(l)}_{ss}(\sin 2b^{(l)}_i - \sin 2a^{(l)}_i) \\ \frac{1}{2}k^{(l)}_{ss}(\sin 2b^{(l)}_i - \sin 2a^{(l)}_i) & k^{(l)}_{cs,t} + k^{(l)}_{ss}(\cos^2 a^{(l)}_i + \cos^2 b^{(l)}_i) \end{pmatrix},$$

$$\mathbf{K}^{(l)}_{s_i s_{i+1},V} = \begin{pmatrix} k^{(l)}_{ss}\sin^2 a^{(l)}_i & \frac{1}{2}k^{(l)}_{ss}\sin 2a^{(l)}_i \\ -\frac{1}{2}k^{(l)}_{ss}\sin 2a^{(l)}_i & -k^{(l)}_{ss}\cos^2 a^{(l)}_i \end{pmatrix}, \tag{4.43h}$$

$$\mathbf{K}^{(l)}_{s_i s_{i-1},V} = \begin{pmatrix} k^{(l)}_{ss}\sin^2 b^{(l)}_i & -\frac{1}{2}k^{(l)}_{ss}\sin 2b^{(l)}_i \\ \frac{1}{2}k^{(l)}_{ss}\sin 2b^{(l)}_i & -k^{(l)}_{ss}\cos^2 b^{(l)}_i \end{pmatrix},$$

$$a^{(l)}_i = \alpha^{(l)}_{i+1} - \alpha^{(l)}_i,\ b^{(l)}_i = \alpha^{(l)}_i - \alpha^{(l)}_{i-1},$$

$$\mathbf{K}_T = \text{diag}(\mathbf{K}_{cc,T}, \underbrace{\mathbf{K}^{(1)}_{s_1 s_1,T}, \mathbf{K}^{(1)}_{s_2 s_2,T}, \ldots}_{N^{(1)}}, \ldots, \underbrace{\mathbf{K}^{(n)}_{s_1 s_1,T}, \mathbf{K}^{(n)}_{s_2 s_2,T}, \ldots}_{N^{(n)}}), \tag{4.43i}$$

$$\mathbf{K}_{cc,T} = \text{diag}(m_c, m_c, 0), \tag{4.43j}$$

$$\mathbf{K}^{(l)}_{s_i s_i,T} = \text{diag}(m^{(l)}_s, m^{(l)}_s). \tag{4.43k}$$

The eigenvalue problem of Eq. (4.42) is

$$(\lambda^2\mathbf{M} + \lambda\Omega\mathbf{G} + \mathbf{K}_V - \Omega^2\mathbf{K}_T)\boldsymbol{\phi} = \mathbf{0}. \tag{4.44}$$

Different sets of parameters apply to the example systems. The parameters in Table 4.1 apply to both example systems in Fig. 4.1, while Table 4.2 provides the parameters that vary between the different systems.

System Parameters	**Value**
C.C. mass, m_c (kg)	20
C.C. moment of inertia along $\mathbf{e}_3$, J_z (kg-m^2)	10.0
C.C. Translational stiffness to non-vibrating rotor, k_c (N/m)	5.2×10^6
C.C. Rotaional stiffness to non-vibrating rotor, $k_{c,R}$ (N-m/rad)	1.0×10^7
Radius of Sub. undeflected position, L_0 (m)	1
Radial stiffness between C.C. and a Sub., $k_{cs,r}^{(1)}$, $k_{cs,r}^{(2)}$ (N/m)	2.0×10^6, 2.5×10^6
Tangential stiffness between C.C. and a Sub., $k_{cs,t}^{(1)}$, $k_{cs,t}^{(2)}$ (N/m)	3.5×10^6, 3.0×10^6
Mass of a substructure, $m_s^{(1)}$, $m_s^{(2)}$(kg)	1.5, 1
Stiffness between substructures, $k_{ss}^{(1)}$, $k_{ss}^{(2)}$ (N/m)	2.5×10^6, 2.0×10^6

Table 4.1: Parameters of the components and coupling elements in Fig. 4.2. These parameters apply to both example systems in Fig. 4.1. Abbreviations C.C. and Sub. represent central component and substructure, respectively, and they are also used in Table 4.2.

System Parameters	**Value**
Multi-stage system with (Fig. 4.1(a))	
Angular positions of Subs., $\alpha_i^{(1)}$ (deg)	15, 87, 159, 231, 303
Angular positions of Subs., $\alpha_i^{(2)}$ (deg)	0, 60, 120, 180, 240, 300
Rotational speed of non-vibrating rotor (rad/s), Ω	100
Multi-stage system with $\mathcal{C}_5$ and $\mathcal{D}_2$ symmetric stages(Fig. 4.1(b))	
Angular positions of Subs., $\alpha_i^{(1)}$ (deg)	10, 82, 154, 226, 298
Angular positions of Subs., $\alpha_i^{(2)}$ (deg)	20, 75, 105, 160, 200, 255, 285, 340
Rotational speed of non-vibrating rotor (rad/s), Ω	0

Table 4.2: Parameters of the components and coupling elements in Fig. 4.2. These parameters vary between the example systems in Fig. 4.1.

Chapter 5

Eigensolution of Multi-Stage Bladed Disks Using Multi-Stage Cyclic Symmetry Reduction with Subspace Iterations

5.1 Introduction

Assemblies of bladed disks in turbomachines have multi-stage structures. Each component stage consists of a central disk and a number of equally spaced blades that are attached to the disk and sometimes shrouded at the blade tips. Each stage is cyclically symmetric, but the full multi-stage structure can be asymmetric because the number of the blades may vary in each stage.

Many current modeling methodologies for multi-stage bladed disks focus on single stage analysis, where each stage of balded disk can be decomposed into identical rotationally

repetitive sectors. The studies of the component stages are independent of each other. Because each stage is cyclically symmetric, the matrix operators in the equation of motion of each stage are circulant in structure [26]. The theory for circulant matrices provides an essential modal property for cyclically symmetric systems: modal deflections of each sectors are identical, but different sectors may vibrate with phase differences characterized by phase indices or number of nodal diameters [9, 26, 29, 105]. Therefore, the model of each full stage is reduced to a series of sector models characterized by phase indexes, each of which is obtained by imposing cyclic symmetry boundary conditions on the sector frontiers with the adjacent sectors [68]. The reduction of modeling size leads to an important improvement of computational efficiency, and the computation can be parallelized because all the sector models (with different phase indices) for all the stages are separate. Single stage models are also extended to study the mistuned bladed discs [82, 95–97, 107].

Despite of its advantages in computational efficiency, single stage analysis is not sufficient to fully understand the dynamics of the multi-stage bladed disks. Bladh et al. [66] demonstrated that the behavior of a stage of bladed disk deviates from its single stage analysis if it is coupled with other stages. The necessity for building multi-stage models comes with the challenge for computational cost. First, such models are usually huge (the number of degrees of freedom for an industrial model can be as large as tens of millions). Also, it is risky (inaccurate in theory although it works sometimes) to apply any cyclic symmetry boundary conditions to reduced the modeling order because the full system can be asymmetric.

Two general strategies are formed to reduce the modeling order for multi-stage bladed disks. Component mode synthesis methods (for example the Criag-Bampton method [80]) provide a divide-and-conquer scheme to obtain the reduced model by decomposing the multi-stage structures into single stages and then assembling the reduced models of the single stages by enforcing the compatibility conditions at the inter-stage interface. To capture the

inter-stage coupling and simultaneously guarantee the size of the reduced models is small, component mode synthesis methods using partial interface modes [108], Gram-Schmidt interface modes [109], or fourier constraint modes [110] are developed in recent years. Mistuning is taken into accounts in recent studies [69, 81, 110] where the component mode synthesis is combined with component mode mistuning [82] or the prestine rogue interface modal expansion (PRIME) [111]. Another strategy to reduce the modeling order for multi-stage bladed disks is the multi-stage cyclic symmetry (MSCS) reduction, first proposed by Laxalde et al [70, 71]. This method applies linear constraints on the inter-stage interface degrees of freedom of the single stage sector models for each stage. The full multi-stage system is reduced into a series of coupled systems consisting of sector models for all stages, but only one or few phase index components are considered for each coupled system. (This process will be reviewed later.) Based on this method, Sternchüss et al [72] introduced inter-disk structures to better capture inter-stage coupling, and Laxalde and Pierre [83] took mistuning into consideration. Tran combined the MSCS reduction with component mode synthesis and improved the MSCS reduction by using a systematic scheme to select the phase index components [73].

Obtaining accurate eigensolutions is important for parametric studies, optimization processes, and studies on dynamic behaviors of tuned multi-stage bladed disks systems. Accurate eigensolutions also provide a foundation to analyze mistuned multi-stage bladed disks through the reduced-order models using the subset of nominal system modes (SNM) [97]. In both the component mode synthesis and the MSCS reduction, however, inaccuracies of obtained eigensolutions introduced by substructuring or omitting a part of phase index components are unavoidable. The subspace iteration method, firstly by Bathe [112], was used to improve and control the accuracy of eigensolutions when substructuring and component mode synthesis apply [113, 114]. The errors in obtained eigensolutions can be reduced to

a desired order. To the authors' knowledge, however, it is still unknown how to improve and control the accuracy of eigensolutions obtained from the MSCS reduction method for multi-stage bladed disks with acceptable sacrifice of computational efficiency.

The aim of this work is to combine the MSCS reduction method and the subspace iteration method to obtain the eigensolutions of multi-stage bladed disks with a controllable precision. The study does not consider the mistunings in bladed disks. The proposed method in this work is formulated with consideration of the cyclic symmetry in each component stage, so that the computational efficiency of the MSCS reduction method is not completely sacrificed for the eigensolution accuracy.

The paper is organized as follows. In Section 5.2, the method of MSCS reduction is revisited. The drawbacks of this method are demonstrated by an example two-stage bladed disks. In Section 5.3, the MSCS reduction method is combined with the subspace iteration method to improve the accuracy of obtained eigensolutions. The formulation of the proposed method is given, and the effectiveness of this method is illustrated by applying the method to the same example two-stage system in Section 5.2.

5.2 Multi-Stage Cyclic Symmetry (MSCS) Reduction

Multi-stage bladed disks in turbinemachines consist of several to tens of component stages, with tens to hundreds of blades in each stage. For industry applications, the finite element analysis usually requires a mesh containing at least thousands of nodes within a sector (a blade and a portion of the disk) of a component stage, and this number of nodes within a sector can be as large as hundreds of thousands in bladed disks with compliant structures. The large size of the full system model for multi-stage bladed disks impedes computing eigensolutions or any other dynamic properties of the full system. To improve

the computational efficiency, multi-stage bladed disks are studied using the multi-stage cyclic symmetry reduction method in many previous works. The method is based on the properties of cyclically symmetric systems, although it is applied to the multi-stage structures that are not symmetric as a whole in general.

5.2.1 Formulation of Multi-Stage Cyclic Symmetry Reduction

The formulation of multi-stage cyclic symmetry (MSCS) reduction is given for reference to complete the full methodology in this work, starting from the sector models of each stage to iteration method for eigensolutions (comes later). The formulation in this section is distilled from Ref. [70]. One of the advantages of this method is that only sector models of component stages are involved, thus, the full multi-stage system model in physical coordinates is not necessary.

According to group theory or equivalently the circulant matrix theory [1, 26, 57], the dynamics of a system with cyclic symmetry can be described by a series of sector models (characterized by phase indices). All these sector models for a cyclic stage are obtained from the same reference sector for the stage. For the reference sector of the ith stage, the matrix operator $\mathbf{D}_i^r$ is in the form of

$$\mathbf{D}_i^r = \mathbf{M}_i^r \frac{\mathrm{d}^2}{\mathrm{d}t^2} + \mathbf{K}_i^r, \tag{5.1}$$

where $\mathbf{M}_i^r$ and $\mathbf{K}_i^r$ are the inertia and stiffness matrices. By categorizing the degrees of freedom of the reference sector according to the node positions, the matrix operator $\mathbf{D}_i^r$ can be partitioned as

$$\mathbf{D}_i^r = \begin{pmatrix} \mathbf{D}_{i,LL}^r & \mathbf{D}_{i,LI}^r & \mathbf{D}_{i,LH}^r \\ \mathbf{D}_{i,IL}^r & \mathbf{D}_{i,II}^r & \mathbf{D}_{i,IH}^r \\ \mathbf{D}_{i,HL}^r & \mathbf{D}_{i,HI}^r & \mathbf{D}_{i,HH}^r \end{pmatrix}, \tag{5.2}$$

where the subscripts L, H, and I represents that the nodes are on the low edge, high edge, and in the interior regions of the sector, respectively. In cyclically symmetric structures, the nodes on the high edge of a sector are simultaneously the nodes on the low edge of the adjacent sector. For a phase index k, the cyclic symmetry boundary condition for the nodes on the low edge and the high edge is

$$\mathbf{q}^r_{i,H} = \mathrm{e}^{k\frac{2\pi \mathrm{j}}{N_i}} \mathbf{q}^r_{i,L}, \tag{5.3}$$

where N_i is the number of blades in the ith stage, and $\mathbf{q}^r_{i,L}$ and $\mathbf{q}^r_{i,H}$ are the degrees of freedom of the nodes on the low edge and high edge of the reference sector, respectively. The matrix operator for the sector models with the cyclic symmetry boundary condition is obtained as

$$\begin{aligned}
\mathbf{D}^{(k)}_i &= \begin{pmatrix} \mathbf{I}^r_{i,L} & \mathbf{0} \\ \mathbf{0} & \mathbf{I}^r_{i,I} \\ \mathrm{e}^{k\frac{2\pi \mathrm{j}}{N_i}} \mathbf{I}^r_{i,L} & \mathbf{0} \end{pmatrix}^T \begin{pmatrix} \mathbf{D}^r_{i,LL} & \mathbf{D}^r_{i,LI} & \mathbf{D}^r_{i,LH} \\ \mathbf{D}^r_{i,IL} & \mathbf{D}^r_{i,II} & \mathbf{D}^r_{i,IH} \\ \mathbf{D}^r_{i,HL} & \mathbf{D}^r_{i,HI} & \mathbf{D}^r_{i,HH} \end{pmatrix} \begin{pmatrix} \mathbf{I}^r_{i,L} & \mathbf{0} \\ \mathbf{0} & \mathbf{I}^r_{i,I} \\ \mathrm{e}^{k\frac{2\pi \mathrm{j}}{N_i}} \mathbf{I}^r_{i,L} & \mathbf{0} \end{pmatrix} \\
&= \begin{pmatrix} \mathbf{D}^r_{i,LL} + \mathbf{D}^r_{i,HH} & \mathbf{D}^r_{i,LI} \\ \mathbf{D}^r_{i,IL} & \mathbf{D}^r_{i,II} \end{pmatrix} + \mathrm{e}^{k\frac{2\pi \mathrm{j}}{N_i}} \begin{pmatrix} \mathbf{D}^r_{i,LH} & \mathbf{0} \\ \mathbf{D}^r_{i,IH} & \mathbf{0} \end{pmatrix} + \mathrm{e}^{-k\frac{2\pi \mathrm{j}}{N_i}} \begin{pmatrix} \mathbf{D}^r_{i,HL} & \mathbf{D}^r_{i,HI} \\ \mathbf{0} & \mathbf{0} \end{pmatrix}
\end{aligned}, \tag{5.4}$$

where $\mathbf{I}^r_{i,L}$ is the identity matrix that has the same dimension of $\mathbf{D}^r_{i,LL}$. The equation of motion for the sector model of the ith stage with phase index k is

$$\mathbf{D}^{(k)}_i \mathbf{q}^{(k)}_i = \mathbf{f}^{(k)}_i, \tag{5.5}$$

where the solution $\mathbf{q}^{(k)}_i$ is the phase index component k for the ith stage. The force vector

in Eq. (5.5) is obtained from the force vector $\mathbf{f}_i$ for the full ith stage through the relation

$$\mathbf{f}_i^{(k)} = (\mathbf{e}_{N_i}^{(k)})^{\mathcal{H}} \otimes \mathbf{f}_i, \tag{5.6a}$$

$$\mathbf{e}_{N_i}^{(k)} = \frac{1}{\sqrt{N_i}} \begin{pmatrix} 1 & \mathrm{e}^{k\frac{2\pi \mathrm{j}}{N_i}} & \mathrm{e}^{k\frac{4\pi \mathrm{j}}{N_i}} & \dots & \mathrm{e}^{k\frac{2(N_i-1)\pi \mathrm{j}}{N_i}} \end{pmatrix}^T \tag{5.6b}$$

where $\mathcal{H}$ is to take the Hermitian transpose of the matrix or vector. The motion of the full ith stage $\mathbf{q}_i$ is

$$\mathbf{q}_i = \sum_{k=0}^{N_i-1} \mathbf{e}_{N_i}^{(k)} \otimes \mathbf{q}_i^{(k)}. \tag{5.7}$$

To add inter-stage boundary conditions for the interface where two stages merge, the sector models (characterized by phase indices) of the merging stages are combined through a linear constraint equation. The $\mathbf{q}_i^{(k)}$ in Eq. (5.5) can be separated as

$$\mathbf{q}_i^{(k)} = (\mathbf{q}_{i,U}^{(k)}, \mathbf{q}_{i,I}^{(k)}, \ \mathbf{q}_{i,D}^{(k)})^T, \tag{5.8}$$

where U denotes the boundary nodes at the inter-stage interface connecting the upper stage (upper frontier), D denotes the boundary nodes at the inter-stage interface connecting the lower stage (lower frontier), and I denotes the interior nodes (relative to the inter-stage interface, instead of the sector cyclic boundaries). The deflections of the nodes on the interface between the ith and the hth stages (the hth stage is the upper stage) can be obtained from the sector models for these two stages. For example, the deflections on the inter-stage interface between the ith and hth stages is the deflections of the nodes at the upper frontier of the ith stage, which can be obtained from

$$\mathbf{q}_{inter,i} = \sum_{k=0}^{N_i-1} \mathbf{e}_{N_i}^{(k)} \otimes \mathbf{q}_{i,U}^{(k)}, \tag{5.9}$$

where $\mathbf{q}_{inter,i}$ is the vector of the nodal deflections on the interface obtained from the sector models of the ith stage. The same nodal deflections on the inter-stage interface can be similarly expressed as

$$\mathbf{q}_{inter,h} = \sum_{k=0}^{N_h-1} \mathbf{e}_{N_h}^{(k)} \otimes \mathbf{q}_{h,D}^{(k)}, \tag{5.10}$$

because the inter-stage interface is also the lower frontier of the hth stage (the upper stage). Considering a general case where the two merging stages are meshed differently on the inter-stage interface, a constraint equation can be formulated as

$$\sum_{k=0}^{N_i-1} \mathbf{e}_{N_i}^{(k)} \otimes \mathbf{q}_{i,U}^{(k)} = \mathbf{B}(i,h) \sum_{l=0}^{N_h-1} \mathbf{e}_{N_h}^{(l)} \otimes \mathbf{q}_{h,D}^{(l)} \tag{5.11}$$

where $\mathbf{B}(i,h)$ is a constraint matrix (multi-point constraint) that makes the two interface meshes compatible. Eq. (5.11) is the inter-stage boundary condition. Combination of Eqs. (5.5) and (5.11) can formulate a multi-stage full coupled system that considers all phase index components of all stages simultaneously [73]. According to Ref. [73], solving this multi-stage full coupled system (Eqs. (5.5) and (5.11)) is equivalent to solving the original full multi-stage system directly. The computational cost for solving this multi-stage full coupled system is even higher than solving the original full multi-stage system directly, because application of multi-stage full coupled system can not reduce the size of the problem but requires calculations to assemble Eqs. (5.5) and (5.11).

Different from the multi-stage full coupled system that considers all phase index components of all stages simultaneously, the MSCS reduction method reduces the modeling order by formulating reduced problems, each of which considers a few (at least one but not all) phase index components of all the component stages simultaneously. To determined the phase index components to be considered simultaneously in one reduced problem, Ref. [73] proposed a mixing scheme of phase index components. By this scheme, all phase index com-

ponents can be mixed into N_{min} sets, where N_{min} is the least number of blades in a single stage, and each phase index component can only appear in one set. In other words, this mixing scheme of phase index components assumes the phase index components in different sets can not couple with each other. In this work, the mixing scheme in Ref. [73] is used for the MSCS reduction method, and the phase index components of a stage are labeled with the stage index. For example, (i,k) denotes the phase index k in the ith stage. Such denoting convention is similar to the symmetry species in Chapter 3.

For a set of phase index components V, the inter-stage boundary condition for the interface between the ith and the hth stages is

$$\sum_{(i,k)\in V} \mathbf{e}_{N_i}^{(k)} \otimes \mathbf{q}_{i,U}^{(k)} = \mathbf{B}(i,h) \sum_{(h,l)\in V} \mathbf{e}_{N_h}^{(l)} \otimes \mathbf{q}_{h,D}^{(l)}. \tag{5.12}$$

Multiplication of Eq. (5.12) by $\mathbf{e}_{N_i}^{(k)} \otimes \mathbf{I}_{i,B}$ from the left yields

$$\mathbf{q}_{i,U}^{(k)} = \sum_{(h,l)\in V} C(i,h,k,l)\ \mathbf{q}_{h,D}^{(l)}, \tag{5.13a}$$

$$C(i,h,k,l) = (\mathbf{e}_{N_i}^{(k)} \otimes \mathbf{I}_{i,U})^{\mathcal{H}}\ \mathbf{B}(i,h)\ (\mathbf{e}_{N_h}^{(l)} \otimes \mathbf{I}_{h,D}). \tag{5.13b}$$

As indicated by Eq. (5.12), on the inter-stage interface, all the phase index components of the ith stage in the set V are represented as a linear combination of the phase index components of the hth stage in the same set.

To assemble the multi-stage model characterized by the phase index component set V, all equations of motions of the sector models of the phase index components in V are appended as one equation,

$$\mathbf{D}^{(V)}\mathbf{q}^{(V)} = \mathbf{f}^{(V)}, \tag{5.14a}$$

$$\mathbf{D}^{(V)} = \mathrm{diag}(\dots, \mathbf{D}_i^{(k)}, \dots, \mathbf{D}_h^{(l)}, \dots), \tag{5.14b}$$

$$\mathbf{q}^{(V)} = (\dots, \mathbf{q}_{i,D}^{(k)}, \mathbf{q}_{i,I}^{(k)}, \mathbf{q}_{i,U}^{(k)}, \dots, \mathbf{q}_{h,D}^{(l)}, \mathbf{q}_{h,I}^{(l)}, \mathbf{q}_{h,U}^{(l)}, \dots)^T, \tag{5.14c}$$

$$\mathbf{f}^{(V)} = (\dots, \mathbf{f}_{i,D}^{(k)}, \mathbf{f}_{i,I}^{(k)}, \mathbf{f}_{i,U}^{(k)}, \dots, \mathbf{f}_{h,D}^{(k)}, \mathbf{f}_{h,I}^{(l)}, \mathbf{f}_{h,U}^{(l)}, \dots)^T, \tag{5.14d}$$

where the couplings between these sector models are not considered. To assemble these sector models, the nodal deflections of the inter-stage interface are represented as the deflections of the lower frontier of the upper stage. For example, at the interface between the ith and the hth stages, the upper frontier nodal deflections of the ith stage are eliminated using Eq. (5.13). Therefore, the new generalized coordinate $\tilde{\mathbf{q}}^{(V)} = (\dots, \mathbf{q}_{i,D}^{(k)}, \mathbf{q}_{i,I}^{(k)}, \dots, \mathbf{q}_{h,D}^{(l)}, \mathbf{q}_{h,I}^{(l)}, \dots)^T$ is related to $\mathbf{q}^{(V)}$ in Eq (5.14) as

$$\mathbf{q}^{(V)} = \mathbf{T}\tilde{\mathbf{q}}^{(V)}, \tag{5.15a}$$

$$\mathbf{T} = \begin{pmatrix} \ddots & & & & & & \\ \dots & \mathbf{I}_{i,D} & \mathbf{0} & \dots & \mathbf{0} & \mathbf{0} & \dots \\ \dots & \mathbf{0} & \mathbf{I}_{i,I} & \dots & \mathbf{0} & \mathbf{0} & \dots \\ \dots & \mathbf{0} & \mathbf{0} & \dots & C(i,h,k,l) & \mathbf{0} & \dots \\ & \vdots & \vdots & \vdots & \vdots & \vdots & \\ \dots & \mathbf{0} & \mathbf{0} & \dots & \mathbf{I}_{h,D} & \mathbf{0} & \dots \\ \dots & \mathbf{0} & \mathbf{0} & \dots & \mathbf{0} & \mathbf{I}_{h,I} & \dots \\ \dots & \mathbf{0} & \mathbf{0} & \dots & \mathbf{0} & \mathbf{0} & \dots \\ & & & & & & \ddots \end{pmatrix}. \tag{5.15b}$$

Substitution of Eq. (5.15) into Eq. (5.14a) and multiplication by $\mathbf{T}^{\mathcal{H}}$ yield the equation of motion of the coupled system by assembling the sector models characterized by the phase

index components in V,

$$\tilde{\mathbf{D}}^{(V)}\tilde{\mathbf{q}}^{(V)} = \tilde{\mathbf{f}}^{(V)}, \tag{5.16a}$$

$$\tilde{\mathbf{D}}^{(V)} = \mathbf{T}^{\mathcal{H}}\mathbf{D}^{(V)}\mathbf{T}, \tag{5.16b}$$

$$\tilde{\mathbf{f}}^{(V)} = \mathbf{T}^{\mathcal{H}}\mathbf{f}^{(V)}, \text{ for } (i,k),(h,l) \in V. \tag{5.16c}$$

The eigenvalue problem of Eq. (5.16) is

$$\tilde{\mathbf{A}}^{(V)}\tilde{\boldsymbol{\phi}}^{(V)} = \mathbf{0} \tag{5.17a}$$

$$\tilde{\boldsymbol{\phi}}^{(V)} = \left(\ldots,\ \tilde{\boldsymbol{\phi}}_{i,D}^{(k)}, \tilde{\boldsymbol{\phi}}_{i,I}^{(k)},\ \ldots,\ \tilde{\boldsymbol{\phi}}_{h,D}^{(l)},\ \tilde{\boldsymbol{\phi}}_{h,I}^{(l)},\ \ldots \right)^T \tag{5.17b}$$

In full system modes (obtained by the MSCS reduction method), the modal deflections of the interior and inter-stage boundary degrees of freedom in the ith stage are expanded as

$$\boldsymbol{\phi}_{i,D}^{(V)} = \sum_{(i,k)\in V} \mathbf{e}_{N_i}^{(k)} \otimes \tilde{\boldsymbol{\phi}}_{i,D}^{(k)} \tag{5.18a}$$

$$\boldsymbol{\phi}_{i,I}^{(V)} = \sum_{(i,k)\in V} \mathbf{e}_{N_i}^{(k)} \otimes \tilde{\boldsymbol{\phi}}_{i,I}^{(k)}, \tag{5.18b}$$

$$\boldsymbol{\phi}_{i,U}^{(V)} = \mathbf{B}(i,h)\boldsymbol{\phi}_{h,D}^{(V)} = \mathbf{B}(i,h) \sum_{(h,l)\in V} \mathbf{e}_{N_h}^{(l)} \otimes \tilde{\boldsymbol{\phi}}_{h,D}^{(l)}, \tag{5.18c}$$

5.2.2 Example Two-Stage Cyclically Symmetric System

A two-stage bladed disks assembly is given as the numerical example throughout this study. As shown in Fig. 5.1, the blades in each stage are shrouded, and the disks are coupled

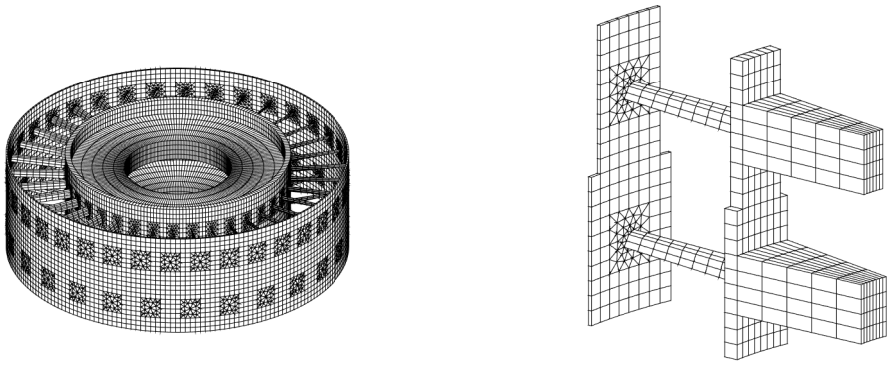

(a) (b)

Figure 5.1: Example two-stage bladed disks. (a). The full two-stage system with meshes for finite element method. (b). Two single stage sectors for the two-stage system. The bottom sector is the sector for the first stage and the top is for the second stage.

through the rims of the disk and the shrouds of the blades. There are 27 and 36 blades in the two stages, respectively. For the two stages, the meshes on the inter-stage interface are compatible, so the constraint matrix $\mathbf{B}$ in Eq. (5.11) is a boolean matrix, where the elements in the matrix are valued with either 1 or 0. The reference sector models of the two stages are illustrated in Fig. 5.1(b), with 1743 and 1413 degrees of freedom, respectively.

5.2.3 Advantages and Drawbacks of MSCS Reduction

The MSCS reduction method is advantageous in improving the computational efficiency, because the full multi-stage system are analyzed using sector-level-sized models. Besides, because all these models are independent, the task of obtaining the full system eigensolutions is decomposed into multiple parallel sub-tasks where the full system eigensolutions are estimated from these sector-level-sized models. Performing such parallel computation provides further reduction of the time cost to obtain the eigensolutions.

Although it improves the computational efficiency, the MSCS reduction method can

not always provide accurate eigensolutions because it relys on the mixing scheme of the phase index components of component stages. The equation of motion of the assembled systems in Eq. (5.16) can describe the dynamics of the actual multi-stage system based on an assumption: the phase index components considered in each set V are assumed to couple with the phase index components within the set V but be uncoupled with the other components excluded from the set (for brevity, the sets are referred to as being independent). Such assumption is analogous to the orthogonality of symmetry species in group theory [1]. In some multi-stage systems with full system symmetry, the phase index components can be mixed perfectly into independent sets. For example, the example system in Fig. 5.1(a) has a cyclic symmetry with order of 9, so the phase index components of the component stages can be mixed into 9 independent sets V_1, V_2, ..., V_9, where $V_i = \{(1,i),(1,i+9),(1,i+18),(2,i),(2,i+9),(2,i+18),(2,i+27)\}$ for i from 0 to 8. Based on this phase index mixing scheme , the assembled system in Eq. (5.16) for the set V_i is equivalent to a 'bigger' sector model of the full system that includes three basic sectors in the first stage and four basic sectors in the second stage. Admittedly, the MSCS reduction method using this phase index mixing scheme for the example system in Fig. (5.1) provides accurate eigensolutions. For general applications, however, it is not always possible or even preferred to re-group the phase index components into independent sets (explained as follows), thus the MSCS reduction method unavoidably provide inaccurate eigensolutions.

The mixing scheme of phase index components can not partition the phase index components into independent sets if a multi-stage system is asymmetric, although each of its component stage is cyclically symmetric. In such a case, all the phase index components of the component stages are coupled, and any partitioning of the phase index components leads to the loss of accuracy occurs in the MSCS reduction. Also, although the phase index components of some multi-stage systems can be partitioned into perfectly independent sets

(e.g., the example in Fig. (5.1), as discussed above), the pursuit of independent phase index component sets is not always preferred because the assembled models (in Eq. (5.16)) can be large sized and the computational efficiency of the MSCS reduction method is largely sacrificed. The trade of computational efficiency for a perfectly mixing of phase index components is not always favorable, especially when the order of cyclic symmetry in the full multi-stage system is much smaller than the minimum number of blades in a component stage. For example, in a system consisting of a 102-bladed stage and 104-bladed stage, the phase index components can be partitioned into two independent sets, the first set contains all the odd phase indices of the two stages (103 phase index components in total), and the second set contains all the even phase indices of the two stages (103 phase index components in total). Despite of its accuracy in obtaining eigensolutions, the MSCS reduction method based on this phase index mixing scheme is less advantageous to improve the computational efficiency than using the mixing schemes that re-group the phase indices into 102 sets (as proposed in Refs. [70, 71, 73], phase indices are partitioned into N_{min} sets, where N_{min} is the minimum number of blades in any component stage). In Ref. [73], a mixing scheme of phase index components is proposed to guarantee the computational efficiency of the MSCS reduction method with a reliable accuracy. The mixing scheme proposed by Tran provides a proper partition of phase index components for the example system in Ref. [73], where the component stages are not shrouded. As shown in the following example, however, the proposed mixing scheme in Ref. [73] unavoidably results in inaccurate eigensolutions when the stages are coupled through compliant structures.

To illustrate the above advantages and drawbacks of the MSCS reduction method, the lowest 500 eigensolutions are solved for the example system in Fig. 5.1 using the full system model and the MSCS reduction method. The phase index components are partitioned into 27 sets (instead of 9 independent sets as forementioned) based on the mixing scheme proposed

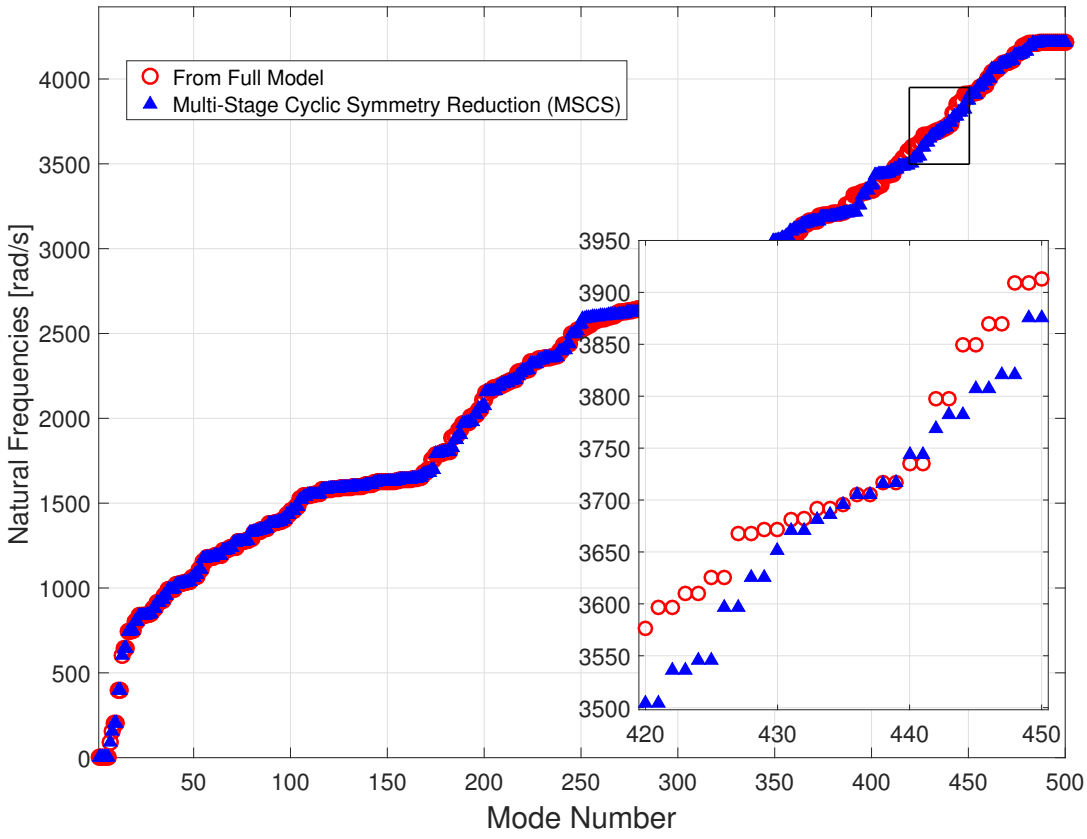

Figure 5.2: Natural frequencies of the system in Fig. 5.1(a).

by Tran [73] to retain the computational efficiency of the MSCS reduction while maximizing the independence between the sets of phase index components.

As shown in Fig. 5.2, comparing the natural frequencies for the same mode number, the relative error of natural frequencies obtained by the MSCS reduction is within 2%. The computational time for solving the full system eigenvalue problem is 763s, while it only takes 32s to obtain the same number of eigensolutions using the MSCS reduction method without parallel computation of Eq. (5.17) with respect to the set V. The computation speed increased by 24 times, and this increase can be larger if Eq. (5.17) for different sets (27 in total) of phase index components are solved simultaneously. The example shows that

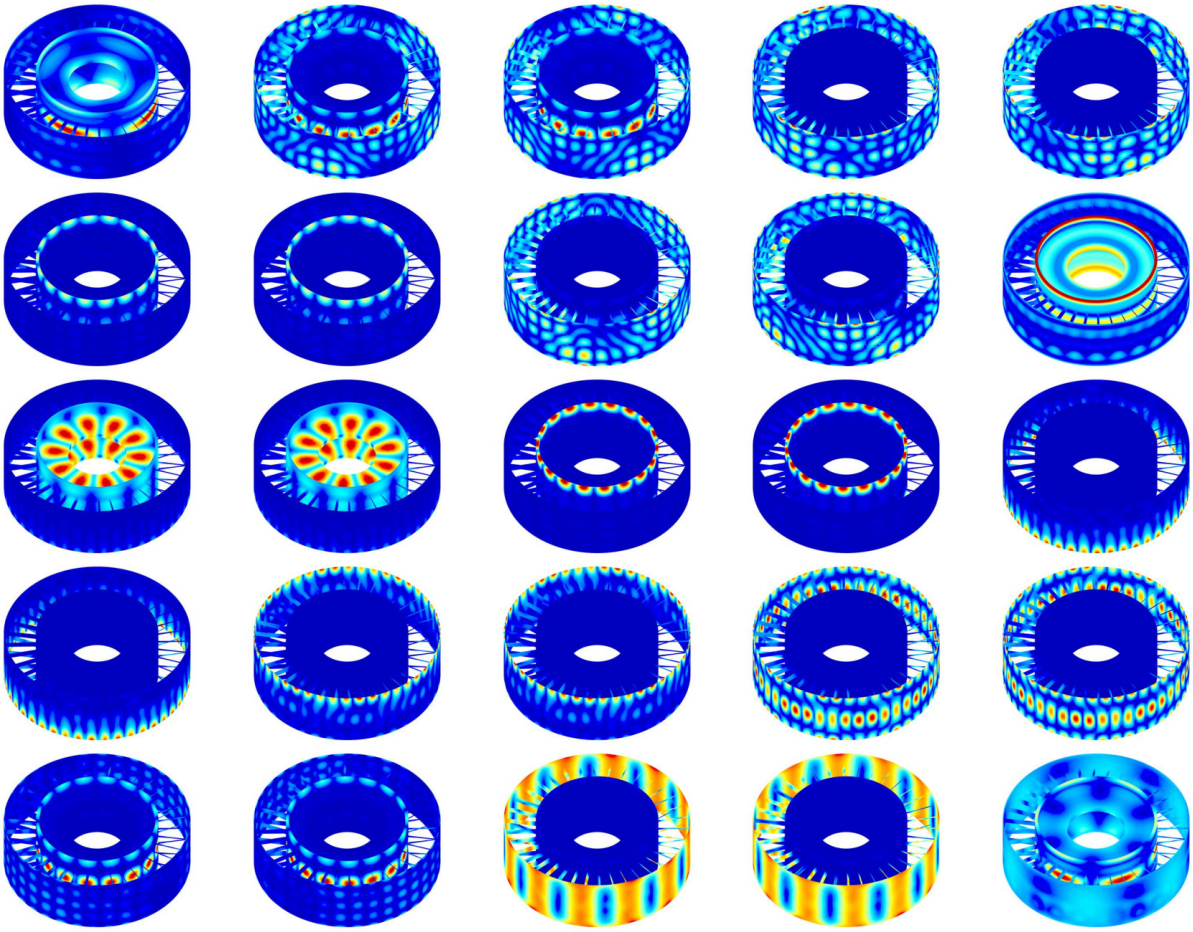

Figure 5.3: Modes of the system in Fig. 5.1(a) obtained from the full system model (with mode number from 426 to 450). The modes are arranged from the left to the right, then from the top to the bottom, in the ascending order of the mode number. For example, the 433rd mode in the third mode in the second row.

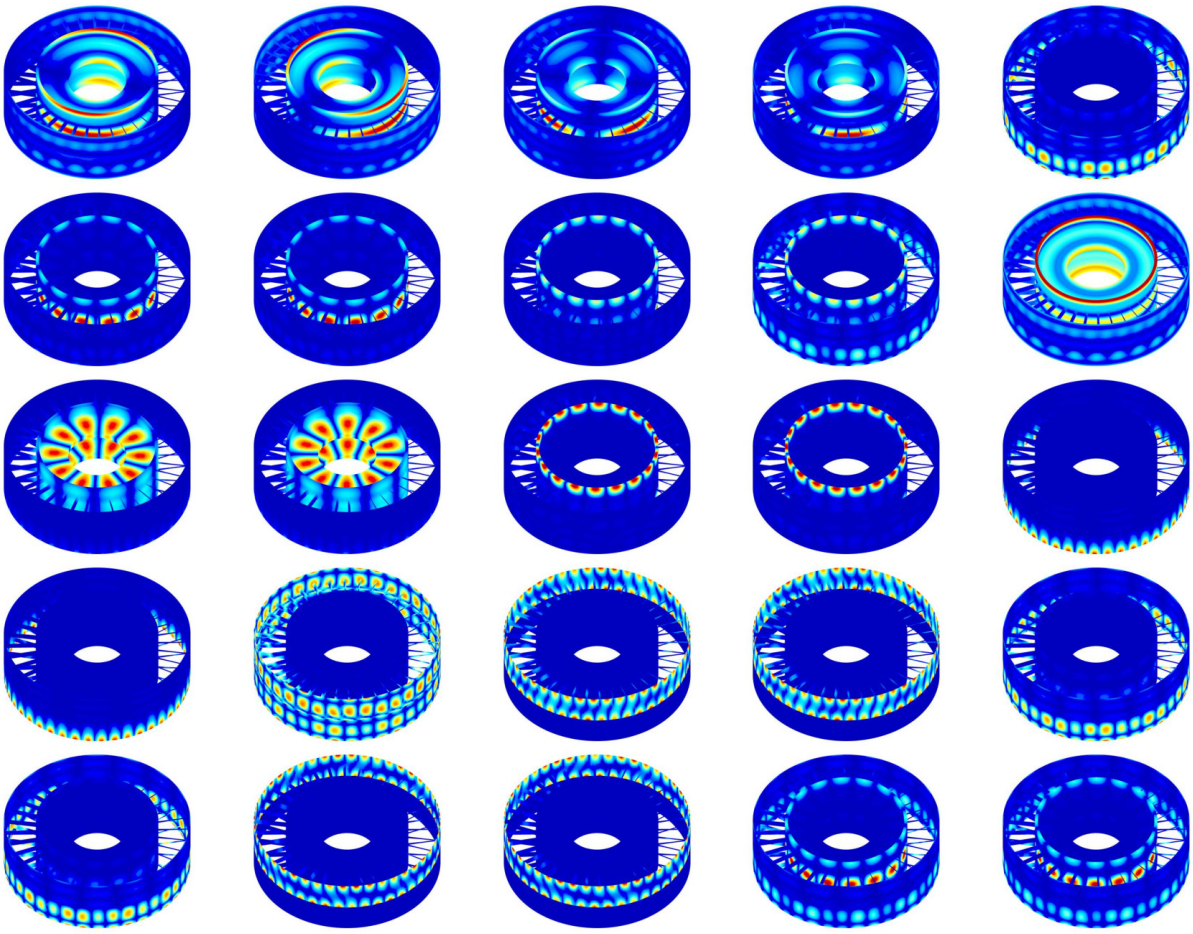

Figure 5.4: Modes of the system in Fig. 5.1(a) obtained from the MSCS reduction (with mode number from 426 to 450).

the MSCS reduction method improves the computational efficiency significantly as discussed previously.

Meanwhile, the example also illustrates that the MSCS reduction method sacrifices the solution accuracy for computational speed. For this example system, Fig. 5.2 shows that the errors in natural frequencies are more likely to occur after mode number 250, above 2500 Hz, where the modal deflections of disks and shrouds can be a combination of phase index components that is not obtained by the phase index mixing scheme in Ref. [73]. Although the errors in natural frequencies are accidentally acceptable, the accuracy of the mode shapes obtained from the MSCS reduction can be unsatisfying. Figures 5.3 and 5.4 illustrate the full system mode shapes (with mode number from 426 to 450) obtained from the full system model and the MSCS reduction method, respectively. With the modes obtained from the full system model as the benchmark, the modes obtained from the MSCS reduction method are unsatisfying for two reasons: a) some of the actual full system modes can not be well estimated (for example, the mode with the mode number 433 in Fig. 5.3); b) the MSCS reduction method provides wrong modes that are not similar to any of the actual full system modes (for example, the mode with the mode number 430 in Fig. 5.4). Because the above two types of errors exist, the comparison between the actual full system modes in Fig. 5.3 and their estimates in Fig. 5.4 more efficiently reveals the inaccuracy of the MSCS method than the comparison of natural frequencies, which are used to validate the accuracy of the MSCS method in Ref. [73].

To better illustrate whether the MSCS reduction can capture the phase index components of the full system modes, Fig. 5.5 compares the nodal diameter components existing in the first 500 modes obtained from the full system model and the those from the MSCS reduction method. For a full system mode $\boldsymbol{\phi}$, regardless of whether it is obtained from the full system model or the MSCS reduction method, the weight of the phase index component

(k,i) (the kth phase index component of the ith stage) can be calculated as

$$w_i^{(k)} = \frac{\left\|\tilde{\boldsymbol{\Phi}}_i^{(k)}\right\|}{\sum_{i=1}^{2}\sum_{k=0}^{N_{i-1}}\left\|\tilde{\boldsymbol{\Phi}}_i^{(k)}\right\|}, \tag{5.19}$$

where

$$\tilde{\boldsymbol{\Phi}}_i^{(k)} = \begin{bmatrix} (\mathbf{e}_{N_i}^{(k)} \otimes \mathbf{I}_{i,I})^{\mathcal{H}} \boldsymbol{\Phi}_{i,I} \\ (\mathbf{e}_{N_i}^{(k)} \otimes \mathbf{I}_{i,B})^{\mathcal{H}} \boldsymbol{\Phi}_{i,B} \end{bmatrix}, \tag{5.20}$$

and $\boldsymbol{\Phi}_{i,I}$ and $\boldsymbol{\Phi}_{i,B}$ are the the modal deflections of the interior and inter-stage boundary degrees of freedom in the ith stage. For brevity, the nodal diameter components instead of phase index components are plotted in Fig. 5.5, because both the kth and the $(N_i - k)$th phase index components of the full system modes has the same nodal diameter k. The weight of the kth nodal diameter components for the ith stage is

$$W_i^k = \begin{cases} w_i^{(k)} + w_i^{(N_i-k)} & k \neq N_i \text{ or } \frac{N_i}{2} \\ w_i^{(k)} & k = N_i, \text{ or } \frac{N_i}{2} \end{cases}, \tag{5.21}$$

where $k = 0, 1, \ldots, N_i/2$ (N_i is even) or $(N_i - 1)/2$ (N_i is odd). The nodal diameter components are said to be dominant if its weight is over 50%, and said to be secondarily dominant if the weight is between 10% and 50%. Both the dominant and secondarily dominant nodal diameter components of a mode are plotted with the same value of the natural frequency for the mode. Compared to Fig. 5.2, Fig. 5.5 provides a more strict criterion to evaluate the accuracy of the MSCS reduction method, because both the natural frequencies and significant nodal diameter components of vibration modes are compared simultaneously.

As illustrated in Fig. 5.5, the MSCS reduction method can not capture all necessary phase index components, even it can accidentally provide relatively accurate natural frequencies (Fig. 5.2).

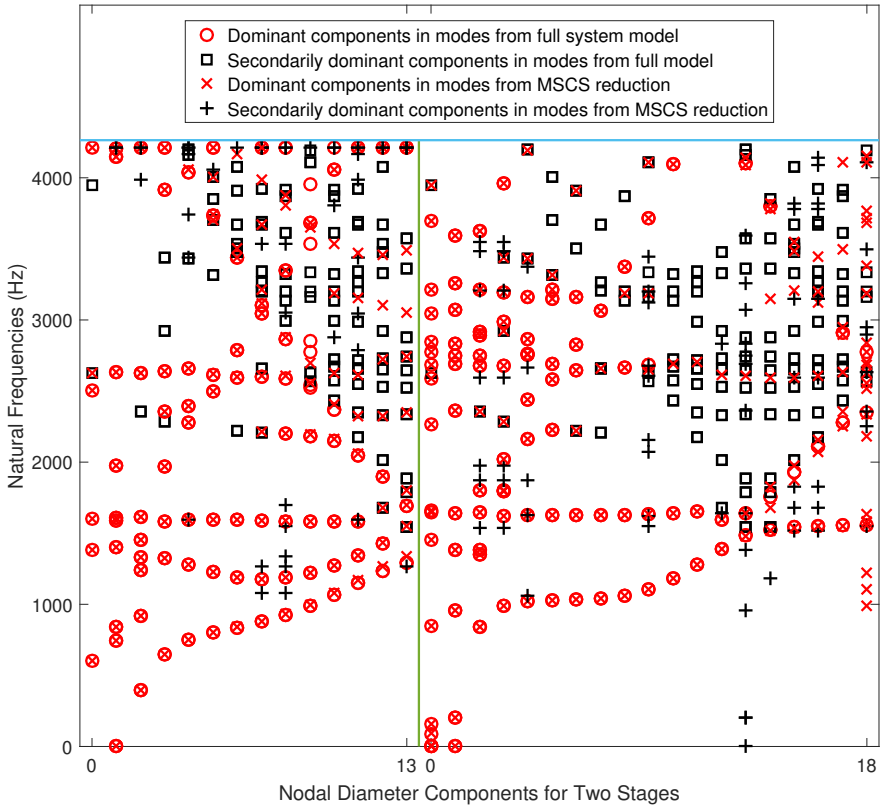

Figure 5.5: Natural frequencies vs nodal diameter components of the eigenvectors of the system in Fig. 5.1(a). On the horizontal axis, the number of nodal diameter for the two stages are labeled and divided by the vertical line. The nodal diameter components for the first stage (number of nodal diameter from 0 to 13 for a 27-bladed stage) are on the left hand side, while those for the second stage are on the right

Therefore, the MSCS reduction method is advantageous in computational speed but not always reliable in providing accurate eigensolutions. The mixing schemes of the phase index components is the foundation of the MSCS reduction method, but it is flawed because the phase index components that are partitioned into different sets can be coupled in any vibration modes. This mixing scheme in Ref. [73] can not guarantee that the MSCS reduction method can captured the coupling between the phase index components. For general multi-stage balded disks where the full system can be asymmetric, no mixing scheme of the phase index components should be expected to be able to simultaneously retain the computational efficiency and accuracy of the MSCS reduction method.

5.3 Subspace Iteration for Multi-Stage Cyclically Symmetric System

The accuracy of the MSCS reduction relies on how unlikely it is for the phase index components from two different partitioned sets to couple with each other. In the previous section, it is shown that the mixing scheme of phase index components can not guarantee that the resulting MSCS reduction can captured the coupling between the phase index components. To improve the accuracy of eigensolutions obtained from the MSCS reduction method, an iterative method based on the subspace iteration [112] is developed for multi-stage bladed disks.

5.3.1 General Subspace Iteration Method

The subspace iteration method developed by Bathe [112] is can solve general eigenvalue problems that take the form of

$$\mathbf{K}\boldsymbol{\phi} = \lambda \mathbf{M}\boldsymbol{\phi}, \tag{5.22}$$

where $\mathbf{K}$ and $\mathbf{M}$ are the stiffness and mass matrices of a finite element system. The eigenvalue problems of the systems with gyroscopic effect can also be transformed into this general form when it is represented in the state space. The subspace iteration method can solve the smallest p eigenvalues λ_n $(n = 1, 2, ..., p)$ and their corresponding eigenvectors $\boldsymbol{\phi}_n$ $(n = 1, 2, ..., p)$, where the eigenvalues are ordered as

$$0 < \lambda_1 \leqslant \lambda_2 \leqslant \cdots \leqslant \lambda_p. \tag{5.23}$$

The number of eigensolutions to be solved (the number p in Eq. (5.23)) is arbitrary as long as it does not exceeds the size of the matrix $\mathbf{K}$ in Eq. (5.22), but in most applications this number is much smaller than the size of $\mathbf{K}$. If the smallest eigenvalue is zero (such case is easy to identify because it indicates rigid body modes exist), a shift can be used to reach the condition in Eq. (5.23) [115].

To solve the p eigensolutions that are ordered as Eq. (5.23), one should start with q starting iteration vectors ($q = max\{p + 8, 2p\}$ according to Ref. [112]) to establish $\mathbf{X}_0$ and iterate in the following process:

$$\mathbf{Y}_{(m-1)} = \mathbf{M}\mathbf{X}_{(m-1)}, \tag{5.24a}$$

$$\mathbf{K}\tilde{\mathbf{X}}_{(m)} = \mathbf{Y}_{(m-1)}, \tag{5.24b}$$

$$\tilde{\mathbf{K}}_{(m)} = \tilde{\mathbf{X}}_{(m)}^{\mathcal{H}}\mathbf{K}\tilde{\mathbf{X}}_{(m)} = \tilde{\mathbf{X}}_{(m)}^{\mathcal{H}}\mathbf{Y}_{(m-1)}, \tag{5.24c}$$

$$\tilde{\mathbf{M}}_{(m)} = \tilde{\mathbf{X}}_{(m)}^{\mathcal{H}}\mathbf{M}\tilde{\mathbf{X}}_{(m)}, \tag{5.24d}$$

$$\tilde{\mathbf{K}}_{(m)}\mathbf{Q}_{(m)} = \tilde{\mathbf{K}}_{(m)}\mathbf{Q}_{(m)}\mathbf{\Lambda}_{(m)}, \tag{5.24e}$$

$$\mathbf{X}_{(m)} = \tilde{\mathbf{X}}_{(m)}\mathbf{Q}_{(m)}, \tag{5.24f}$$

where $m = 1, 2, 3, ...$ labels the iteration times. For each iteration, the columns of $\mathbf{X}_{m-1}$ for $m > 1$ in Eq. (5.24a) are the estimated eigenvectors obtained from the last iteration. After the matrix $\mathbf{Y}_{(m-1)}$ is calculated from Eq. (5.24a), the matrix $\tilde{\mathbf{X}}_{(m)}$ is obtained by solving Eq. (5.24b). The columns of the matrix $\tilde{\mathbf{X}}_{(m)}$ are used as the basis to span a subspace of the full eigenspace, and the full system matrices $\mathbf{M}$ and $\mathbf{K}$ are projected to the subspace through Eqs. (5.24c-5.24d). The dimension of the reduced matrix operators $\tilde{\mathbf{M}}$ and $\tilde{\mathbf{K}}$ is $q \times q$. By solving the eigenvalue problem in Eq. (5.24e), the diagonal matrix $\mathbf{\Lambda}_{(m)}$ contains

the updated estimation of the q eigenvalues (with subscript (m)),

$$\mathbf{\Lambda}_{(m)} = \begin{pmatrix} \lambda_{(m),1} & & & \\ & \lambda_{(m),2} & & \\ & & \ddots & \\ & & & \lambda_{(m),q} \end{pmatrix}, \tag{5.25}$$

and $\mathbf{Q}_{(m)}$ is a square matrix containing the reduced eigenvectors in the mth iteration. Through Eq. (5.24f), the updated full system eigenvectors are obtained as the columns of $\mathbf{X}_{(m)}$. Convergence of eigenvalues is checked after each iteration. The iterative process will stop if all the ratios $\left|\lambda_{(m),n} - \lambda_{(m-1),n}\right| / \left|\lambda_{(m),n}\right|$ for $n = 1, 2, \ldots, p$ are within the desired tolerance. Otherwise, the iteration will continue.

According to the iteration process in Eq. (5.24), the quality of starting iteration vectors ($\mathbf{X}_0$ in Eq. (5.24)) is important for the rate of convergence. If the subspace spanned by the starting iteration vectors contains the exact vectors, a single iteration can provide the exact eigenvalues and eigenvectors. A source of starting iteration vectors with good quality is the modes of a system that is similar to the system to be solved, and such cases occur in structure optimization problems where the natural frequencies are calculated as the structure changes [115]. In this work, the full system modes obtained from the MSCS reduction method are used as the starting iteration vectors ($\mathbf{X}_{i,(0)}$ in Eq. (5.24)). These vectors are considered as ideal starting iteration vectors because solving the coupled systems assembled by sector models in Eq. (5.16) are equivalent to solving the full system with constraints at the inter-stage interface. These constraints are resulted from the facts that not all the phase index components are considered simultaneously within a coupled system assembled by sector models, and the full original systems is equivalent to the coupled system that assembled by all sector models with all phase index components. These constraints differentiate the

coupled systems in Eq. (5.16) from the original full system model, but the modes from the MSCS reduction method are starting iteration vectors with reliable quality. And this will be validated by the later numerical example.

With starting iteration vectors from the MSCS reduction method, better estimation of eigensolutions can be obtained through the iteration in Eq. (5.24), and the estimation will finally converge to the eigensolutions in Eq. (5.22)). When the iteration process in Eq. (5.24) applies, the matrix operators in the iterative process ($\mathbf{M}$ and $\mathbf{K}$ in Eq. (5.24)) are those for the full multi-stage model. This path to improving accuracy works, however, it has a significant drawback. The full system matrix operators in Eq. (5.24) can be very large in industrial applications, so it is not convenient to conduct iterations with respect to these huge matrices. In practice, building and storing such huge matrices can be inconvenient. Therefore, it is necessary to improve the subspace iteration method so that the iterations with respect to these huge full system matrices can be avoided.

5.3.2 Combination of Subspace Iteration and Multi-Stage Cyclic Symmetry Reduction

The combination of the subspace iteration with the MSCS reduction is more than simply using the estimated full system modes obtained from the MSCS reduction method as the starting iteration vectors in the general subspace iteration in Eq. (5.24). In this section, an improved subspace iteration that only requires sector-level-sized calculations is formulated. Parallel computation can also be applied to the proposed iterative process to further improve the computational speed. The matrix operators for the full multi-stage system or its component stages are not necessary in the final formulation, although they are used in the following derivation leading to the final formulation.

To reduce the computational cost in Eq. (5.24), the full multi-stage bladed disks is considered as an assembly of component stages (bladed disks). All the calculations involving full system matrices in Eq. (5.24) are firstly replaced by those involving the matrices for component stages. The component stages are viewed as 'hyper-finite elements' that are connected at the inter-stage interfaces. The full system matrices in Eq. (5.24) can be considered as being generated by assembling these 'hyper-finite elements', although these full system matrices are not ever generated or stored in practice. Starting from the first iteration, the estimated full system eigenvectors obtained from the MSCS reduction method can be partitioned into subvectors that describe the estimated modal deflections of each component stage. These subvectors are used as the starting iteration vectors for the component stages. For the ith and hth stages, the starting iteration vectors for the two stages establish the matrices

$$\mathbf{X}_{i,(0)} = \begin{pmatrix} \dots & \boldsymbol{\phi}_{i,D}^{(V)} & \dots \\ \dots & \boldsymbol{\phi}_{i,I}^{(V)} & \dots \\ \dots & \boldsymbol{\phi}_{i,U}^{(V)} & \dots \end{pmatrix}, \tag{5.26a}$$

$$\mathbf{X}_{h,(0)} = \begin{pmatrix} \dots & \boldsymbol{\phi}_{h,D}^{(V)} & \dots \\ \dots & \boldsymbol{\phi}_{h,I}^{(V)} & \dots \\ \dots & \boldsymbol{\phi}_{h,U}^{(V)} & \dots \end{pmatrix}, \tag{5.26b}$$

where the subvectors in the $\mathbf{X}_{i,(0)}$ and $\mathbf{X}_{h,(0)}$ can be directly obtained through Eq. (5.18). These subvectors in $\mathbf{X}_{i,(0)}$ and $\mathbf{X}_{h,(0)}$ are subvectors of estimated modes (by the MSCS reduction method) that are associated with the lowest q eigenvalues ($q = max\{p + 8, 2p\}$ according to Ref. [112]). For the mth iteration, the contribution to $\mathbf{Y}_{(m-1)}$ in Eq. (5.24a)

from the ith stage (or hyper-finite element) is

$$\mathbf{Y}_{i,(m-1)} = \mathbf{M}_i \mathbf{X}_{i,(m-1)}, \tag{5.27}$$

where $\mathbf{M}_i$ is the full inertia matrix for the ith stage.

To obtain $\tilde{\mathbf{X}}_{(m)}$ in Eq. (5.24b), or equivalently the part of $\tilde{\mathbf{X}}_{(m)}$ for each stage ($\tilde{\mathbf{X}}_{i,(m)}$ for the ith stage), Eq. (5.24b) can be regarded as a static full system force-displacement relation, where $\mathbf{Y}_{(m-1)}$ is the matrix containing q pseudo-loads (the q columns in $\mathbf{Y}_{(m-1)}$). Similarly, by treating $\mathbf{Y}_{i,(m-1)}$ in Eq. (5.27) as pseudo-load matrix, the force-displacement relation for the ith stage is

$$\begin{aligned} &\mathbf{K}_i \tilde{\mathbf{X}}_{i,(m)} = \mathbf{Y}_{i,(m-1)} \\ &= \begin{pmatrix} \mathbf{K}_{i,II} & \mathbf{K}_{i,IB} \\ \mathbf{K}_{i,BI} & \mathbf{K}_{i,BB} \end{pmatrix} \begin{pmatrix} \tilde{\mathbf{X}}_{i,I,(m)} \\ \tilde{\mathbf{X}}_{i,B,(m)} \end{pmatrix} = \begin{pmatrix} \mathbf{Y}_{i,I,(m-1)} \\ \mathbf{Y}_{i,B,(m-1)} \end{pmatrix}, \end{aligned} \tag{5.28}$$

where the subscript B denotes the inter-stage boundary degrees of freedom which include the degrees of freedom with the subscripts U and D in Eq. (5.26). By assembling the force-displacement relations of all component stages (a series of equations in the form of Eq. (5.28)) using finite element assembling process, the assembled full system force-displacement relation (a coupled equation) is equivalent to Eq. (5.24b). This methodology of directly assembling all component stage force-displacement relations, however, is not helpful to reduce the computational cost of solving Eq. (5.24b), because the size of the obtained coupled equation is of a similar, if not identical, size with Eq. (5.24b). Instead of this method, the force-displacement relations of all component stages are used to assemble a force-displacement relation in terms of only the boundary degrees of freedom by using the static condensation procedure [116]. For this purpose, the interior degrees of freedom of the ith stage $\tilde{\mathbf{X}}_{i,I,(m)}$ in

Eq. (5.28) are eliminated, and Eq. (5.28) can be rewritten as

$$(\mathbf{K}_{i,BB} + \mathbf{K}_{i,BI}\mathbf{P}_i)\tilde{\mathbf{X}}_{i,B,(m)} = \mathbf{Y}_{i,B,(m-1)} + (\mathbf{P}_i)^{\mathcal{H}}\mathbf{Y}_{i,I,(m-1)}, \tag{5.29a}$$

$$\mathbf{P}_i = -[\mathbf{K}_{i,II}]^{-1}\mathbf{K}_{i,IB}. \tag{5.29b}$$

Eq. (5.29) can be regarded as the force-displacement relation for a new type of hyper-finite element that only contains the inter-stage boundary degrees of freedom in a stage. A global generalized coordinate $\mathbf{q}_B$ is built by assembling all the inter-stage boundary degrees of freedom. For example, only the lower frontier of the upper stages are retained in $\mathbf{q}_B$ when two stages merge. The inter-stage boundary degrees of freedom in the ith stage $\mathbf{q}_{i,B}$ is related to $\mathbf{q}_B$ by a constraint equation,

$$\mathbf{q}_{i,B} = \tilde{\mathbf{B}}(i)\mathbf{q}_B, \tag{5.30}$$

where $\tilde{\mathbf{B}}(i)$ is the matrix that transforms the global inter-stage boundary degrees of freedom to the local inter-stage boundary degrees of freedom in the ith stage. The force-displacement relation in terms of the global boundary degrees of freedom is assembled as

$$\sum_i \tilde{\mathbf{B}}(i)^T\tilde{\mathbf{K}}_{i,BB}\tilde{\mathbf{B}}(i)\tilde{\mathbf{X}}_{B,(m)} = \sum_i \tilde{\mathbf{B}}(i)^T\tilde{\mathbf{Y}}_{i,B,(m-1)}, \tag{5.31a}$$

$$\tilde{\mathbf{K}}_{i,BB} = \mathbf{K}_{i,BB} + \mathbf{K}_{i,BI}\mathbf{P}_i, \tag{5.31b}$$

$$\tilde{\mathbf{Y}}_{i,B,(m-1)} = \mathbf{Y}_{i,B,(m-1)} + (\mathbf{P}_i)^{\mathcal{H}}\mathbf{Y}_{i,I,(m-1)}. \tag{5.31c}$$

After $\tilde{\mathbf{X}}_{B,(m)}$ is solved from Eq. (5.31), $\tilde{\mathbf{X}}_{B,(m)}$ and $\tilde{\mathbf{X}}_{i,(m)}$ in Eq. (5.28) can be obtained through

$$\tilde{\mathbf{X}}_{i,B,(m)} = \tilde{\mathbf{B}}(i)\tilde{\mathbf{X}}_{B,(m)} \tag{5.32a}$$

$$\tilde{\mathbf{X}}_{i,I,(m)} = [\mathbf{K}_{i,II}]^{-1}\mathbf{Y}_{i,I,(m-1)} + \mathbf{P}_i\tilde{\mathbf{X}}_{i,B,(m)} \tag{5.32b}$$

where Eq. (5.32a) is based on the relation in Eq. (5.30), and Eq. (5.32b) is obtained from manipulation of Eqs. (5.28) and (5.29b). Therefore, the part of $\tilde{\mathbf{X}}_{(m)}$ for each stage, *e.g.*, $\tilde{\mathbf{X}}_{i,(m)} = (\tilde{\mathbf{X}}_{i,I,(m)}, \tilde{\mathbf{X}}_{i,B,(m)})^T$ for the ith stage, is obtained by using matrix operators for single stages, and it process is equivalent to obtain $\tilde{\mathbf{X}}_{(m)}$ in Eq. (5.24b).

Compared to solving Eq. (5.24b), the process from Eq. (5.28) to (5.32) avoids the full system matrices and reduces the size of the linear equations from the full system size to the size of single stages. The inverse of $\mathbf{K}_{i,II}$ in Eqs. (5.29b) and (5.32b) is not calculated in practice for large system. $\mathbf{P}_i$ in Eq. (5.29b), for example, is the solution of linear equation $\mathbf{K}_{i,II}\mathbf{P}_i = -\mathbf{K}_{i,IB}$, which can be solved by efficient decomposition procedures, such as forward and backward substitutions. Also, the decomposition of $\mathbf{K}_{i,II}$ and the calculation of $\mathbf{P}_i$ in Eq. (5.29b) are performed only once because they are not changed in iterative process.

To further increase the computational speed, the process from Eq. (5.27) to (5.32) can also be equivalently performed without using the matrices for full single stages. Because each single stage of bladed disk is cyclically symmetric, the calculations with respect to a full single stage can be replaced by calculations with respect to single stage sector models with different phase indices. For this purpose, the phase index components of $\mathbf{X}_{i,(m-1)}$ in Eq. (5.27) for the mth iteration are calculated as

$$\mathbf{X}^{(k)}_{i,(m-1)} = \begin{pmatrix} (\mathbf{e}^{(k)}_{N_i} \otimes \mathbf{I}_{i,I})^{\mathcal{H}} & \mathbf{0} \\ \mathbf{0} & (\mathbf{e}^{(k)}_{N_i} \otimes \mathbf{I}_{i,B})^{\mathcal{H}} \end{pmatrix} \mathbf{X}_{i,(m-1)}, \tag{5.33}$$

where $k = 0, 1, ..., N_i - 1$ is the phase index. Then phase index components of $\mathbf{Y}_{i,(m-1)}$ in

Eq. (5.28) can be calculated as

$$\mathbf{Y}^{(k)}_{i,(m-1)} = \mathbf{M}^{(k)}_i \mathbf{X}^{(k)}_{i,(m-1)}, \tag{5.34}$$

where $\mathbf{M}^{(k)}_i$ (a part of $\mathbf{D}^{(k)}_i$ in Eq. (5.4)) is the inertia matrix of the sector model with the phase index k for the ith stage. Similar to Eq. (5.29), the force-displacement relation for the inter-stage boundary degrees of freedom in the kth sector model of the ith stage can be written as

$$(\mathbf{K}^{(k)}_{i,BB} + \mathbf{K}^{(k)}_{i,BI}\mathbf{P}^{(k)}_i)\tilde{\mathbf{X}}^{(k)}_{i,B,(m)} = \mathbf{Y}^{(k)}_{i,B,(m-1)} + (\mathbf{P}^{(k)}_i)^{\mathcal{H}}\mathbf{Y}^{(k)}_{i,I,(m-1)}, \tag{5.35a}$$

$$\mathbf{P}^{(k)}_i = -[\mathbf{K}^{(k)}_{i,II}]^{-1}\mathbf{K}^{(k)}_{i,IB}, \tag{5.35b}$$

where $\mathbf{K}^{(k)}_{i,II}$, $\mathbf{K}^{(k)}_{i,IB}$, $\mathbf{K}^{(k)}_{i,BI}$, and $\mathbf{K}^{(k)}_{i,BB}$ are submatrices of the stiffness matrix for the kth sector model of the ith stage $\mathbf{K}^{(k)}_i$. Columns of $\tilde{\mathbf{X}}^{(k)}_{i,B,(m)}$ can be regarded as displacement vectors of a hyper-finite element that contains only the inter-stage boundary degrees of freedom in the sector model characterized by the phase index k of the ith stage. Similar to the assembling process of hyper-finite elements in Eqs. (5.30) and (5.31), the force-displacement relation in terms of the global boundary degrees of freedom is assemble as

$$\sum_i \tilde{\mathbf{B}}(i)^T \tilde{\mathbf{K}}_{i,BB}\tilde{\mathbf{B}}(i)\tilde{\mathbf{X}}_{B,(m)} = \sum_i \tilde{\mathbf{B}}(i)^T \tilde{\mathbf{Y}}_{i,B,(m-1)}, \tag{5.36a}$$

$$\tilde{\mathbf{K}}_{i,BB} = \sum_{k=1}^{N_i} (\mathbf{e}^{(k)}_{N_i} \otimes \mathbf{I}_{i,B})(\mathbf{K}^{(k)}_{i,BB} + \mathbf{K}^{(k)}_{i,BI}\mathbf{P}^{(k)}_i)(\mathbf{e}^{(k)}_{N_i} \otimes \mathbf{I}_{i,B})^{\mathcal{H}}, \tag{5.36b}$$

$$\tilde{\mathbf{Y}}_{i,B,(m-1)} = \sum_{k=1}^{N_i} (\mathbf{e}^{(k)}_{N_i} \otimes \mathbf{I}_{i,B})(\mathbf{Y}^{(k)}_{i,B,(m-1)} + (\mathbf{P}^{(k)}_i)^{\mathcal{H}}\mathbf{Y}^{(k)}_{i,I,(m-1)}), \tag{5.36c}$$

where the displacement matrix $\tilde{\mathbf{X}}_{B,(m)}$ for the global boundary degrees of freedom is related

to $\tilde{\mathbf{X}}^{(k)}_{i,B,(m)}$ in Eq. (5.35) by the constraint equation

$$\sum_{k=1}^{N_i} \mathbf{e}^{(k)}_{N_i} \otimes \tilde{\mathbf{X}}^{(k)}_{i,B,(m)} = \tilde{\mathbf{B}}(i)\tilde{\mathbf{X}}_{B,(m)}. \tag{5.37}$$

After solving for $\tilde{\mathbf{X}}_{B,(m)}$ in Eq. (5.36), the phase index component (with the phase index k in the ith stage) of $\tilde{\mathbf{X}}_{(m)}$ in Eq. (5.24b) is obtained as

$$\tilde{\mathbf{X}}^{(k)}_{i,(m)} = \begin{pmatrix} \tilde{\mathbf{X}}^{(k)}_{i,I,(m)} \\ \tilde{\mathbf{X}}^{(k)}_{i,B,(m)} \end{pmatrix}, \tag{5.38a}$$

$$\tilde{\mathbf{X}}^{(k)}_{i,B,(m)} = (\mathbf{e}^{(k)}_{N_i} \otimes \mathbf{I}_{i,B})^{\mathcal{H}} \tilde{\mathbf{B}}(i)\tilde{\mathbf{X}}_{B,(m)}, \tag{5.38b}$$

$$\tilde{\mathbf{X}}^{(k)}_{i,I,(m)} = [\mathbf{K}^{(k)}_{i,II}]^{-1}\mathbf{Y}^{(k)}_{i,I,(m-1)} + \mathbf{P}^{(k)}_{i}\tilde{\mathbf{X}}^{(k)}_{i,B,(m)}. \tag{5.38c}$$

With $\tilde{\mathbf{X}}^{(k)}_{i,(m)}$ in Eq. (5.38) for all the phase index components of all the component stages being obtained, $\tilde{\mathbf{X}}_{(m)}$ in Eq. (5.24b) is equivalently obtained, although generating $\tilde{\mathbf{X}}_{(m)}$ from $\tilde{\mathbf{X}}^{(k)}_{i,(m)}$ is not necessary in practice.

In Eqs. (5.24c) and (5.24d), the full system matrices are projected onto the space spanned by the columns of $\tilde{\mathbf{X}}_{(m)}$ in Eq. (5.24b). To replace Eqs. (5.24c) and (5.24d), the matrices of sector models are projected onto $\tilde{\mathbf{X}}^{(k)}_{i,(m)}$ in Eq. (5.38) as

$$\tilde{\mathbf{K}}_{i,k,(m)} = (\tilde{\mathbf{X}}^{(k)}_{i,(m)})^{\mathcal{H}} \mathbf{K}^{(k)}_{i} \tilde{\mathbf{X}}^{(k)}_{i,(m)}, \tag{5.39a}$$

$$\tilde{\mathbf{M}}_{i,k,(m)} = (\tilde{\mathbf{X}}^{(k)}_{i,(m)})^{\mathcal{H}} \mathbf{M}^{(k)}_{i} \tilde{\mathbf{X}}^{(k)}_{i,(m)}. \tag{5.39b}$$

The size of $\tilde{\mathbf{K}}_{i,k,(m)}$ (or $\tilde{\mathbf{M}}_{i,k,(m)}$) is q by q, which is equal to the size of $\tilde{\mathbf{K}}_{(m)}$ in Eq. (5.24c). Because $\tilde{\mathbf{X}}_{(m)}$ and $\mathbf{K}$ (or $\mathbf{M}$) in Eq. (5.24) are respectively replaced by the phase index components and sector models of all individual stages, the summation of the projected matrices, $\tilde{\mathbf{K}}_{i,k,(m)}$ and $\tilde{\mathbf{M}}_{i,k,(m)}$ in Eq. (5.39), over all phase indices of all stages yields the

alternative formulation of Eqs. (5.24c) and (5.24d),

$$\tilde{\mathbf{K}}_{(m)} = \sum_{i} \sum_{k=0}^{N_i-1} \tilde{\mathbf{K}}_{i,k,(m)} \tag{5.40a}$$

$$\tilde{\mathbf{M}}_{(m)} = \sum_{i} \sum_{k=0}^{N_i-1} \tilde{\mathbf{M}}_{i,k,(m)} \tag{5.40b}$$

where only matrices of sector models and $\tilde{\mathbf{X}}^{(k)}_{i,(m)}$ in Eq. (5.38) are involved. The reduced eigenvalue problem in Eq. (5.24e) is then solved, and the estimated eigenvalues are contained in the $\mathbf{\Lambda}_{(m)}$ in Eq. (5.24e). Analogous to Eq. (5.24f), the kth phase index component in the ith stage of the updated estimated eigenvectors is obtained as

$$\mathbf{X}^{(k)}_{i,(m)} = \tilde{\mathbf{X}}^{(k)}_{i,(m)} \mathbf{Q}_{(m)}. \tag{5.41}$$

Until all the ratios $\left|\lambda_{(m),n} - \lambda_{(m-1),n}\right| / \left|\lambda_{(m),n}\right|$ for $n = 1, 2, \ldots, p$ are within the desired tolerance, a new iteration will start from Eq. (5.34) with the updated $\mathbf{X}^{(k)}_{i,(m)}$ in Eq. (5.41). If the eigenvalues converge in the mth iteration, the modal deflections of the ith stage are columns of the matrix

$$\mathbf{X}_{i,(m)} = \sum_{k=0}^{N_i-1} \begin{pmatrix} \mathbf{e}^{(k)}_{N_i} \otimes \mathbf{X}^{(k)}_{i,I,(m)} \\ \mathbf{e}^{(k)}_{N_i} \otimes \mathbf{X}^{(k)}_{i,B,(m)} \end{pmatrix}, \tag{5.42}$$

where the first p columns are the modal deflections of the ith stage in the first p full system mode.

The subspace iteration method for multi-stage bladed disks is summarized as follow:

1. The estimated full system modes that are associated with the lowest q estimated eigenvalues ($q = max\{p + 8, 2p\}$, p is the number of eigensolutions to be solved) obtained from the MSCS reduction method are selected as the starting iteration vectors. The matrix of these vectors is partitioned into submatrices for each single stage as shown

in Eq. (5.26).

2. The phase index components of the submatrices obtained in Step 1 are calculated as $\mathbf{X}^{(k)}_{i,(m-1)}$ through Eq. (5.33) for the first iteration ($m = 1$).

3. Based on Eq. (5.35b), decomposition of $\mathbf{K}^{(k)}_{i,II}$ is performed and stored, and $\mathbf{P}^{(k)}_{i}$ for each phase index in each stage is calculated and stored.

4. $\mathbf{Y}^{(k)}_{i,(m-1)}$ in Eq. (5.34) is calculated for all the phase indices in all stages.

5. The force-displacement relation of the hyper-finite elements containing only inter-stage boundary degrees of freedom is assemble based on Eq. (5.36).

6. Based on Eq. (5.38), $\tilde{\mathbf{X}}^{(k)}_{i,(m)}$ for each phase index components of each component stages is obtained.

7. The reduced eigenvalue problem in Eq. (5.24e) is formulated based on Eqs. (5.39) and (5.40). After solving the Eq. (5.24e), the phase index component (with phase index k) in the ith stage of the updated estimated full system eigenvectors is obtained as $\mathbf{X}^{(k)}_{i,(m)}$ in Eq. (5.41).

8. The convergence of the first p eigenvalues (p is the number of desired eigenvalues) is checked: whether all the ratios $\left|\lambda_{(m),n} - \lambda_{(m-1),n}\right| / \left|\lambda_{(m),n}\right|$ for $n = 1, 2, \ldots, p$ are within the desired tolerance. If the convergence is not reached, $\mathbf{X}^{(k)}_{i,(m)}$ in Eq. (5.41) is returned to Step 4 for a new iteration, because the first three steps are not necessary after the first iteration.

9. With convergence of eigenvalues, the part of the eigenvectors for the each stage is generated by Eq. (5.42). The desired p eigenvectors are the first p columns of $\mathbf{X}_{i,(m)}$ in Eq. (5.42) after the columns of $\mathbf{X}_{i,(m)}$ are sorted according to the eigenvalues.

Compared to the general subspace iteration method in Section 5.3.1, the iterative process above is advantageous in storage size and computational speed. First, in the iterative process proposed in this section, full system matrices are not necessary to be generated or stored. Instead, only matrices of the sector models in single stages are needed. This feature provides a significant advantage over the general subspace iteration method in industrial applications, where the full system matrices consumes large storage space. Secondly, all the calculations in the iterative process in this section are within sector level, and the computational expensive step (Step 3) is only performed once. Compared to solving Eq. (5.24b), the process from Step 3 to Step 6 involves calculation with smaller sizes, so the proposed method provides higher computational efficiency for the iterations after the first one than the general subspace iteration method. More importantly, parallel computations can be performed in many steps of the proposed iterative process. Parallel computations can be involved in Steps 3, 4, 6, 8, and the assembling process in Step 5 and 7. The increase of computational speed by performing parallel computations can be significant if the size of full system is large (for system with small sizes, performing parallel computations is not always beneficial). The benefit of parallel computations is especially significant if the large size of multi-stage systems is a result of having a large number of stages and/or having a large number of blades (sectors) within each stage.

5.3.3 Numerical Validation

To validate the proposed subspace iteration method in Section 5.3.2, the eigensolutions of the two-stage bladed disk in Fig. 5.1 (a) are solved. Starting with 1000 estimated full system modes obtained from the MSCS reduction method, the lowest 500 natural frequencies converge within a relative error of 0.01% in three iterations. In Fig. 5.6, the natural frequencies of the example systems obtained from different methods are illustrated. As shown

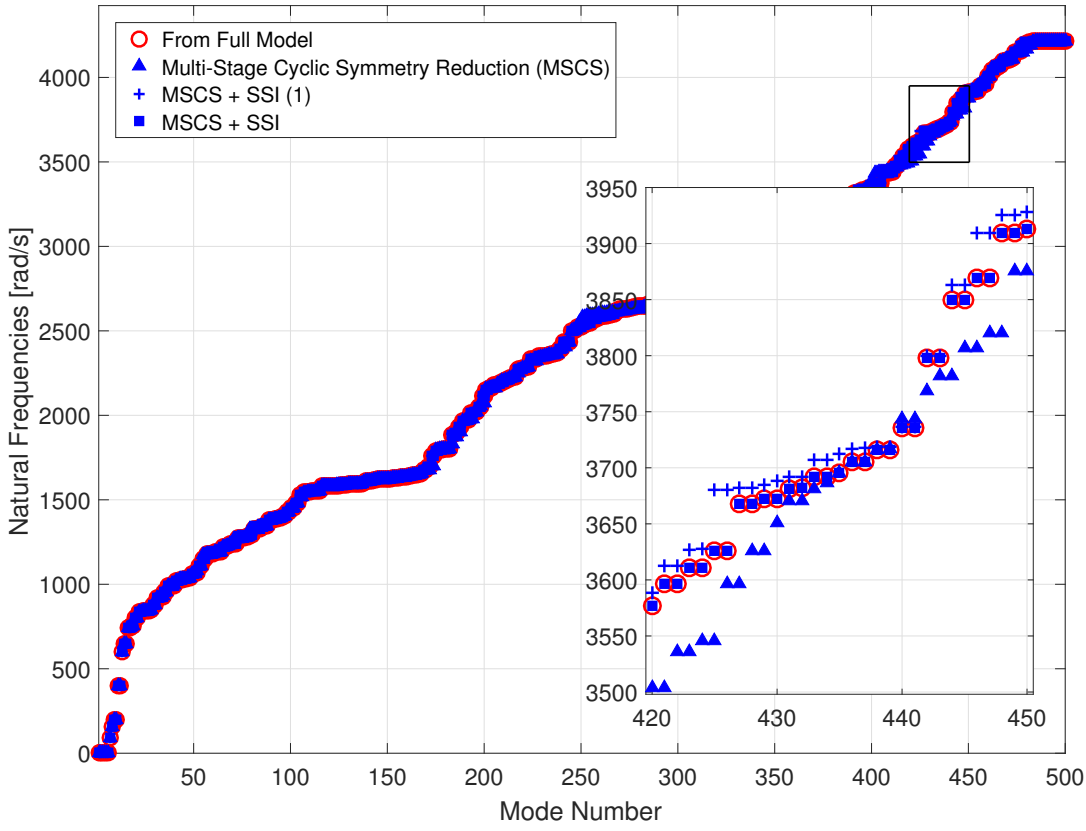

Figure 5.6: Natural frequencies of the example system in Fig 5.1(a). '+' marks the results after one subspace iteration (SSI) with the starting vectors from the MSCS reduction method. The square marks the final converged results obtained by using the proposed subspace iteration with the starting vectors from the MSCS reduction method.

in Fig. 5.6, the natural frequencies converge to the accurate values in few steps because the starting vectors provided by the MSCS reduction method are of good quality as discussed in Section 5.3.1.

By using the proposed subspace iteration after the MSCS reduction method, both the natural frequencies and the associated mode shapes are accurate. For the purpose of validation, Fig. 5.7 illustrates whether the eigenvectors obtained from the proposed subspace iteration method can capture the accurate combinations of nodal diameter components with

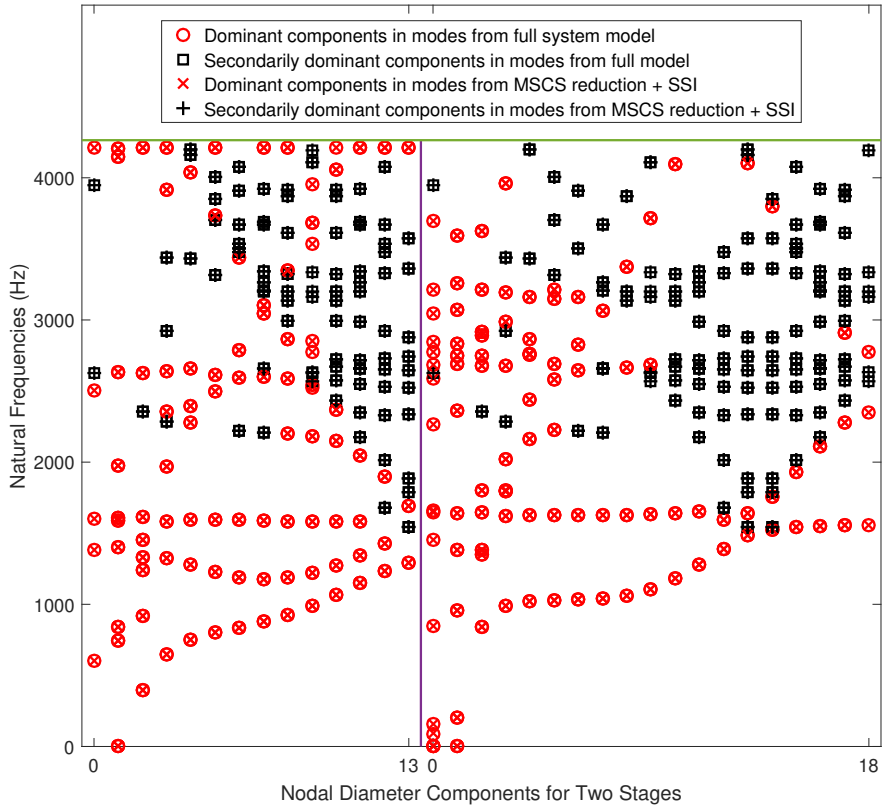

Figure 5.7: Natural frequencies vs nodal diameter components of the eigenvectors for the system in Fig. 5.1(a).

the accurate natural frequencies. As Fig. 5.7 shows, by analyzing the combination of nodal diameter components, the eigenvectors obtained from the proposed subspace iterations are as accurate as the ones obtained from the full system model. Compared to the results by using the MSCS reduction method alone (Fig. 5.5), the improvement of accuracy for obtained eigenvectors is significant. In Fig. 5.8, 25 full system modes (with mode number 426-450) obtained from the MSCS reduction combined with the proposed subspace iteration method are provided to ensure that the accuracy of mode shapes illustrated by Fig. 5.7 is reliable. The mode shapes in Fig. 5.8 are almost identical to those with the same mode number in Fig. 5.3, and the only difference between the modes with the same mode number is due to that some modes are associated with degenerate natural frequencies. Therefore, the proposed subspace iteration method is demonstrated to be effective to obtain accurate

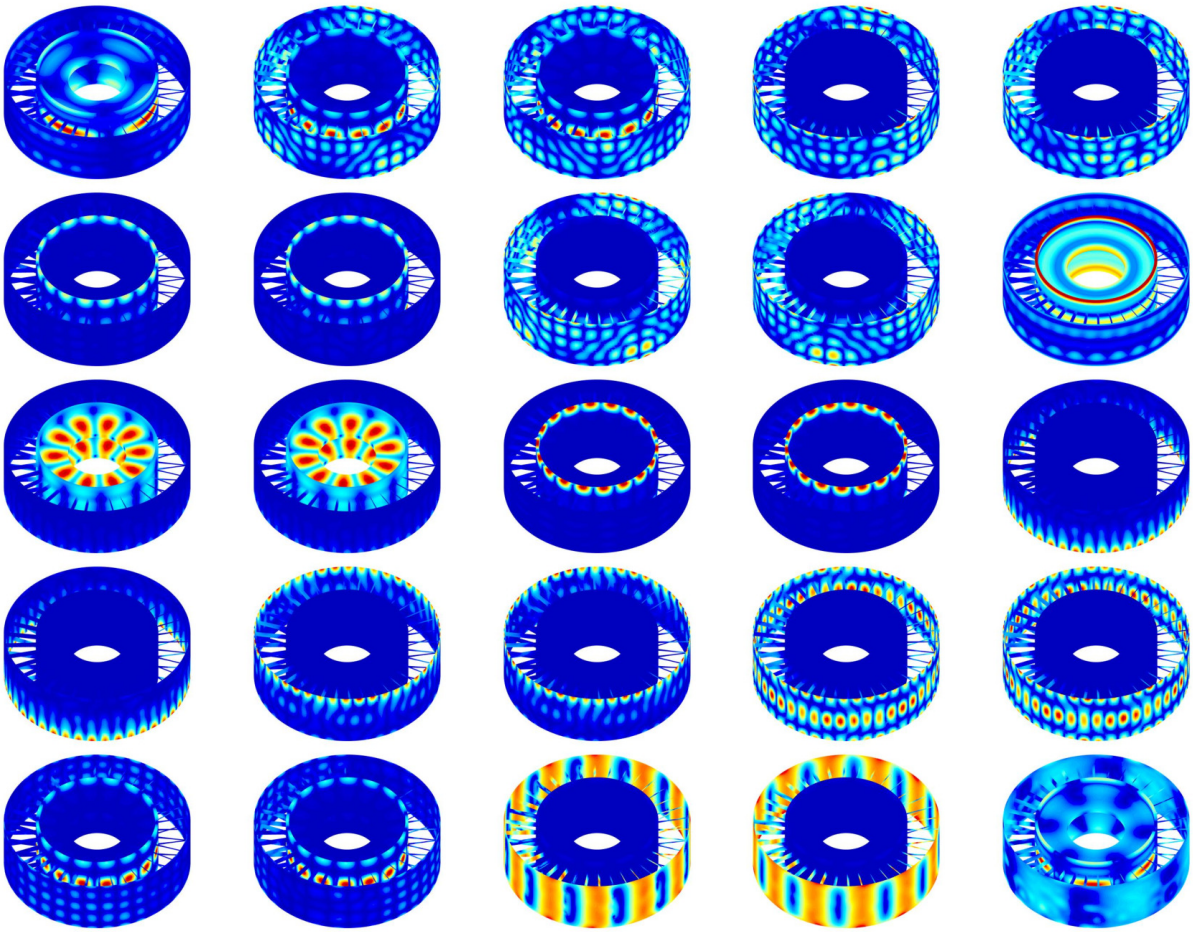

Figure 5.8: Modes (with mode number 426-450) of the example system in Fig 5.1(a) obtained from MSCS reduction combined with subspace iteration.

eigensolutions.

To compare the computational speed of the MSCS reduction combined with the proposed subspace iteration method, Fig. 5.9 illustrates the time ratio for solving the full system eigensolutions using different methods. In Fig. 5.9, the time for using the MSCS reduction combined with the proposed subspace iteration method is 76% of the time for solving the full system eigenvalue problems directly, if no parallel computation is performed in the proposed subspace iteration method. By analyzing the proportions of time taken during the proposed procedure, most of the computational time (83%) is consumed by the parallelizable steps in

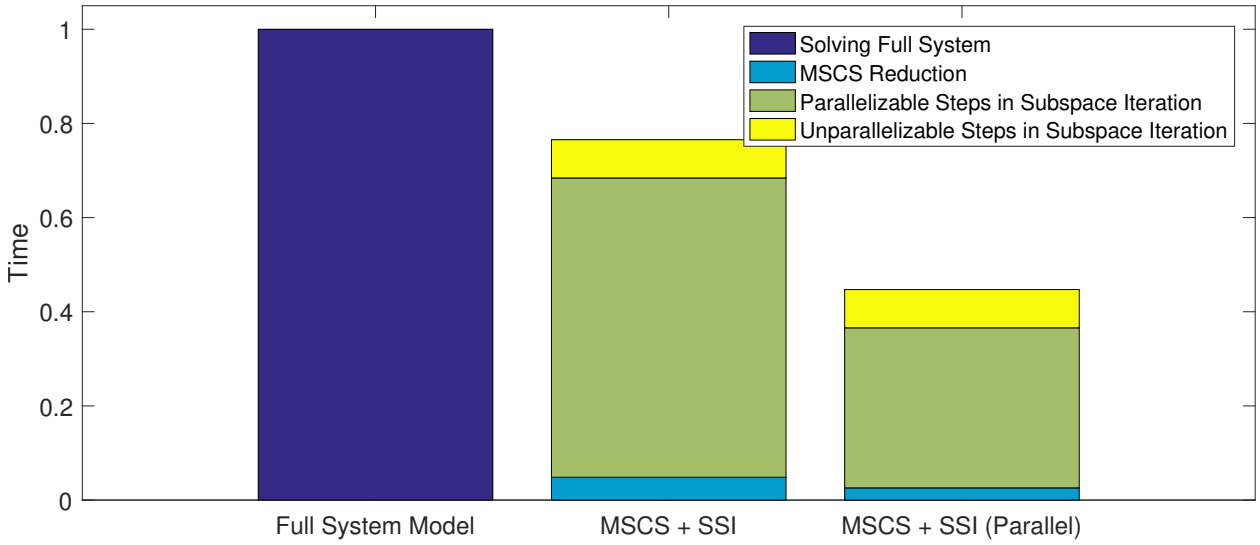

Figure 5.9: Time for solving the first 500 eigenvalues of the example system in Fig 5.1(a). The time for solving the full system model is set as the benchmark. The time for using the MSCS reduction and the proposed subspace iteration method is given as ratios to the benchmark.

the proposed subspace iterations. By applying parallel computation (4 cores as workers), both the time consumed by the MSCS reduction method and the parallelizable steps in the proposed subspace iteration are reduced, and the total time for using the proposed subspace iteration combined with the MSCS reduction is only 45% of the time for solving the full system eigenvalue problems. Because the size of the example system is not large, the reduction of computational time is not significant compared to the number of cores used for parallel computations. For industrial applications, where the number of degrees of freedom can be enormously large (tens or hundreds of millions), the MSCS reduction combined with the proposed subspace iteration method can reduce the computational time for full multi-stage systems dramatically, because parallel computations are allowed in most steps of the full procedure.

Another important feature of the proposed method is all computations are performed without generating any full system matrix operators. Specifically, because of this feature,

only the matrices for the two sectors in Fig. 5.1 (b) are needed, instead of the full system matrices as large as 94932 by 94932 (number of total degrees of freedom). For industrial applications, the size of full system matrices can be too large to be stored or read in further computations. By using the MSCS reduction method with the proposed subspace iteration, the obstacles of storing full system matrices are overcome because only matrices of sector level size are involved.

5.4 Conclusions

In industrial finite element models of multi-stage bladed disks, obtaining eigensolutions for the full multi-stage structure is hard because of the large number of degrees of freedom in the full system model. In this work, a method to solve the eigensolutions of multi-stage bladed disks is proposed. By combining the multi-stage cyclic symmetry reduction method and the subspace iteration, both natural frequencies and associated eigenvectors are obtained accurately. In the proposed method, all computations are performed without generating or storing the matrix operators for the full multi-stage bladed disks.

The main drawback of the multi-stage cyclic symmetry reduction method is that the accuracy of obtained full system eigenvectors is not reliable although the obtained natural frequencies coincidentally match the ones from the full multi-stage system model. To overcome this drawback, the subspace iteration method is applied to improve the accuracy of obtained eigen pairs. With the full system eigenvectors obtained from the multi-stage cyclic symmetry reduction method as the starting iteration vectors, accurate eigensolutions are obtained within a small number of iterations.

In this work, the subspace iteration method is improved for solving multi-stage bladed disks. In the proposed subspace iteration method, cyclic symmetry of each stage is con-

sidered, and the iteration can be performed by using single stage sector models only. This feature overcomes the difficulties in generating, storing, and reading the large-sized full system matrices in industrial applications. Meanwhile, parallel computation can be performed in most steps of the proposed subspace iteration method. Because parallel computation can also be performed in the multi-stage cyclic symmetry reduction method, the time for using the proposed method (the multi-stage cyclic symmetry reduction combined with the proposed subspace iteration method) to obtain full system eigensolutions is reduced significantly when multiple computational cores are available. The reduction of computational time can be more significant when the proposed method is applied to industrial multi-stage bladed disks systems with tens to hundreds of blades within each stage.

Bibliography

[1] R. McWeeny, Symmetry: an introduction to group theory and its applications, Pergamon Press, New York, 1963.

[2] D. J. Ewins, Vibration characteristics of bladed disc assemblies, Journal of Mechanical Engineering Science 15 (1973) 165–186.

[3] G. S. Óttarsson, Dynamic modeling and vibration analysis of mistuned bladed disks, PhD Thesis, University of Michigan, Ann Arbor, Michigan, 1994.

[4] B. J. Olson, S. W. Shaw, Vibration absorbers for a rotating flexible structure with cyclic symmetry: nonlinear path design, Nonlinear Dyn 60 (2009) 149–182.

[5] R. G. Parker, C. D. Mote Jr., Tuning of the natural frequency spectrum of a circular plate by in-plate stress, Journal of Sound and Vibration 145 (1991) 95–110.

[6] X. Wu, R. G. Parker, Vibration of rings on a general elastic foundation, Journal of Sound and Vibration 295 (2006) 194–213.

[7] D. Zhang, S. Wang, J. Liu, Analytical prediction for free response of rotationally ring-shaped periodic structures, Journal of Vibration and Acoustics 136 (2014) 041016–041016–12.

[8] S. Wang, W. Sun, Y. Wang, Instantaneous mode contamination and parametric combination instability of spinning cyclically symmetric ring structures with expanding application to planetary gear ring, Journal of Sound and Vibration 375 (2016) 366–385.

[9] H. Kim, I. Y. Shen, Ground-based vibration response of a spinning, cyclic, symmetric rotor with gyroscopic and centrifugal softening effects, Journal of Vibration and Acoustics 131 (2009) 021007–021007.

[10] H. Kim, N. T. K. Colonnese, I. Y. Shen, Mode evolution of cyclic symmetric rotors assembled to flexible bearings and housing, Journal of Vibration and Acoustics 131 (2009) 051008–051008.

[11] A. Kahraman, Natural modes of planetary gear trains, Journal of Sound and Vibration 173 (1994) 125–130.

[12] J. Lin, R. G. Parker, Analytical characterization of the unique properties of planetary gear free vibration, Journal of Vibration and Acoustics 121 (1999) 316–321.

[13] J. Lin, R. G. Parker, Natural frequency veering in planetary gears, Mechanics of Structures and Machines 29 (2001) 411–429.

[14] R. G. Parker, A physical explanation for the effectiveness of planet phasing to suppress planetary gear vibration, Journal of Sound and Vibration 236 (2000) 561–573.

[15] X. Wu, R. G. Parker, Modal properties of planetary gears with an elastic continuum ring gear, Journal of Applied Mechanics 75 (2008) 031014–1–12.

[16] C. G. Cooley, R. G. Parker, Vibration properties of high-speed planetary gears with gyroscopic effects, Journal of Vibration and Acoustics 134 (2012) 061014–061014.

[17] B. J. Olson, Order-tuned vibration absorbers for systems with cyclic symmetry with applications to turbomachinery, PhD Thesis, Michigan State University, East Lansing, Michigan, 2006.

[18] C. Shi, R. G. Parker, Modal properties and stability of centrifugal pendulum vibration absorber systems with equally spaced, identical absorbers, Journal of Sound and Vibration 331 (2012) 4807–4824.

[19] C. Shi, R. G. Parker, Modal structure of centrifugal pendulum vibration absorber systems with multiple cyclically symmetric groups of absorbers, Journal of Sound and Vibration 332 (2013) 4339–4353.

[20] C. Shi, R. G. Parker, S. W. Shaw, Tuning of centrifugal pendulum vibration absorbers for translational and rotational vibration reduction, Mechanism and Machine Theory 66 (2013) 56–65.

[21] C. Shi, R. G. Parker, Vibration modes and natural frequency veering in three-dimensional, cyclically symmetric centrifugal pendulum vibration absorber systems, Journal of Vibration and Acoustics 136 (2013) 011014–011014.

[22] R. M. Orris, M. Petyt, A finite element study of harmonic wave propagation in periodic structures, Journal of Sound and Vibration 33 (1974) 223–236.

[23] D. L. Thomas, Standing waves in rotationally periodic structures, Journal of Sound and Vibration 37 (1974) 288–290.

[24] D. L. Thomas, Dynamics of rotationally periodic structures, International Journal for Numerical Methods in Engineering 14 (1979) 81–102.

[25] P. J. Davis, Circulant matrices, John Wiley and Sons, New York, 2nd edition, 1979.

[26] B. J. Olson, S. W. Shaw, C. Shi, C. Pierre, R. G. Parker, Circulant matrices and their application to vibration analysis, Applied Mechanics Reviews 66 (2014) 040803–040803.

[27] T. M. Ericson, R. G. Parker, Planetary gear modal vibration experiments and correlation against lumped-parameter and finite element models, Journal of Sound and Vibration 332 (2013) 2350–2375.

[28] T. M. Ericson, R. G. Parker, Natural frequency clusters in planetary gear vibration, Journal of Vibration and Acoustics 135 (2013) 061002–061002–13.

[29] C. Shi, R. G. Parker, Vibration mode structure and simplified modelling of cyclically symmetric or rotationally periodic systems, Proceedings of the Royal Society A 471 (2015) 20140672.

[30] T. Eritenel, R. G. Parker, Modal properties of three-dimensional helical planetary gears, Journal of Sound and Vibration 325 (2009) 397–420.

[31] A. F. Vakakis, Dynamics of a nonlinear periodic structure with cyclic symmetry, Acta Mechanica 95 (1992) 197–226.

[32] A. Vakais, C. Cetinkaya, Mode localization in a class of multidegree-of-freedom nonlinear systems with cyclic symmetry, SIAM Journal on Applied Mathematics 53 (1993) 265–282.

[33] A. Vakakis, T. Nayfeh, M. King, A multiple-scales analysis of nonlinear, localized modes in a cyclic periodic system, Journal of Applied Mechanics 60 (1993) 388–397.

[34] M. E. King, A. F. Vakakis, A very complicated structure of resonances in a nonlinear system with cyclic symmetry: nonlinear forced localization, Nonlinear Dynamics 7 (1995) 85–104.

[35] F. Georgiades, M. Peeters, G. Kerschen, J. C. Golinval, M. Ruzzene, Modal analysis of a nonlinear periodic structure with cyclic symmetry, AIAA Journal 47 (2009) 1014–1025.

[36] A. F. Vakakis, Non-linear normal modes (NNMs) and their applications in vibration theory: an overview, Mechanical Systems and Signal Processing 11 (1997) 3–22.

[37] S. W. Shaw, C. Pierre, Normal modes for non-linear vibratory systems, Journal of Sound and Vibration 164 (1993) 85–124.

[38] S. W. Shaw, C. Pierre, Normal modes of vibration for non-linear continuous systems, Journal of Sound and Vibration 169 (1994) 319–347.

[39] C.-P. Chao, S. W. Shaw, C.-T. Lee, Stability of the unison response for a rotating system with multiple tautochronic pendulum vibration absorbers, Journal of Applied Mechanics 64 (1997) 149–156.

[40] C.-P. Chao, C.-T. Lee, S. Shaw, Non-unison dynamics of multiple centrifugal pendulum vibration absorbers, Journal of Sound and Vibration 204 (1997) 769–794.

[41] A. S. Alsuwaiyan, S. W. Shaw, Performance and dynamics stability of general-path centrifugal pendulum vibration absorbers, Journal of Sound and Vibration 252 (2002) 791–815.

[42] C. T. Lee, S. W. Shaw, On the counteraction of periodic torques for rotating systems using centrifugally driven vibration absorbers, Journal of Sound and Vibration 191 (1996) 695–719.

[43] C.-T. Lee, S. W. Shaw, V. T. Coppola, A subharmonic vibration absorber for rotating machinery, Journal of Vibration and Acoustics 119 (1997) 590–595.

[44] B. J. Olson, S. W. Shaw, Vibration absorbers for a rotating flexible structure with cyclic symmetry: nonlinear path design, Nonlinear Dynamics 60 (2010) 149–182.

[45] V. K. Ambarisha, R. G. Parker, Suppression of planet mode response in planetary gear dynamics through mesh phasing, Journal of Vibration and Acoustics 128 (2005) 133–142.

[46] V. K. Ambarisha, R. G. Parker, Nonlinear dynamics of planetary gears using analytical and finite element models, Journal of Sound and Vibration 302 (2007) 577–595.

[47] C.-J. Bahk, R. G. Parker, Analytical solution for the nonlinear dynamics of planetary gears, Journal of Computational and Nonlinear Dynamics 6 (2010) 021007–021007.

[48] Y. Guo, R. G. Parker, Dynamic analysis of planetary gears with bearing clearance, Journal of Computational and Nonlinear Dynamics 7 (2012) 041002–041002.

[49] Y. Guo, R. G. Parker, Dynamic modeling and analysis of a spur planetary gear involving tooth wedging and bearing clearance nonlinearity, European Journal of Mechanics - A/Solids 29 (2010) 1022–1033.

[50] Y. Guo, J. Keller, R. G. Parker, Nonlinear dynamics and stability of wind turbine planetary gear sets under gravity effects, European Journal of Mechanics - A/Solids 47 (2014) 45–57.

[51] C.-J. Bahk, R. G. Parker, Analytical investigation of tooth profile modification effects on planetary gear dynamics, Mechanism and Machine Theory 70 (2013) 298–319.

[52] M. S. Dresselhaus, G. Dresselhaus, J. Ado, Group theory - application to the physics of condensed matter, Springer, Berlin, 2008.

[53] B. Werner, A. Spence, The computation of symmetry-breaking bifurcation points, SIAM Journal on Numerical Analysis 21 (1984) 388–399.

[54] T. J. Healey, A group-theoretic approach to computational bifurcation problems with symmetry, Computer Methods in Applied Mechanics and Engineering 67 (1988) 257–295.

[55] M. Dellnitz, B. Werner, Computational methods for bifurcation problems with symmetrieswith special attention to steady state and Hopf bifurcation points, Journal of Computational and Applied Mathematics 26 (1989) 97–123.

[56] A. Zingoni, An efficient computational scheme for the vibration analysis of high tension cable nets, Journal of Sound and Vibration 189 (1996) 55–79.

[57] A. Zingoni, Group-theoretic insights on the vibration of symmetric structures in engineering, Philosophical Transactions of the Royal Society A 372 (2014).

[58] S. J. Mohan, R. Pratap, A group theoretic approach to the linear free vibration analysis of shells with dihedral symmetry, Journal of Sound and Vibration 252 (2002) 317–341.

[59] S. J. Mohan, R. Pratap, A natural classification of vibration modes of polygonal ducts based on group theoretic analysis, Journal of Sound and Vibration 269 (2004) 745–764.

[60] J. C. Wohlever, Some computational aspects of a group theoretic finite element approach to the buckling and postbuckling analyses of plates and shells-of-revolution, Computer Methods in Applied Mechanics and Engineering 170 (1999) 373–406.

[61] A. Zingoni, A group-theoretic finite-difference formulation for plate eigenvalue problems, Computers & Structures 112-113 (2012) 266–282.

[62] T. J. Healey, J. A. Treacy, Exact block diagonalization of large eigenvalue problems for structures with symmetry, International Journal for Numerical Methods in Engineering 31 (1991) 265–285.

[63] A. Zingoni, A group-theoretic formulation for symmetric finite elements, Finite Elements in Analysis and Design 41 (2005) 615–635.

[64] G. Zlokovi, T. Maneski, M. Nestorovi, Group theoretical formulation of quadrilateral and hexahedral isoparametric finite elements, Computers & Structures 82 (2004) 883–899.

[65] R. D. Kangwai, S. D. Guest, S. Pellegrino, An introduction to the analysis of symmetric structures, Computers & Structures 71 (1999) 671–688.

[66] R. Bladh, M. P. Castanier, C. Pierre, Effects of multistage coupling and disk flexibility on mistuned bladed disk dynamics, Journal of Engineering for Gas Turbines and Power 125 (2003) 121.

[67] S. H. Song, M. P. Castanier, C. Pierre, Multi-stage modeling of turbine engine rotor vibration, International Design Engineering Technical Conferences 2005-85740 (2005) 1533–1543.

[68] M. P. Castanier, C. Pierre, Modeling and analysis of mistuned bladed disk vibration: current status and emerging directions, Journal of Propulsion and Power 22 (2006) 384–396.

[69] K. D'Souza, A. Saito, B. I. Epureanu, Reduced-order modeling for nonlinear analysis of cracked mistuned multistage bladed-disk systems, AIAA Journal 50 (2012) 304–312.

[70] D. Laxalde, J.-P. Lombard, F. Thouverez, Dynamics of multistage bladed disks systems, Journal of Engineering for Gas Turbines and Power 129 (2007) 1058–1064.

[71] D. Laxalde, F. Thouverez, J. P. Lombard, Dynamical analysis of multi-stage cyclic structures, Mechanics Research Communications 34 (2007) 379–384.

[72] A. Sternchss, E. Balms, P. Jean, J.-P. Lombard, Reduction of multistage disk models: application to an industrial rotor, Journal of Engineering for Gas Turbines and Power 131 (2008) 012502–012502–14.

[73] D.-M. Tran, Reduced models of multi-stage cyclic structures using cyclic symmetry reduction and component mode synthesis, Journal of Sound and Vibration 333 (2014) 5443–5463.

[74] D. R. Kiracofe, R. G. Parker, Structured vibration modes of general compound planetary gear systems, Journal of Vibration and Acoustics 129 (2006) 1–16.

[75] R. G. Parker, Natural frequencies and modal properties of compound planetary gears, Gear Solution (2008) 26–35.

[76] Y. Guo, R. G. Parker, Purely rotational model and vibration modes of compound planetary gears, Mechanism and Machine Theory 45 (2010) 365–377.

[77] Y. Guo, R. G. Parker, Sensitivity of general compound planetary gear natural frequencies and vibration modes to model parameters, Journal of Vibration and Acoustics 132 (2010) 011006–011006.

[78] Y. Guo, R. G. Parker, Analytical determination of mesh phase relations in general compound planetary gears, Mechanism and Machine Theory 46 (2011) 1869–1887.

[79] C. Shi, S. W. Shaw, R. G. Parker, Vibration reduction in a tilting rotor using centrifugal pendulum vibration absorbers, Journal of Sound and Vibration 385 (2016) 55–68.

[80] R. R. Craig Jr., M. C. C. Bampton, Coupling of substructures for dynamic analyses., AIAA Journal 6 (1968) 1313–1319.

[81] K. X. D'Souza, B. I. Epureanu, A statistical characterization of the effects of mistuning in multistage bladed disks, Journal of Engineering for Gas Turbines and Power 134 (2011) 012503–012503–8.

[82] S.-H. Lim, R. Bladh, M. P. Castanier, C. Pierre, Compact, generalized component mode mistuning representation for modeling bladed disk vibration, AIAA Journal 45 (2007) 2285–2298.

[83] D. Laxalde, C. Pierre, Modelling and analysis of multi-stage systems of mistuned bladed disks, Computers & Structures 89 (2011) 316–324.

[84] A. Sinha, Reduced-order model of a mistuned multi-stage bladed rotor, International Journal of Turbo and Jet Engines 25 (2008) 145–154.

[85] C. H. Hodges, Confinement of vibration by structural irregularity, Journal of Sound and Vibration 82 (1982) 411–424.

[86] S.-T. Wei, C. Pierre, Localization phenomena in mistuned assemblies with cyclic symmetry Part I: free vibrations, Journal of Vibration and Acoustics 110 (1988) 429–438.

[87] S.-T. Wei, C. Pierre, Localization phenomena in mistuned assemblies with cyclic symmetry Part II: forced vibrations, Journal of Vibration and Acoustics 110 (1988) 439–449.

[88] P. W. Anderson, Absence of diffusion in certain random lattices, Physical Review 109 (1958) 1492–1505.

[89] A. Sinha, S. Chen, A higher order technique to compute the statistics of forced response of a mistuned bladed disk assembly, Journal of Sound and Vibration 130 (1989) 207–221.

[90] M. P. Mignolet, W. Hu, Direct prediction of the effects of mistuning on the forced response of bladed disks, Journal of Engineering for Gas Turbines and Power 120 (1998) 626–634.

[91] M. P. Mignolet, A. RivasGuerra, B. LaBorde, Towards a comprehensive direct prediction strategy of the effects of mistuning on the forced response of turbomachinery blades, Aircraft Engineering and Aerospace Technology 71 (1999) 462–469.

[92] M. P. Mignolet, C.-C. Lin, B. H. LaBorde, A novel limit distribution for the analysis of randomly mistuned bladed disks, Journal of Engineering for Gas Turbines and Power 123 (2000) 388–394.

[93] R. Bladh, C. Pierre, M. P. Castanier, M. J. Kruse, Dynamic response predictions for a mistuned industrial turbomachinery rotor using reduced-order modeling, Journal of Engineering for Gas Turbines and Power 124 (2002) 311–324.

[94] M. P. Castanier, G. Óttarsson, C. Pierre, A reduced order modeling technique for mistuned bladed disks, Journal of Vibration and Acoustics 119 (1997) 439–447.

[95] R. Bladh, M. P. Castanier, C. Pierre, Reduced order modeling and vibration analysis of mistuned bladed disk assemblies with shrouds, Journal of Engineering for Gas Turbines and Power 121 (1999) 515–522.

[96] M.-T. Yang, J. H. Griffin, A normalized modal eigenvalue approach for resolving modal interaction, Journal of Engineering for Gas Turbines and Power 119 (1997) 647–650.

[97] M.-T. Yang, J. H. Griffin, A reduced-order model of mistuning using a subset of nominal system modes, Journal of Engineering for Gas Turbines and Power 123 (1999) 893–900.

[98] R.-C. Yu, C. D. Mote Jr., Vibration of circular saws containing slots, Holz als Roh-und Werkstoff 45 (1987) 155–160.

[99] J.-G. Tseng, J. A. Wickert, On the vibration of bolted plate and flange assemblies, Journal of Vibration and Acoustics 116 (1994) 468–473.

[100] L. Brillouin, Wave propagation in periodic structures: electric filters and crystal lattices, International series in pure and applied physics, McGraw-Hill Book Company, Inc., New York, 1946.

[101] N. W. Ashcroft, N. D. Mermin, Solid state physics, Holt, Rinehart and Winston, New York, 1976.

[102] L. Meirovitch, Principles and techniques of vibrations, Prentice-Hall, Inc., Upper Saddle River, New Jersey, 07458, 1997.

[103] C. G. Cooley, R. G. Parker, Mechanical stability of high-speed planetary gears, International Journal of Mechanical Sciences 69 (2013) 59–71.

[104] R. C. Yu, C. D. Mote Jr., Vibration and parametric excitation in asymmetric circular plates under moving loads, Journal of Sound and Vibration 119 (1987) 409–427.

[105] B. Dong, R. G. Parker, Modal properties of cyclically symmetric systems with central components vibrating as three-dimensional rigid bodies, Journal of Sound and Vibration 435 (2018) 350–371.

[106] A. Zingoni, Group-theoretic exploitations of symmetry in computational solid and structural mechanics, International Journal for Numerical Methods in Engineering 79 (2009) 253–289.

[107] D. M. Feiner, J. H. Griffin, A fundamental model of mistuning for a single family of modes, Journal of Turbomachinery 124 (2002) 597–605.

[108] D.-M. Tran, Component mode synthesis methods using partial interface modes: Application to tuned and mistuned structures with cyclic symmetry, Computers & Structures 87 (2009) 1141–1153.

[109] G. Battiato, C. M. Firrone, T. M. Berruti, B. I. Epureanu, Reduction and coupling of substructures via GramSchmidt Interface modes, Computer Methods in Applied Mechanics and Engineering 336 (2018) 187–212.

[110] E. Kurstak, K. D'Souza, Multistage blisk and large mistuning modeling using Fourier constraint modes and PRIME, Journal of Engineering for Gas Turbines and Power 140 (2018) 072505–072505–10.

[111] A. Madden, B. I. Epureanu, S. Filippi, Reduced-order modeling approach for blisks with large mass, stiffness, and geometric mistuning, AIAA Journal 50 (2012) 366–374.

[112] K.-J. Bathe, The subspace iteration method - revisited, Computers & Structures 126 (2013) 177–183.

[113] J. S. Arora, D. T. Nguyen, Eigensolution for large structural systems with substructures, International Journal for Numerical Methods in Engineering 15 (1980) 333–341.

[114] K.-J. Bathe, J. Dong, Component mode synthesis with subspace iterations for controlled accuracy of frequency and mode shape solutions, Computers & Structures 139 (2014) 28–32.

[115] K.-J. Bathe, Finite element procedures, Prentice Hall, 2006.

[116] M. Paz, W. Leigh, Integrated matrix analysis of structures: theory and computation, Springer US, 2001.